Modulated Signal Impact on Multibeam Echosounder Bathymetry

Pauline Vincent

N° d'ordre : 2013telb0275

Sous le sceau de l'Université européenne de Bretagne

Télécom Bretagne

En habilitation conjointe avec l'Université de Rennes 1

Ecole Doctorale – MATISSE

IMPACT DES SIGNAUX MODULES SUR LA PRECISION DES MESURES BATHYMETRIQUES ISSUES DE SONDEURS MULTIFAISCEAUX

-

MODULATED SIGNAL IMPACT ON MULTIBEAM ECHOSOUNDER BATHYMETRY

Thèse de Doctorat

Mention : *Traitement du signal et Télécommunications*

Présentée par **Pauline Vincent**

Département : Image et Traitement de l'Information

Laboratoire : Lab-STICC - Pôle CID

Directeur de thèse : René Garello

Soutenue le 28 mai 2013

Jury :

M. Pierre Cervenka, Directeur de recherche CNRS (Rapporteur-Président du Jury)
M .Thomas Weber, Professeur à l'UNH (Rapporteur)
M. René Garello, Professeur à Telecom Bretagne (Directeur de thèse)
M. Xavier Lurton, Chercheur à l'IFREMER (Co-Directeur de thèse)
M. Frédéric Maussang, Maitre de Conférences à Telecom Bretagne (Examinateur)
M. Odd Arne Almskår, Ingénieur de Recherche à Kongsberg Maritime (Examinateur)
M. Pierre Palud, Ingénieur à Simrad Spain - France (Invité)

Acknowledgements

This manuscript is the result of a long work which has involved several people I would like to thank here.

First of all, my gratitude comes to all the jury members.

I thank P. Cervanka (Universty P.Curie Paris6, France) for honouring me with accepting the role of jury president, as well as for his precise in-depth review and evaluation of the presented work. I also thank T. Weber (University of New Hamphire, USA) for his visit to Brest and his enhancive and kind review he made to this manuscript.

In addition, I am really grateful to the people who have advised and supervised this work during these last few years.

I would like to thank R. Garello (Telecom Bretagne, France) for being present to handle all the administrative matters and especially for his unfailing support he gave to me and this work. I am really thankful to X. Lurton (Ifremer, France) for our weekly discussions. I am conscious that without his advices, peer expertise and his meticulous sense this work would not have reached this level of quality. In addition, a great thank to F. Maussang (Telecom Bretagne, France) for having accepted to be my advisor and for his enthusiasm and his encouragement he gave throughout these years. I have particularly appreciated his trust in my abilities.

As the PhD work has been conducted under a "Cifre" contract, I would like to thank the industrial partners. I express my thanks to O. A. Almskår (Kongsberg Maritime, Norway) for being my personal contact with Kongsberg Maritime and also for his real kindness in our exchanges and his reactivity, and also to P. Palud (Simrad Spain, France) on the side of Simrad Spain.

I would like to thank Kongsberg Maritime (Norway) via acknowledging S. Tetlie and B. Horvei for the PhD funding. I am also grateful to the multibeam R&D team for entrusting me to this research subject. I particularly thank R. Eckhoff and O.A. Almskår for the time they took to collect data aboard M/K Simrad Echo with the different signal shapes I proposed (several series of measurements). These data have majorly contributed to enhance the quality of this PhD work and reinforce its conclusions.

I express also a thank to Ch. Sintes (Telecom Bretagne, France) for introducing me to Kongsberg Maritime and for his advices during the first year of this work.

I also add a special acknowledgement to my colleagues and friends from Telecom Bretagne and Ifremer. I will particularly miss the warm atmosphere of the morning coffee break at Ifremer, as well as friendly atmosphere created by PhD students, post doc and training students at Telecom Bretagne. I have a special thought to the IEEE student branch and to the 'bureau des doctorants' members of Telecom Bretagne, may their activities continue without me.

I do not forget J. Beaudoin (UNH, USA) for his permission for the use of some images illustrating the arguments in sections 1.6 and 2.2.3 taken from his reports [Bea, 2012, Bea, 2013].

And at last but not least, I would like to thank my dear friends and my family: my parents, my sisters, their spouses and my little nephew for providing me with their support and their affection.

Contents

List of Figures

Introduction - Context

The use of acoustical waves (which have good propagation properties in underwater medium compared to electromagnetic waves) as a mean of subsea exploration has been introduced during the First World War in order to detect and combat submarine attacks. Thus, since the beginning of the 20th century, sonar systems using acoustical waves have appeared as a priviliged tool for ocean seafloor exploration. The first applications has been seafloor echo-sounding in order to complete nautical charts to ensure navigation safety. But bathymetry (measurement of seafloor depth) and imaging are important issues for several other applications in various fields: environmental sciences, economic exploitation, military strategy... The needs linked to offshore oil exploration and exploitation, as well as in mine warfare, caused in the 70's a really breakthrough, boosting the development of seafloor sonar mapping systems. Bathymetric multibeam echo sounders are today's favorite systems for suchapplications since they allow to explore and map large areas in a short time. In addition to seafloor mapping, the data from such systems also make it possible the localisation, imaging and measurement of wrecks, bubble plumes... and the monitoring of industrial installations (such as pipelines) and geological/geophysical sea-bottom evolution.

The main cause of measurement limitation for bathymetric multibeam echo sounders is the ambient noise which can degrade the seafloor echoes when it is needed to explore deeper seafloor or reach wider swath. To overcome this and increase the achievable swath widths while keeping an accurate resolution, modern multibeam echosounders make use of modulated signals providing a gain in processing (pulse compression, thanks to matched filter). Modulation allows to break the link between the pulse bandwidth and its duration: the bandwidth inverse gives the equivalent pulse duration after pulse compression, which characterises the new range resolution. It is thus possible to increase the transmitted energy thanks to the pulse duration without damaging the range resolution. The increase of transmitted energy is found back in the received backscattered signal. Moreover, this energy is compressed in a shorter pulse and the resulting signal to noise ratio is improved.

However, it seems that the various systems using this principle cannot meet the expected improvements of performances [Bea, 2012, Bea, 2013, Hug, 2010] that are normally linked to it, and indeed met in other realms of radar or sonar. This observation has been made on systems from different constructors (Reson Seabat 7150 as well as Kongsberg EM 122, 302 and 710) (see more details in section 1.6). The question is why the bathymetry measured by MBES using modulated signal are observed noisier whereas the use of modulated signal should (and is used in order to) improve the signal to noise ratio. The aim of my PhD is to explain this observation which looks paradoxical.

A first interpretation is related to the presence of Doppler effect impacting the quality of received signals and hence degrading the result of matched filtering. Indeed because of the

motion of the array platform (fixed on the ship hull) caused by the ship motion (due to roll, heave, pitch, yaw, sway, surge), the received signal is misshapened and the matched filter is unadapted. An important issue was to better understand the effect of Doppler upon the FM signal processing considered from the bathymetry accuracy point of view; to extract from these results useful orders of magnitude; to possibly identify other causes of bathymetry performance losses, and finally to propose strategies of improvements (either linked to processing or to the design of new signals).

This manuscript is divided into three main chapters.

The first chapter entitled 'state of the Art' aims at initiating the reader to the different basic notions necessary to better understand the fundamentals of this PhD work such as the multibeam echo sounder system principles and its associated signal processing to process the bathymetric measurement, or pulse compression concept and the different kinds of modulation.

The second chapter focuses on the causes of bathymetric degradation (considering the signal approach), and aims at explaining why the degradation observed when using modulated signals. This chapter is divided into three parts. The first one could stand for any multibeam echo sounder systems. It builds a model of bathymetric noise level prediction as a function of signal pulse shape. Parts 2.2 and 2.3 deal with specific causes of degradations. The second part of this chapter ((2.2) explores the first assumption of bathymetry quality loss caused by Doppler effect. The degradation might be due to the Doppler effect, since as said previously, it could affect more FM signals than CW (because of the unadatpted matched filtering). Bathymetric damage caused by Doppler effect has been studied from two aspects: measurement bias and statistics change (using theoretical and simulation approaches). Doppler effect is finally concluded, at the end of this part, as an unsatisfying explanation of the observed degradation. However, the simulations conducted to support the argumentation of this part have shown that the use of modulated signals damages the quality of the bathymetric echo signal. The last part of the second chapter (2.3) thus focuses on another explanation, based on the intrinsic signal noise (baseline decorrelation). Indeed since the signal to noise ratio is theoretically improved by matched filtering, and the interferometric signal is observed noisier, it can be assumed that degradation when using FM signals is effectively caused by some kind of intrinsic-signal noise. Thus, section 2.3 focuses on the impact of intrinsic noise which has been introduced in the first section of the same chapter. It will be seen that the presence of sidelobes in the pulse compression shape (when using modulated signal) lengthens the instantaneous footprint, decorrelating the interferometric signals used for the detection. This observation will be confirmed by three approaches: derivations, simulations and field data tests.

The last chapter 3 exposes improvement solution to reduce the impact of sidelobe. Three main approaches are considered. The first one is at transmission by using a smoother envelope. Smoothing the envelope reduces the sidelobe level and thus the decorrelation from baseline decorrelation. The problem is this method also reduces the transmitted energy and thus the benefit of using modulated signal concerning relative additive noise level reduction. The second idea is thus to keep a transmitted signal with a maximum energy and work at reception proposing matched filtering allowing to reduce sidelobes. This method provides sidelobe reduction but also lengthens the main lobe of the compressed pulse (introducing also coherence loss via baseline decorrela tion). Depending on interferometer configuration, this technique is more or less relevant. The third idea is to keep the transmitted energy at its maximum (i.e transmitted in a rectangular pulse) but to use another frequency modulation function

(non linear) providing low sidelobe levels after pulse compression. This last method seems promising, but has not been tested in real field. At the end of chapter 3, the three proposals are compared.

Chapter 1

State of the Art

Many types of acoustical systems are used to investigate the sea bottoms (single beam sounder, multibeam echosounder, side scan sonar, synthetic aperture sonar...). It has been chosen not to extend the discussion to these different systems and rather go directly into the topic under considerations. Only multibeam echo sounder systems (MBES) are described here. It is the same for the rest of this dissertation. The presented developments are focused on the problematic: understanding why modulated signals do not meet the expected bathymetric-quality improvement, finding general solutions and finally improving MBES bathymetry measurement quality. Of course, some of the presented phenomena could be transposed to other systems (notably interferometric ones), which could fall under the interest of the reader.

The aim of this first chapter is thus not to provide the readers with a wide collection of information on sonar system history or principles. Rather, it presents useful information to them in order about the different key notions approached along this PhD study:

- Bathymetric multibeam echosounder systems;
- Matched filter and pulse compression;
- Doppler effect;
- Modulated signals.
- External bathymetric degradation causes

1.1 General introduction on MBES

1.1.1 Principles

MBES systems are constituted by two array antennas (a transmitting and a receiving one). The arrays are large compared to the wave length, so that their directivity patterns (of transmission and reception) are narrow.

The principle of Bathymetric MBES is as follows:

- The sounder system is mounted on a ship hull or an underwater vehicule. The transmitting array sends a wave (pulsed signal) toward the bottom. The transmitting array long side is on the along direction. Thus, the transmitting pattern is narrow in the

along-ship direction. The illuminated footprint on the seafloor is thus a narrow stripe in the across-ship direction;

- The transmitted signal along its propagation scans the seafloor and is backscattered toward the receiving array;
- The reception is made by a fan of beams whose (conversely to the transmission) pattern is narrow in the across-ship direction (the receiving array being longer in the across direction). For a given beam the contributed signal is thus backscatter from the intersection of transmitting and receiving beam footprints (Figure 1.1.1). The fan of beams is created by beamforming (the process is exposed in the following section 1.1.2) and by steering the receiving beams at different angles.

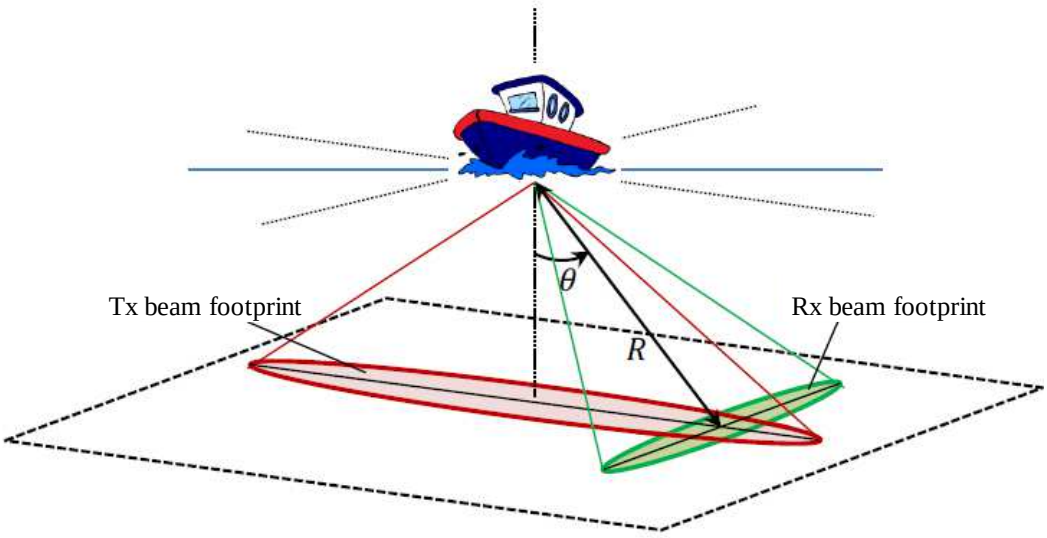

Figure 1.1.1: MBES Principle

Bathymetry consists in estimating the couple (θ, R) from the echo signal using the configuration presented in Figure 1.1.1 where R is estimated from the echo delay τ. The couple is unique. Considering that the sound speed c in the water is constant, the delay gives the lateral range by using the equation (1.1.1).

$$\tau = \frac{2R}{c} \tag{1.1.1}$$

The measurement is made for one ping in the plane defined by the across-ship axis and depth axis, the transmitted beam being considered narrow enough in the along ship direction to validate this hypothesis. The couple (θ,R) can be transformed into (x, z)Cartesian coordinates along depth and across-ship axis; so that $(x, z) = (R\sin\theta, R\cos\theta)$, on the ship referential. The y-axis (along ship axis) is scanned while the ship moves forward. A motion compensation (see section 1.5.1) using the attitude data recorded by the motion reference unit (gyroscopes and accelerometers) is necessary in order to express correctly the coordinates on the ship referential. The coordinates after motion compensation can then be replaced in a global referential such as in example WGS84, by using a GNSS positioning.

1.1.1.1 Transmission sectors

Many current systems use several sectors in transmission [Kon, EM122, Kon, EM302, Kon, EM710]. The transmission is made successively in different angular sectors (in the plane of measurement (x and z axis)). Figure 1.1.2 illustrates this configuration considering the across ship section as an example with three transmission sectors (case of $e.g$ EM710). The sectors are built by beamforming (process described in section 1.1.2) of the transmitting array in the across ship plane (rotation around the along ship axis).

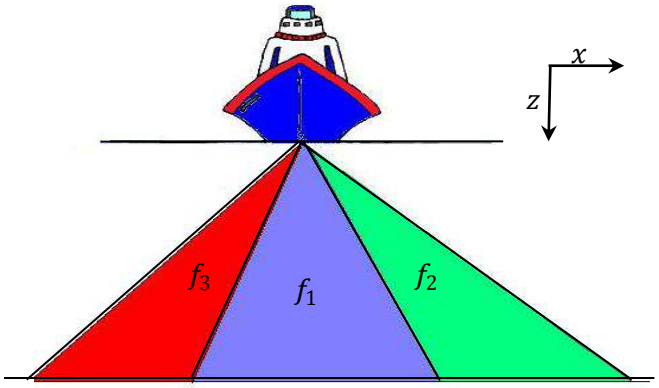

Figure 1.1.2: Transmission sectors (example of 3 sectors)

The interest of using several transmission sectors is multi-fold. The carrier frequency f_i is associated with its transmitting sector i . This allows for a considered angular area to reject after filtering the frequencies from the contribution of the other sectors. It makes it possible to reject the strong specular echo from the side sectors. In addition, since the angular width is reduced, the antenna can concentrate the transmitted energy in a spatially reduced area, and the signal power is increased improving the final received signal to noise ratio. In addition, it maintains the angular wave reception power as constant on the whole swath reducing the transmission pattern shape influence. Even, if necessary, it also makes it possible to increase the transmitted power in side sector since ambient noise is relatively more important in these beams with respect to the backscattered signal which is really attenuated by propagation. Furthermore, for the same reason, the presence of sectors allows the introduction of modulated signal in side sectors. Indeed modulated signals (section 1.4) are used to this purpose: reducing to the relative additive noise level thanks to matched filtering (section 1.2).

The carrier frequencies (f_1, f_2, f_3) are little different from one sector to the others, in order to keep the optimum transducer frequency domain and also similar beam characteristics (and thus keep close bathymetric measurement statistics). Let us point out that the available frequency band between sector carrier is a limitation factor for modulated signal bandwidths (to avoid inter sector crosstalk).

1.1.2 Beamforming

Beamforming is a signal processing method designed to spatially explore in angles an observed space with a multi-sensors array. This processing is used in every multibeam echo sounder.

The aim of this part is to shortly describe the principles of this method. The objective of beamforming is to steer the antenna array and so explore space in angles. The resulting signal observed on the whole array is maximum if the source (backscattering target) is located along the observed direction (due to constructive interferences).

1.1.2.1 Array steering

Actually, a receiving array is desired to be steered in order to investigate in one particular direction θ. Physically, steering the antenna with an angle θ, considering the target in far field, is equivalent to add up delayed version of the stave signals (Figure 1.1.3). The delay observed in each sensor (stave) n of the array is proportional to its abscissa along the array nl and is such as: [Lur, 2010a, Puj, 2007]

$$\delta t_{n,\theta} = \frac{nl}{c}\sin\theta \tag{1.1.2}$$

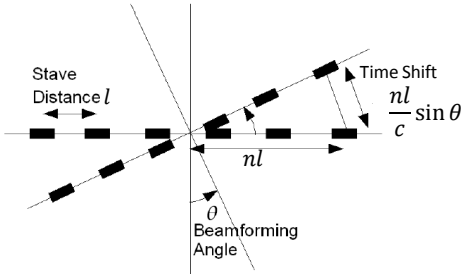

Figure 1.1.3: Array steering

For each sensor n, the received signal $S_{n,\theta}(t)$ on a steered array (steering angle θ) is given as a time-shifted version (by $\delta t_{n,\theta}$) of the received signal $S_n(t)$.

$$S_{n,\theta}(t) = S_n(t - \delta t_{n,\theta}) = S_n(t - \frac{nl}{c}\sin\theta) \tag{1.1.3}$$

Considering that the number of sensors in the array is N and the stave spacing is l, the resulting signal, when steering the antenna, becomes:

$$S = \sum_{n=-(N-1)/2}^{(N-1)/2} S_n\left(t - n\frac{l}{c}\sin\theta\right) \tag{1.1.4}$$

The practical problem is how to shift accurately in time a signal which have been sampled.

1.1.2.2 Phase beamforming

When considering a non-modulated signal (CW) (or FM-pulse-compressed signal) on the carrier frequency f_c, the time delay can be approximated by a phase shift. The resulting signal is:

$$S = \sum_{n=(1-N)/2}^{(N-1)/2} S_n(t)e^{-2\pi j.f_c n\frac{l}{c}\sin\theta} \tag{1.1.5}$$

With narrow-band signals, multiplying the measured signal from each sensor by the associated phase shift is the standard way to apply the steering of the antenna. But approximating the time delay by a phase shift becomes less and less accurate as the bandwidth of the signal increases.

1.1.2.3 Time beamforming

If the time delay to apply on the sensor is higher than the sampling period, another solution is to take the closest data sample arriving to the sensor and apply the rest of the delay by multiplying by the associate phase shift. This method gives a resulting signal closer to the one which would have been received by really steering the antenna array. And it is a better solution with relative large frequency bandwidths. So processing this solution amounts to (Figure 1.1.4):

- first, calculating the delay $\delta t_{n,\theta}$ on each sensor for each steering angle and defining it associated closest sample as $\lfloor \delta t_{n,\theta}/T_s \rfloor$ (where T_s is the sample rate and $\lfloor . \rfloor$ round value);
- defining the residual phase term to be multiplied on.

The expression at instant kT_s (k^{th} sample) is:

$$S_{n,\theta}(kT_s) = S_n\left(kTs - E\left\lfloor \delta t_{n,\theta}/T_s \right\rfloor T_s\right) e^{-2\pi j.f_c\left[n\frac{l}{c}\sin\theta - \left\lfloor \delta t_{n,\theta}/T_s \right\rfloor T_s\right]} \tag{1.1.6}$$

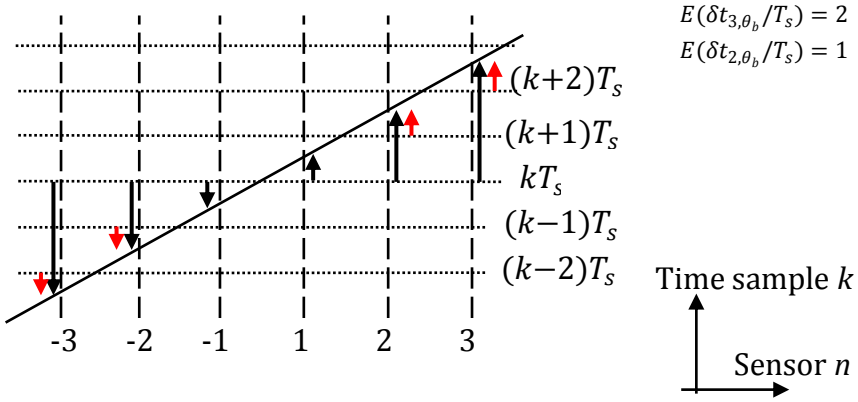

Figure 1.1.4: Time beamforming

Moreover, there is another possibility, nevertheless more computing-resources consuming. It consists in estimating the value of the delayed data for one sensor using the previous and next closest samples by a linear interpolation. [Puj, 2007]

The sounders considered in this PhD work (such as EM-210 and EM-710) actually apply the time beamforming method: picking the closest sample and correcting with the phase associated with the rest of the time delay.

1.1.2.4 Interferometry

The principle of interferometry is based on the measurement of the path difference between two sensors, extracted from the measurement of the phase differences of a coherent wave. It is used in MBES under the name of 'phase' when the seafloor detection is made in 'phase detection' of the seafloor (see next paragraph 1.1.3.2).

Optical principles Interferometers use two coherent sources (with a long coherence duration). In the 19th century, they were designed in order to prove the wave nature of light in opposition to the corpuscular theory introduced by Newton in the beginning of the 18th century [You, 1804]. The principle is to create fringes pattern of interference on a screen by using the constructive or destructive superposition of two waves.

The electromagnetic field of the two sources at a given point of the space is a monochromatic wave (only one frequency f_c) and thus given as $E_i = A_i \exp(\omega t + \phi_i)$ $(i = 1, 2)$ where ϕ_i is a phase term depending on the position (wave propagation delay) and $\omega = 2\pi f_c$. The two sources are actually created from a same source separated into two waves with different propagation paths. The intensity at this point given by the superposition of the waves is given by:

$$I = A_1^2 + A_2^2 + A_1 A_2 \cos(\phi_1 - \phi_2) \tag{1.1.7}$$

The resulting intensity depends on the phase difference between the two waves, *i.e.* to the propagation path difference between the two waves.

Sonar application By analogy with optics, some sonars use interferometry, thus the phase difference of the wave received by two sensors, in order to estimate the path difference and thus localise the source (here backscattering target, thus the seafloor).

Most often in MBES, the receiving array is divided into two sub arrays whose associated signals (summation on the stave signals) are S_a and S_b. The division is characterized by the parameter b which is called baseline and designs the length and the spacing of the sub arrays. Baseline b is given by the ratio between spacing of the subarray center a and the whole receiving array length L. The length of the subarrays is given by $(1 - b)$ of the whole array length. Commonly, b takes the value $1/2$ or $1/3$. f the backscattering wave is considered as a monochromatic wave, interferometry can be used.

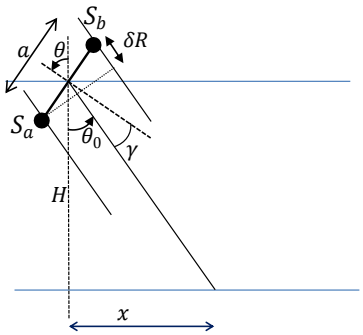

Figure 1.1.5: Interferometry configuration geometry

The phase difference between the two array centres is given by (Figure 1.1.5):

$$\psi = 2\pi \frac{f_c}{c} \delta R = 2\pi \frac{f_c}{c} a \sin(\theta - \theta_0) = 2\pi \frac{f_c}{c} a \sin \gamma \tag{1.1.8}$$

This phase difference is estimated from the measurement of the phase of $S_a S_b^*(\Delta\phi = \arg\{S_a S_b^*\})$. The estimation is made with an ambiguity modulo 2π.

1.1.3 Bathymetry detection

The bathymetry measurement consists in estimating parameters θ and τ corresponding to a point on the seafloor surface. There are two possible approaches:

- Define, for a given instant τ, the associated θ corresponding to the seafloor localisation;
- Or conversely, search the associated time delay τ for a given angle θ.

In the nowadays MBES systems, the beam angle θ is considered well defined and the second approach (consisting in searching the delay associated with θ) is preferably used. Then the search of the detection instant could be made by two ways:

- estimation on the beam signal amplitude
- estimation on the interferometric phase (zero crossing of the phase ramp)

1.1.3.1 Amplitude detection

he arrival time is estimated as the beam time-envelope COG (centre of gravity) of the signal received in a beam steered at angle θ. Unfortunately, as the beam angle θ increases, the time spreading of the signal envelope increases. In addition, the level of the expected temporal beam envelope decreases as a function beam angle (see Figure 1.1.6and additive noise becomes relatively high. The increasing of the envelope and relative additive noise directly impact on the precision of the measurement of the COG. Hence this arrival time detection estimator is poorly efficient for highly-steered beams.

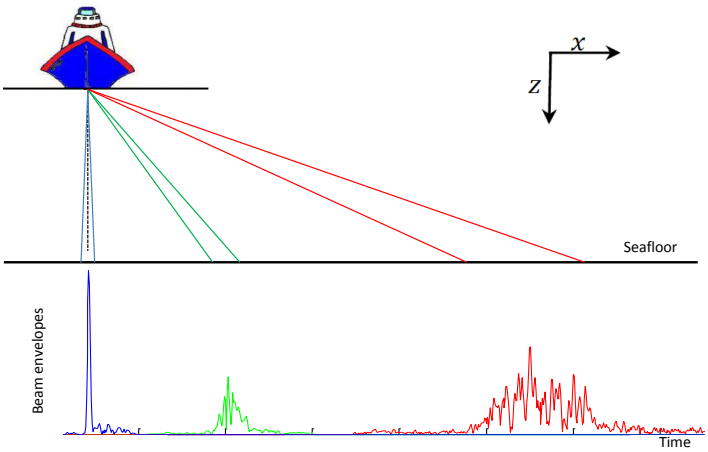

Figure 1.1.6: Amplitude detection - envelope spread as a function of beam angle

1.1.3.2 Phase detection

The whole receiving array is split into two sub arrays S_a and S_b. Phase detection is made by using the interferometric signal phase difference (using $\arg\{S_a S_b^*\}$). Indeed the phase difference directly associated with the propagation path difference between the sub-array signals S_a and S_b is estimated from the phase of $S_a S_b^*$(where * denotes the conjugate operator). It can be noticed that the seafloor point situated in the middle of the beam footprint has a null path difference between the two sub-arrays. The resulting phase difference is null.

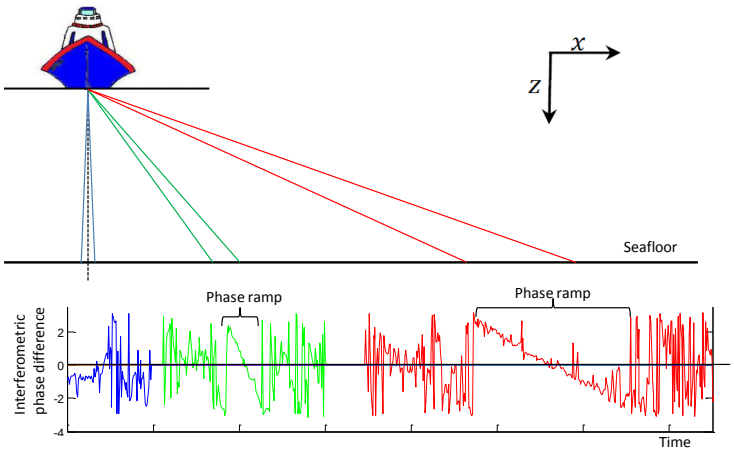

Figure 1.1.7: Phase detection- phase ramp zeros crossing

By considering the contributions of the point scatterers (scanned along time by the signal), it can been seen that the interferometric phase forms a ramp as a function of time which crosses zero at the delay instant corresponding to the seafloor point situated at the exact angular beam direction (see Figure 1.1.7). The phase ramp can be eventually extended modulo 2π. This could give zero-crossing ambiguities. However, most often in MBES, the beam is narrow enough to consider that the zero-crossing detection can be done without ambiguity. Thus for a given beam, the time arrival detection is made by the zero crossing of the phase ramp. At the vertical beam almost every point of the footprint will respond simultaneously making phase measurement really noisy. However, when the beam steering angle increases, the phase ramp is longer and with a better quality, and this detection method becomes more efficient. Finally, phase detection is a really complementary detection method compared with amplitude detection.

By analogy, it is possible to use the phase ramp outside its zero-crossing, and find its crossing instant to an other phase value. The resulting soundings (time detection) are then not associated with the beam angle but toward another axis dependent on the setting phase values. This method makes it possible to extract multiple soundings from a phase ramp [Ron, 1999].

1.2 Matched filtering

Matched filtering is applied in radar or sonar systems when using modulated signal in MBES (different types of modulation will be exposed in part 2.2.1.2). Here, the two-fold interest

of the matched filter is reminded. Firstly, this linear filter allows to maximize the signal to noise ratio (SNR). Moreover used with modulated signal, the technique allows to increase the transmitted energy thanks to a pulse-duration lengthening, without damaging the localisation precision. This is possible by using the pulse compression process naturally induced by this filtering.

1.2.1 Maximizing the signal to noise ratio

Most of the time, in active remote sensing detection, only a small part of the transmitted energy is backscattered by the target towards the receiver. Thus, at last, the received signal is a really low amplitude completely surrounded in the ambient noise. This is all the more critical in sonar application since the propagation of acoustic waves in water induces a strong attenuation. It is thus natural to search a way of filtering optimally the signal in order to make the detection easier. Here, it is desired to find a linear filter which maximizes the signal/noise ratio.

Figure 1.2.1: Optimal Filter scheme

Consider the situation described in Figure 1.2.1, tthe received signal is composed of two terms: a useful signal which is here considered as the transmitted signal delayed by τ, $s(t-\tau)$ and an additive noise term $n(t)$. The noise is white and its power spectral density is N_0. After filtering, the output signal is the summation of two terms corresponding respectively to the useful signal and to noise. Let $g(t)$ be the useful signal filtered by the optimal filter and $n_f(t)$ the noise term.

$$\begin{aligned} g(t) &= (s * \delta_\tau * h)(t) = \int_{-\infty}^{+\infty} s(t-u-\tau)h(u)du \\ n_f(t) &= (n * h)(t) = \int_{-\infty}^{+\infty} n(t-u)h(u)du \end{aligned} \tag{1.2.1}$$

The instantaneous signal to noise ratio (SNR) has the following expression:

$$(S/N)_{out} = |g(t)|^2/(E[|n_f(t)|^2]) = \frac{\left|\int_{-\infty}^{+\infty} s(t-u-\tau)h(u)du\right|^2}{N_0 \int_{-\infty}^{+\infty} |h(u)|^2 \, du} \tag{1.2.2}$$

According to the Cauchy-Schwarz inequality:

$$\begin{aligned} \left|\int_{-\infty}^{+\infty} s(t-u-\tau)h(u)du\right|^2 &\leq \int_{-\infty}^{+\infty} |s(t-u-\tau)|^2 du \int_{-\infty}^{+\infty} |h(u)|^2 du \\ &\leq E_0 . \int_{-\infty}^{+\infty} |h(u)|^2 du \end{aligned} \tag{1.2.3}$$

So, the SNR has a boundary. According the Cauchy-Schwarz relation, this boundary is reached when both signals are colinear (one proportional to the other conjugate), so that finally to optimize the signal to noise ratio the impulse response of the filter should be:

$$h(u) = k.\overline{s(t-u-\tau)} \tag{1.2.4}$$

Where $\overline{X}$ denotes the conjugate of X. To maximize the SNR ratio at $t = \tau$, the final expression of the optimal filter is:

$$h(t) = k.\overline{s(-t)} \tag{1.2.5}$$

Then by using the optimal filter also named 'matched filter' (since the filter matches the transmitted signal as a reverse conjugate copy of it), the output SNR becomes:

$$(S/N)_{out} = E_0/N_0 \tag{1.2.6}$$

While the input signal to noise was:

$$(S/N)_{in} = \frac{\max|s(t)|^2}{N_0 B} \tag{1.2.7}$$

The matched filter is thus a linear filter allowing to maximize the output signal to noise ratio. This is really convenient in active systems since the received backscattered signal shape is known and expected as the delayed transmitted signal.

1.2.2 Pulse Compression using Modulated Signal

here is another interest in using the matched filter: the pulse compression. Indeed, since the backscattered signal power level is low, it is intended to find a way to increase the backscattered intensity, especially when studying deep sea bottom surfaces or wider side swath (which means high propagation attenuation). One solution is to light the scene more by transmitting more energy in the medium. The whole transmitted energy varies as A^2T (case of rectangular envelope) where A and T represent respectively the amplitude of the transmitted signal, and its duration. However, the amplitude A is limited by the characteristics of the sounder device and the power electronics technology. The duration T can be relatively longer. However, by increasing T, the problem is this leads to a loss of depth detection accuracy. Indeed, the range resolution is $c.T/2$.

The other solution is then to use a modulated signal combined with the matched filter and use the resulting pulse compression, theoretically allowing to increase T as much as desired, without to loose in resolution. Indeed the final pulse-compressed duration (signal after matched filtering) is approximately equal to the inverse of the signal bandwidth. Modulation makes it possible to include a variability in the signal which makes it possible to increase the factor $B.T$ of a signal (equal to 1 in case of non modulated signal). Different kinds of modulations will be presented in section 1.4.

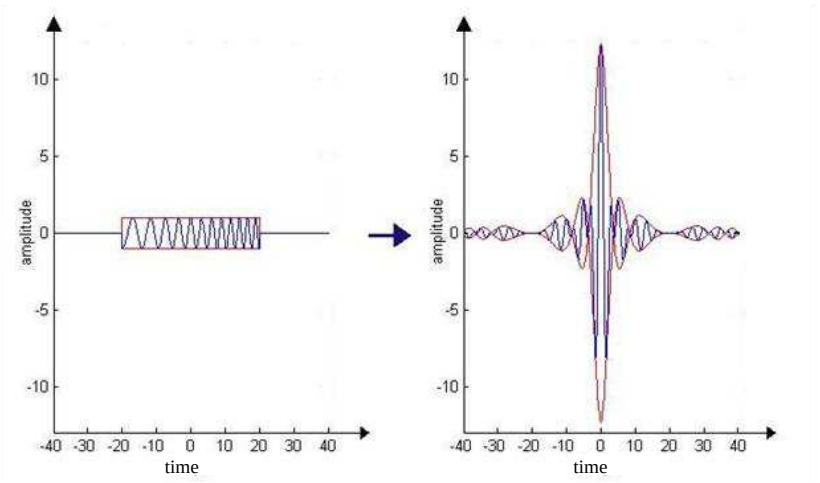

Figure 1.2.2: Chirp pulse compression

To illustrate the phenomenon described above let us take an example. A linear chirp (linear frequency modulated signal) is a signal whose instantaneous frequency is varying linearly with time. Its expression is given as:

$$s(t) = e^{2\pi i(f_c t + \frac{B}{2T}t^2)} \qquad \text{for} - T/2 \leq t \leq T/2, \ =0 \text{ otherwise} \tag{1.2.8}$$

Here the chirp is considered in a rectangular envelope whose duration is T. During its whole duration, its instantaneous frequency sweeps the bandwidth B. Thus its swept-bandwidth is B.

The pulse-compressed shape (1.2.9)(after matched filter) of such a signal is given in [Hei, 2004] (see calculation in Appendix D).

$$w(t) = \int_{-\infty}^{+\infty} s(u-\tau)\overline{s(u-t)}du = e^{2\pi i f_c t} T\Lambda(\frac{t-\tau}{T})\text{sinc}\left(2\pi\frac{B}{2}(t-\tau)\Lambda(\frac{t-\tau}{T})\right) \tag{1.2.9}$$

where $\Lambda(t)$ denotes the triangle function whose maximum value is 1 at 0 and values are null if $t \leq -1$ or $t \geq 1$.

It can be seen from (1.2.9) with the sinc part (assuming $BT \gg 1$, if $t < 1/B$, $\Lambda(\frac{t-\tau}{T}) \approx 1$ and by considering the width of $\text{sinc}\,(\pi B(t-\tau))$) that the envelope of the pulse compressed signal $w(t)$ has a duration equivalent to the inverse of B. Thus the equivalent signal duration is no longer T but $1/B$ which is really shorter. For MBES, typical pulse compressing factor BT is 10. Pulse compression is illustrated in Figure 1.2.2.

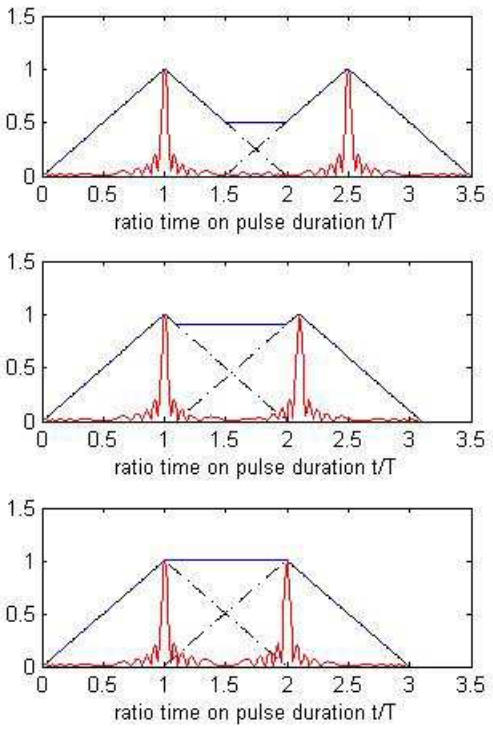

Figure 1.2.3: Resolution: capability to separate two successive echoes (after matched filtering: blue: CW, red: FM) interest of modulation using pulse compression

It means that instead of being dispatched on the whole signal with the duration T, the energy of the signal after filtering is mainly concentrated around τ (expected detection instant) in the time width $1/B$. A factor TB is actually gained on the SNR at the instant τ. In addition, since the compressed signal is shorter, the system gains also in resolution. Figure 1.2.3 shows this improvement in resolution by using modulated signal (here linear frequency modulation) with matched filtering (using pulse compression) compared to a non-modulated pulse (CW) with the same duration at transmission.

The pulse compression of a modulated signal is defined in the ambiguity function (which will be introduced later in paragraph 1.3.2 and specified in 1.4) in setting the Doppler shift to 0.

1.3 Doppler effect

The Doppler effect was initially suspected to be the first factor of bathymetric degradation by using frequency modulated signal with pulse compression on MBES (received signal does not match the matched filtering). The phenomenon and its impact on bathymetric measurement will be widely studied in Chapter 2.2. This part goes through the basics of Doppler effect phenomenon.

1.3.1 Introduction

The arrays mounted on the ship's hull (Figure 1.3.1) are submitted to the ship's motion (heave, roll, pitch, yaw). Thus, since the transmitter and the receiver are moving, the received signal is distorted by the Doppler effect.

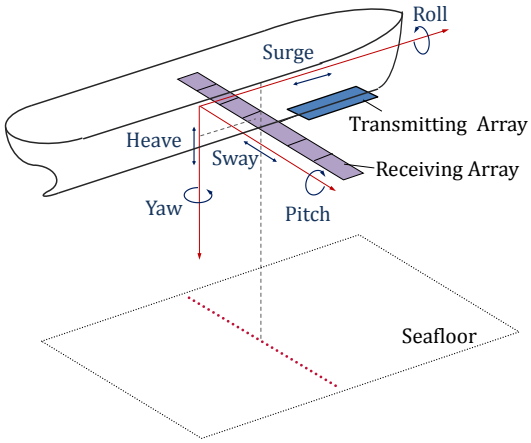

Figure 1.3.1: Array motions description

In general, the Doppler effect is a phenomenon affecting a signal when the transmitter, receiver or target (in case of backscattered signal) are in motion. In the case of bathymetric MBES, the target is motionless, and only transmitter and receiver move. To define the resulting Doppler effect on the received signal, here, let us present an infinitesimal development linking the signal received at a given instant t_r as a function of the signal transmitted at t_e. This development will be divided considering the two parts of the propagation:

- from the transmitter to the target (seafloor)
- from the target to the receiver

Let the signal obtained at the instant t_r from the receiver be assumed as actually being the signal reflected from the bottom (or target) at the instant t_b, this last one being the transmitted signal at the instant t_e .

To be simple, what is caught at t_r was what is sent at t_e. There is a relation between these different moments t_r, t_b, t_e due to the propagation. Knowing this relation between t_r and t_e, like $t_e = f(t_r)$, will make it possible to express the received signal at t_r and understand the deformation due to the Doppler effect (or array motions).

Let us consider the propagation from the transmitter to the bottom (Figure 1.3.2)

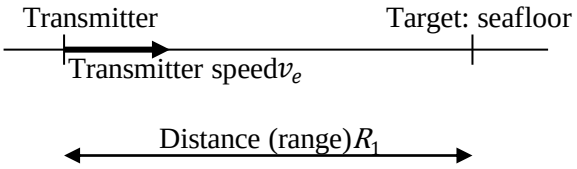

Figure 1.3.2: Propagation from the transmitter to the target

The link between the receiving instant at the bottom and the transmitting instant given by propagation delay is expressed in Table 1.2.

Transmitting time	Effective covered distance	Receiving time at the target
t_e	R_1	$t_b = R_1/c + t_e$
$t_e + \delta t_e$	$R_1 - v_e(t_e)\delta t_e$	$t_b + \delta t_b = (R_1 - v_e(t_e)\delta t_e)/c + t_e + \delta t_e$

Table 1.1: Propagation from the transmitter to the target

$$\delta t_b = -\frac{v_e(t_e)}{c}\delta t_e + \delta t_e = (1 - \frac{v_e(t_e)}{c})\delta t_e \tag{1.3.1}$$

Consider now the propagation from the bottom to the receiver (Figure 1.3.3)

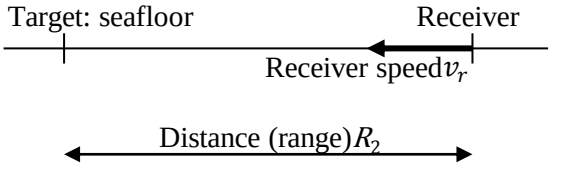

Figure 1.3.3: Transmission from the target to the receiver

Transmitting time at the target	Effective covered distance	Receiving time
t_b	R_2	$t_r = R_2/c + t_b$
$t_b + \delta t_b$	$R_2 - v_r(t_r)\delta t_r$	$t_r + \delta t_r = (R_2 - v_r(t_r)\delta t_r)/c + t_b + \delta t_b$

Table 1.2: Propagation from the transmitter to the target

The link between the receiving instant and the transmitting instant (at seafloor bottom) (see Table 1.2) is:

$$\delta t_r = -\frac{v_r(t_r)}{c}\delta t_r + \delta t_b = \frac{1}{1+\frac{v_r(t_r)}{c}}\delta t_b \tag{1.3.2}$$

Combining equations (1.3.1)and (1.3.2) leads to the differential equation:

$$\delta t_r \left(1+\frac{v_r(t_r)}{c}\right) = \delta t_e \left(1-\frac{v_e(t_e)}{c}\right) \tag{1.3.3}$$

Case of Constant Speeds

Assuming v_e and v_r as constant makes it easy to solve the previous differential equation. It leads to

$$t_e = \eta(t_r - \tau) \quad \text{with} \quad \eta = \frac{c+v_r}{c-v_e}, \tau = R/c \tag{1.3.4}$$

R being the initial spacing between the transmitter and the receiver. The received signal at instant t_r is the transmitted signal at instant t_e, so that, in the case of constant speeds, it is found out as:

$$S_r(t_r) = s(t_e) = s(f(t_r)) = s(\eta(t_r - \tau)) \tag{1.3.5}$$

In case of constant speeds, the relation between the received signal and the transmitted shape is a time compression or dilation by the factor η. Indeed, the received signal sampled with a sample rate δt looks like the transmitted pulse delayed by τ and sampled at $\eta\delta t$. Since, the Doppler effect does not change the signal energy, the received signal is:

$$S_r(t) = \frac{1}{\sqrt{\eta}} s(\eta(t-\tau)) \tag{1.3.6}$$

Taking the Fourier transform $\sqrt{k}S(\nu/k)$ (ν being the frequency variable), the frequency shift commonly associated with the Doppler Effect is retrieved. This shift, under the condition that $BT(\eta-1) \ll 1$ [Coo, 1993], is often considered as not affecting the envelope shape of the signal. And the Doppler effect is approximated to be the transmitted pulse multiplied by the phase term corresponding to the frequency shift $(\eta-1)f_c$ where $\eta = \frac{c+v_e}{c-v_r} \approx 1 + \frac{v_e+v_r}{c}$.

$$S_r(t) = s(t-\tau)e^{2\pi i f_c(\eta-1)(t-\tau)} \tag{1.3.7}$$

Case of Varying Speeds as a function of time

Let the speeds be varying functions of time. The infinitesimal approach and the differential equation defined in (1.3.3) is still valid. Integrating the two parts of the differential equation leads to:

$$\int \left(1+\frac{v_r(t_r)}{c}\right) dt_r = \int \left(1-\frac{v_e(t_e)}{c}\right) dt_e \tag{1.3.8}$$

Let us introduce the varying distance from transmitter to target $d_e(t)$ and $d_r(t)$ the distance from target to receiver. By adapting the sign since speeds in the previous paragraph were counted as positive towards the direction of the target (positive speeds inducing distance diminution), $d_e(t)$ and $d_r(t)$ are respectively primitives of $-v_e(t)$ and $-v_r(t)$.

$$t_r - \frac{d_r(t_r)}{c} = t_e + \frac{d_e(t_e)}{c} + A \tag{1.3.9}$$

Finding the integration constant A applies a limit condition *i.e.* the link between the arrival instant τ with the transmitted instant 0 (τ is the propagation delay from the transmitter at instant 0 to the target then from the target to the receiver position at τ (instant associated with 0 at transmission)).

$$A = \tau - \left(\frac{d_r(\tau)}{c} + \frac{d_e(0)}{c}\right) = \tau - \tau = 0 \tag{1.3.10}$$

And finally,

$$t_r - \frac{d_r(t_r)}{c} = t_e + \frac{d_e(t_e)}{c} \tag{1.3.11}$$

Finally, the Doppler effect equation is the same as the propagation equation. It links the receiving instant to the transmitting instant by equalling the delay between transmission and reception with the propagation delay associated with the effective distance to cover.

1.3.2 Ambiguity function

In order to study the Doppler effect impact on the pulse compression of modulated signals, it is defined the "ambiguity function" as :

$$A(\tau, \eta) = \frac{\int_{-\infty}^{+\infty} s(\eta t)\overline{s(\tau - t)}dt}{\int_{-\infty}^{+\infty} |s(t)|^2 dt} \tag{1.3.12}$$

where η is the Doppler shift defined as in 1.3.4 and often approximated by $\eta = 1 + \frac{v_d}{c} = 1 + \frac{v_r + v_e}{c}$.

The ambiguity function [Bur, 1989] is the result of the matched filter output (convolution with the time reverse conjugate signal) of the Dopplerized signal (by the Doppler shift η). This output is often normalized by the pulse energy. It can be noticed that when $\eta = 1$, the ambiguity function gives the pulse compression of the pulse signal s. Defined like this, the ambiguity function in absolute value presents its maximum in $(0, 0)$ equals to 1.

If the Doppler shift is low (typically if $BT(\eta - 1) \ll 1$), it does not influence much the signal envelope. The Dopplerized signal is then just shifted in frequency.

$$s(kt) = e^{2\pi i f_d t} s(t) \tag{1.3.13}$$

Where f_d is the Doppler frequency shift equal to $(\eta - 1)f_c$ (f_c being the central frequency of the pulse $s(t)$). In such conditions, the ambiguity function becomes :

$$A(\tau, f_d) = \frac{\int_{-\infty}^{+\infty} e^{2\pi i f_d t} s(t)\overline{s(\tau - t)}dt}{\int_{-\infty}^{+\infty} |s(t)|^2 dt} \tag{1.3.14}$$

The ambiguity function is a useful tool to characterise the different kinds of modulation which are the object of the next paragraph 1.4.

In MBES, the array motion period is pretty low considering the transmitted pulse duration (roll, heave *etc* periods are about 10 s while transmitted signal duration is some milliseconds). This leads to consider the motion speed (Doppler shift η) as constant which simplifies the analysis.

1.4 Different kinds of modulations

The modulation aims at introducing a frequency variety in the signals in order to spread the signal bandwidth in the frequency domain. For CW classic pulse, the bandwidth B equals its duration inverse $B = 1/T$. Using modulation allows to separate the signal bandwidth from the signal duration so that $B \gg 1/T$. Combined with matched filtering, the bandwidth increase allows the pulse compression. Indeed, the signal (main lobe) is compressed into the duration $1/B$ rather than being spread over T. There are three kinds of modulations: amplitude (AM or ASK), phase (PSK), frequency (hopping FSK, continuous FM).

Sections 1.4.1 and 1.4.2 detail amplitude, phase and frequency modulations. The different kinds of modulations are characterised by their ambiguity function (1.3.14) (see section 2.2) which describes the pulse compression performance (matched filter output). The ambiguity function at zero Doppler shift is the expected pulse compression: it shows the range accuracy improvement (temporal main lobe width). In Radar application, it is also usual to reduce the response of the ambiguity function for non-null Doppler shift. The ideal Ambiguity function has a "thumbtack" shape. Of course with such conditions, the moving target with unknown speed can be undetected with the standard matched filter. But Doppler processing can be independently performed (thanks for example to moving target indicator or pulse Doppler processing [Ric, 2005, Lev, 1988]). Knowing the precise Doppler frequency and adapting accordingly the matched filter allows to range the target without ambiguity.

However, MBES do not use Doppler processing: such processing needs data from several pings [Ric, 2005]and the period of the platform motion is not constant at this time scale. Thus the ambiguity function needs to keep a certain stability to Doppler shift. Nevertheless, since it is not the target which moves but the platform, it is possible to estimate the array speed from external attitude sensor data and thus the associated Doppler shift for a given beam. Thus signals with low tolerance to Doppler shift now discorded in MBES could be still interesting. In addition, Radar processing processes the detection in the amplitude of the received backscattered signal, when MBES uses the interferometric phase for the detection for outer beam detection. Hence, the expectations considering wave shape can be slightly different, especially when using Radar/Sonar single target system or MBES since its target is extended (target not presenting spatially relative same speed).

1.4.1 Amplitude and Phase modulation

1.4.1.1 Continuous amplitude modulation

The modulation is given by a modulation shape $a(t)$ on a carrier frequency f_c.

$$s(t) = a(t)e^{2\pi i f_c t} \tag{1.4.1}$$

The variation on $a(t)$ gives the bandwidth occupation.

In practise, phase or frequency modulation is preferred to amplitude modulation, because the amplitude modulation reduces the power efficiency, and is more sensitive to noise.

1.4.1.2 Phase and amplitude coded modulation

The modulated signal takes the following mathematical expression:

$$s(t) = \sum_{n=1}^{N} C_n \mathbf{\Pi}(\frac{N}{T}t - n - \frac{1}{2}) e^{2\pi i f_c t} \tag{1.4.2}$$

Where f_c is the carrier frequency. Such a signal has a duration equalling T and changing modulation states every T/N instant (N state changes in a pulse). This type of modulation is using signal discontinuities to increase the bandwidth. The code C_n are complex numbers, and denotes the different states of the modulation. To keep a maximum of power and thus of transmitted energy, the different C_n modulus are set constant, equal to 1. The modulation expressed in (1.4.2) which can be considered as a quadratic amplitude modulation (QAM), is actually equivalent to a phase shift keying (PSK) modulation. Indeed since$|C_n| = 1$, it can be written C_n as equal to $e^{2\pi\Phi_n}$ with the ϕ_i constituting the phase states of the PSK modulation. In a two-state modulation, the C_n can take two values -1 and 1. The associated phase modulation is ϕ_i taking the values 0 and π. Considering the sea medium and backscattering characteristics, due to their impact on the phase discontinuities, the signal well supports only phase modulation with two states, maybe four (QPSK) but hardly modulation using more states (to preserve the coherence between received pulse and transmitted one, and not damage the pulse compression).

1.4.1.3 Phase modulation: 2 states

The sequence of C_n is chosen in order to process the pulse compression with the lowest sidelobe level possible. The width of the main lobe (ambiguity function cross-section on zero Doppler shift) is given as a function of the number N of transmitted signal state changes equalling T/N.

The Barker codes are often described in the radar literature [Ric, 2005, Coo, 1993, Lev, 1988]
.

Their advantage is that the cross-correlation of a Barker sequence equals N at the centre and 0 or 1 otherwise. It means that the sidelobe level of the pulse compression shape is lower than $1/N$. However there is a limited number of such sequences where the maximum number of state changes N is 13. Table 1.3 presents the different Barker sequences. In current MBES, the compression factor which equals the ratio between before and after pulse-compression durations (also product of the signal duration with its frequency-domain bandwidth) is commonly equal to 10. The interesting Barker sequences are the last three lines of Table 1.3.

N	C_n
2	-1 +1
3	+1 +1 -1
4	+1 +1 +1 -1
4	+1 +1 -1 +1
5	+1 +1 +1 -1 +1
7	+1 +1 +1 -1 -1 +1 -1
11	+1 +1 +1 -1 -1 -1 +1 -1 -1 +1 -1
13	+1 +1 +1 +1 +1 -1-1 +1 +1 -1 +1 -1 +1

Table 1.3: Barker sequence

Figure 1.4.1a presents the ambiguity function of the signal using the Barker sequence of length 11. (f_c= 73 kHz, T= 20 ms). It can be seen that the sidelobes level is low for no-Dopplerized signal matched filter output. However this characteristic disappears when the Doppler shift is not null. In addition, there is no time-frequency dependency as in frequency modulation (see paragraph 1.4.2.2). This is an advantage for single target detection since the target could be then detected without ambiguity in range and in Doppler (speed).

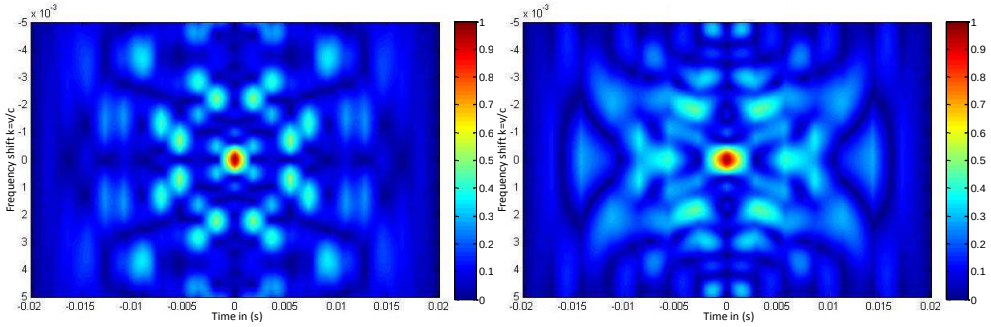

(a) Barker Code (b) Binary code

Figure 1.4.1: Ambiguity function for 2-state phase modulation

Another family of binary phase modulations is built around pseudo-random codes which can be generated using linear feedback shift registers. The length of such codes is necessarily $2^m - 1$ (m being an integer). Their interest is that they can give modulated signal with longer sequences than Barker (and thus improve the pulse compression factor $BT = N$). This family of modulation allows pulse compression with relatively low sidelobes (however higher than for Barker code) and with no time frequency dependency (no ambiguity). An example with N=7 is plotted in Figure 1.4.1b.

1.4.1.4 Phase modulation: 4 states

The main disadvantage of two states phase modulation is their sensitivity to Doppler shift. If the Doppler effect is not well estimated the target can be undetected. Polyphase modulation

breaks with this property, designing pulses with high response even in case of Doppler shift. Their design is most of the time made to fit a linear or hyperbolic frequency modulation. Many polyphase codes have been proposed [Jam, 2008, Yan, 2007]. Here, only Frank codes which is the most commonly described[Lev, 1988, Mit, 1985] is exposed. The Frank codes need to have a length of N as a square of an integer. ($N = M^2$) As previously the Time-Bandwidth factor is equal to N. It can be seen as a generation of M sequences of length M. The phase of the the qth element of the pth sequence is given by:

$$\phi_{p,q} = \frac{2\pi}{M}(p-1)(q-1) \tag{1.4.3}$$

$C_{n=4p+q} = \exp(j\phi_{p,q})$, By considering N=16 the phase coding matrix is given by:

$$\phi_{p,q} = \begin{matrix} 0 & 0 & 0 & 0 \\ 0 & \pi/2 & \pi & 3\pi/2 \\ 0 & \pi & 2\pi & 3\pi \\ 0 & 3\pi/2 & 3\pi & 9\pi/2 \end{matrix} \tag{1.4.4}$$

The ambiguity function of the Frank code modulation is close to the linear frequency modulation, presenting the similar linear ambiguity coupling between Doppler and time shifts (Figure 1.4.2). Like the linear frequency modulation presented in the next paragraph (paragraph 1.4.2) the ambiguity function is stable with Doppler shift.

The similarity comes from that the phase changes seem to follow (discretely) the phase function (as a function of time) of the linear frequency modulation. Frank code has lower performances in reducing the sidelobe level compared with Barker codes. In addition, they are more difficult to implement (increase of the number of modulation states).

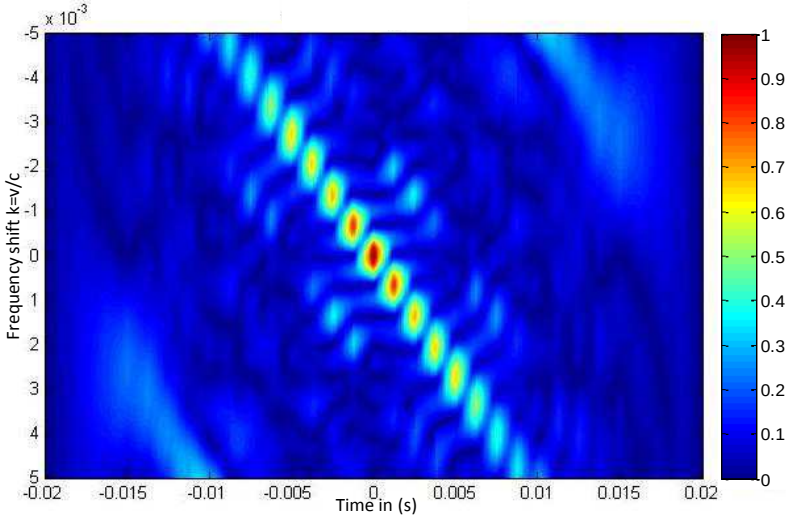

Figure 1.4.2: Ambiguity function of a 4 states phase modulation: Frank codes

1.4.2 Frequency modulation

1.4.2.1 Costas code: frequency modulation by frequency discontinuities

Costas wave form [Cos, 1984] is a modulation using frequency hopping [Lev, 1988, Ric, 2005]. The wave is divided into N subpulses being a single frequency wave at frequency carrier f_n.

$$s(t) = \sum_{n=1}^{N} x_n(t - n\frac{T}{N} - \frac{T}{2}) \tag{1.4.5}$$

$$x_n(t) = \begin{cases} \exp(if_n\frac{B}{N}t) & \text{if } -\frac{T}{2N} \leq t \leq \frac{T}{2N} \\ 0 & \text{otherwise} \end{cases} \tag{1.4.6}$$

The bandwidth is thus covered thanks to the single frequencies repartition. The frequency hopping repartition is chosen to minimize the sidelobes of the ambiguity function. In this purpose, a matrix of coding is associated to the Costa wave. The costas matrix contains on each column and raw only one element non null. The interpretation is made considering the column as a subpulse number and the raw number associated with its non-null element as its frequency number. An example of such matrix is presented below for a costas coded wave with length 7.

	1					
			1			
				1		
1						
						1
					1	
		1				

Example of Costas code matrix

The cross-correlation between the sub-signals at different single frequencies approach zero if the frequency difference is large enough compared to the inverse of the signal duration (see Figure 1.4.3). Thus, the cross-correlation (and ambiguity function) of the Costas code is equivalent to search the matching between the Costas code matrix by itself with a shifted replica (shifted in time and frequency) of it.

At (0,0), the match between the Costas code matrix and its replica is maximum (equalling 7 in this example). Otherwise, whatever the time and frequency shift of the replica is aimed at matching with maximally one element. A coding matrix of Costas signal is filled to respect this property.

Since the cross-correlation of Costas code matrix is maximum equal to 1, the ambiguity function of Costas signals thus presents low sidelobes. This wave form is interesting in this respect. In addition, it is also possible by this same way to predict the localisation of the ambiguity function sidelobe. However, nowadays, since the Doppler effect is not taken into account before matched filtering in MBES applications, such signals are not convenient. Moreover, the sidelobes on the ambiguity function of Costas coded wave (close to the origin) are higher compared with binary phase modulation [Mil, 1990], that is why despites its simplicity of modulation and the numerous possibilities of coding matrix, Costas wave are less used than Binary phase modulation (such as Barker or Pseudo binary code).

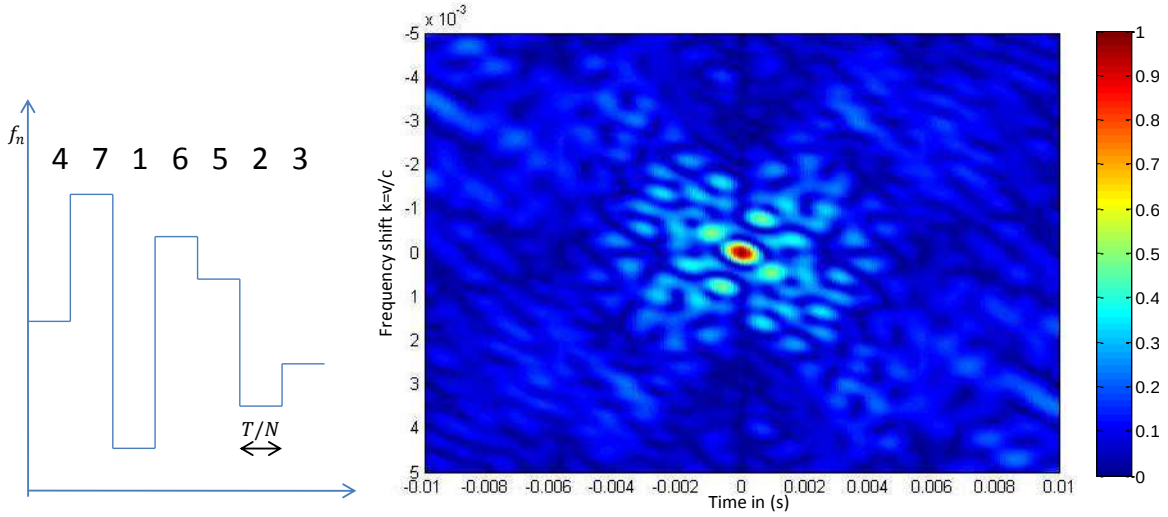

Figure 1.4.3: Frequency hoppings of Costas signal and its associated ambiguity function

1.4.2.2 Continuous frequency modulation

The pulse frequency can also be modulated as continuous function of time. Such pulses are called 'chirp'. Equation 1.4.7 is the mathematical expression of frequency modulated signals (where $a(t)$ is the pulse envelope and f_c the carrier frequency). The instantaneous frequency is given by the differential of the phase function $\omega(t)$. $f(t) = \frac{1}{2\pi}\omega'(t)$. The pulse occupies the frequency band swept by the instantaneous frequency.

$$s(t) = a(t)e^{2\pi j\omega(t)}e^{2\pi j f_c t} \tag{1.4.7}$$

The frequency sweep can be done by different functions.

The best-known and simplest is the linear modulation, *i.e* $f_i(t) = \frac{1}{2\pi}\omega'(t) = \frac{B}{T}t$ thus $\omega(t) = \frac{B}{2T}t^2$. The bandwidth B is swept linearly from $-B/2$ to $B/2$ during the duration T (t from $-T/2$ to $T/2$).

This shape is commonly used in MBES when using modulated signals [Kon, EM122, Kon, EM302, Kon, EM710].

Another well-known modulation shape is the hyperbolic frequency modulation given by :

$$s(t) = a(t)e^{-2\pi j f_c P \ln(1-\frac{t}{P})} \tag{1.4.8}$$

The instantaneous frequency of such a pulse is given by:

$$f_i(t) = \frac{f_c}{1-\frac{t}{P}} \tag{1.4.9}$$

The main interest of hyperbolic chirp is its robustness to the Doppler effect. It can be noticed that the instantaneous frequency of a Dopplerized hyperbolic modulated pulse is given by:

$$f_{i,\eta}(t) = \frac{\eta f_c}{1-\eta\frac{t}{P}} \tag{1.4.10}$$

The instantaneous frequency of a delayed copy (δt) of the hyperbolic modulated signal is:

$$f_{i,\delta t}(t) = \frac{f_c}{1 - \frac{t-\delta t}{P}} \tag{1.4.11}$$

The two expressions (1.4.10) and (1.4.11) equal if $\delta t = \frac{(1-\eta)P}{\eta}$. The Dopplerized hyperbolic modulated signal thus matches with a delayed copy of itself. The matched-filtering output amplitude is maximum (despite of a slight loss due to mismatch of the whole bandwidth, and maximum localisation shifted by δt). In the case of linear modulation the instantaneous frequencies do not match exactly. This induces additive amplitude loss (beside the consideration of bandwidth mismatch). But this effect can be neglected by considering that $B \ll f_c$

Considering that the swept bandwidth is again B, the parameter P in the hyperbolic modulation has to be set to:

$$P = \frac{T}{2B}\left(f_c + \sqrt{f_c^2 + B^2}\right) \tag{1.4.12}$$

In practice, taking into account the swept bandwidth used in MBES compared to the carrier frequency $B \ll f_c$, the hyperbolic modulation is really close to the linear modulation. Indeed in such condition, $P \approx \frac{T}{B} f_c$ and $f_i(t) = \frac{f_c}{1-\frac{t}{P}} \approx f_c + \frac{B}{T}t$.

The modulation can be other function. Part (3.5) proposes and discusses the use of different continuous frequency modulation function as possible improvements prone to increase the bathymetric quality.

Figure 1.4.4 represents the frequency ambiguity of a linear frequency modulated pulse with T = 20 ms, F_c= 73 kHz, B = 500 Hz. Its particularity is the ambiguity in time-frequency which is linked to the modulation function. It is a drawback for many systems since the target can not be localised precisely in range and speed (an error in range gives an error on speed estimation). However, bathymetric MBES do not aim at localising the target in speed. In addition the motion of the array can be known thanks to the ship's attitude data. The received signal being filtered by the matched filter adapted to the transmitted pulse, the Doppler tolerance can even be considered as an advantage since it allows to keep a high response peak (inducing a good signal to noise ratio whatever the Doppler shift). Of course the peak localisation is biased (time shifted) but if the speed of the array is known (estimated from the motion sensors), this can be corrected in post-processing. This does not need pre-Doppler estimation to adapt the matched filtering.

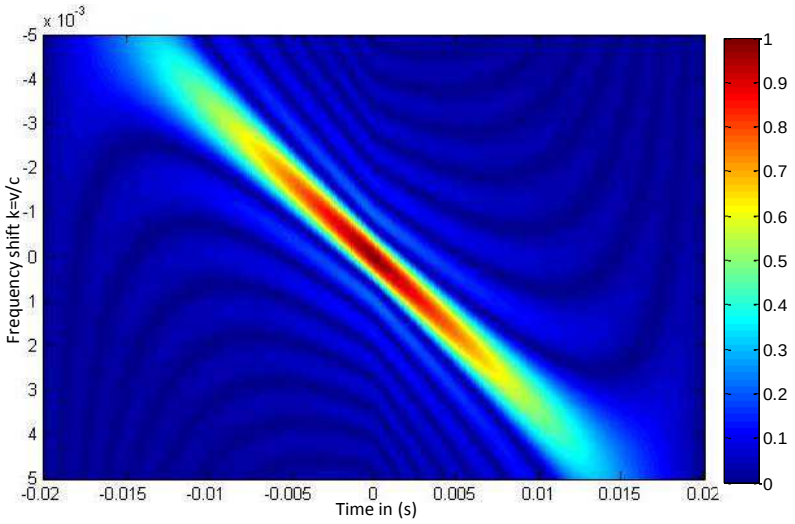

Figure 1.4.4: Ambiguity function for a Linear frequency modulation

Fourier transform of a linear frequency modulated signal (Chirp) Considering the case of linear chirp (linear modulation) in a rectangular envelope, its Fourier transform envelope is approximatively a rectangular function of frequency. Indeed, such a signal is mathematically defined as:

$$\left\{ \begin{array}{rcl} a(t) & = & \mathbf{\Pi}(\frac{t}{T}) \\ \omega(t) & = & f_c t + \frac{B}{2T} t^2 \end{array} \right. \tag{1.4.13}$$

where$\Pi(t)$ denotes the rectangular function which equals 1 on the time interval $[-\frac{1}{2} : \frac{1}{2}]$ and 0 otherwise. By using the stationary phase criterion defined in (A.1.3) in this case it becomes $\nu = \omega'(t) = f_c + \frac{B}{T}t$ (the time-frequency relation is linear). The inverse of this relation gives $t_\nu = T/B(\nu - f_c)$. Finally, using the results on (A.1.10) from the associated development of the stationary phase method.

$$|S(\nu)| \approx \mathbf{\Pi}\left(\frac{\nu - f_c}{B}\right)\sqrt{\frac{T}{B}} \tag{1.4.14}$$

Equation (1.4.14) is the expected approximation. Indeed, the Fourier transform of a chirp is commonly approximated by a rectangular function with a bandwidth equal to B (if the product BT is high enough).

Considering any temporal pulse shape $a(t)$ with a linear frequency modulation, the frequency spectrum (the stationary phase approximation) can be given as a first approximation by:

$$|S(\nu)| \approx a(T\frac{\nu - f_c}{B})\sqrt{\frac{T}{B}} \tag{1.4.15}$$

In practice, in MBES applications, the modulation as continuous frequency modulation is most often chosen. Indeed other kinds of modulations with discontinuities (phase or frequency-hopping) suffer more in case of decorrelation introduced by the backscattering process or

the propagation medium. In addition, continuous frequency modulation presents a certain tolerance to the Doppler effect, which is an advantage since the Doppler effect is not estimated before the pulse compression. Hence despite the platform motion, the signal is still powerful enough to process the detection. Of course ignoring the Doppler effect influence on the detection introduces a bias due to the frequency-time ambiguity from the modulation function and has to be compensated.

1.5 External bathymetric degradation causes

The MBES has to take into account data from external sensors in order to correct potential external errors [Har, 1995]. Indeed the bathymetric measurement is affected by two main types of errors:

- The first one comes from the signal itself: whatever the measurement technique, the bathymetric detection (time angle) fluctuates depending on the received signal fluctuation (SNR). This aspect will be studied in section 2.1

- n addition, the bathymetric measurement IS also biased by external causes (motion of the platform or non-constant sound velocity profile). Specified external sensors have to be operated and their data processed to correct these uncertainties.

Let us shortly present, in the rest of this section, how the last point affects the bathymetric measurement and how it is corrected via data from other sensors. For the rest of the work, the measurement uncertainties brought by external causes will not be considered, and assumed to be already corrected; or at least, since they stem from external causes, their affect is assumed to be the same when using classic pulse CW or modulated pulse (not depending on the signal used).

1.5.1 Platform motion

The bathymetric measurement is made by estimating the angle in the vertical/across-ship plane and the time delay. The platform motion affects the measurement when it is translated from the inertial referential (linked to ship motion) to the global ship's referential. The correction can be done by considering the data from attitude sensors which register the angular motions (roll α , pitch β, yaw γ)as well as the translation motions (heave, sway and surge).

Each sounding made in the vessel's inertial referential (XYZ) has to translated to the referential (xyz) (global referential centered on a reference point of the vessel) using the rotation matrix linked to roll, heave, pitch (Figure 1.5.1) and the translation array linked to heave surge and sway.

$$\begin{pmatrix} x \\ y \\ z \end{pmatrix} = \begin{pmatrix} 1 & 0 & 0 \\ 0 & \cos\gamma & \sin\gamma \\ 0 & -\sin\gamma & \cos\gamma \end{pmatrix} \begin{pmatrix} \cos\beta & \sin\beta & 0 \\ -\sin\beta & \cos\beta & 0 \\ 0 & 0 & 1 \end{pmatrix} \begin{pmatrix} \cos\alpha & 0 & \sin\alpha \\ 0 & 1 & 0 \\ -\sin\alpha & 0 & \cos\alpha \end{pmatrix} \begin{pmatrix} X \\ Y \\ Z \end{pmatrix} + \begin{pmatrix} T_x \\ T_y \\ T_z \end{pmatrix} \tag{1.5.1}$$

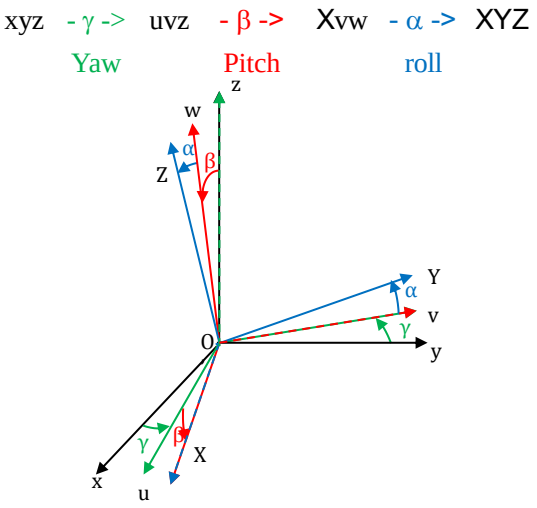

Figure 1.5.1: Ship's inertial referential angular motion

The data from the attitude sensors are also used for real time stabilisation.

1. In reception, a real time stabilisation in roll can be done. The beam steering is applied as a function of the vertical of the global referential and not the inertial vessel's referential, in order to stabilise the swath in the global referential.
2. In transmission, three types of real time stabilisation can be done:
   - pitch stabilisation (to transmit in the across and depth axis plane (xOz) rather than in (XOZ) which does not follow the vertical direction (Oz) (nadir direction)).
   - roll stabilisation (to maintain the transmitting sector angles)
   - yaw stabilisation, using the transmitted sectors (to avoid the sounding line crossings). (see Figure 1.5.2

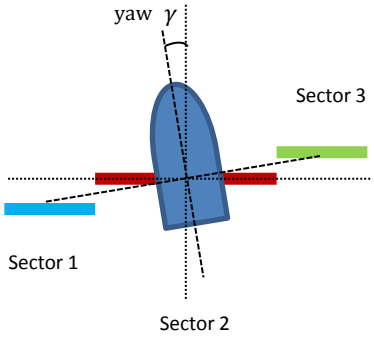

Figure 1.5.2: real-time yaw stabilisation in transmission

Not processing the real-time stabilisation does not impact the bathymetry measurement precision. The real-time stabilisation aims at improving the spatial regularity of the bathymetric data used in the building of digital terrain model.

1.5.2 Velocity profile

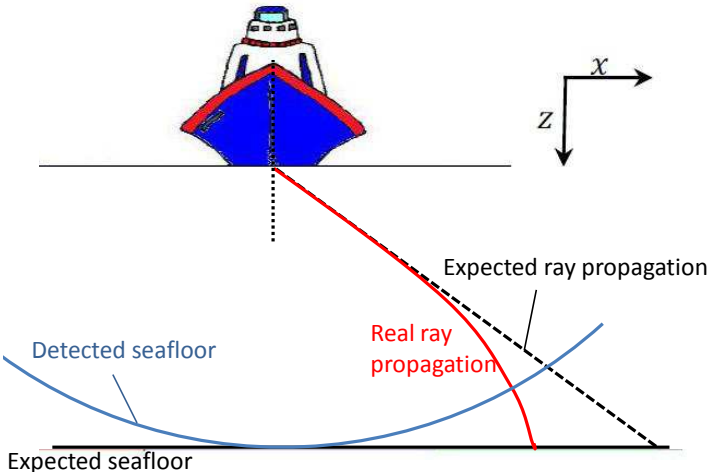

Figure 1.5.3: Impact of not taking into account sound speed profile

It is necessary to know the sound speed profile on the considered water medium, in order to process a correct bathymetric detection. Because of variation in pressure, temperature and salinity, the sound velocity varies along the propagation path. Affected by refraction, the propagation rays are not straight (see Figure 1.5.3). And this could introduce mistakes in the detection localisation. In practice during a bathymetric survey, the sound speed profile is measured and updated.

The external bathymetric degradations are independent of the acoustic signal and are corrected in the same way whatever the transmitted pulse characteristic s. However, bathymetric degradation may happen when modulated signals, as it will be presented in the following section (section 1.6). The external causes could thus not explain this observation.

1.6 Observation of bathymetry quality caused by modulated signals

It has been observed that the bathymetric quality when using frequency-modulated signals (linear frequency modulation) is damaged [Bea, 2012, Bea, 2013, Hug, 2010].

Such observations have been done one several sounders. In the next two paragraphs (1.6.1 & 1.6.2), bathymetric measurement quality estimation is considered for two different Kongsberg echo sounders EM 302 and EM 710 mounted on *R/V Falkor* (Shmidt Oceans Institute). Figures and statistics plots have been extracted from [Bea, 2012, Bea, 2013] and images used by courtesy of J. Beaudoin, UNH/CCOM.

Paragraph 1.6.3 will also show the same kind of observation when using EM 122 from *R/V L'Atalante* (Ifremer).

1.6.1 EM 710

Figure 1.6.1 [Bea, 2013] gives the measured bathymetry on a 500 m-deep bottom using the *R/V Falkor* 's EM710. EM710 features three transmitting sectors [Kon, EM710]. The measurement has been done using MEDIUM and DEEP modes (Table 1.4). MEDIUM mode uses CW wave signals on the whole swath. DEEP mode uses linear frequency modulated signal on outer sectors. Transitions between sectors happen at beam angles -40° and 40°.

sector	1	2	3
MEDIUM	CW T=2ms Fc= 73kHz	CW T=2ms Fc= 79kHz	CW T=2ms Fc=76kHz
DEEP	FM T=20ms Fc= 73kHz	CW T=2ms Fc= 79kHz	FM T=20ms Fc=76kHz

Table 1.4: MEDIUM & DEEP mode description: 3 sectors of the EM710

Due to the high frequency of the EM710 (around 75 kHz) the swath by using CW is limited by additive noise (left on Figure 1.6.1). The bathymetric results when switching to DEEP mode is plotted on the right in Figure 1.6.1 on the right part. The use of FM on side sectors increases the swath. However, it is clearly visible at the inter-sector transition that the bathymetric measurement gets noisier.

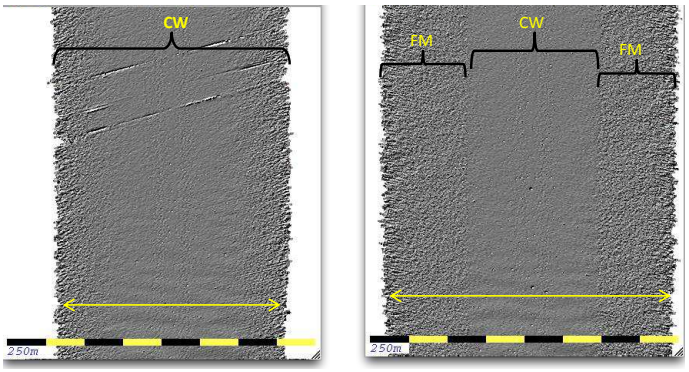

Figure 1.6.1: Measured bathymetry EM710

The bathymetric measurement quality estimated from the data plotted in Figure 1.6.1 is represented as a function of beam angle in Figure 1.6.2. The quality is estimated as the ratio between the standard deviation of the measurement and the actual depth value. The first plot (in Figure 1.6.2) displays the standard deviation of the depth estimation (relatively to the actual depth) as a function of beam angle. The EM710 has the particularity to be able to send simultaneously two pings (multi-ping or dual swath). The two lines (red-light blue for central sectors, blue and magenta for outer sectors) correspond to statistics estimated on these two pings at slightly different along-ship angles. The higher the curves in Figure 1.6.2) , the noisier the bathymetric measurement. The transition between the sectors (at -40° and 40°), clearly shows that the use of modulated signals damages the resulting bathymetric

quality. The second depicts the bathymetric measurement bias around the reference surface and shows that the error is centred : measurement bias is induced by the change to modulated signals.

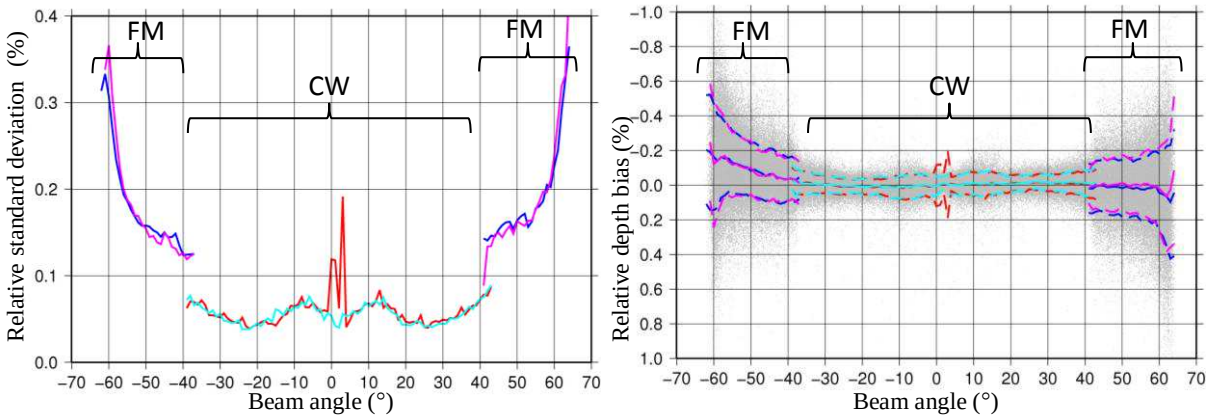

Figure 1.6.2: Bathymetry quality estimated on *R/V Falkor* 's EM710 data, expressed in term of standard deviation and measurement bias on a reference surface as a function of beam angle (sector tansition at -40° and 40°)

The noise level on bathymetry when switching from CW to FM is found to be approximately twice higher (at transition, relative standard deviation jumps from 0.07% to 0.15%).

1.6.2 EM 302

The estimation of bathymetric quality (Figure 1.6.3) has also been done on data recorded with an EM302 on a 1200-m-deep seafloor area [Bea, 2012]. EM 302 can transmit up to 8 transmitting sectors [Kon, EM302] (transitions happening at beam angles 51°, 36°, 20°, 0°, -20, -36°, -51° (see Table 1.5)).

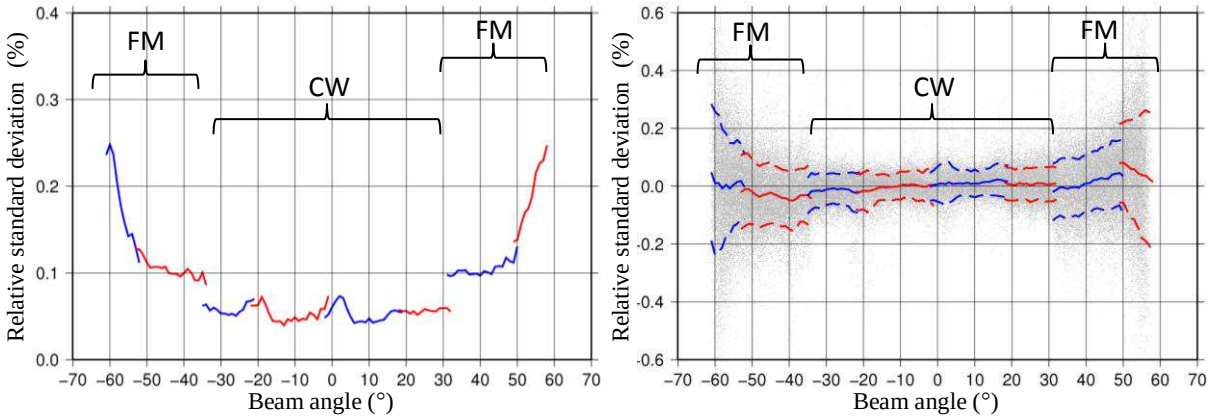

Figure 1.6.3: Bathymetry quality estimated on *R/V Falkor* 's EM302 data, expressed in term of standard deviation and measurement bias on a reference surface as a function of beam angle (tansition CW to FM at -36° and 36°)

Here, it is also clearly visible (Figure 1.6.3) that, at the transition between FM and CW (sectors #2-3, and #6-7), bathymetry quality is damaged when using FM signals. Once again, the standard deviation around the surface reference of the bathymetric measurement is twice higher when using FM than when using CW pulses.

sector	1	2	3	4	5	6	7	8
DEEP	FM	FM	CW	CW	CW	CW	FM	FM
T=	100ms	60ms	5ms	5ms	5ms	5ms	60ms	100ms
Fc=	26.5kHz	27.5kHz	28.5kHz	29.5kHz	30kHz	29kHz	28kHz	27kHz

Table 1.5: DEEP mode description: 8 sectors for EM302

1.6.3 EM 122

The same kind of observation can be done on EM122 data set from *R/V L'Atalante* (Ifremer). The data presented here was recorded on a 2200-m-deep seafloor. EM 122 can transmit on 8 sectors (Table 1.6) with double swath mode [Kon, EM122]. Sector transitions happen at 52°, 35°, 18°, 0°, -18°, -35°, -52°.

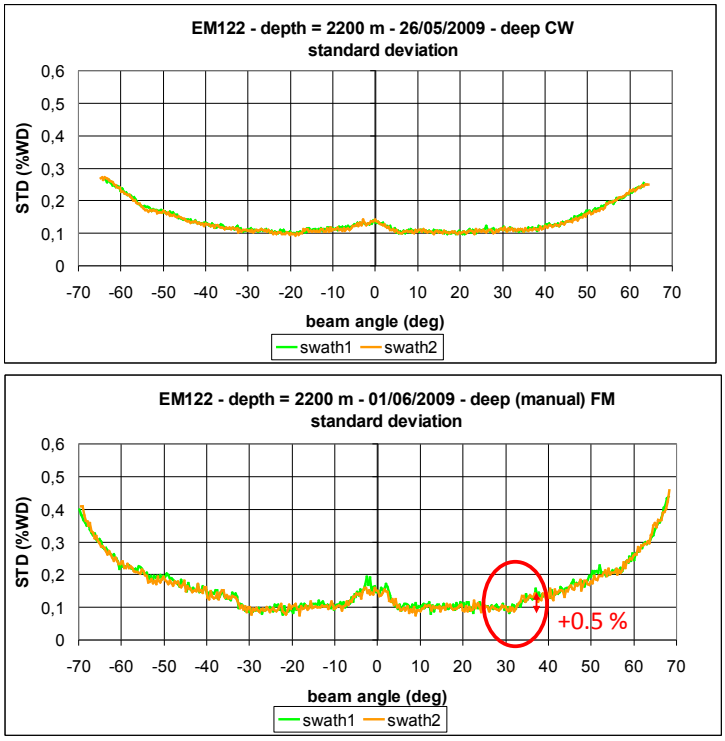

Figure 1.6.4: Bathymetric measurement quality degradation at the sector transition 35° and -35° (central beams using CW outer beams using FM); estimation on *R/V L'Atalante* EM 122 data by relative standard deviation of the measurement as a function of beam angle

The first graph in Figure 1.6.4 presents the result of estimated bathymetric standard

deviation with CW over the whole swath. The second graph below shows the bathymetric quality estimation when FM mode (use of linear-frequency modulated signal) has been applied in the outer sectors (beam angle over 35°). Here the distinction between sectors is not made, green and yellow shows the respective statistics for each ping of the double swath.

sector	1	2	3	4	5	6	7	8
DEEP 1	CW	CW	CW	CW	CW	CW	FM	FM
T=	15ms	15ms	15ms	8ms	8ms	15ms	15ms	15ms
Fc=	11.5kHz	11kHz	12kHz	12.5kHz	12.85kHz	12.25kHz	11.75kHz	11.25kHz
DEEP 2	FM	FM	CW	CW	CW	CW	FM	FM
T=	100ms	60ms	15ms	8ms	8ms	15ms	60ms	100ms
Fc=	11.5kHz	11kHz	12kHz	12.5kHz	12.85kHz	12.25kHz	11.75kHz	11.25kHz

Table 1.6: DEEP mode description (EM 122) 8 sectors

Beyond this particular set of observations, the same type of degradation on bathymetric measurement quality is observed on many systems (EM 710, 302 and 122). This seems to be in contradiction with the well-known statement setting that matched filtering optimises the output signal to noise ratio (see paragraph 1.2). Why does this degradation happen whereas these signal shapes are expected to improve the signal to noise ratio regards to additive noise? This is the question addressed in the next Chapter and the key point of the work presented.

Chapter 2

Analysis of Bathymetric Degradation caused by using modulated signals in MBES

The first Chapter aimed at making the reader familiar with the different notions and elements of processing which are useful to the understanding of this PhD work. It presented the principles of the bathymetric measurement using MBES. It introduced the particular processing linked to modulated signals, using pulse compression which theoretically improves the output signal to noise ratio. However, it was also presented many examples showing a bathymetry measurement damage when using modulated signal. The second chapter will focus on the PhD problematic: explaining why the bathymetric measurement can be noisier when using modulated signals. Commonly-used modulated signals follow a linear frequency modulation function (LFM).

This Chapter is divided into three sections:

1. Bathymetric noise level prediction;
2. Impact of the Doppler effect;
3. Intrinsic noise due to the presence of sidelobes in the compressed pulse.

The first section of this chapter is attached to build a model in order to make the prediction of the noise level observed on bathymetric measurement considering any kind of pulse shape: FM or CW. The detection process is assumed to be applied on the phase difference of the interferometric signals. Indeed, the use of FM signal aims at increasing the swath and thus is used for outer beams where phase detection is processed.

The second part deals with the impact of Doppler effect on the bathymetric measurement. Indeed, the FM signals are impacted differently by the Doppler effect (mismatch of the pulse compression) than CW pulse. Thus, the Doppler effect was firstly assumed to be the causes of bathymetric degradation.

The third part focuses on the main cause of bathymetric degradation caused by FM signals. Considering that pulse-compressed FM are alike to non-modulated signals, the only difference between pulse-compressed signals and common CW is their envelope shape. The measurement degradation is interpreted as the impact of the presence of pulse compression sidelobes, which increase the instantaneous footprint and introduce decorrelation in interferometric signals.

2.1 Noise modeling for Bathymetry measurements

Since the modulated signals are mostly used in the side sectors, the study mainly deals with noise prediction over the phase ramp. The aim of this section is to define the different causes of noise present in the bathymetric measurement. It will explain why the modulated signal can give in certain conditions noisier bathymetric measurement, whereas in the common understanding, it is designed to reduce the noise level relatively to the signal. First, the origins of noise (section 2.1.1 are identified and described, making the distinction between additive and intrinsic noise. The prediction of the additive and intrinsic noise level impacts are first made separately (in sections 2.1.2 and 2.1.3) to be combined (section 2.1.4). The noise level prediction over the phase ramps is expressed in section 2.1.5 using the notions of interferometric signals coherence level and signal to noise ratio introduced in the sections 2.1.2, 2.1.3 & 2.1.4. Finally, the expression in terms of final noise level on bathymetry is made at the end of this chapter, in section 2.1.6. To sum up, throughout this chapter, a complete noise level prediction model is built, which enables to better understand and also predict the degradations observed in bathymetric measurement.

2.1.1 Noise origins

Four types of noise can be considered

- Ambient noise: considered as additive noise;
- Multi path interference (here neglected since the bottom is deep enough)
- Spatial decorrelation or shift footprint
- Angular decorrelation or baseline decorrelation.

Additive noise Ambient noise is certainly not the main cause of bathymetric degradation when using FM. Indeed the theory of pulse compression using matched filter raises the signal to noise ratio with a coefficient BT. Thus, the signal to noise ratio (due to additive noise) is typically 10 times higher when using FM signals than CW. Moreover, the additive noise is not taken into account in the simulations showing the FM-caused degradation. However it is interesting to quantify its impact in term of signal to noise ratio and its final impact on the phase ramp statistics, in order to fully understand and predict the behaviour of the actual bathymetry measurement statistics.

Intrinsic noise 1: Spatial decorrelation or footprint shift At a given observation time, the footprints observed by the sub-arrays are slightly shifted (see Figure 2.1.1). This phenomenon is called spatial decorrelation.

Let the resolution cell size be noted Δ_x and the footprint shift be δ_x. The two signals S_a and S_b are coherent and interfere along length $\Delta_x - \delta_x$. The contribution from the non-common part of the footprints could be considered as being a noise. The resolution cell length at grazing incident angle (high beam angle) [Lur, 2001][Sin, 2010] is approximated as:

$$\Delta_x = \frac{cT}{2\sin(\theta_0)} \tag{2.1.1}$$

And the shift of the footprints comes as [1]:

$$\delta_x = \frac{a\sin(\theta - \theta_0)}{2\sin(\theta_0)} \tag{2.1.2}$$

Here it can be noticed that the ratio between the non-coherent part of the footprints over the coherent is minimized when the footprints are around the interferometer axis direction *i.e.* when$\theta_0 = \theta$. Since the noise level over the phase ramp is evaluated around the zero-crossing (time sample when the footprint is in the beam axis direction), this phenomenon can be neglected in MBES, in a first approximation.

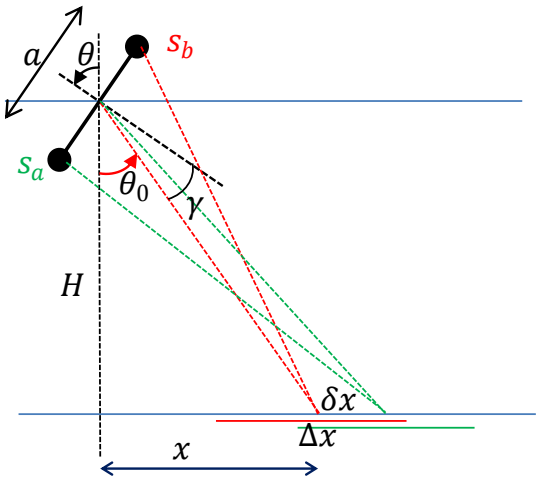

Figure 2.1.1: Footprint shift: at a given instant, the footprints seen by the two sub-arrays are slightly different

Intrinsic noise 2: Angular or baseline decorrelation Consider a part of the bottom at one instant which is illuminated and backscatters the signal. This footprint can be considered as a sound source with its own pattern of transmission (defined as a function of angle direction). The larger the footprint, the more fluctuating the directivity pattern. The footprint seen as a new sound sources sees the centres of the sub-arrays along two different angular directions. Due to fluctuating directivity pattern, the power observed by the two receivers can be really different, resulting in a decorrelation of the two interferometric signals (see Figure 2.1.2). This phenomenon is called angular decorrelation or baseline decorrelation [Jin, 1996] and is often likened to speckle. Indeed, all the contributions of the different points of the resolution cell (considered as wide and homogeneous) are summed so that the received signal follows a Rayleigh law for its amplitude with a random phase (uniform). However, speckle

[1] The covered propagation distance from transmitter to centers of the two different footprints and then to their respective receivers should be equal:
$\sqrt{H^2+x^2} + \sqrt{(H+\frac{a}{2}\sin\theta)^2 + (x-\frac{a}{2}\cos\theta)^2} = \sqrt{H^2+(\delta x+x)^2} + \sqrt{(H-\frac{a}{2}\sin\theta)^2 + (x+\delta x+\frac{a}{2}\cos\theta)^2}$
Considering that δ_x and a are low compared to H and x, this conducts to:
$\frac{a}{2}\frac{H\sin\theta - x\cos\theta}{\sqrt{H^2+x^2}} = 2\delta x\frac{x}{\sqrt{H^2+x^2}} - \frac{a}{2}\frac{H\sin\theta - x\cos\theta}{\sqrt{H^2+x^2}}$
And by using trigonometry and expression of sine and cosine as a function of distance ratio, it is possible to express the footprint shift as:
$2\delta x\sin\theta_0 = a\left(\cos\theta_0\sin\theta - \sin\theta_0\cos\theta\right) = a\sin(\theta-\theta_0)$

only describes the resulting amplitude fluctuation of the scatter in process, while baseline or angular decorrelation denotes the coherence loss of signals from two receivers.

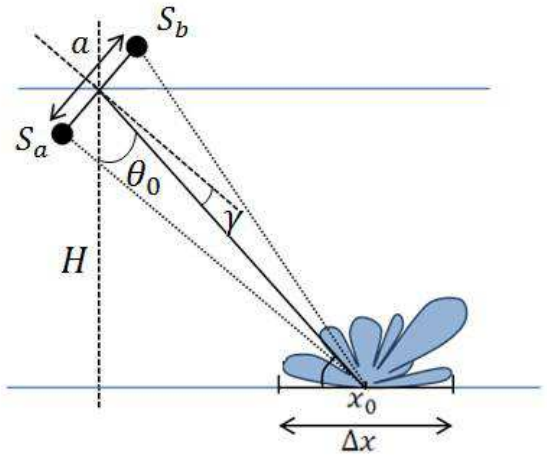

Figure 2.1.2: Directivity pattern fluctuation of the backscattering footprint considered as an extended sound source. The more extended the footprint, the more fluctuating its directivity pattern, introducing decorrelation of received sub-array signals (called baseline decorrelation).

The noise observed with FM signals is probably due to this last phenomenon. Indeed, additional noise is reduced by matched filtering and footprint shift can be neglected since the detection is always processed when the seafloor is towards the beam angle.

2.1.2 Additive noise prediction

The signal to noise ratio (equation (2.1.3)) in reception can be obtained from the energy budget. The expected backscattered intensity (pressure field measured in µPa at 1m of the receiver) and noise level received by the sounder system is predicted by the well known active sonar equation [Ain, 2010] and expressed as follows [Lur, 2010a]:

$$SNR = SL - 2TL + TS + DI - NL + PG \tag{2.1.3}$$

Where :

- SNR is the signal to noise ratio;
- SL denotes the transmitted energy level in dB re 1µPa@1m. The transmitted level is specific to the considered sounder system;
- TL the transmission loss (divergence loss PL+ absorption loss AL);
- TS the target strength of the illuminated seafloor footprint;
- DI is the directivity gain of the receiving array;
- NL the additive noise level in dB re 1µPa@1m
- PG denotes the processing gain due to the pulse compression.

The different terms of this equation are discussed and detailed in the following paragraphs.

2.1.2.1 Sonar equation

Transmitted energy level This term depends on the sounder system and its actual setting. The sounder specifications from manufacturers specifies the maximum level depending on the sounder mode.

Here there are some axamples of Kongsberg MBES configurations [Kon, EM122, Kon, EM302, Kon, EM710]:

- **EM 710** (Very Shallow (2-100 m)=225 dB 1μPa@1m; Shallow (100-200 m)=224 dB 1μPa@1m; Medium and deep (200-500 m)=225 dB 1μPa@1m, veryDeep(500-2000 m)=229 dB 1μPa@1m)
- **EM 122** (Shallow and medium (10-1000 m)=235 dB; Deep (1000-9000 m)=239 dB 1μPa@1m; Very Deep (9000-11000 m)=241 dB 1μPa@1m)
- **EM 302** (Shallow and medium (10-750 m)=232 dB 1μPa@1m; Deep and Very Deep (750-7000 m) 237 dB 1μPa@1m)

Propagation loss When they propagate, acoustical waves are submitted to intensity loss [Bur, 1989] due to mainly two phenomenon:

- geometrical divergence loss PL common to any spherical wave
- absorption loss AL from the medium itself.

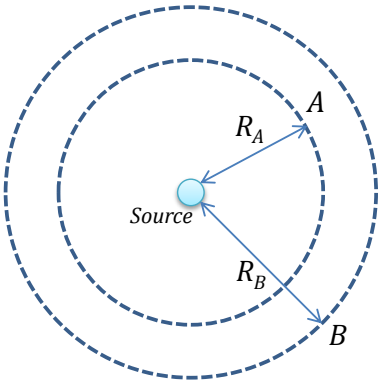

Figure 2.1.3: Wave spherical propagation: wave intensity spread on the sphere surface increasing with the radius (propagation distance)

Geometrical divergence loss: Considering a spherical propagation in an homogeneous medium (Figure), the propagation of the energy transmitted by a point source (as centre of the spherical pattern) goes through spherical surfaces that grow surface with the square of their distance to the source ($S = 4\pi R^2$). The energy of the wave is constant but is spread over the sphere (so that $E = 4\pi R^2 I(R)$). Thus the ratio of the intensity at points A and B situated respectively at distances $R_A$and R_B to the source is:

$$\frac{I(R_A)}{I(R_B)} = \left(\frac{R_B}{R_A}\right)^2 \tag{2.1.4}$$

By considering this ratio with the reference as the unity sphere ($R_0 = 1$ m), the loss due to the geometric divergence of spherical wave in dB at the observation distance R is:

$$PL = 20\log(\frac{R}{R_0}) \tag{2.1.5}$$

medium absorption loss : The propagation medium (sea water) is dissipative and the energy of the wave is absorbed by the medium. The wave is submitted to an amplitude damping, so that the amplitude decreases exponentially with the propagation distance. Thus the pressure field is expressed as::

$$p(r,t) = \frac{p_0}{R} e^{-\gamma R} e^{j(\omega_0 t - kR)} \tag{2.1.6}$$

where γ is the medium absorption coefficient (in Nepers by meter). Most of the time the attenuation is expressed in dB/km to fit the energetic equation which is expressed in dB as in (2.1.3). So, the attenuation loss is:

$$AL = -\alpha R/1000 \tag{2.1.7}$$

Where α is equal to $1000\,.\,20\gamma\log(e)$.

The parameter α (as well as γ) depends on wave frequency and water conditions: salinity, temperature, pressure.

Many models have been developed, such as the one proposed in [Fra, 1982a] and [Fra, 1982b] which is today the most commonly used.

F(kHz)	0.1	0.3	1	3	10	30	100	300	1000
α(dB/km)	0.001	0.01	0.07	0.1	1	5	30	100	500

Table 2.1: attenuation coefficient as a function of the wave frequency

Table 2.1 gives the attenuation parameter α as a function of frequency. These values are average values since, as it was previously mentioned, α depends on several other parameters.

Considering the value of parameter α corresponding to attenuation loss, it is easy to understand that systems at different frequencies will reach swath width of very different extent. As orders of magnitude using 10 kHz systems, with 1 dB/km as attenuation coefficient, allows to reach swath around a dozen of km, while systems working at 100 kHz would hardly be efficient for swath above 1 km. The practical frequency limitation for MBES is 1MHz, since such systems would maximally reach a swath of a few hundred meters.

Total transmission loss : Considering a one-way propagation transmission loss is the sum of the divergence loss and attenuation loss:

$$TL = 20\log(R) + \alpha R/1000 \tag{2.1.8}$$

n the case of MBES the propagated signal goes through a two-way flight which explains the factor 2 in the sonar equation (2.1.3).

Backscattered energy The backscattered signal strength will depend on the seafloor nature and structure (rocks, mud, sand...), the characteristics of the incidence signal (angle and frequency) but also the area of the footprint which scattered the signal.

$$TS = BS(\theta) + 10\log(S) \tag{2.1.9}$$

Where S is the surface of the footprint and $BS(\theta)$ is the backscattering index of the target (expressed in $\mathrm{dB/m^2}$) which depends on the observing (or beam) angle θ, at a given frequency.

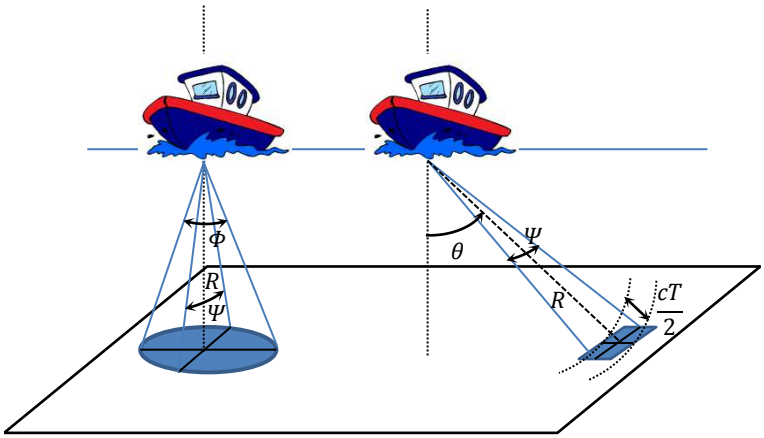

Figure 2.1.4: Backscattering footprint geometry depending on beam angle

At small angle θ , the footprint is delimited by the projection (see Figure 2.1.4) of the beam aperture on the seafloor so that:

$$S = \Psi\Phi R^2 \tag{2.1.10}$$

Considering that θ is large the footprint is delimited on the transverse direction by the projection of the spatial duration of the signal on the seafloor and the surface S becomes:

$$S = \Psi R \frac{cT}{2\sin\theta} \tag{2.1.11}$$

Complex models have been developed to predict $BS(\theta)$, however here it will only be considered that the backscattering index of the target follows the Lambert's law:

$$BS(\theta) = BS_0 + 20\log(\cos\theta) \tag{2.1.12}$$

Where in practice BS_0 takes its value on the range from -10 to -40 dB/m. Despite its simplicity, Lambert's law practically fit the observed backscattering index in many case, and constitutes a good first approximation at grazing incidence angles (high beam angles). Additive noise is strongly present on outer beam angles and its prediction is precisely the most important in such beams. In central sectors (vertical beams) the bathymetric noise will be less affected by the additive noise and its contribution part in the final SNR could even be neglected compared to intrinsic noise (see sections 2.1.3 and 2.1.4).The prediction of target strength will be done by using (2.1.11) and (2.1.12) in (2.1.9).

Directivity gain The directivity gain denotes the SNR improvement brought by using directive arrays. In case of active systems such as MBES, there is a double advantage in using directive arrays, one in transmission (concentration of the energy along one direction) and one in reception (focusing the 'listening' towards a given direction).

First, consider the directivity function $D(\theta, \phi)$ which is the angle-dependent capability to receive or transmit a wave for a single element (stave) or several (array). To define the directivity of an array composed from several single elements (stave), the elementary directivity functions of the stave $D_{stave}(\theta, \phi)$ and the array geometry $D_{array}(\theta, \phi)$ have to be known. The product of both gives a resulting directivity function.

$$D_{tot} = D_{stave}.D_{array} \tag{2.1.13}$$

In the same way by combining the directivity functions of the transmitting array and receiving array, the directivity of the sounder system is given as the product of the transmitting array T_x and receiving array R_x.

$$D_{syst} = D_{T_x}.D_{R_x} \tag{2.1.14}$$

At the transmission, the directivity gain denotes the 'energetic spatial gain' obtained by a directive antenna as comparison to an omnidirectional antenna. It corresponds to the ratio between double integral on space of the directivity function of the transmitting element (or transmission pattern) and its equivalent for an omnidirectional antenna whose integral value is 4π (directivity function equals a constant value) [Bou, 1992, Ain, 2010, Bur, 1989]. And the directivity gain (directivity index) is expressed as in (2.1.15) where Ω is the solid angle.

$$DI = -10\log\left(\frac{\int\int D(\theta,\phi)d\Omega}{\int\int d\Omega}\right) = -10\log\left(\frac{1}{4\pi}\int\int D(\theta,\phi)d\Omega\right) \tag{2.1.15}$$

The gain from the directivity of the transmitted antenna is already taken into account inside the term SL in equation (2.1.3).

In the reception, the notion of directivity gain (denoted here as array gain $AG$is slightly different since it gives the equivalent noise diminution due to the directivity of the antenna as comparison to the omnidirectional antenna. Indeed, the antenna directivity allows to 'listen' only from a given direction. Focusing the attention on this particular direction makes the perceptive noise decrease. AG is the ratio between the signal to noise ratio perceived by the directional array over the signal to noise ratio at the output of the omnidirectional receiver.

$$AG = 10\log\left(\frac{\int\int D(\theta,\phi)S(\theta,\phi)d\Omega}{\int\int D(\theta,\phi)N(\theta,\phi)d\Omega}\right) - 10\log\left(\frac{\int\int S(\theta,\phi)d\Omega}{\int\int N(\theta,\phi)d\Omega}\right) \tag{2.1.16}$$

Where $S(\theta, \phi)$ and $N(\theta, \phi)$ are the spatial density of acoustic field respectively the signal and the ambient noise. To be rigorous, AG should replace DI in the signal to noise equation (2.1.3) (considering the reception point of view). However, the two definitions of the directivity gain are equivalent when considering these two hypotheses:

- noise as spatially-isotropic, spatial density of noise is constant $N(\theta, \phi) = N$.
- received wave as plane (which can be justified since the backscattering seafloor is in the far field of the array). $S = S(\theta, \phi)\delta_{\theta-\theta_0}$

Indeed, under these conditions, the array gain in signal to noise ratio AG in (2.1.16) can be simplified to the directivity index of the array DI as in (2.1.15). That is why, finally, DI from (2.1.15) is used in the final signal to noise (2.1.3).

DI\$ definition uses the beam directivity function of the whole system (taking into account transmission and reception). The beam directivity function is characterised by MBES manufacturers thanks to their angular aperture parametersΨ and Φ which correspond to their -3 dB angular apertures. Considering these parameters, the directivity gain can be approximately given by:

$$DI = -10\log(\frac{\Psi\Phi}{4\pi}) \tag{2.1.17}$$

2.1.2.2 Additive noise level

Sea water constitutes a noisy medium for acoustical waves. The ambient noise is the signal received by the receiver array in absence of useful signal. The spectral density function of the ambient noise depends on the considered central frequency [Bou, 1992, Bur, 1989].

- From 10 Hz to 1 kHz, ambient noise is mainly due to the traffic noise (the level depends on the considered area);
- From some hundreds of Hz to a dozen of kHz, the main cause of the noise is the surface agitation (bubble clapping at the sea surface, depending on wind strength, rain...);
- Around 100 kHz and above, noise is mainly due to the self noise of the acoustical system (thermal noise).

The noise level taken into account inside the sonar equation is given by its spectral density integration over the band considered by the system (bandwidth being inversely proportional to the signal duration T_{eq} (in case of CW signal, or equivalent pulse compressed duration in case of FM). Taking into account that the bandwidth is relatively short in comparison to the carrier frequency, the noise spectral density is assumed to be constant depending only of the central frequency ($N_0(f_c)$ expressed as dB ref 1μPa/$\sqrt{\text{Hz}}$). Finally, the noise level is defined as:

$$NL = N_0(f_c) + 10\log(\frac{1}{T_{eq}}) \tag{2.1.18}$$

2.1.2.3 Processing gain

The pulse compression improves the signal to noise ratio and the term PG in the sonar equation denotes this improvement. Considering the received signal as a delayed copy of the transmitted signal, the signal to noise ratio before pulse compression is (see in 1.2.1):

$$SNR_0 = \frac{\max|s|^2}{N_0/T_{eq}} \tag{2.1.19}$$

The signal to noise ratio at the output of the matched filter is

$$SNR_1 = \frac{\int|s|^2dt}{N_0} = E/N_0 \tag{2.1.20}$$

The level of improvement is given as:

$$PG = 10\log(\frac{\int |s|^2 dt}{\max |s|^2 T_{eq}}) \tag{2.1.21}$$

2.1.2.4 Signal to noise ratio as a function of depth and beam angle

To sum up, the signal to noise (expressed in dB) ratio considering additive noise (ambiant noise) is thus predicted by the equation:

$$SNR = SL - 2TL + TS + DI - NL + PG \tag{2.1.22}$$

in which is given

$$\begin{cases} 2TL & = 40\log(\frac{H}{\cos\theta}) + 2\alpha\frac{H}{\cos\theta}/1000 \\ TS & = BS_0 + 20\log(\cos\theta) + 10\log(\Psi\frac{H}{\cos\theta}\frac{cT_{eq}}{2\sin\theta}) \\ DI & = -10\log(\frac{\Psi\Phi}{4\pi}) \\ NL & = N_0 + 10\log(\frac{1}{T_{eq}}) \\ PG & = 10\log(\frac{\int |s|^2 dt}{\max |s|^2 T_{eq}}) \end{cases} \tag{2.1.23}$$

The natural expression of signal to noise ratio is given by:

$$d_{ad} = 10^{\frac{SNR}{10}} \tag{2.1.24}$$

Example with EM 710

SL	224dB re 1µPa@1m
BS_0	-28dB/m^2
N_0	37dB/$\sqrt{\text{Hz}}$
$\Psi\Phi$	1°*26°
α	23dB/km

2.1.3 Intrinsic noise: baseline decorrelation and footprint shift

2.1.3.1 Coherence coefficient of interferometric signals

The coherence coefficient μ between two signals S_a and S_b (here the interferometric signals) is defined [Lur, 2010a, Cer, 2012, Jin, 1996, Sin, 2010, Puj, 2007] as the ratio between the expected value of the signal $S_a\overline{S_b}$ and the square root of the product of their expected values. This coefficient gives the level of likelihood between the two signals. It is used here as a parameter of the interferometry performance of the two signals.

$$\mu = \frac{\left|\left\langle S_a\overline{S_b}\right\rangle\right|}{\sqrt{\left\langle S_a\overline{S_a}\right\rangle\left\langle S_b\overline{S_b}\right\rangle}} \tag{2.1.25}$$

In (2.1.25), the operator$\langle . \rangle$ denotes the operator expected value and$|.|$the absolute value.

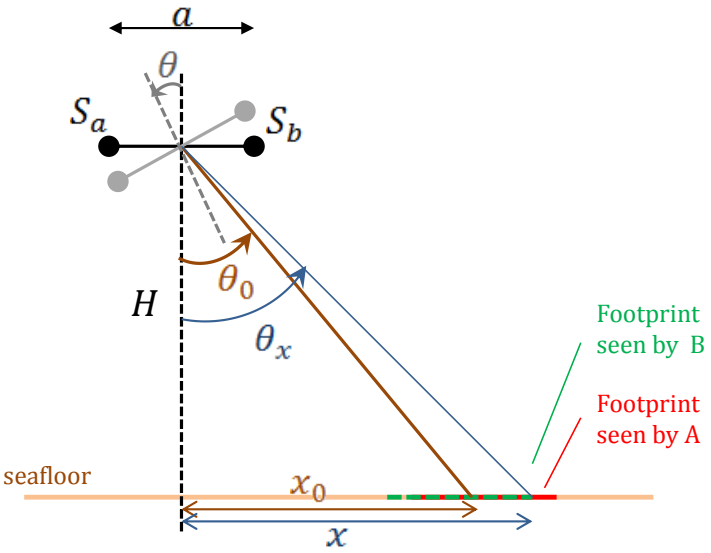

Figure 2.1.5: receiving configuration allowing to expressed the interferometric signals S_a and S_b

To predict the coherence coefficient of the two interferometric signals S_a, S_b (signals from the receiving sub array), the expressions of the expected signals on these subarrays have to be calculated. To simplify the calculation, the subarray signal is modelled as signal received from a point receiver at the subarray phase centre (see in Figure 2.1.5). The received signal is the convolution product of the transmitted signal with the seafloor impulse response. The bottom is considered a line of elementary scatterers, which should tends to a continuous integral summation (on the line axis: x-axis). A scatterer situated at x sends back a delayed copy of the transmitted signal to the array centre (corresponding to propagation delay τ_x) and multiplied by a random backscattering coefficient a_x depending on its position. This backscattering coefficient commonly follows a Rayleigh law in amplitude and uniform phase distribution [Hel, 2003, Hel,1998, Che, 2004].

Then, the received signals can be expressed as (2.1.26).

$$\begin{aligned} S_a &= s * \overbrace{\int_{-\infty}^{+\infty} a_x \delta_{\tau_x + \frac{a}{2c}\sin\theta_x} dx}^{\text{seafloor impulse response seen by A}} \\ S_b &= s * \underbrace{\int_{-\infty}^{+\infty} a_x \delta_{\tau_x - \frac{a}{2c}\sin\theta_x} dx}_{\text{seafloor impulse response seen by B}} \end{aligned} \tag{2.1.26}$$

In(2.1.26),$\delta_\tau$is the Dirac distribution, representing the delay τ due to signal propagation. τ_x is the propagation delay equalling $\frac{2H}{c\cos\theta_x}$ corresponding to twice the way from the array centre to the elementary backscatterer situated at x in the transversal axis (θ_x being the angular position of the backscatterer located at x). (see Figure (2.1.5)). Considering that the incident wave is plane, the wave observed by receivers A and B is delayed by $\pm\frac{a}{2c}\sin\theta_x$ as comparison to the receiving array centre (see Figure 2.1.5).

The originality here is to consider the whole expressions of S_a and S_b. This gives directly the joint impact of the two types of intrinsic noise: spatial decorrelation (footprint shift) and angular decorrelation (baseline decorrelation). In many publications [Jin, 1996, Lur, 2001, Puj, 2007, Sin, 2002] only one of these two impacts is considered at once and the two phenomena are studied separately. However, they are thereafter aimed at being gathered to express their final impact on the bathymetric measurement.

Before considering the interferometry, the signals S_a and S_b are delayed by the beamforming steering according to the steering angle θ. Here this delay is introduced directly, corresponding to the time beamforming case.

$$\begin{aligned} S_a &= \int_{-\infty}^{+\infty} a_x s\left(t - \tau_x - \frac{a}{2c}\left(\sin\theta_x - \sin\theta\right)\right) dx \\ S_b &= \int_{-\infty}^{+\infty} a_x s\left(t - \tau_x + \frac{a}{2c}\left(\sin\theta_x - \sin\theta\right)\right) dx \end{aligned} \tag{2.1.27}$$

The expected value of the interferometric term $\left\langle S_a \bar{S}_b \right\rangle$is:

$$\begin{aligned} \left\langle S_a \overline{S_b} \right\rangle &= \iint \left\langle a_x a_{x'} \right\rangle s\left(t - \tau_x - \frac{a}{2c}\left(\sin\theta_x - \sin\theta\right)\right) \overline{s\left(t - \tau_{x'} + \frac{a}{2c}\left(\sin\theta_{x'} - \sin\theta\right)\right)} dx dx' \\ &= \left\langle a^2 \right\rangle \int s\left(t - \tau_x - \frac{a}{2c}\left(\sin\theta_x - \sin\theta\right)\right) \overline{s\left(t - \tau_x + \frac{a}{2c}\left(\sin\theta_x - \sin\theta\right)\right)} dx \end{aligned} \tag{2.1.28}$$

The random coefficients from the different scatterers are commonly-assumed to be independent from each other. Thus $\langle a_x a_{x'} \rangle$is null if x is different from x'. Let us consider that the contributed scatterers at a given instant can be gathered constituting a footprint located in average along the direction θ_0. The propagation delay associated with the responding footprint centre (situated on the direction θ_0) is τ_0. Considering that the footprint dimension is small compared to depth H and lateral distance x, a first-order Taylor series approximation can be performed.

$$\begin{cases} \tau_x = \tau_0 + \dfrac{2}{c}\sin\theta_0 (x - x_0) = \tau_0 + T\dfrac{x - x_0}{\Delta x} \\ \sin\theta_x = \sin\theta_0 + \dfrac{x - x_0}{H}\cos^3\theta_0 \end{cases} \tag{2.1.29}$$

By replacing in(2.1.28), and by taking $t = \tau_0$ (which is equivalent to study the coherence level of interferometric signals at the detection instant), the coherence ratio becomes:

$$\begin{aligned} \left\langle S_a \overline{S_b} \right\rangle &= \left\langle a^2 \right\rangle \int s\left(T\frac{(x - x_0)}{\Delta x}(1 - \beta) - \kappa\right) \overline{s\left(T\frac{(x - x_0)}{\Delta x}(1 + \beta) + \kappa\right)} dx \\ &= \left\langle a^2 \right\rangle \frac{\Delta_x}{T} \int s\left((1 - \beta)\, t - \kappa\right) \overline{s\left((1 + \beta)\, t + \kappa\right)} dt \end{aligned} \tag{2.1.30}$$

Where the factor β and κ have been set as:

$$\begin{cases} \beta = \frac{a}{2cT}\frac{\Delta x}{H}\cos^3\theta_0 = \frac{1}{4}\frac{a}{H}\frac{\cos^2\theta_0}{\tan\theta_0} \\ \kappa = \frac{a}{2c}\left(\sin\theta_0 - \sin\theta\right) = \frac{1}{2}\frac{\delta_x}{\Delta x}T. \end{cases} \tag{2.1.31}$$

By a similar development, it can be shown that:

$$\left\langle S_a \overline{S_a} \right\rangle = \left\langle S_b \overline{S_b} \right\rangle = \left\langle a^2 \right\rangle \frac{\Delta_x}{T} \int s\left(t\right) \overline{s\left(t\right)} dt \tag{2.1.32}$$

Then the coherence ratio can be expressed thanks to (2.1.33) . It takes the form of the ambiguity function (wideband-signal ambiguity function (Wigner-Ville transform)) of the transmitted signal and depending on the interferometer and environmental condition parameters such as depth, interferometer space, sound speed. Such a similar expression has been presented in several papers [Cer, 2012] and [Bir, 2005] (noting that, in the latter, the factor β has been neglected).

$$\mu = \frac{\int s\left(\left(1-\beta\right)t - \kappa\right) \overline{s\left(\left(1+\beta\right)t + \kappa\right)} dt}{\int s\left(t\right) \overline{s\left(t\right)} dt} \tag{2.1.33}$$

This expression quantifies the self similarity of the transmitted signal s when it is delayed by a factor κ and stretched by the factor β. Hence, it can be seen that the loss of coherence between the two interferometric signals S_a and S_b comes from two effects quantified respectively by parameters κ and β. Here, the two kinds of intrinsic noise described in section 2.1.1 are thus well taken into account and described in equation 2.1.33. Indeed, parameter κ denotes the effect caused by the shift of the footprints (first kind of intrinsic noise causing interferometric signal coherence loss), while β refers to the other kind of intrinsic noise that is baseline decorrelation.

By neglecting β and considering only κ and that the transmitted signal is a rectangular CW signal whose duration is T , the well know expression ([Lur, 2001]) of the interferometric coherence coefficient is found back.

$$\mu = \frac{\int s\left(t-\kappa\right) \overline{s\left(t+\kappa\right)} dt}{\int s\left(t\right) \overline{s\left(t\right)} dt} = \frac{T - 2\kappa}{T} = \frac{T - T\delta_x/\Delta_x}{T} = \frac{\Delta_x - \delta_x}{\Delta_x} \tag{2.1.34}$$

2.1.3.2 Coherence coefficient considering baseline decorrelation only

In the case of MBES processing, the detection is made when the footprints are along the beam axis direction so that θ equals θ_0. In this particular case the term κ becomes null and the phenomenon of footprint shift disappears. Only baseline decorrelation then plays a role in the coherence ratio of the interferometric signals. Neglecting the footprint shift is equivalent to consider the coherence ratio as the ambiguity function of the signal when the time delay is null.

$$\mu = \frac{\int s\left(\left(1-\beta\right)t\right) \overline{s\left(\left(1+\beta\right)t\right)} dt}{\int |s|^2 dt} \tag{2.1.35}$$

In the case of a CW signal (or pulse compressed signal $s(t) = |s| e^{2\pi i f_c t}$), the ambiguity function can be simplified (time delay being still null). Indeed, the distortion of the whole envelope can be neglected since $\beta \ll 1$, and $s\left(\left(1 \pm \beta\right)t\right) \simeq |s(t)|\, e^{2\pi i f_c (1\pm\beta) t}$. Finally, the dilation or the compression of the signal is approximated by a frequency shift (common radar-community approximation).

$$\mu = \frac{\int |s|^2 e^{-2\pi i f_c(2\beta t)} dt}{\int |s|^2 dt} = \frac{\mathrm{FT}[|s|^2](2f_c\beta)}{\mathrm{FT}[|s|^2](0)} = \frac{\mathrm{FT}[|s|^2](f_c \frac{1}{2}\frac{a}{H}\frac{\cos^2\theta_0}{\tan\theta_0})}{\mathrm{FT}[|s|^2](0)} \tag{2.1.36}$$

It can be seen from (2.1.36) that, in case of neglecting the footprint shift effect and using CW signal, the coherence ratio between interferometric signals is a particular point of the normalized Fourier transform of the transmitted signal envelope which depends on the interferometer parameters.

In the particular case of a CW transmitted in a square envelope the coherence coefficient being a particular point of its Fourier transform, the development above leads to the sinc expression defined in [Jin, 1996, Lur, 2001, Sin, 2010, Puj, 2007].

$$\mu = \mathrm{sinc}\left(\pi f_c T \frac{1}{2}\frac{a}{H}\frac{\cos^2\theta_0}{\tan\theta_0}\right) \tag{2.1.37}$$

Note: In the case of an FM signal, equation (2.1.36) is still valid if the pulse-compressed envelope is considered as the transmitted envelope.

2.1.3.3 Expression as a signal to noise ratio

From the interferometric-signal coherence coefficient, it is possible to define a signal to noise ratio [Gat, 1994, Bir, 2005, Jin, 1996, Sin, 2002, Puj, 2007, Lur, 2001]

Let us assume that the interferometric signals can be written as the combination of a useful part C which is the common part of the signals that contributes on the coherence and a noise N including any type of degradation.

$$\begin{cases} S_a = & C.N_{a,in} \\ S_b = & C.N_{b,in} \end{cases} \tag{2.1.38}$$

The noise $N_{a,in}$ and $N_{b,in}$ are independent, with the same mean m and standard deviation σ (standard deviation denoting the noise level due to intrinsic degradation on the signals S_a and S_b).

$$\mu = \frac{\left|\left\langle S_a \overline{S_b}\right\rangle\right|}{\sqrt{\left\langle S_a \overline{S_a}\right\rangle \left\langle S_b \overline{S_b}\right\rangle}} = \left|\frac{|C|^2 m^2}{|C|^2 (\sigma^2 + m^2)}\right| = \frac{m^2/\sigma^2}{m^2/\sigma^2 + 1} = \frac{d_{in}}{1 + d_{in}} \tag{2.1.39}$$

Where d_{in} denotes the natural signal to noise ratio between the useful interferometric signal and the noise associated with the degradation (taking into consideration the intrinsic noise). Indeed, classic signal to noise ratio is given in case of random signals is given by the ratio of the squared expected value value m^2 over its variance σ^2 .

Inversing (2.1.39) to express the signal to noise ratio as a coherence coefficient function gives:

$$d_{in} = \frac{\mu_{in}}{1 - \mu_{in}} \quad \text{with } \mu_{in}\text{define as in(2.1.35)} \tag{2.1.40}$$

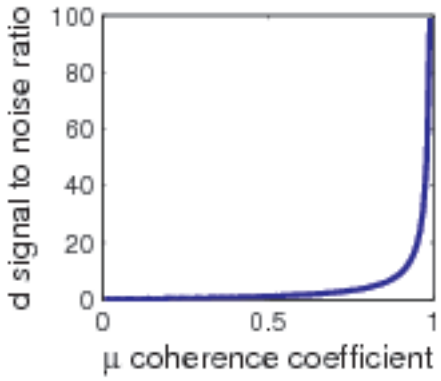

Figure 2.1.6: signal to noise ratio as a function of coherence coefficient

Defined in (2.1.40), the signal to noise ratio (considering the intrinsic noise) is an increasing function of the interferometric signal coherence. This seems natural, the more coherent the interferometric signals are, the better the resulting interferometric signal to noise ratio is. The function SNR as a function of coherence coefficient $f : \mu \to d$ is a bijection from/ to their respective definition domains $[0;1] \to [0;+\infty[$.

2.1.4 Combination of both effect: Additive and Intrinsic noise

This paragraph aims at combining the two kinds of noise, additive and intrinsic noise. Many publications [Puj, 2007]consider individually bathymetric error from additive and intrinsic noise and sum up their contribution it quadratically.

$$\delta_{tot}{}^2 = \delta_{ad}{}^2 + \delta_{it}{}^2 \tag{2.1.41}$$

Other publications [Lur, 2001] propose to consider the final noise N_{tot} as the sum of the individual two kinds of noise (N_{ad} for additive noise andN_{in} for intrinsic noise) as $N_{tot} = N_{ad} + N_{in}$and thus define a final signal to noise ratio ($d_{tot} = S/(N_{ad} + N_{in})$) by the inverse of the sum of individual signal to noise ratio inverses.

$$\frac{1}{d_{tot}} = \frac{1}{d_{ad}} + \frac{1}{d_{in}} \tag{2.1.42}$$

These two combination methods even if they give good approximations can seem a bit rough. The model exposed here (developed in [Sin, 2002] and [Zeb, 1992]but only considering square CW signal) aims at combining additive and intrinsic noise with no rough assumptions. The expression of the total resulting signal to noise ratio will be given as a function of the individually-taken signal to noise ratios which have been defined in the previous sections 2.1.2 and 2.1.3 (from additive and intrinsic noises).

Let the received signal by subarray A (res. B) signal $S_{a,tot}$ (res. $S_{b,tot}$) be considered as the summation of the S_a (res. S_b) which is the same as the one defined in paragraph 2.1.3.1 with an additive noise N_a (res. N_b).

$$\begin{cases} S_{a,tot} = S_a + N_a \\ S_{b,tot} = S_b + N_b \end{cases} \tag{2.1.43}$$

The corresponding interferometric coherence coefficient follows its definition in (2.1.25):

$$\mu_{tot} = \frac{\left|\left\langle S_{a,tot}\overline{S_{b,tot}}\right\rangle\right|}{\sqrt{\left\langle S_{a,tot}\overline{S_{a,tot}}\right\rangle \left\langle S_{b,tot}\overline{S_{b,tot}}\right\rangle}} \tag{2.1.44}$$

By estimating the expected value of the terms impacting the interferometric coefficient, it is possible to express the later μ_{tot} as as a function of the coherence coefficient defined in (2.1.36) (it will be noted here as μ_{in}) taking into account only the intrinsic noise and signal to noise ratio from additive noise. The expected value of the interferometric term $\left\langle S_{a,tot}\overline{S_{b,tot}}\right\rangle$ is:

$$\left\langle S_{a,tot}\overline{S_{b,tot}}\right\rangle = \left\langle S_a\overline{S_b}\right\rangle + \left\langle S_a\overline{N_b}\right\rangle + \left\langle N_a\overline{S_b}\right\rangle + \left\langle N_a\overline{N_b}\right\rangle \tag{2.1.45}$$

Assuming that the noise terms on the two subarrays N_a and N_b are independent from one to the other and independent from signals S_a and S_b (common hypothesis) and that their expected value are null.

$$\left\langle S_{a,tot}\overline{S_{b,tot}}\right\rangle = \left\langle S_a\overline{S_b}\right\rangle \tag{2.1.46}$$

Considering the denominator of (2.1.44) which can be expressed by using:

$$\begin{cases} \left\langle S_{a,tot}\overline{S_{a,tot}}\right\rangle = \left\langle S_a\overline{S_a}\right\rangle + \underbrace{\left\langle S_a\overline{N_a}\right\rangle + \left\langle N_a\overline{S_a}\right\rangle}_{=0} + \left\langle N_a\overline{N_a}\right\rangle = \left\langle S_a\overline{S_a}\right\rangle \left(1+\frac{1}{d_{ad}}\right) \\ \left\langle S_{b,tot}S^*_{b,tot}\right\rangle = \left\langle S_b\overline{S_b}\right\rangle + \underbrace{\left\langle S_b\overline{N_b}\right\rangle + \left\langle N_b\overline{S_b}\right\rangle}_{=0} + \left\langle N_b\overline{N_b}\right\rangle = \left\langle S_b\overline{S_b}\right\rangle \left(1+\frac{1}{d_{ad}}\right) \end{cases} \tag{2.1.47}$$

the coherence coefficient is thus equal to:

$$\mu_{tot} = \frac{\left|\left\langle S_a\overline{S_b}\right\rangle\right|}{\sqrt{\left\langle S_a\overline{S_a}\right\rangle \left\langle S_b\overline{S_b}\right\rangle}.\left(1+\frac{1}{d_{ad}}\right)} = \frac{\mu_{in}}{\left(1+\frac{1}{d_{ad}}\right)} \tag{2.1.48}$$

By considering the general link between the coherence coefficient and the signal to noise ratios as $d = \frac{\mu}{1-\mu}$ or by its inversion $\mu = \frac{d}{1+d} = \frac{1}{1+1/d}$, it can be shown that the global coherence ratio is the product of intrinsic coherence ratio and the coherence ratio defined as a function of the signal to additive noise ratio (2.1.49).

$$\mu_{tot} = \mu_{in}\mu_{ad} \qquad \text{with} \qquad \mu_{ad} = \frac{d_{ad}}{(1+d_{ad})} \tag{2.1.49}$$

In addition by substituting the coherence ratio by their expression as a function of the signal to noise ratio as in (2.1.50), , it can be shown that :

$$\frac{1}{\left(1+\frac{1}{d_{tot}}\right)} = \frac{1}{\left(1+\frac{1}{d_{ad}}\right)\left(1+\frac{1}{d_{in}}\right)} \tag{2.1.50}$$

It leads to the expression of the global SNR as a function of additive-noise and intrinsic-noise SNRs :

$$\frac{1}{d_{tot}} = \frac{1}{d_{ad}} + \frac{1}{d_{in}} + \frac{1}{d_{ad}d_{in}} \tag{2.1.51}$$

It can be noticed a certain similitude between (2.1.42) and(2.1.51). A difference is made by the cross term of signal to noise ratio (intrinsic and additive). This term plays a role only when additive noise and intrinsic noise are high and equivalent in amplitude, which is rarely the case, excepted for central beams with a very deep seafloor.

2.1.5 Noise level on phase ramps

The aim of this part is to analyse the statistical properties of the phase difference of the interferometric signals $S_a$and S_b, more precisely, its mean (which would give the eventual bias) and its standard deviation (which would give the noise level of the phase difference measurement). Indeed, the phase ramp (phase of $S_aS_b^*$) is the phase difference between the two interferometric signals S_a and S_b.

2.1.5.1 Statistics on the interferometric signal phase difference

Consider that the interferometric signals S_a and S_b are random variables modelled as Gaussian-distributed. This hypothesis could be justified by the backscattering formation of the received signal. Indeed by considering that the number of scatterers is statistically high in a resolution cell, the central limit theorem confirms this Gaussian statistic model [Hel, 2003, Hel,1998, Che, 2004]. In addition the additive noise is considered as Gaussian as well. And thus, the summation of the contribution of the backscatterers (which constituted a Gaussian variable thanks to the central limit theorem) plus a Gaussian additive noise, has a random Gaussian behaviour which is modelled by:

$$\begin{cases} S_a &= x_a + iy_a = r_a e^{i\varphi_a} \\ S_b &= x_b + iy_b = r_b e^{i\varphi_b} \end{cases} \tag{2.1.52}$$

Where x_i and y_i are zeros mean Gaussian variables and thus r_i presents a Rayleigh distribution with parameter σ^2 (equal for the two sensors since the two signals statistics have same amplitude) and φ_i is uniformly distributed between $-\pi$ and π. It is reminded that we search the statistic (density, mean, standard deviation) of the random variable $\Delta\phi$ defined as $\Delta\phi = \arg(S_aS_b^*) = \varphi_a - \varphi_b$. The different steps of calculation are developed in Appendix B.

Probability density Let us introduce the correlation coefficient η

$$\eta = \frac{\langle S_aS_b^* \rangle}{\sqrt{\langle S_aS_b^* \rangle \langle S_bS_b^* \rangle}} = \mu e^{i\psi} \tag{2.1.53}$$

In equation (2.1.53), the coherence coefficient μ as it has previously been defined in (2.1.44), is used.

The probability density of the phase difference between S_a and $S_b$is given by: (see calculation development on Appendix B)

$$f(\Delta\phi) = \frac{(1-\mu^2)}{2\pi}\left[\frac{1}{1-Y^2} + \frac{Y}{(1-Y^2)^{3/2}}\left(\frac{\pi}{2} + \text{asin}Y\right)\right] \tag{2.1.54}$$

With:

$$Y = \mu \cos(\varphi_a - \varphi_b - \psi) = \mu \cos(\Delta\phi - \psi) \tag{2.1.55}$$

It can be noticed from this expression than when the coherence μ between the two interferometric signals drops to 0, the density repartition of the phase difference between these two signals tends to an uniform function on the interval -π toπ. This seems evident if the two signals S_a and S_b do not have any coherent part, that the phase difference between can take any value between -π and π with equi-chance. If the coherence reaches one the repartition function looks like to a Dirac function in ψ. Let us remember that ψ is the phase of the expected value of $S_a S_b^*(\psi = \arg(\langle S_a S_b^* \rangle))$, which is slightly different to the expected value of the phase of $S_a S_b^*$ (parameter which is aimed to be calculated in the next section and named as $\langle \Delta\phi \rangle = \langle \arg(S_a S_b^*) \rangle$) . $\psi$is the parameter which is search to be estimated.

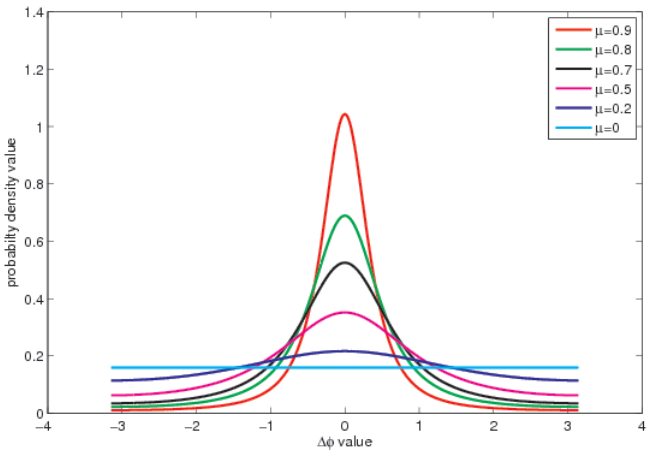

Figure 2.1.7: Probability density of the phase difference of two signals depending on their coherence ratio with$\psi = 0$

Let note that if $\psi = 0$ which is the case at the theoretical instant of detection the probability density of $\Delta\phi$ is centered thus the expected value of $\Delta\phi$ should be zero and equal to ψ. The estimator$\Delta\phi$ is thus unbiased (see next paragraph on the expected value). In addition by considering that ψ is null, the probability density depends only on the coherence coefficient μ. The lower the coherence ratio μ, the more spread the probability density (until reach the equiprobable repartition when $\mu = 0$) see Figure (2.1.7). This tends to affirm that the variance (spread of the density probability around the mean) is a decreasing function of the coherence ratio. Finally the noise level on the phase difference estimator (standard deviation or square root of the variance) increases with the coherence level drop down (see: next paragraph on variance).

Phase difference Expected value By definition the expected value of$\langle \Delta\phi \rangle$is:

$$\langle \Delta\phi \rangle = \int_{-\pi}^{\pi} \Delta\phi \, f(\Delta\phi) \, d\Delta\phi \tag{2.1.56}$$

Going through different steps of calculation (see Appendix B), final expression of the expected value of $\Delta\phi$is:

$$\langle\Delta\phi\rangle = \frac{\mu\sin\psi}{\sqrt{1-(\mu\cos\psi)^2}}\text{acos}\left(\mu\cos\psi\right) \tag{2.1.57}$$

As expected when the coherence between the 2 interferometric signals drops to 0, the mean value of the phase difference tends to 0 whatever the value ofψ. This is predictable since in this case, it tends to be the expected value of a uniform random variable whose value is between $-\pi$and π (see Figure 2.1.7). If the coherence value tends to 1, the expected value of the phase difference tends to ψ and the estimator is unbiased. Here it is found back that if ψ equals zeros (case at the theoretical detection instant) the expected value is null and the estimator is unbiased.

If ψ is not null and the coherence level of interferometric signal is low, the estimator of ψ given by the phase difference of the interferometric signals is bias. (i.e $\langle\arg S_aS_b^*\rangle \neq \arg\langle S_aS_b^*\rangle$) This can be explained by the fact that the expected value operator $\langle.\rangle$ processed before the operator arg{.} operates as a smoothing operation. If the operator arg{.} is process before when the coherence level of interferometric signal is low, the phase of $S_aS_b^*$is really noisy and have a non null probability to jump over π or below $-\pi$. If in addition ψ is not null for example positive, the phase has more chances to jump over π. Since the operator arg{.} is defined modulo 2π the observed phase is pulled down. And thus its expected value of the estimator is biased.

Phase difference Variance By definition the variance is expressed as:

$$\text{var}\left\{\Delta\phi\right\} = \left\langle\Delta\phi^2\right\rangle - \langle\Delta\phi\rangle^2 \tag{2.1.58}$$

Going through different steps of calculation (Appendix B) , final expression of the expected value of $\Delta\phi^2$is:

$$\left\langle\Delta\phi^2\right\rangle = \frac{\pi^2}{3} - \pi\text{acos}\left(\mu\cos\psi\right) + \left[\text{acos}\left(\mu\cos\psi\right)\right]^2 - \frac{1}{2}\sum_{i=1}^{\infty}\frac{\mu^{2i}}{i^2} \tag{2.1.59}$$

then the variance is [Puj, 2007, Sin, 2002, Oli, 1996]:

$$\text{var}\left\{\Delta\phi\right\} = \frac{1-\mu^2}{1-(\mu\cos\psi)^2}\left(\frac{\pi^2}{4} - \pi\text{asin}\left(\mu\cos\psi\right) + \left[\text{asin}\left(\mu\cos\psi\right)\right]^2\right) + \frac{1}{2}\sum_{i=1}^{\infty}\frac{1-\mu^{2i}}{i^2} \tag{2.1.60}$$

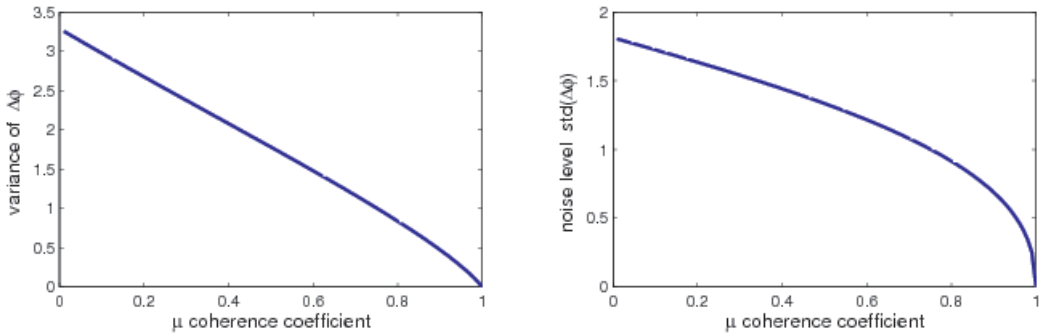

(a) Variance of $\Delta\phi$ (b) Standard deviation of (noise level on) $\Delta\phi$

Figure 2.1.8: Variance and standard deviation of the phase difference $\Delta\phi$as a function of coherence ratio μ

As expected the variance of the phase difference $\Delta\phi$ is a decreasing function of the coherence level of the interferometric signals (Figure 2.1.8). The variance is maximal when the coherence is null and equals $\pi^2/3$ (uniformly distributed random variable between $-\pi$ and π) and minimum equalling 0 when interferometric signals are fully coherent $\mu = 1$.

The standard deviation of the interferometric phase difference is not a linear function of the coherence ratio (Figure 2.1.8). It means that a really little decrease of interferometric signals coherence will much increase the noise level observed in their phase difference (noise level throughout the phase ramp) measurement.

2.1.5.2 Approximation as signal to noise ratio function

A approximations of (2.1.60) has been proposed in [Lur, 2001] with the use of the signal to noise ratio$d$ defined as $d = \mu/(1-\mu)$.

$$\sigma_1(\Delta\phi) = \sqrt{\mathrm{var}\,(\Delta\phi)} = \frac{2}{\sqrt{\frac{12}{\pi^2} + d}\left(1 - 0.05\frac{d}{d+1}\ln d\right)} \tag{2.1.61}$$

A second approximation has more-recently been proposed as:

$$\sigma_2(\Delta\phi) = 2\sqrt{\frac{1 + \frac{d}{d+1}\left(-0.435 + 0.25\ln d\right)}{\frac{12}{\pi^2} + \frac{1}{1/d + 1/d^2}}} \tag{2.1.62}$$

These two formulas (blue : equation (2.1.61) ; red: equation (2.1.62)) have been represented in Figure 3.3.4 as a function of $\log(d)$. They show really close results.

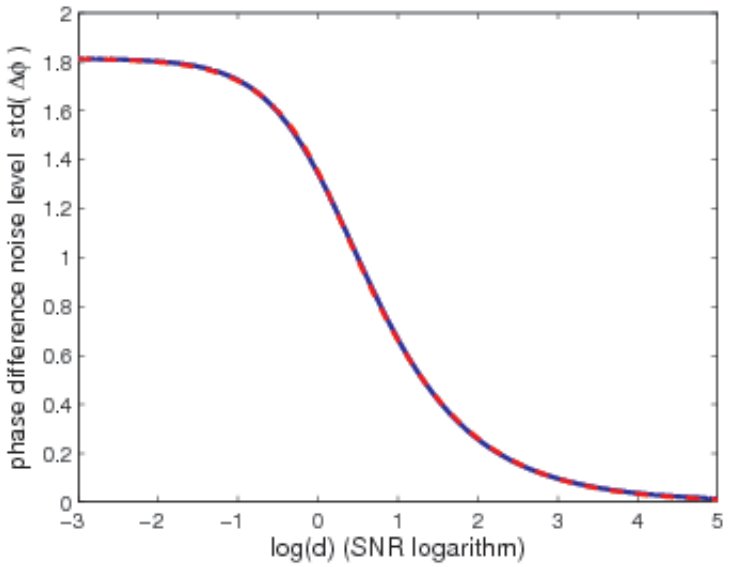

Figure 2.1.9: Noise level on phase difference as a function of the SNR (blue : equation (2.1.61); red: equation (2.1.62))

As expected, the noise level observed on the interferometric phase is a decreasing function of signal to noise ratio. When signal to noise ratio tends to be null the noise level equals $\pi/\sqrt{3}$ (which is predictable; as the SNR tends to zeros, the interferometric coherence ratio tends to 0. Hence the phase difference of incoherent signals is a uniformly distributed random variable whose standard deviation is $\pi/\sqrt{3}$). Conversely, while the SNR becomes higher, the interferometric signal become more coherent and the standard deviation of their phase difference decreases to becomes null.

2.1.6 Final bathymetry measurement noise using phase detection

Around the detection instant, the interferometric phase difference is approximated by a linear phase ramp whose equation is $\alpha t + \beta$ with an additive noise $n(t)$ whose expected value is $\langle\Delta\phi\rangle - \psi$ with$\langle\Delta\phi\rangle$ given in (2.1.57) and variance is the one predicted in (2.1.60). In first approximation, the expected value of $n(t)$ can can be considered as constant equalling 0. This becomes true by considering that the interferometric signals are coherent enough (interferometric signal coherence level is high in MBES). Its variance is constant on the considered window, which is generally the case if the coherence coefficient of the interferometric signal is high (mainly the case in MBES).

$$\Delta\phi(t) = \alpha t + \beta + n(t) \tag{2.1.63}$$

α and β depend on the interferometer and the seafloor configuration. Considering the seafloor as flat the linearisation of the phase ramp gives the parameters $\alpha$and β of the phase ramp.

$$\begin{cases} t-\tau & = \left[\frac{2H}{c\cos\theta(t)} - \frac{2H}{c\cos\theta}\right] = \frac{2H\tan\theta}{c\cos\theta}\left(\theta(t)-\theta\right) \\ \Delta\phi(t) & = 2\pi f_c \frac{a}{c}\left(\sin\theta(t)-\sin\theta\right) = 2\pi f_c \frac{a}{c}\left(\sin\theta(t)-\sin\theta\right) = 2\pi f_c \frac{a}{c}\left(\theta(t)-\theta\right)\cos\theta \end{cases} \tag{2.1.64}$$

The expected phase ramp as a function of time can be approximated by:

$$\Delta\phi(t) = 2\pi f_c \frac{a}{2H}\frac{\cos^2\theta}{\tan\theta}\left(t-\tau\right) \tag{2.1.65}$$

The linear regression consists in estimating α and β minimizing the quadratic error between the regression and the real phase ramp so that:

$$[\widehat{a},\widehat{b}] = \min_{a,b}\sum_{i=1}^{N}\left(\Delta\phi(t_i) - at_i - b\right)^2 \tag{2.1.66}$$

Here the linear regression is made on N samples.

Finally the estimator takes the values:

$$\begin{cases} \widehat{a} & = \frac{\sum_{i=1}^{N}(\Delta\phi(t_i)-\tilde{\Delta\phi})(t_i-\tilde{t})}{\sum_{i=1}^{N}(t_i-\tilde{t})^2} = a + \frac{\sum_{i=1}^{N}(n_i-\tilde{n})(t_i-\tilde{t})}{\sum_{i=1}^{N}(t_i-\tilde{t})^2} \\ \widehat{b} & = \tilde{\Delta\phi} - \widehat{a}\tilde{t} = b + (a-\widehat{a})\tilde{t} + \tilde{n} \end{cases} \tag{2.1.67}$$

Where $\tilde{\Delta\phi}$and $\tilde{t}$ are respectively the mean on the detection windows of the phase difference value and the time. $\tilde{\Delta\phi} = \frac{1}{N}\sum_{i=1}^{N}\Delta\phi(t_i)$ and $\tilde{t} = \frac{1}{N}\sum_{i=1}^{N}t_i$. From Gauss-Markov theorem, the estimators $\widehat{a}$ and $\widehat{b}$ is the best linear unbiased estimators of α andβ.

The detection instant is estimated by:

$$\widehat{\tau} = -\frac{\widehat{b}}{\widehat{a}} \tag{2.1.68}$$

Unfortunately, the variance of such an estimator is not immediate to calculate. The evaluation of standard deviation of the detected instant estimate is made from the variability (standard deviation) of the processed linear phase ramp. Phase ramp variability is evaluated around the detection instant and projected on the abscissa axis (instant axis), to give the time variability. If the detection window is centred on the expected detection instant the standard deviation of the time detection (see Appendix C) is given by (same as in [Lur, 2010b]):

$$\mathrm{std}\left\{\widehat{\tau}\right\} = \frac{\mathrm{std}\left\{\Delta\phi\right\}}{\alpha\sqrt{N}} \tag{2.1.69}$$

And finally the relative bathymetric measurement error (relative noise level on the detection) is equals to:

$$\frac{\delta H}{H} = \frac{\mathrm{std}\left\{\widehat{\tau}\right\}}{\tau} = \frac{\mathrm{std}\left\{\Delta\phi\right\}}{\beta\sqrt{N}} = \frac{\mathrm{std}\left\{\Delta\phi\right\}}{2\pi f_c \frac{a}{c}\frac{\cos\theta}{\tan\theta}\sqrt{N}} \tag{2.1.70}$$

In addition from the phase ramp regression it is possible to have an unbiased estimator of the noise level over the phase ramp by:

$$\text{std}\left\{\Delta\phi\right\}^2 = \frac{1}{N-2}\sum_{i=1}^{N} e_i^2 = \frac{1}{N-2}\sum_{i=1}^{N}\left(\Delta\phi(t_i) - \widehat{a}t_i - \widehat{b}\right)^2 \tag{2.1.71}$$

Thanks to the theoretical approach exposed in this section, it is possible to express the expected relative bathymetric error with (2.1.70) in case of phase detection, via the noise level on the interferometric phase difference. The phase noise level is calculated from the coherence coefficient of the interferometric signals (expectation from model) which is impacted by intrinsic noise (baseline decorrelation) and additive noise (multiplication of coherence coefficient of the both noise considered separately). The coherence ratio considering additive noise only is predicted using the sonar equation. Whereas, the coherence ratio considering the intrinsic noise only has been found being a particular point of the Fourier transform of the transmitted pulse envelope square (in case of FM, the pulse-compressed squared envelope).

2.2 The Doppler Effect Impact

The Doppler effect has been first assumed to be the main cause of bathymetric degradation when using frequency modulated signals. This section presents the results of the model [Vin, 2011b, Vin, 2011a] predicting the bathymetric Doppler effect impact. The Doppler effect has been studied on two aspects:

- introduction of a measurement bias
- change of the measurement noise level

2.2.1 Bathymetric measurement bias

This part aims at determining how the Doppler effect affects the multibeam beamformed signals, more precisely by estimating the induced bathymetric measurement bias. If the Doppler effect is largely studied and well known, little work has been conducted to understand its impact on the final bathymetric measurement. Bathymetric measurement bias δH (2.2.1) can be induced by two estimation errors: the first one being an error of the arrival time estimation δt, the second one an error on the observed angle estimation $\delta\theta$.

$$\frac{\delta H}{H} = \frac{\delta t}{t} + \tan\theta.\delta\theta \tag{2.2.1}$$

Here let us introduce two kinds of Doppler effects which could influence the received signal and their possible impact on the beamformed signal:

- **Constant Doppler throughout the antenna array** (all the sensor speeds are equal, *e.g.* caused by heave): Impact depends on which kind of beamforming is applied. If the beamforming is processed with adding a phase shift, since this phase is depending on the signal frequency which is Doppler shifted, an effect/error on the beamforming angle could be observed. By applying a spatial beamforming in time domain, this effect should be limited.
- **Differential Doppler on the two interferometer sources S_a and S_b**: interferometry is applied on two signals with slightly different frequencies (this phenomenon

can be induced by the roll). The question is whether it has an impact on the final interferometry signal.

Nowadays, the precision aimed for the relative error $\frac{\delta H}{H}$ in bathymetry is 10^{-3}.

2.2.1.1 First idea of the Doppler effect on beamformed signal

To have a really rapid first idea of the Doppler effect on beamformed signal, a simple case is first simulated considering only one backscattering point on the seafloor at the direction θ (here as example 40°). The aim is to show the effect of the Doppler on the localization of this scatterer. The received signal is simulated (with matched filtering in case of FM signal then beamforming with the steering of the array (phase or time beamforming)). The array is divided into two sub arrays $S_a$and S_b) is a complex signal in function of the steering angle and the time which can be studied in phase and amplitude. The error in the localization of a scatterer on the seafloor can thus come from two aspects: the steering angle (angular localization) and the time (range localization). The simulation can compute linear FM signal (linear chirp) and CW signal. Their envelope is not smoothed and is a simple rectangular function. The following parameters have been chosen: the linear chirp parameters are:

- Central frequency 73kHz
- Bandwidth 0.5kHz
- Duration 20ms

Other simulations are conducted with an equivalent CW signal with the following

- Central frequency 73kHz
- Duration 2ms (reverse to the chirp bandwidth so that the two compared signal CW and FM present equivalent bandwidth)

The array is 1 m long and features 128 sensors. The chosen baseline spacing is 1/3 of the whole array length. The sound speed velocity is 1500m and the seafloor is flat and 500m-deep.

The results in the localization of the scatterer in the interferometry map (in angle and time) are presented in the following table, considering the two ways of beamforming (phase or time beamforming) (sensors speed is vertical equal to 2m/s or on rotation 1°/s)

	Phase beamforming	**Time beamforming**
CW without Doppler	40° - 876.1ms	40° - 876.1ms
CW with Doppler in transmission	**40.05°** - 876.1ms	40° - 876.1ms
CW with Doppler in reception	40° - 876.1ms	**39.95°** - 876.1ms
CW with differential Doppler	40° - 876.1ms	40° - 876.1ms
FM without Doppler	40° - 876.1ms	40° - 876.1 ms
FM with Doppler in transmission	**40,02°** - **873.4 ms**	40° - **873.4 ms**
FM with Doppler in reception	**39.98°** - **873.4 ms**	**39.95°** - **873.4 ms**
FM with differential Doppler	40° - 876.1ms	40° - 876.1 ms

Table 2.2: Simulation result localisation of one single backscatterer in case of the Doppler effect

Depending on the type of signal and beamforming, the error observed on localization can be in angle (highlighted in red in Table 2.2) or in range (highlighted in blue in Table 2.2).

This short section points out the Doppler effect on the beamformed output can take two different aspects:

- a time detection error due to the matched filtering mismatch in case of FM signals use. This phenomenon is well known and predictable.
- a bias on the beam steering angle direction. This aspect was until now not known and not taken into account on the final bathymetry measurement.

Section 2.2.1.2 aims at modelling and quantifying the Doppler effect on the beamformed signal in case of FM and CW depending on the beamformer type. It will confirm the two errors in: beam angular steering and time detection. Section 2.2.1.2 will also describe the impact of the beam steering error on the time detection estimation.

2.2.1.2 Modelling

The signal received on each subarray is modelled by its resultant component at the subarray phase centre. It remains to consider 2 single receivers rather than taking a receiver array.

The complex array motion is assumed to be possibly divided into two simple components:

- Translation (heave, sway) of the array centre in a given direction: the array motion in this case is a constant speed movement of the two subarray phase centres (same amplitude, same direction)
- Rotation (roll, pitch and yaw) applied on the array considering its centre as rotation centre: the array motion is a constant speed movement of the two subarray phase centres with same amplitude but opposite direction.

To simplify the problem, consider one single scatterer located at angular position $\gamma$and in range R. A delay τ is associated with the two-way time $\tau = 2R/c$. By expressing the effective propagation distance (taking into account the motion), it is possible to get an expression of the signal received at the instant t_r as function to the signal transmitted at the instant t_e. The sensor speeds are assumed constant and are expressed as their projection on the scatterer angular direction.

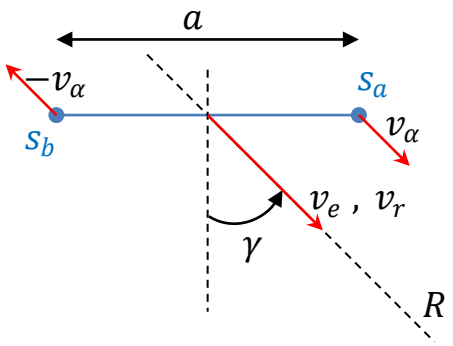

Figure 2.2.1: Doppler effect modelling : geometrical configuration

A temporal expression of the received signal can be expressed for sensor #1 as:

$$c.(t_r - t_e) = (R - v_e t_e) + \left(R - (v_r + v_\alpha)(t_r - \tau) - \frac{a}{2}\sin\gamma\right) \tag{2.2.2}$$

By expressing t_r as a function of t_e, the received signal expression is deducted as the delayed version of the transmitted signal.

$$s_a(t) = s\left(\frac{k_{r1}}{k_e}(t-\tau) + \frac{1}{k_e}\frac{a\sin\gamma}{2c}\right) \quad \text{with } k_e = 1 - \frac{v_e}{c} \text{ and } k_{r1} = 1 + \frac{v_r + v_\alpha}{c} \tag{2.2.3}$$

Similarly for sensor #2:

$$s_b(t) = s\left(\frac{k_{r2}}{k_e}(t-\tau) - \frac{1}{k_e}\frac{a\sin\gamma}{2c}\right) \quad \text{with } k_e = 1 - \frac{v_e}{c} \text{ and } k_{r2} = 1 + \frac{v_r - v_\alpha}{c} \tag{2.2.4}$$

The Doppler effect on CW signals In case of a CW signal the received signal is on a single frequency f_c so that the considered signal s is $e^{2\pi i f_c t}$, the localisation of the scatterer is made after beamforming by annulling the phase difference of the two received signal s_a and s_b. The effect on the localisation will be different according to the type of beamforming used.

Phase beamforming When beamforming at angle θ, the steering is introduced as a phase compensation term. The phase difference between s_a and s_b is:

$$\Delta\phi = 2\pi f_c\left(\left(\frac{k_{r2}}{k_e}(t-\tau) - \frac{1}{k_e}\frac{a\sin\gamma}{2c} + \frac{a\sin\theta}{2c}\right) - \left(\frac{k_{r1}}{k_e}(t-\tau) + \frac{1}{k_e}\frac{a\sin\gamma}{2c} - \frac{a\sin\theta}{2c}\right)\right) \tag{2.2.5}$$

Annulling the phase difference leads to:

$$2v_\alpha(t-\tau) + a\sin\gamma - (1 - \frac{v_e}{c})a\sin\theta = 0 \tag{2.2.6}$$

Here it can be found that the scatterer is localised when beam angle $\theta = \text{asin}\left[\frac{\sin\gamma}{1-\frac{v_e}{c}}\right]$ and $t = \tau$, the scatterer is well localised in range (time) but the Doppler effect introduces a bias in its angular localisation $\delta\theta$ (scatterer estimated at$\theta = \gamma + \delta\gamma$ instead of γ).

$$\delta\gamma = \text{asin}\left[\frac{\sin\gamma}{1-\frac{v_e}{c}}\right] - \gamma = \frac{1}{\sqrt{1+\sin^2\gamma}}\frac{v_e}{c}\sin\gamma = \frac{v_e}{c}\tan\gamma \approx \frac{v_e}{c}\tan\theta \tag{2.2.7}$$

The beam axis is along the angular direction γ (equal $\theta - \delta\gamma$) rather than the expected θ. Considering positive speed, γ is lower than θ. It explains why in the case of a single backscatterer the target is observed in a beam angle with a positive angle error (see Table 2.2) The error in beam angle steering induces an error on seafloor localisation (see Figure 2.2.2)

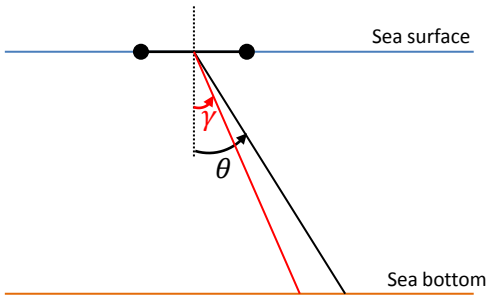

Figure 2.2.2: Impact of angle steering error #1

Time beamforming when beamforming at angle θ, the steering is introduced as a temporal delay. The phase difference between s_a and s_b after compensation is thus:

$$\Delta\phi = 2\pi f_c \left[\left(\frac{k_{r2}}{k_e}(t - \tau + \frac{a\sin\theta}{2c}) - \frac{1}{k_e}\frac{a\sin\gamma}{2c} \right) - \left(\frac{k_{r1}}{k_e}(t - \tau - \frac{a\sin\theta}{2c}) + \frac{1}{k_e}\frac{a\sin\gamma}{2c} \right) \right] \tag{2.2.8}$$

Annulling the phase difference leads to:

$$2v_\alpha(t-\tau) + a\sin\gamma - (1 + \frac{v_r}{c})a\sin\theta = 0 \tag{2.2.9}$$

As for phase beamforming case, it can be noticed that the scatterer is well localised in range (time delay equals τ) while the Doppler effect has introduced a bias in the angular localisation (angular estimation being in this case $\theta = \text{asin}\left[\frac{\sin\gamma}{1+\frac{v_r}{c}}\right]$). The introduced bias is:

$$\delta\gamma = \text{asin}\left[\frac{\sin\gamma}{1+\frac{v_r}{c}}\right] - \gamma = -\frac{v_r}{c}\tan\gamma \tag{2.2.10}$$

Inversely to the previous case, here only the receiving array motion plays a role in the scatterer localisation error. The beam axis is along the angular direction γ (equal $\theta - \delta\gamma$) rather than the expected θ. Considering positive speed, γ is more important than θ. In this condition, the single backscatterer is observed in a beam angle with a negative angle error (see Table 2.2) As previously, the error in beam angle steering induces an error on seafloor localisation. In the case of flat seafloor, the beam oriented toward γ will meet deeper seafloor that the expected one at θ (see Figure 2.2.3).

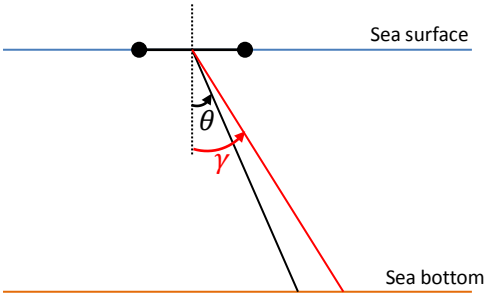

Figure 2.2.3: Impact of angle steering error #2

The Doppler effect on LFM signals In the case of LFM signal, the received signals after pulse compression are:

$$\begin{cases} w_a(t) = \int_{-\infty}^{+\infty} s\left(\frac{k_{r1}}{k_e}(u-\tau) + \frac{1}{k_e}\frac{a\sin\gamma}{2c}\right)\overline{s(u-t)}du & \text{with } k_e = 1-\frac{v_e}{c} \text{ and } k_{r1} = 1+\frac{v_r+v_\alpha}{c} \\ w_b(t) = \int_{-\infty}^{+\infty} s\left(\frac{k_{r2}}{k_e}(u-\tau) - \frac{1}{k_e}\frac{a\sin\gamma}{2c}\right)\overline{s(u-t)}du & \text{with } k_e = 1-\frac{v_e}{c} \text{ and } k_{r2} = 1+\frac{v_r-v_\alpha}{c} \end{cases} \tag{2.2.11}$$

The dopplerised signal by the factor η filtered by the matched filter is known as (see Appendix (D)):

$$w(t) = \int_{-\infty}^{+\infty} s(\eta u)\overline{s(u-t)}du \approx e^{2\pi i f_c(1+\frac{\alpha}{2})t} T\Lambda(\frac{t}{T})\text{sinc}\left[\pi\left(f_c\alpha + \frac{B}{T}t\right)T\Lambda(\frac{t}{T})\right] \tag{2.2.12}$$

by using the variable change $\frac{k_{r1}}{k_e}v = \frac{k_{r1}}{k_e}(u-\tau) - \frac{1}{k_e}\frac{a\sin\gamma}{2c} = \frac{k_{r1}}{k_e}v$ for sensor A and $\frac{k_{r2}}{k_e}v + \frac{k_{r2}}{k_e}(u-\tau) + \frac{1}{k_e}\frac{a\sin\gamma}{2c} = \frac{k_{r2}}{k_e}v$ for sensor B in (2.2.11), the expression of the interferometric signals is obtained as follows.

$$\begin{cases} w_a(t) \approx e^{2\pi i f_c(1+\frac{\alpha_1}{2})(t-\tau+\frac{1}{k_{r1}}\frac{a\sin\gamma}{2c})} T\mathbf{\Lambda}(\frac{t}{T})\text{sinc}\left[\pi\left(f_c\alpha_1 + \frac{B}{T}(t-\tau+\frac{1}{k_{r1}}\frac{a\sin\gamma}{2c})\right)T\mathbf{\Lambda}\left(\frac{t-\tau+\frac{1}{k_{r1}}\frac{a\sin\gamma}{2c}}{T}\right)\right] \\ w_b(t) \approx e^{2\pi i f_c(1+\frac{\alpha_2}{2})(t-\tau-\frac{1}{k_{r2}}\frac{a\sin\gamma}{2c})} T\mathbf{\Lambda}(\frac{t}{T})\text{sinc}\left[\pi\left(f_c\alpha_2 + \frac{B}{T}(t-\tau-\frac{1}{k_{r2}}\frac{a\sin\gamma}{2c})\right)T\mathbf{\Lambda}\left(\frac{t-\tau-\frac{1}{k_{r2}}\frac{a\sin\gamma}{2c}}{T}\right)\right] \end{cases} \tag{2.2.13}$$

From this expression, the envelopes of w_a and w_b are obviously shifted. The global time shift on the envelope of $w_a w_b^*$ happens when annulling the term $f_c\alpha + \frac{B}{T}(t-\tau-(1-\frac{v_e}{c})\frac{a\sin\gamma}{2c})$ (with α the mean of $\alpha_1 = \frac{k_{r1}}{k_e} - 1$and $\alpha_2 = \frac{k_{r2}}{k_e} - 1$) which can be simplified by the annullation of $f_c\alpha + \frac{B}{T}(t-\tau)$ taking into account the parameter dimension.

$$\delta_t = -\alpha\frac{f_c}{B}T = -\left(\frac{k_{r1}+k_{r2}}{2k_e} - 1\right)\frac{f_c}{B}T = -\frac{v_e+v_r}{c}\frac{f_c}{B}T \tag{2.2.14}$$

The first impact of the Doppler effect will be to introduce a time shift in the time detection (range estimation).

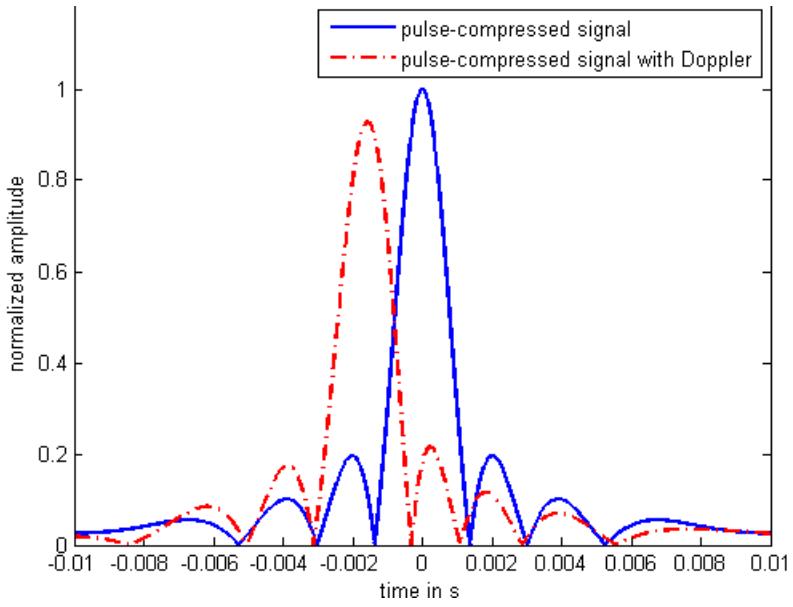

Figure 2.2.4: Matched filter output of a Dopplerized signal, illustrating the time shift of the envelope

As for CW, the two cases of phase beamforming and time beamforming are studied.

Phase beamforming The phase difference of the interferometric signals after compensation (with phase beamforming) is:

$$\Delta\phi = 2\pi f_c \left(\left((1+\frac{\alpha_2}{2})(t-\tau-\frac{1}{k_{r2}}\frac{a\sin\gamma}{2c}) + \frac{a\sin\theta}{2c} \right) - \left((1+\frac{\alpha_1}{2})(t-\tau+\frac{1}{k_{r1}}\frac{a\sin\gamma}{2c}) - \frac{a\sin\theta}{2c} \right) \right) \tag{2.2.15}$$

Annulling the phase difference leads to:

$$2v_\alpha(t-\tau)+\frac{1}{2}(\frac{1+\frac{\alpha_2}{2}}{k_{r2}}+\frac{1+\frac{\alpha_1}{2}}{k_{r1}})a\sin\gamma - a\sin\theta \approx 2v_\alpha(t-\tau)+(1-\frac{v_r}{2c}+\frac{v_e}{2c})a\sin\gamma - a\sin\theta = 0 \tag{2.2.16}$$

Here it can be found that the scatterer is localised when $\theta = \text{asin}\left[\frac{\sin\gamma}{1-\frac{v_r}{2c}+\frac{v_e}{2c}}\right]$ and $t=\tau$, the scatterer is well localised in range (time) but the Doppler effect introduces a bias in its angular localisation $\delta\theta$ (scatterer estimated at$\theta = \gamma + \delta\gamma$ instead of γ).

$$\delta\gamma = \text{asin}\left[\frac{\sin\gamma}{1-\frac{v_r}{2c}+\frac{v_e}{2c}}\right] - \gamma = \frac{v_r - v_e}{2c}\tan\gamma \approx \frac{v_r - v_e}{2c}\tan\theta \tag{2.2.17}$$

In this case, Tx and Rx speeds impact the detection. Assuming that v_r is null and v_e positive, the beam axis being along γ rather that θ, the beam steering error is positive. a little less steered than expected (beam pointing towardγ rather than the expected θ). The angular localisation of a single scatterers is thus negative. It is the opposite when considering v_e as null and v_r positive. In case of continuous seafloor the beam steering error will introduce an error in range localisation.

Time beamforming The phase difference between w_a and w_b after compensation (time beamforming) is :

$$\Delta\phi = 2\pi f_c \left[(1+\frac{\alpha_2}{2}) \left(t - \tau - \frac{1}{k_{r2}} \frac{a\sin\gamma}{2c} + \frac{a\sin\theta}{2c} \right) - (1+\frac{\alpha_1}{2}) \left(t - \tau + \frac{1}{k_{r1}} \frac{a\sin\gamma}{2c} - \frac{a\sin\theta}{2c} \right) \right] \tag{2.2.18}$$

Annulling the phase difference leads to:

$$\begin{aligned} 2v_\alpha(t-\tau) + \frac{1}{2}(\frac{1+\frac{\alpha_2}{2}}{k_{r2}} + \frac{1+\frac{\alpha_1}{2}}{k_{r1}}) a\sin\gamma - (1+\alpha_1+\alpha_2) a\sin\theta = \\ 2v_\alpha(t-\tau) + (1 - \frac{v_r - v_e}{2c}) a\sin\gamma - (1+\frac{v_r+v_e}{2c}) a\sin\theta = 0 \end{aligned} \tag{2.2.19}$$

The same as for the phase beamforming case, it can be noticed that the scatterer is well localised in range (time delay equals τ) while the Doppler effect has introduced a bias in the angular localisation (angular estimation being in this case $\theta = \text{asin}\left[\frac{1+\frac{v_r+v_e}{2c}}{1-\frac{v_r-v_e}{2c}}\sin\gamma\right]$). The introduced bias is:

$$\delta\theta = \text{asin}\left[\frac{1+\frac{v_r+v_e}{2c}}{1-\frac{v_r-v_e}{2c}}\sin\gamma\right] - \gamma = -\frac{v_r}{c}\tan\gamma \tag{2.2.20}$$

When time beamforming, the beam steering error is the same for CW and FM signals. Of course in the case of FM, the time shift from the mismatch of the pulse compression has to be added.

Theoretical Doppler Impact summary To sum up (Table 2.3) , the errors made in the localization of one scatterer can be in angle (steering bias) and in time (shift resulting from the pulse compression of FM signals).

	Phase beamforming			Time beamforming		
	Error $\delta\gamma$ on single scatterer localisation	Errorδt due to beam steering error $\delta\theta$	Error δt due to pulse compression mismatch	Error $\delta\gamma$on single scatterer localisation	Errorδt due to beam steering error $\delta\theta$	Error δt due to pulse compression mismatch
CW - Tx Doppler	$\frac{v_e}{c}\tan\theta$	$-\frac{v_e}{c}\frac{2H}{c}\frac{\tan^2\theta}{\cos\theta}$	0	0	0	0
CW - Rx Doppler	0	0	0	$-\frac{v_r}{c}\tan\theta$	$\frac{v_r}{c}\frac{2H}{c}\frac{\tan^2\theta}{\cos\theta}$	0
FM - Tx Doppler	$\frac{v_e}{2c}\tan\theta$	$-\frac{v_e}{2c}\frac{2H}{c}\frac{\tan^2\theta}{\cos\theta}$	$-\frac{v_e}{c}\frac{f_c}{B}T$	0	0	$-\frac{v_e}{c}\frac{f_c}{B}T$
FM - Rx Doppler	$-\frac{v_r}{2c}\tan\theta$	$\frac{v_r}{2c}\frac{2H}{c}\frac{\tan^2\theta}{\cos\theta}$	$-\frac{v_r}{c}\frac{f_c}{B}T$	$-\frac{v_r}{c}\tan\theta$	$\frac{v_r}{c}\frac{2H}{c}\frac{\tan^2\theta}{\cos\theta}$	$-\frac{v_r}{c}\frac{f_c}{B}T$

Table 2.3: Doppler estimation bias

The estimated orders of magnitude fit the simulated observations. For a vertical speed v=2m/s, projected on the direction of the observation 40° , the steering error is $\delta\theta = \frac{v}{c}\sin\theta$=0.049° , the same as the error on the simulated results (Section 2.2.1.1).

In case of continuous seafloor the error in beam steering angle causes an error in range localisation (time error), since the time delay is given by:

$$t = \frac{2H}{c\cos\theta} \tag{2.2.21}$$

The time error caused by the beam angle bias is:

$$\delta t = \frac{2H}{c}\frac{\tan\theta}{\cos\theta}\delta\theta = -\frac{2H}{c}\frac{\tan\theta}{\cos\theta}\delta\gamma \tag{2.2.22}$$

Equation (2.2.22) was used to fill Table (2.3).

Finally the relative bathymetric error ($\delta H/H = \delta t/t$) caused by the Doppler effect is presented in Table (2.4).

	Phase beamforming		Time beamforming	
	Error $\delta t/t$ due to the beam steering error	Error $\delta t/t$ due to dopplerized matched filter	Error $\delta t/t$ due to the beam steering error	Error $\delta t/t$ due to dopplerized matched filter
CW	$-\frac{v_e}{c}\tan^2\theta$	0	$\frac{v_r}{c}\tan^2\theta$	0
FM	$\frac{v_r - v_e}{2c}\tan^2\theta$	$-\frac{v_r+v_e}{2H}\frac{f_c}{B}T\cos\theta$	$\frac{v_r}{c}\tan^2\theta$	$-\frac{v_r+v_e}{2H}\frac{f_c}{B}T$

Table 2.4: Doppler estimation bias on relative bathymetry measurments

The time error (δt) introduced by the matched filtering mismatch is independent to the depth and depends on array motion, beam angle and chirp parameters. The error from the beam steering bias increases with depth and beam angle, precisely when other bathymetric degradations (such as additive noise) are more important. It explains why this phenomenon has not been observed before. However, its order of magnitude is about the nowadays requirement (relative bathymetric quality measured as relative error being about 10^{-3}).

2.2.1.3 Validation from simulation

A simulation has been conducted in order to simulate the effect of the Doppler on the final signal $S_a S_b^*$ and its impact on the seafloor detection. The results are to the theoretical prediction made part 2.2.1.2.

Simulation description A flat seafloor is modelled by an array of scatterers. The number of scatterers inside a resolution cell is equal to 20. A random multiplicative coefficient is associated with each scatterer with the form $\alpha = X + iY$ (X and Y being centered Gaussian random variables) which is equivalent to a Rayleigh distribution for the amplitude of α and an uniform-distribution for its phase.

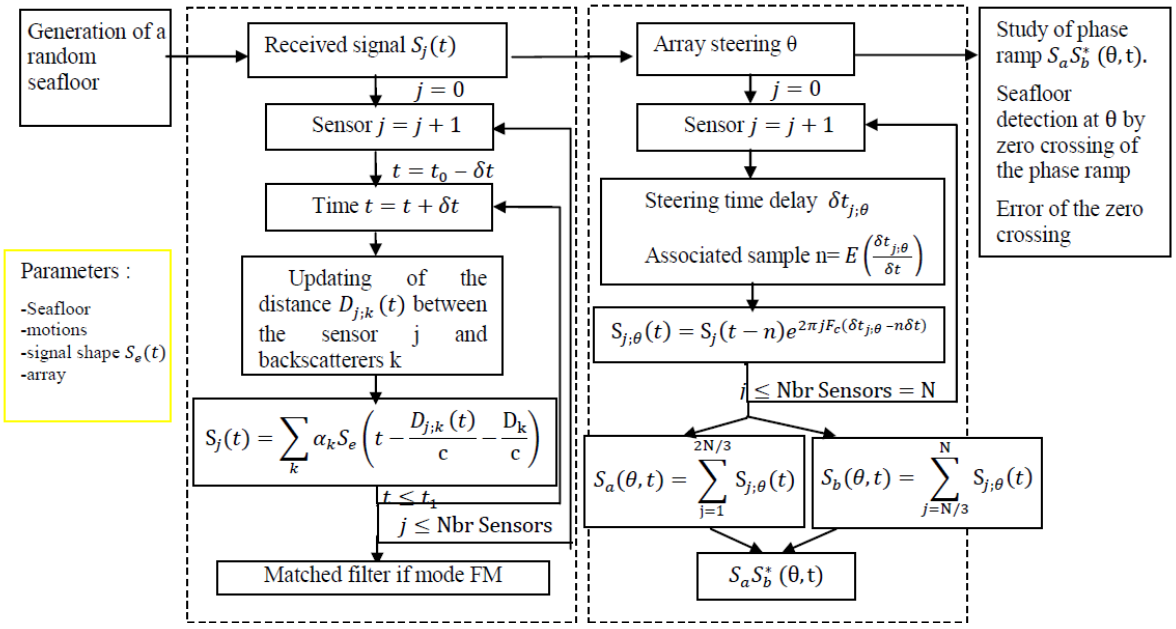

Figure 2.2.5: Simulation scenario

The simulation computes at each instant the distance between each elementary scatterer and array stave element. It identifies the contributing scatterers on a given stave and computes received signal. Since the arrays are in relative motion the distance between a stave receiver and a scatterer is varying depending on time, Doppler effect is included in this range variation. The rest of the processing is classic (Figure 2.2.5) : once the received signals have been calculated, the beam is steered by using time beamforming as described in section 1.1.2.3 and the summation is made one two third of the array. Then the phase of $S_a S_b*$ (phase difference of the interferometric signals) is processed. For each beam angle θ the phase ramp, statistics is evaluated. The TOA is estimated at the zero crossing of the phase ramp. Time uncertainty caused by the Doppler effect is calculated and compared to the model prediction (Table 2.3).

Heave simulations Simulations have been for different motions of the array. The motion considered here is vertical and sinusoidal (simulating the heave effect) following the form $A\sin(2\pi(t-\tau)/T)$. The simulated cases are not realistic taking extreme value parameters (ex: simulation 2 and 3) in order to visually observe phenomenon on the temporal signal.

	A	T
Simulation 0 (without Doppler)	0m	10s
Simulation 1	1m	10s
Simulation 2	5m	10s
Simulation 3	10m	10s

Table 2.5: Simulation heave parameters

The simulated seafloor is constant for all the simulations in order to compare the results. The results are considered at beam 40°. Since the receiving array speed is not null in this

direction. Doppler effect should impact the beamformed signal in terms of angular and time localisation as predicted in section 2.2.1.2. Figure 2.2.6 presents the amplitude of $S_a S_b*$ around the considered beam at 40° [Vin, 2011a, Vin, 2011b]. In this Figure, it can be seen that highlight spots are shifted by the Doppler effect. This shift is both in angle (toward smaller angle) and time (toward smaller delay). Here the speeds are positive (counted toward the bottom). The received signal is thus compressed in time by the Doppler effect. The time shift after pulse compression is thus negative. In addition, in such a condition, the beam steering angle error is positive and the angular error in the localisation of one single scatterer (likened to highlight spot) is negative. Model in section 2.2.1.2 tends to support the observations made in Figure 2.2.6.

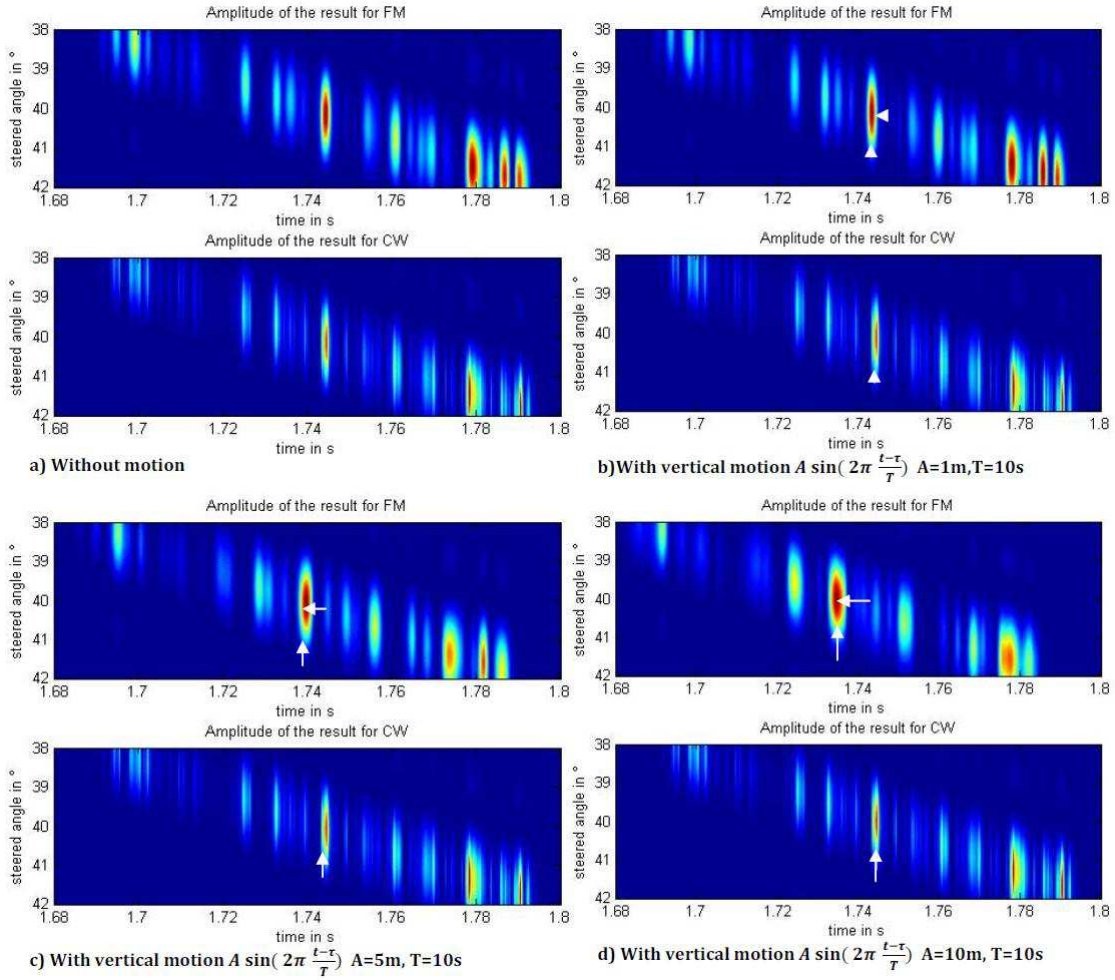

Figure 2.2.6: Amplitude of $S_a S_b^*$ for various different Doppler cases: (heave effect modelled as a sine function with different amplitude) for CW and FM, illustrating the time shift from the matched filter (FM) and the steering angle bias (FM and CW).

Figure 2.2.7 presents the result of $S_a S_b^*$ in term of phase for the beam expected at 40°. The estimation in term of zero-crossing of the phase ramp gives the measurement bias caused

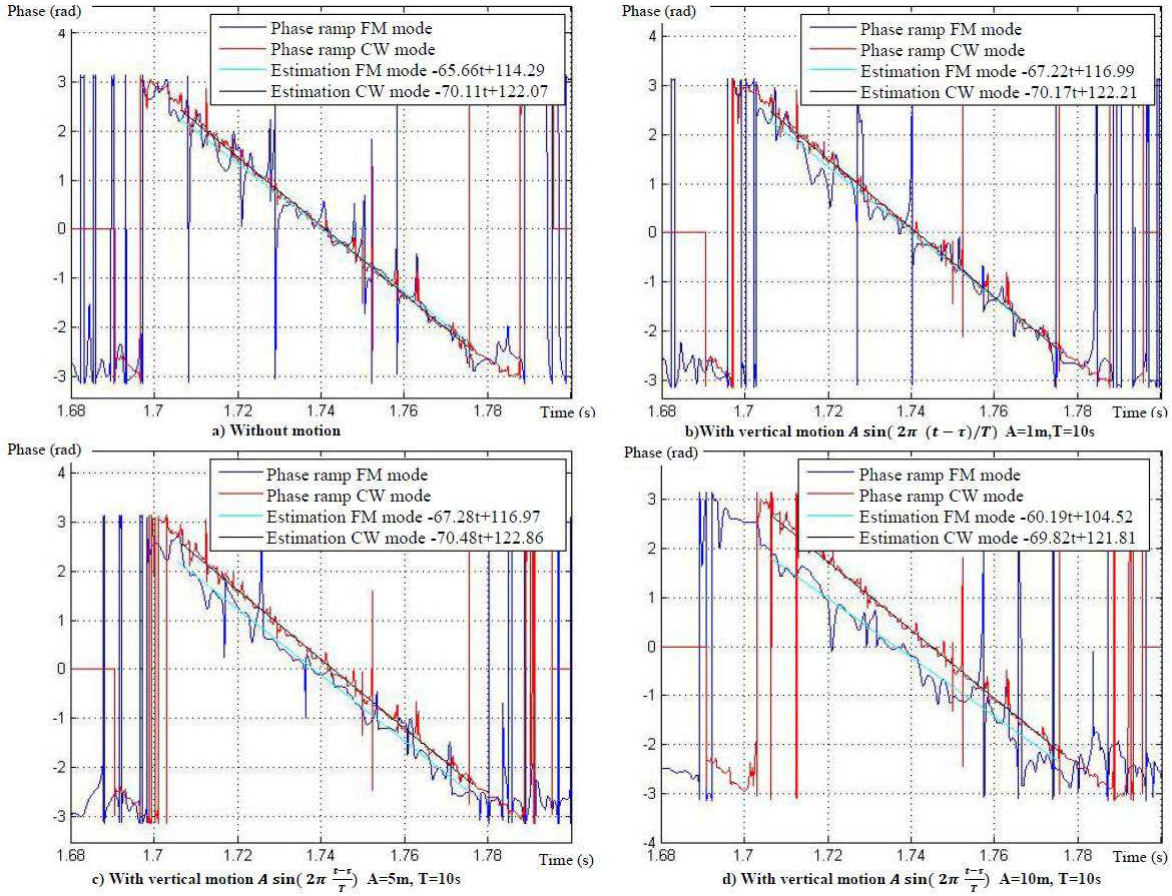

Figure 2.2.7: Phase ramp (beam 40°) in different Doppler effect cases (heave modeled as sine function with different amplitude A) subplot a) without Doppler effect A=0m, subplots b) c) d) with the Doppler Effect resp. A= 1, 5, 10 m.

by Doppler effect. Estimation from simulations are presented in Table 2.6.

Simulation	Without motion	Vertical motion A=1m,T=10s	Vertical motion A=5m,T=10s	Vertical motion A=10m,T=10s
Noise on CW	0.138 rad	0.143 rad	0.146 rad	0.299 rad
Noise on FM	0.452 rad	0.392 rad	0.245 rad	0.551 rad
Time error on CW	0 s	4.0 10^{-4} s	2.0 10^{-3} s	3.9 10^{-3} s
Time error on FM	0 s	-3.0 10^{-4} s	-2.7 10^{-3} s	-5.4 10^{-3} s

Table 2.6: Time detection error and noise estimation from simulations with the various Doppler cases, case 1: without Doppler (reference) cases 2, 3 4: with heave motion as a sine function with amplitude 1, 5, 10 m

It confirms that the simulation results using FM pulse presents a really noisier phase ramp

than the CW. The noise level is almost three times the value observed with CW pulse, this is due to baseline decorrelation and will be explain in the next chapter 2.3. Without getting into details, the expected noise level caused by baseline decorrelation alone is around 0.13 rad for CW, against 0.37 rad for FM. This is due to the impact of the pulse shape and notably the compressed pulse sidelobe impact. This will be discussed more in section 2.2.2.2.

The results from Table 2.6 in terms of time detection error is compared to prediction of the model developed in section 2.2.1.2.

It is reminded that the time error from the steering angle bias caused by the Doppler effect is:

$$\delta t_1 = \frac{2H}{c}\frac{v_r}{c}\frac{\tan^2\theta}{\cos\theta} \tag{2.2.23}$$

and from the mismatched of the Dopplerized signal and matched filter:

$$\delta t_2 = -\frac{v_r}{c}\frac{f_c}{B}T \tag{2.2.24}$$

Finally ,the calculation in our case with $v_r = 2\pi A/T$ with its projection on the θ direction gives the following theoretical results presented in Table 2.6.

Theory	Vertical motion A=1m,T=10s	Vertical motion A=5m,T=10s	Vertical motion A=10m,T=10s
Error δt due to $\delta\theta$	3.9 10^{-4} s	2.0 10^{-3} s	3.9 10^{-3} s
Error δt due to matched filter	-9.4 10^{-4} s	-4.7 10^{-3} s	-9.4 10^{-3} s
CW theoretical results	3.9 10^{-4}s	2.0 10^{-3} s	3.9 10^{-3} s
FM theoretical results	-5.4 10^{-4} s	-2.7 10^{-3} s	-5.4 10^{-3} s

Table 2.7: Numerical results from model for the different Doppler (heave motion as sine function with amplitude 1, 5 , 10m) cases on beam 40°

Conclusion: The comparison between the simulation results in Table 2.6 and the model estimation in Table 2.7 gives the same orders of magnitude, thus validating the model exposed in 2.2.1.2, regarding the bathymetric error caused by the Doppler effect. In the case of FM, the error is twofold. First the signal envelope is shifted in time due to the matched filtering mismatch. This is routinely corrected by a predicted linear time shift (from the time-frequency FM ambiguity). In addition, there is an error due to an uncertainty in the beam steering angle. This happens also on CW signals. This aspect of things was not known before this study and should be taken into account to improve bathymetric measurements. Since it impacts more at large beam angles, and its effect could have been vanished into other degradation causes, such as additive noise impact. It has not been perceived as a limitation for CW and has been neglected until now. Considering that the time shift due to pulse compression mismatch is well corrected, Doppler effect does not affect more bathymetric signal from FM than the one from CW.

Roll simulation Another set of simulations has been conducted to simulate differential Doppler effect from rotation motion such as roll (rotation motion follows the form $A\sin(2\pi(t-\tau)/T)$). It is reminded that prediction has concluded that the roll does not affect the bathymetry results (no measurement bias).

	A	T
Simulation 0 (without Doppler)	0°	10s
Simulation 1	5°	10s

Table 2.8: Roll simulation description, differential doppler

Moreover, the simulated seafloor is the same for all simulations in order to compare the results. Figure 2.2.8 presents the results in amplitude of $S_a S_b^*$ around the steering angle 40°. This figure shows no apparent difference between the case without Doppler and the case with the roll motion effect, as predicted.

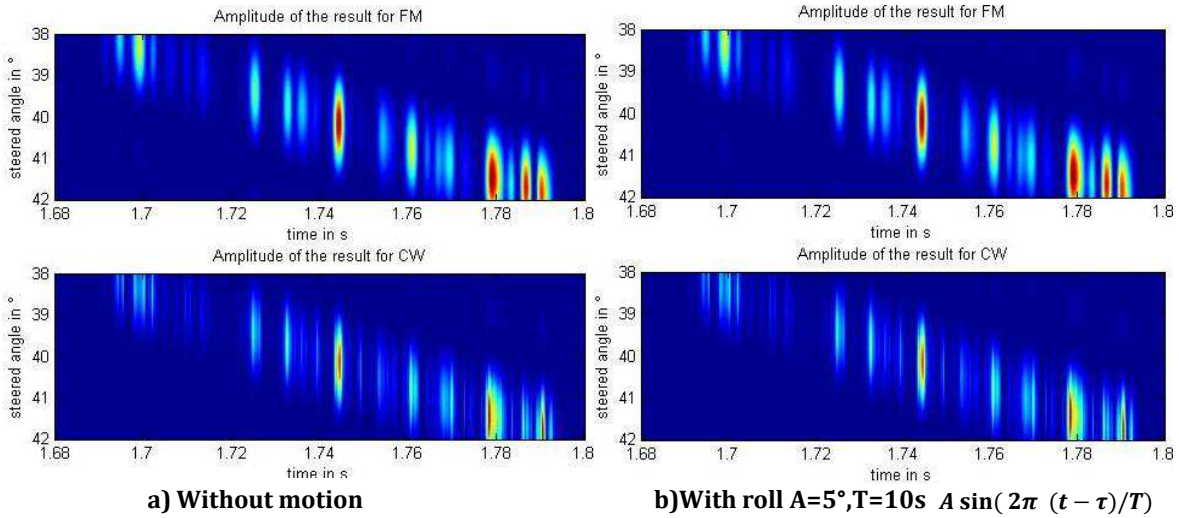

Figure 2.2.8: Amplitude of $S_a S_b^*$ without and with Roll, subplot a) without Doppler (reference), subplot b) with Doppler (roll modeled as a sin function with amplitude 5°)

The phase ramp of the beam expected to be at 40° is shown in Figure 2.2.9 , with the linear regression processed in order to find its zero crossing and also evaluate the phase ramp noise level.

From Figure 2.2.9 , It can be seen that the Doppler effect due to roll (differential Doppler) does not affect FM more than CW, and that Doppler does not affect the time detection. The phase ramp is modified since the antenna is physically steered by roll, apart from the theoretical time detection. The level of noise on FM and CW has the same order of magnitude with or without roll effect.

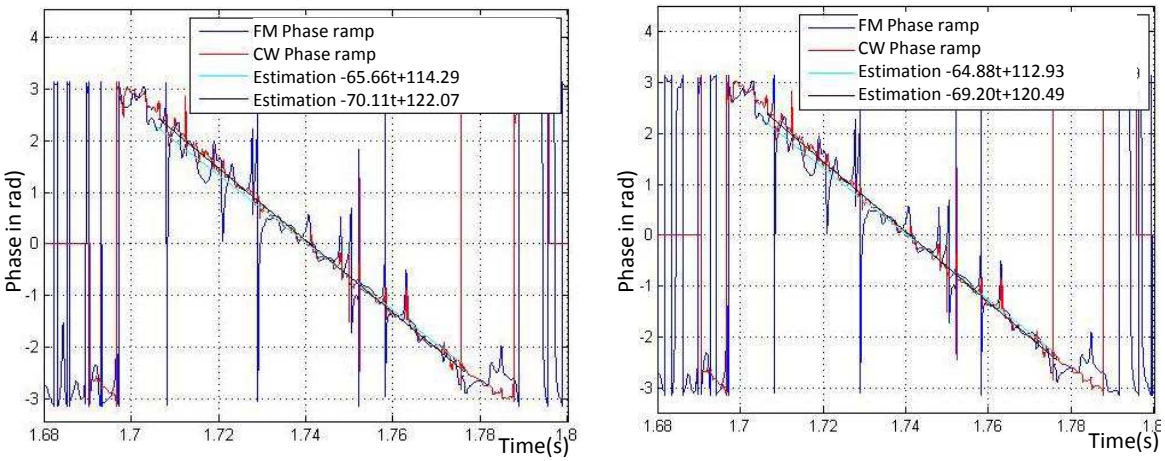

Figure 2.2.9: Phase ramp $S_a S_b^*$(beam angle 40°) without and with roll, subplot a) without Doppler (reference), subplot b) with Doppler (roll modeled as a sin function with amplitude 5°)

Table 2.9 shows the estimated noise variance.

	Without Doppler	With Roll
Estimated standard deviation in CW mode	0.14 rad	0.14 rad
Estimated standard deviation in FM mode	0.45 rad	0.44 rad

Table 2.9: Phase ramp noise level on simulations with or without roll

The differential Doppler introduced by roll does not impact the statistics of the phase ramp (Table 2.9) either considering CW or FM.

2.2.2 Bathymetric measurement statistics

It has been shown that the Doppler effect induces measurement biases. Here, the question is how the Doppler can affect the measurement statistics. First, the Doppler mismatches the matched filter so that the compressed pulse maximum decreases. This will be discussed in the first part of this section 2.2.2.1.

2.2.2.1 SNR loss due to the Doppler effect considering additive noise

Due to the matched filter on the Dopplerized signal the pulse compression is no more optimal and there is a signal to noise loss [Vin, 2012b].

It is reminded the signal Dopplerised by the factor η filtered by the matched filter expresses as (see Appendix D):

$$\begin{aligned} w(t) &= \int_{-\infty}^{+\infty} s(\eta(u-\tau))\overline{s(u-t)}du \\ &\approx e^{2\pi i f_c(1+\frac{\alpha}{2})(t-\tau)} T\mathbf{\Lambda}(\frac{t-\tau}{T})\text{sinc}\left[\pi\left(f_c\alpha + \frac{B}{T}(t-\tau)\right)T\mathbf{\Lambda}(\frac{t-\tau}{T})\right] \end{aligned} \tag{2.2.25}$$

where $\mathbf{\Lambda}$ denotes the triangular function which maximum value is 1 at 0 and which is null for $t \notin [-1/2, 1/2]$.

The maximum of this function is when the cardinal sine argument becomes null at τ_m so that:

$$f_c\alpha + \frac{B}{T}(\tau_m - \tau) = 0 \Leftrightarrow \tau_m = \tau - \frac{T}{B}f_c\alpha = \tau - \frac{T}{B}f_c(k-1) = \tau - \frac{T}{B}f_c\frac{v_d}{c} \tag{2.2.26}$$

Due to the triangular function the maximum is not 1 but is equal to $\mathbf{\Lambda}(\frac{f_c}{B}\frac{v_d}{c}) = 1 - \frac{f_c}{B}\frac{v_d}{c}$.
The SNR loss in term is thus:

$$SNR_{loss} = 20\log\left[1 - \frac{f_c}{B}\frac{v_d}{c}\right] \tag{2.2.27}$$

Considering usual MBES parameters the loss is about -1 dB, which is negligible by considering that the improvement from pulse compression in $10\log(BT) \backsimeq 10$.

Thus phase ramps from FM should statistically not be more sensitive to the Doppler effect than the ones from CW.

2.2.2.2 Impact on phase ramp statistics considering intrinsic noise

Simulations have been conducted on a flat seafloor for 20 realisations considering a vertical Doppler shift of 1 m/s. The pulse is a LFM (duration= 20 ms, sweep bandwidth=830 Hz). The receiving array is a full array of 128 sensors. The interferometer spacing is 0.33 m (a third of the whole array length). The result of the noise level estimation on the processed phase ramp is presented table 2.10.

Beam angle	20°	30°	40°	50°
Estimated phase ramp noise (without Doppler)	0.69 rad	0.58 rad	0.39 rad	0.25 rad
Estimated phase ramp noise (with Doppler)	0.75 rad	0.58 rad	0.39 rad	0.28 rad

Table 2.10: Doppler effect impact on phase ramp statistics for FM ($T = 20$ ms, $B = 830$ Hz) (considering only intrinsic noise)

From Table 2.10, it can be seen that the Doppler effect does not impact significantly the phase ramp in term of statistics.

In addition, as seen in the results from simulation in previous paragraph, the noise level for FM signal is high compared to the one observed for CW. Indeed, even without the Doppler effect interferometric phase ramps from FM signals were observed three-time-higher for CW see Tables 2.9 and 2.2. Thus, the Doppler effect is not a satisfying explanation of the noise level observed when using FM signals.

2.2.3 Discussion on post-processing compensation of the Doppler Effect

In MBES systems, Doppler-caused measurement biases are actually corrected as a post-processing detection-time compensation [Yuf, 2011]. The system processes first the detection and corrects the Doppler effect from the matched filter by introducing the predicted delay considering the array speed measurement. The instantaneous speeds of the array phase centers is given by the MRU aboard the carrier vehicule, the data of which is converted into the array speed. The measurement rate from the MRU is high typically every 1 ms, hence accurately following the array motion whose period is about 10 s (typical period of roll, pitch, heave...).

The interest of this process is to reduce the processing load of pre-compensating the Doppler effect: by compressing or distending the received signal before the matched filtering. Indeed, LFM signals are pretty well tolerant to Doppler effect (few energy loss (relatively low signal to noise degradation regarding additive noise)) and behave nicely introducing linear predictable bias. Moreover, it have been shown that the Doppler effect does not impact much the statistics of the detections but only introduces a bias. Correcting this bias after detection rather than before is more computer-resources efficient to correct this bias after detection than before, since the final statistics should not be improved by the second way.

However, post-processing time compensation can cause errors, notably when the MRU data does not behave properly. An example is presented here. Data was recorded from the EM710 on *R/V Falkor* [Bea, 2012] on a 400-m-deep seafloor in DEEP and VERY DEEP modes. The attitude data used for the Doppler post-correction were undersampled. Thus the correction was applied but with inrelevant speed values, causing additional noise on bathymetry. Figure 2.2.10 shows the bathymetric measurement results in this condition: the seafloor measurement presents a kind of "wobble" structure in FM mode (with no-compliant Doppler correction). When changing to VERY DEEP mode (FM switched on), this 'wobble' structure is also present on the centre sector

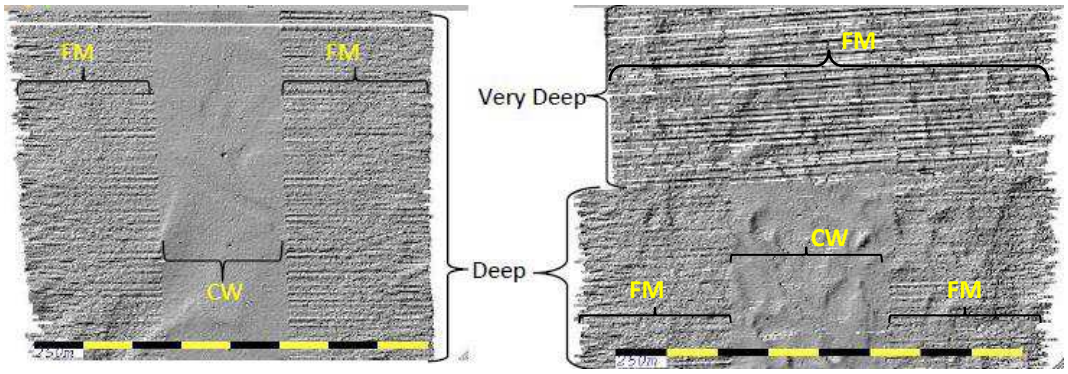

Figure 2.2.10: Bathymetric measurement with FM signal using Doppler effect compensation in post-correction with under-sampled MRU data

Figure 2.2.11 depicts the statistics estimated on the data of the first plot in Figure 2.2.10. It should be compared to Figure 1.6.2. It can be seen that the undersampled attitude data introduces an additionnal noise on the bathymetric measurement. Indeed, instead of being multiplied by two, the noise level when using FM (sector transition) is three/four times higher than CW bathymetric noise level, this extra-noise being due to the under-sampling.

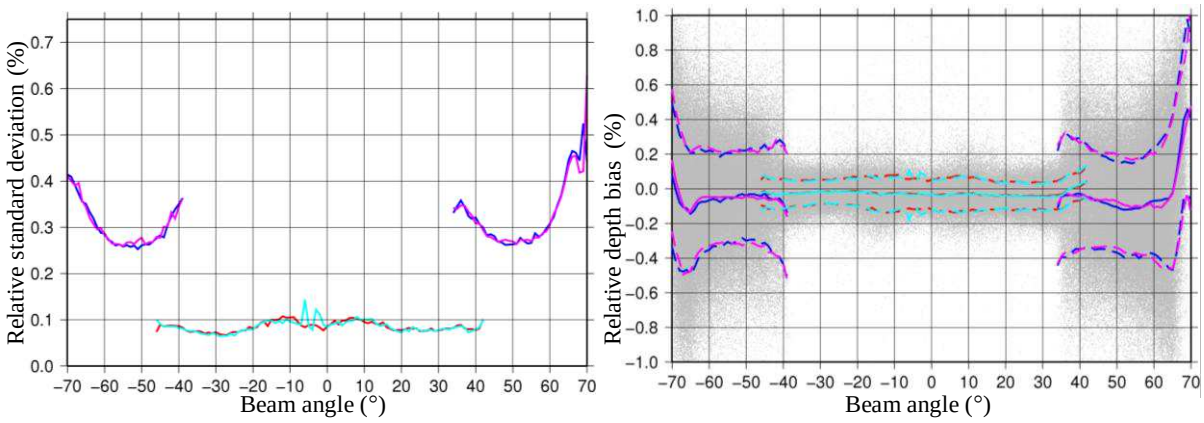

Figure 2.2.11: Impact on bathymetry quality due to undersampled attitude data

Finally, the Doppler correction in post processing is convenient as regards to many aspects (gain an computer operation complexity), however it must be applied with caution (assuming the integrity of attitude motion data).

Even if the Doppler effect is correctly compensated, the bathymetric data quality is lower when using modulated signal (confirmed on simulations, phase ramp noise level in the case of no-Doppler). In the rest of this chapter, Doppler effect will be not considered or assumed to have been well-corrected.

2.3 Baseline decorrelation or impact of pulse compression sidelobes

The Doppler effect has not been found a good explanation of the bathymetry quality loss when using modulated signals. It introduces a measurement bias which is normally taken into account and compensated for post processing compensation. This error is considered as being well estimated and thus corrected from the projection on the array localisation of speeds measured by the attitude sensors. In addition, the presence of the Doppler effect does not influence the measurement statistics. In these conditions, with the objective of only correcting the bias, estimating the Doppler effect from the signal itself and compensating it on pre-processing at the transmission or by adaptive matched filter has been judged being really time-consumming and lacking of interest. However, it has been clearly visible on simulated data that even without Doppler effect the phase ramp looks really noisier with modulated signal compared to CW.

By considering that the propagation, backscattering and filtering are linear processes, at the reception after matched filtering, the signal is equivalent to the one received if the compressed pulse was transmitted. Since the compressed signal is a no-more modulated, the only difference between CW and modulated signal are the envelope shape and namely the presence of sidelobes. The idea is that the sidelobes cause a specific noise on the phase ramp. This confirms the physical intuition that the wider the instantaneous footprint is, the more decorrelated the interferometric signals are. Indeed, because of sidelobes the actual effective pulse is longer than its pulse-compressed main lobe. This section aims at studying the impact of sidelobes as intrinsic noise on the phase ramp statistics and thus on the final bathymetric

measurement performance.

2.3.1 Signal shape design and sidelobes level

The signal shapes used for CW and FM are modulated by an amplitude envelope smoothing the edges of the transmitted signals. Indeed the sonar hardware cannot stand signal sharp edges, and the signal is naturally smoothed by the system. Since it is important to know accurately the transmitted shape in order to apply matched filtering, it is better that the tapering is already defined and controlled at transmission.

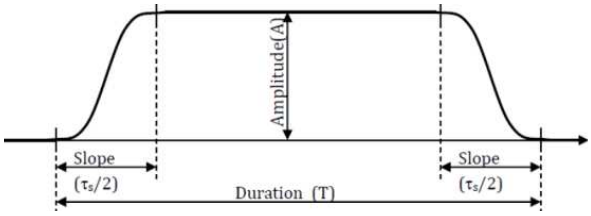

Figure 2.3.1: Transmitted signal envelope with tapered ends

The whole duration is T and the duration associated with the two tapered ends is τ. The envelope computed takes the form:

$$a(t) = \begin{cases} A\sin^2\left(\pi\frac{t+T/2}{\tau}\right) & \text{for } -T/2 \leq t < -(T-\tau)/2 \\ A & \text{for } -(T-\tau)/2 \leq t \leq (T-\tau)/2 \\ A\sin^2\left(\pi\frac{T/2-t}{\tau}\right) & \text{for}(T-\tau)/2 < t \leq T/2 \end{cases} \tag{2.3.1}$$

The tapering coefficient α as the ratio between the tapered end duration and the whole transmitted signal duration.

$$\alpha = \frac{\tau}{T} \tag{2.3.2}$$

Finally the transmitted signal is for CW

$$s(t) = a(t).e^{2i\pi f_c t} \tag{2.3.3}$$

and for FM:

$$s(t) = a(t).e^{2i\pi(f_c t+\beta t^2)} \tag{2.3.4}$$

With $\beta = B/(2T)$. B is the total bandwidth swept by the signal over is whole duration . This is different from the bandwidth occupied by the signal frequency spectrum. Indeed by changing the tapering, the equivalent bandwidth is prone to change while the parameter B is constant. Applying the stationary phase theorem (see Appendix A), the Fourier transform of the signal defined in (2.3.4) is approximated by:

$$S(\nu) \approx \frac{a(t_\nu)}{\sqrt{\omega''(t_\nu)}} e^{-2\pi j(\nu t_\nu - \omega(t_\nu))} e^{j\frac{\pi}{4}} \tag{2.3.5}$$

with $t_\nu = \frac{T}{B}(\nu - f_c)$ and $\omega''(t_\nu) = \frac{B}{T}$

Thus:

$$S(\nu) \approx \sqrt{\frac{T}{B}} a(\frac{T}{B}(\nu - f_c)) e^{-2\pi j \frac{T}{2B}(\nu - f_c)^2} e^{j\frac{\pi}{4}} \tag{2.3.6}$$

Different parameters can be defined characterizing the FM transmitted signal [Bur, 1989].

$T_{ef} = \frac{\int \lvert s\rvert^2 dt}{\max \lvert s\rvert^2}$	$T(1-\alpha) + \alpha\frac{3}{8}T = T(1 - \frac{5}{8}\alpha)$
$B_{ef} = \frac{\int \lvert S\rvert^2 d\nu}{\max \lvert S\rvert^2}$	$B(1 - \frac{5}{8}\alpha)$
B_{-3dB}	$B(1 - 0.6360\alpha)$

Table 2.11: FM parameters

Throughout this chapter, the performance of bathymetric measurement using equivalent pulses (CW pulse in a 100% tapered envelope LFM pulses in a 10% tapered envelope) will be compared. The FM pulse is modulated by an almost-square envelope in the objective to maximize the transmitted energy, and thus the benefit of the pulse compression is maximal. However since the envelope is rectangular, the pulse spectrum is rectangular (equation (2.3.6), Appendix A), and thus the pulse compression has high sidelobes.

The sweep bandwidth of the signal is chosen to make the compressed signal comparable to the CW signal. The -3 dB bandwidth of the CW Fourier transform being 500 Hz, the commonly associated LFM signal is a 10% tapered LFM whose sweep bandwidth is 500 Hz. But its compressed pulse presents a larger main lobe compare to the CW duration. To study the impact of only the sidelobes another LFM signal is designed. Its sweep bandwidth has been chosen in order to have the compressed pluse main lobe as close as possible to the CW pulse (minimisation of the quadratic error between the two pulses on the CW duration). (F_c =73 kHz, B=830 Hz and T=20 ms.)

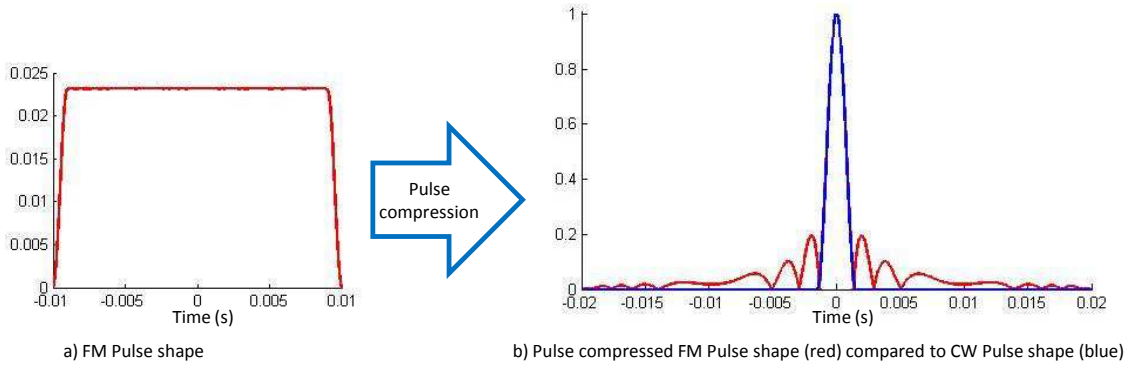

a) FM Pulse shape

b) Pulse compressed FM Pulse shape (red) compared to CW Pulse shape (blue)

Figure 2.3.2: Pulse-compressed-FM B=830Hz *vs* CW shape (close main lobe)

2.3.2 Sidelobe impact on interferometric signal coherence level

Up to this point, the transmitted signal has been characterized by its bandwidth occupation (defined at -3 dB). However, its frequency spectrum, more than its conventional occupied bandwidth, is the key of the noise level observed on the interferometric phase ramps

[Vin, 2012a]. Indeed, it has been shown in section (2.1.3) that the coherence ratio is one particular point of the Fourier transform of the squared signal envelope after normalisation (when considering baseline decorrelation). Thus, it also can be seen as the normalized self-convolution of the Fourier transform of the transmitted signal envelope.

For a FM signal, the transmitted signal shape to consider is the compressed signal (using matched filter).

Considering a CW pulse in a rectangular envelope, its Fourier transform is a cardinal sine whose auto-convolution is also a cardinal sine. Considering now a pulse-compressed chirp (FM) originally in a rectangular envelope, its Fourier transform is more or less a rectangular function, whose self convolution is a triangular function.

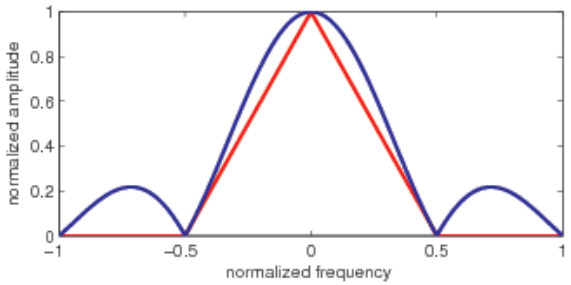

Figure 2.3.3: Normalized Fourier transform auto-correlation giving coherence level (red=FM signal, blue=CW signal)

The triangular function (for FM) and the cardinal sine (for CW) are normalized (maximum equals 1 at $f = 0$) and have the same base width since the compressed FM and CW signals have the same duration and bandwidth. The triangle is thus 'inside' the cardinal sine (Figure 3.3.3). Since the coherence ratio for FM and CW is a particular point of respectively the cardinal sine and the triangle, the conclusion is that the coherence level is always lower for FM than for CW:

$$\mu_{FM} \leq \mu_{CW} \tag{2.3.7}$$

Since the correlation level of S_a and S_b is lower in using FM, the signal to noise (an increasing function of the correlation level) is also lower, (using equation (2.1.37)).

$$d_{FM} \leq d_{CW} \tag{2.3.8}$$

The noise over phase ramps results to be higher (using equation 2.1.62), as well as the final uncertainties on depth detection.

$$\sigma\{\Delta\phi_{FM}\} \geq \sigma\{\Delta\phi_{CW}\} \tag{2.3.9}$$

This conclusion comes when only considering baseline decorrelation alone.

Of course, to get a complete description of the phase ramp noise level (taking intrinsic and additive noise into account) the combination signal to noise ratios from intrinsic and additive noise as it was exposed in the section 2.1.4 has to be used The result of this combination will be presented in section 3.4.

Regardless, the conclusion that the SNR is decreased because of the sidelobes (via intrinsic noise, here baseline decorrelation) can explain why bathymetry results look noisier when using FM signal. Indeed in a area where the additive noise is insignificant regarding the intrinsic noise (moderate values of depth and swath width), the bathymetric noise is mainly due to the baseline decorrelation. The transition between central and lateral sectors happen in this configuration and this explains the gap observed in bathymetric quality at this junction.

2.3.3 Prediction of the phase ramp noise level

The noise level on the phase ramps is modelled here for the three comparable signals defined in 2.3.1. Their respective characteristics (based on EM 710 characteristics) are:

- a 100% tapered CW pulse whose duration is 3 ms and occupied bandwidth (-3 dB) is 500 Hz;
- a LFM in a 10% tapered envelope with a sweep bandwidth of 500 Hz;
- and a LFM in a 10% tapered envelope with a sweep bandwidth of 830 Hz.

2.3.3.1 Without Doppler

The coherence coefficient of the interferometric signals is first calculated for each beam angle (depending on the seafloor configuration) as the special point of the Fourier transform of the square envelope of the pulse compressed signals. Here and for the rest of the PhD dissertation, the seafloor is 200-m-deep, and the interferometer spacing equals 0.33 m.

Figure 2.3.4 shows the normalized Fourier transform of the square envelope of the pulse compressed signals (FM) or the signal envelope (CW). The triangular shape in the case of FM pulses comes from their rectangular frequency spectrum.

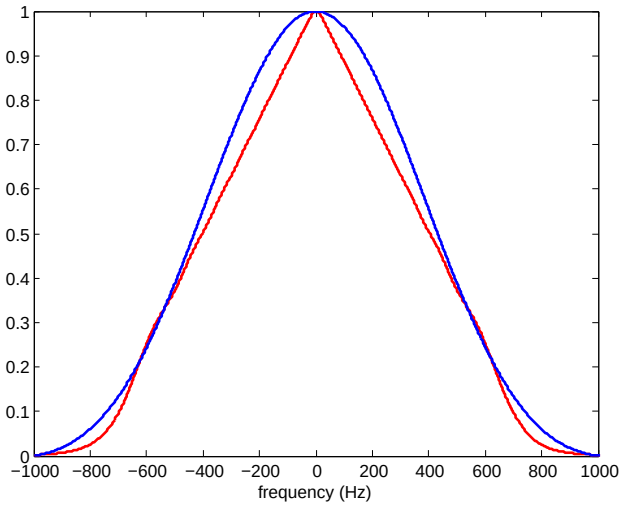

Figure 2.3.4: Normalized Fourier transform auto-correlation giving coherence level (red=FM signal B=830 Hz, blue=CW signal)

It can be seen that the CW curve (blue) is higher than the FM curve (red) this for any frequency. It means that whatever the interferometric configuration the coherence coefficient will be better (considering only baseline decorrelation) than with FM pulses.

Equation (2.1.36) makes it possible to calculate the coherence coefficient as a function of beam angle. The using equation (2.1.60) makes it possible to express the interferometric phase difference noise level as a function of beam angle. phase ramp noise level is illustrated in Figure 2.3.5? confirming that the noise over phase ramp is lower in CW.

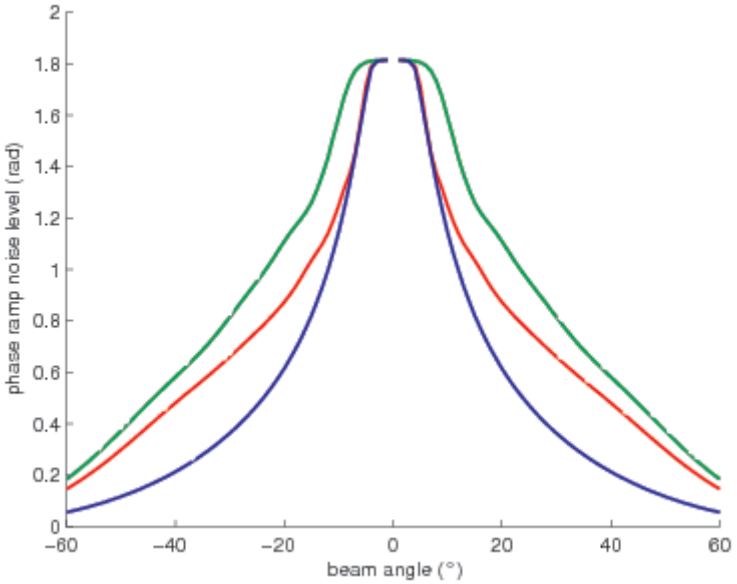

Figure 2.3.5: Phase ramp noise level Prediction: impact of pulse compressed sidelobes, blue: CW pulse, red: FM 830Hz, green FM 500Hz.

In this configuration the noise level observed on the phase ramp is three times higher at 40° with FM pulse compared to CW. Indeed, the sounder switches from CW to FM modes at this beam angle. The detection window length (which is the same for both FM or CW) is used to expressed the relative bathymetric error. For a given beam angle, relative bathymetric error is proportional to phase ramp noise. Thus, if phase ramp noise is observed twice higher, relative bathymetry error will also be twice higher.

A more physical/intuitive approach can also explain why compressed pulse sidelobes affect the phase ramp. For a given beamθ, the phase difference between interferometric signals $\Delta\phi$ is linked to the average angular position of the instantaneous footprint $\hat{\theta}$ by:

$$\Delta\phi = 2\pi f_c \frac{a}{c}(\sin\hat{\theta} - \sin\theta) \tag{2.3.10}$$

At the theoretical detection instant, the footprint is expected to be located towards the beam angle, and thus the expected value of $\Delta\phi$ is null. However, the presence of sidelobe increases the instantaneous responding footprint width (and angular width) seen by the sounder. The variance of $\hat{\theta}$ is thus more important (angular position of footprint seen by the sounder influences by all the scatterers present in the footprint). Hence, using equation 2.3.10, the interferometric noise difference is also noisier.

2.3.3.2 The case with Doppler

In the case of the Doppler Effect, the coherence can be found using the ambiguity function of the pulse. Indeed, the whole responding footprint contribution at a given instant can be considered suffering from the same Doppler shift as a first approximation. If the footprint is angularly narrow, all the scatterer can be assumed to be from almost the same angular direction, so that the radial speeds (projection of the speeds on the scatterer direction) is the same for all the scaterrers.

And the received signals S_a and S_b can be expressed as:

$$\begin{aligned} S_a &= \int_{\Delta_x} a_x s\left(\frac{k_r}{k_e}(t-\tau_x) - \frac{a}{2c}\frac{1}{k_e}\sin\theta_x\right) dx \\ S_b &= \int_{\Delta_x} a_x s\left(\frac{k_r}{k_e}(t-\tau_x) - \frac{a}{2c}\frac{1}{k_e}\sin\theta_x\right) dx \end{aligned} \tag{2.3.11}$$

In the case of the Doppler effect, the pulse compression (matched filtering output) is given by the ambiguity function. Since the Doppler shift is the same for all the instantaneous contributing scatterers, it is equivalent to consider that the transmitted pulse shape is the dopplerised compressed pulse.

If the Dopplerized compressed signal is considered as no more modulated, the developments made in Chapter 2.1 to predict the coherence level of the interferometric signal is still valid. Thus, considering intrinsic noise (baseline decorrelation), the coherence coefficient is given by a particular point of the normalized Fourier transform of the square of the Dopplerized compressed envelope. Thus it can be expressed thanks to the ambiguity function $A(\eta, t)$ (function of time and Doppler shift defined in section 1.3.2). If the received signal suffers from a Doppler shift η, the coherence ratio becomes (see Appendix E):

$$\mu(\eta) \approx \frac{\mathrm{FT}[|\,|A(t,\eta)|^2](f_c \frac{1}{2}\frac{a}{H}\frac{\cos^2\theta_0}{\tan\theta_0})}{\mathrm{FT}[|A(t,\eta)|^2](0)} \tag{2.3.12}$$

2.3.4 Validation from simulations

A series of simulations has been run and compared to the predictions made in paragraph 2.3.3. The simulation process follow the schema defined in 3.2.2. For each simulation, the arrays are considered as motionless. The number of scatterers has been chosen as 10 by resolution cell. The additive noise is considered as null, since only baseline decorrelation effect is under consideration. The simulations are conducted with each kind of signals defined in the previous section.

- CW in a 100% tapered envelope whose whole duration equals 3ms;
- Two linear frequency modulated signals (FM) whose duration equals 20ms and envelope is 10%-tapered.
  - The first one with a sweep bandwidth of 500 Hz,
  - The second one with a bandwidth 830 Hz, so that compressed main lobe fits the CW pulse.

The beamforming is processed in time. The sub array spacing is 0.33 m.

The noise level throughout the phase ramps is estimated by 3 methods:

1. Standard deviation at the closest sample of the detection instant of the phase of $S_a S_b^*$ for the different beam angle over 20 realizations (blue line in Figure 2.3.6)

2. Square root of the squared error between the phase ramp and linear regression for each beam angles and realization see equation (2.1.71) (results averaged over the 20 realizations) (green line in Figure 2.3.6)

3. Standard deviation of $S_a S_b^*$ phase for a window around the detection instant and averaging the results on this window. (black line in Figure 2.3.6)

The results are plotted in Figure 2.3.6. The first method of phase ramp noise level estimation is a good estimator, unfortunately the number of realizations (20) is low and the resulting estimations are really noisy. The second method is more robust (since it is averaged on the 20 realizations). Unfortunately, the number of samples taken for the central beams is low and the processed linear regression and thus fluctuation measurement over the phase ramp (square root of the quadratic error) is not relevant to the noise level on the interferometric phase difference. The last estimator is close to the first one. But it is less noisy, it takes the advantages of being averaged on the window. So, the estimation is less noisy than by taking the standard deviation only at the detection sample.

Phase ramp noise level estimation shows good agreement compared to the prediction Figure 2.3.6. Another visualisation of the results is plotted in Figure 2.3.7 and confirms that the phase noise is higher for FM signals.

The agreement between the simulation estimation (considering the third estimator) and the prediction has been measured by two indices. The first one g_1 is the mean on the beam angle of the relative error between the prediction $p(\theta)$ and the estimation $e(\theta)$.

$$g_1 = \frac{1}{N_b} \left| \sum_{\text{beam}} \frac{p(\theta) - e(\theta)}{p(\theta)} \right| \tag{2.3.13}$$

The second one g_2 is the mean quadratic error between the prediction and the estimation (expressed in rad).

$$g_2 = \sqrt{\frac{1}{N_b} \sum_{\text{beam}} (p(\theta) - e(\theta))^2} \tag{2.3.14}$$

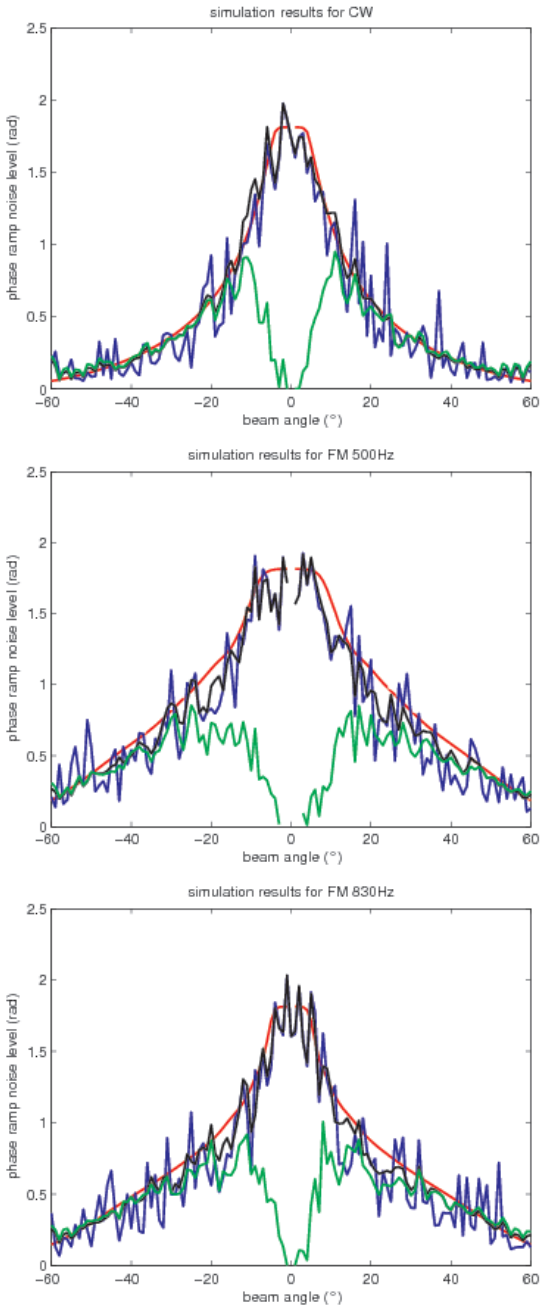

Figure 2.3.6: Phase ramp noise simulation results for the different pulse shape: CW (upper) FM 500 Hz (middle) FM 830 Hz (lower), estimation (blue, green, red as defined on the preceding page) prediction (red).

The indices of agreement between estimation and prediction are presented in Table 2.12. The relative errors are, for the different pulses, lower than 10% (FM 500 Hz presents a small bias between prediction and estimation, but the level of noise estimation is higher than for the other pulses). The mean square error is about 0.10 rad which is good if compared to the amplitude of values that the phase ramp noise level can take.

	CW	FM 500Hz	FM 830Hz
index 1: g_1	2%	9.1%	4.8%
index 2:g_2	0.08rad	0.13 rad	0.11 rad

Table 2.12: indexes of agreement between prediction and estimation

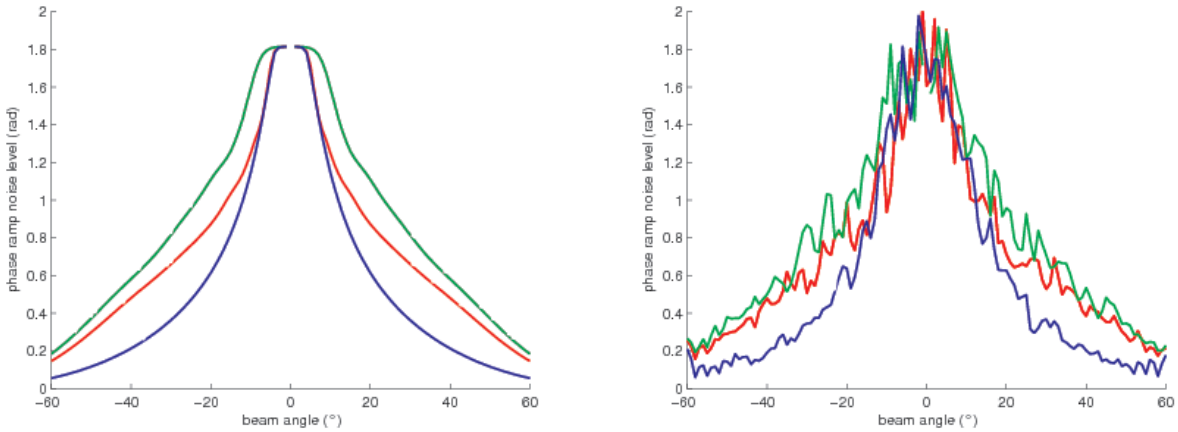

(a) model prediction

(b) simulation (estimator #3)

Figure 2.3.7: Phase ramp noise estimation results compared to model prediction. CW (blue), FM 500 Hz (green), FM 830 Hz (red)

2.3.5 On Survey data

A series of acquisitions has been recorded by Kongsberg Maritime (with courtesy of O. A. Almskar and R. Eckhoff) with the EM 710 mounted on *R/V Simrad echo* in a 200-m-deep seafloor and with special care on the transmitted signal shape (described in Table 2.13). The weather conditions and sea state were calm, and the acquisition could have been done with almost no platform motion (no Doppler influence). During the acquisition, the ship was immobile in order to guaranty that the system always pings almost the same area. This aimed at ensuring that the ping-to-ping statistics of the seafloor measurements was constant. The series corresponds to different maximum levels of transmitted power in order to separate the impacts of baseline decorrelation and additive noise.

file name	signal type	duration	sweep band	tapering rate	transmitted level
F09	CW	3ms		100%	0dB
F10	FM	20ms	830Hz	10%	0dB
F15	FM	20ms	500Hz	10%	0dB
F18	CW	3ms		100%	-20dB
F19	FM	20ms	830Hz	10%	-20dB
F25	FM	20ms	500Hz	10%	-20dB

Table 2.13: Data series description

The transmitted level column of Table2.13 denotes the signal power compared to the maximum power available at transmission of the ($SL_{\max} = 224$dB re 1µPa@1m). The series at 0 dB aims at studying the impact of baseline decorrelation since the received signal is then powerful enough to be insensitive to additive noise. In the series at -20 dB the additive noise impact is more visible. Thanks to this series it is possible to observe the impact of the transmitted energy loss due to the envelope tapering (which reduces processing gain for additive noise consideration).

As in paragraph 2.3.4, the noise level over the phase ramp can be estimated by three methods :

1. Standard deviation at the closest sample of detection instant of the phase of $S_a S_b^*$ for the different beam angle over 100 pings

2. From the re-processed phase ramp linear regression: square root of the squared error between the phase ramp and linear regression for each beam angle and realization see equation (2.1.71) (results averaged over 100 pings)

3. Standard deviation of $S_a S_b^*$ phase for a window around the detection instant and averaging the results on this window.

The results considering the third estimator are plotted in Figure 2.3.8.

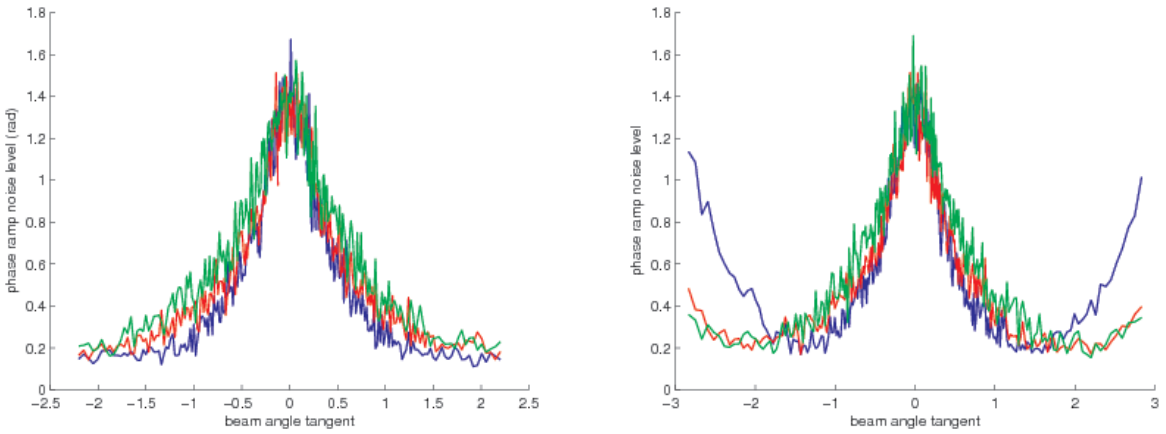

(a) Data series at 0dB

(b) Data series at -20dB

Figure 2.3.8: Noise level throughout the phase ramp as a function of the beam angle tangent (proportional to across distance), CW (blue); FM 830 Hz (red); FM 500 Hz (green).

Figure 2.3.8 shows some interesting expected aspects. First of all, it displays that in case of negligible additive noise (case of transmission at 0dB power) CW shows better performance than any FM pulse. Indeed, in this case only baseline decorrelation affects the phase ramps. The fact that the 500-Hz-bandwidth pulse compression duration is longer (larger main lobe and high sidelobe) creates a decorrelation of the interferometric signals. The same effect is caused by the presence of sidelobes for FM pulse whose sweep-band is 830Hz. That is why phase ramps are noisier due to intrinsic noise (baseline decorrelation) when using FM. It is

observable also on the second subplot of Figure 2.3.8. On the central beams, additive noise is low compared to received backscattered signals. Phase ramps are though more impacted by baseline decorrelation than by the additive noise. For outer beams, the additive noise level increases relatively to the backscattered signal. Phase ramps are thus more impacted by additive noise than by baseline decorrelation. This explains the behaviour at outer beams, in case of low power signal where additive noise is the main limitation. CW phase ramps are then noisier than FM phase ramps. The two FM pulses have the same envelope, and thus, contain the same energy. The final SNR after matched filter considering only additive noise is thus the same for the two FM pulses. It explains why the two FM pulses present the same level of performance when the additive noise is the main cause of phase ramp noise.

2.3.5.1 Comparison between survey and prediction

The survey results (phase ramp noise level estimated with the third method defined on the preceding page) is compared with the prediction made by using the theoretical development of section 2.1. The model presented in this section already takes into account the baseline decorrelation and in addition includes the impact of additive noise.

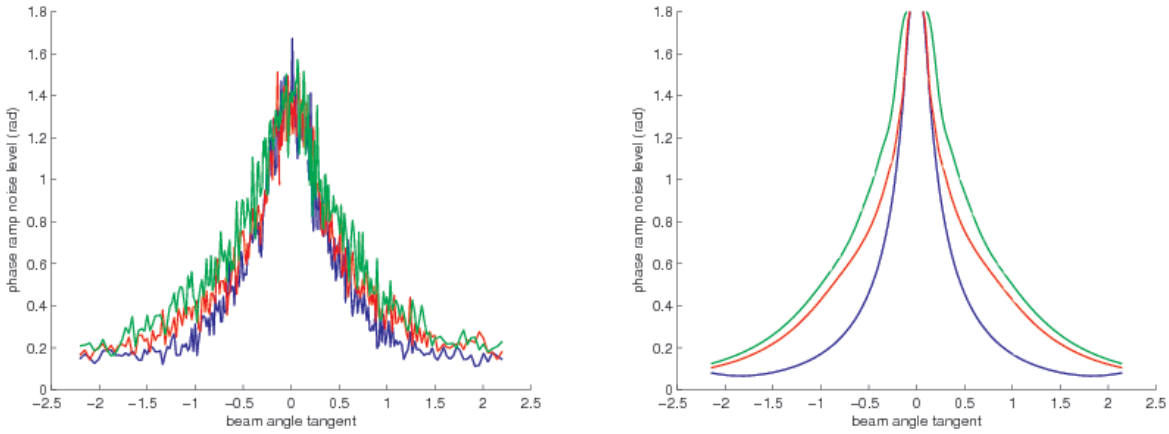

(a) Survey (b) Prediction

Figure 2.3.9: Comparison of the phase ramp noise level estimated on survey (left) with model prediction (right), transmitted level 0dB CW (blue), FM 500Hz (green), FM 830 Hz (red)

Figures 2.3.9 & 2.3.10 plot the results prediction made thanks to the equations presented in paragraph 2.1 with results from the estimation on the recorded field data. It can be noticed that globally their behaviours (prediction *vs* field data estimation) are really close.

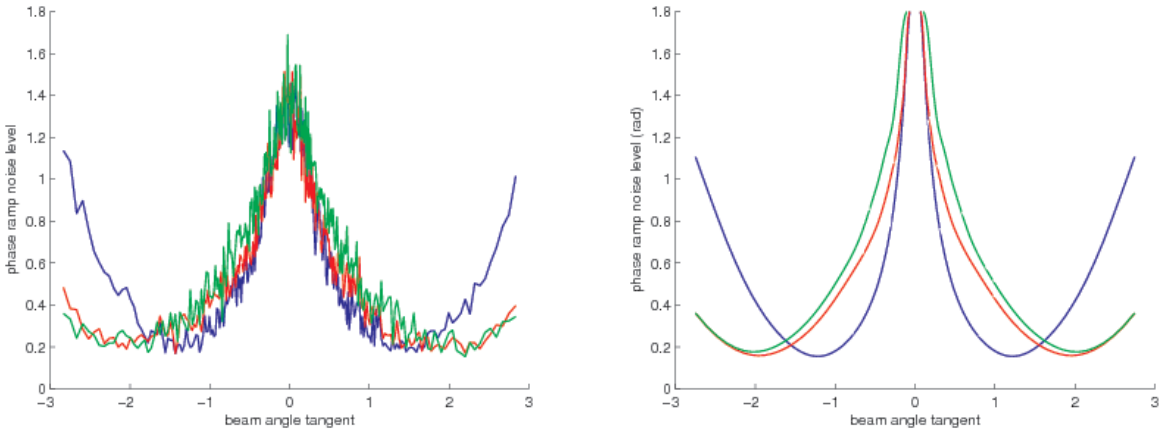

(a) Survey (b) Prediction

Figure 2.3.10: Comparison between the phase ramp noise level estimated on survey (left) and model prediction (right), transmitted level -20dB. CW (blue), FM 500 Hz (green), FM 830 Hz (red)

However, the prediction does not fit exactly the estimation from data recorded during the survey (Figures 2.3.9 & 2.3.10). This is particularly visible for the results from CW pulse in medium swath beams (beam angle tangent between 0.5 to 1.2). Indeed, the results on data give noisier estimated phase ramps.

However, the part where the additive noise is dominant is well predicted, for outer beams (beam angle tangent higher than 1.2). In this case whatever the pulse shape, prediction and data estimation show good agreement. And it can be concluded that additive noise impact have been well-predicted and introduced in prediction model.

Separation between prediction and estimation on survey happens in configurations where baseline decorrelation is the main cause of phase ramp noise.This happens as the interferometric signals S_a and S_b suffer of another cause of decoherence. A probable explanation is exposed in the following section (section 2.3.5.2).

2.3.5.2 Two layered seafloor structure

By looking at the vertical beam, the profile seems to show the presence of an additional backscattering layer around 3 m below the first seafloor backscattering layer. This is not much unexpected since the seafloor where the data was collected is really soft. And it is very not impossible that signals have penetrated a first layer of sediment to meet then a second backscattering layer. In addition, the echos from the second layer are really powerful. The backscattered signal from the second layer is even strong enough to perturb the detection on the vertical beam (detection jumps from the first layer to the second).

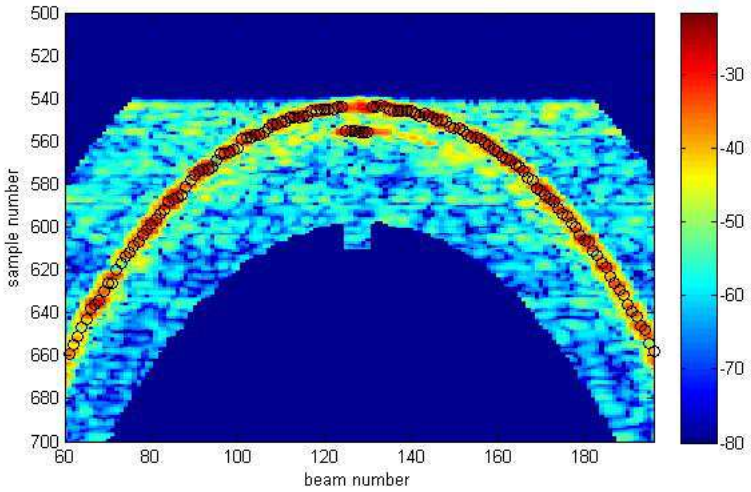

Figure 2.3.11: Beamformed signal amplitude in dB as a function of sample and beam numbers with detection (black circle points): confusion on the vertical beam, confirmation of a second layer presence

Figure 2.3.11 presents an example where the second layer has perturbed the detection. It represents the beamformed signal amplitude (dB) for a given ping of file #9 corresponding to data recorded using CW signals. For this ping, the detection (represented as circle black points) is attached the second layer echo for vertical beams. Bathymetry detection is thus blurred by the second layer. In this case, the second echo is even stronger than the first layer (upper layer) echo.

In the vertical beam (#128), the two layer echoes are clearly separated (Figure 2.3.12), the delay measured between the response peaks indicates that the layers are separated by 3 m.

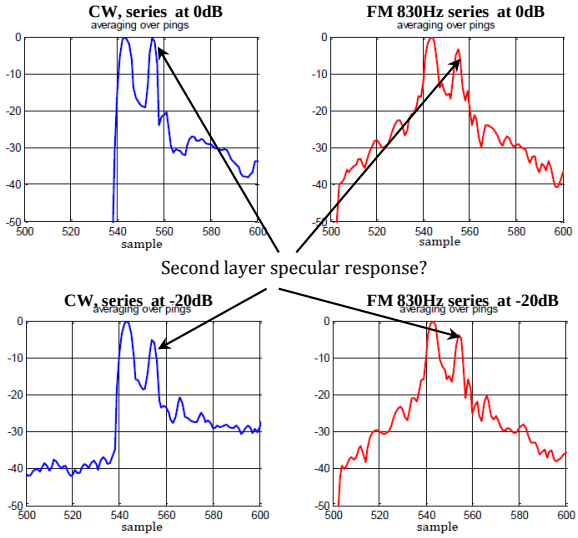

Figure 2.3.12: Vertical beam amplitude averaged on 50 pings: presence of a second layer

The analysis of vertical beam data shows that in the area surveyed, the sea bottom features two main layers. The issue is the lower layer impact upon the interferometric signals coherence (via baseline decorrelation). A model of this impact in term of interferometric signal coherence loss has been developed and is presented in Appendix F.

The signal penetration inside the seabed has been concluded not to affect significantly the interferometric signal coherence if the penetration depth is low compared to the seafloor depth (typically when the ratio between them are less than 10^{-2}, penetration of some cm). Indeed in this condition, the scatterers are still gathered in the same area, and the angular aperture of the footprint seen by the sounder stays unchanged.

However, here, the presence of the underlying layer increases the noise on the phase ramp. Indeed, since the second layer is deep enough to increase the angular aperture of the instantaneous contributing scatterers seen by the sounder, and the standard deviation on the observed angular footprint localisation is increased. The part of the received signals from the second layer impacts as a noise on the coherence part of the signal from the main layer.

Figure 2.3.13 presents the impact of the presence of the second layer on the phase ramp noise level on a CW 100% tapered pulse (3 ms). The water depth is 200 m and the second layer is 3 m below the interface.

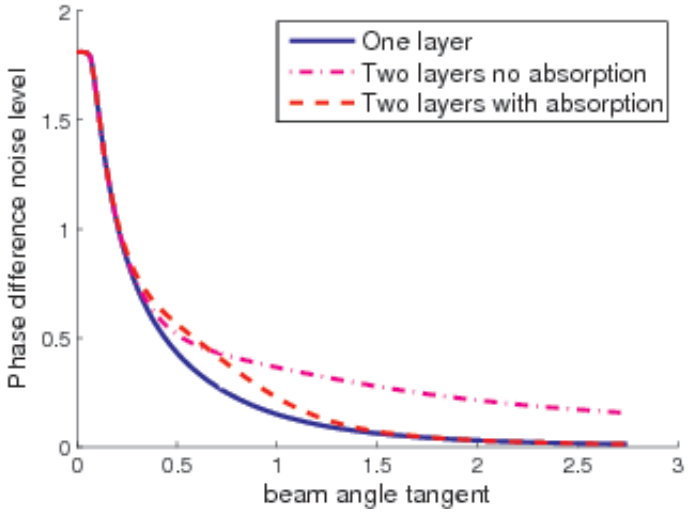

Figure 2.3.13: Influence of second layer on phase difference noise level as a function of beam angle tangent , noise with only one layer (blue), noise with the presence of a 3-m-below second layer (magenta), noise with the presence of a 3-m-below second layer including absorption in the first layer -5dB/m (red).

2.3.5.3 Comparison of real data and model prediction considering the two layers

Figure 2.3.14 shows the comparison results between the phase-ramp noise level estimated on the field data and the model prediction of a second layer burried 3 m below the interface. The attenuation in the first layer is 5dB/m. The estimation of noise level has been done on the series at -20dB following the three methods that were defined on page 86.

In Figure 2.3.14, the agreement between the prediction considering the two layers and the data estimation is clear. This shows that the hypothesis setting that the presence of a second

layer damages the interferometric coherence can explain conveniently why the first prediction (considering a single interface) and the noise level of the phase ramp estimated from the field data did not agree.

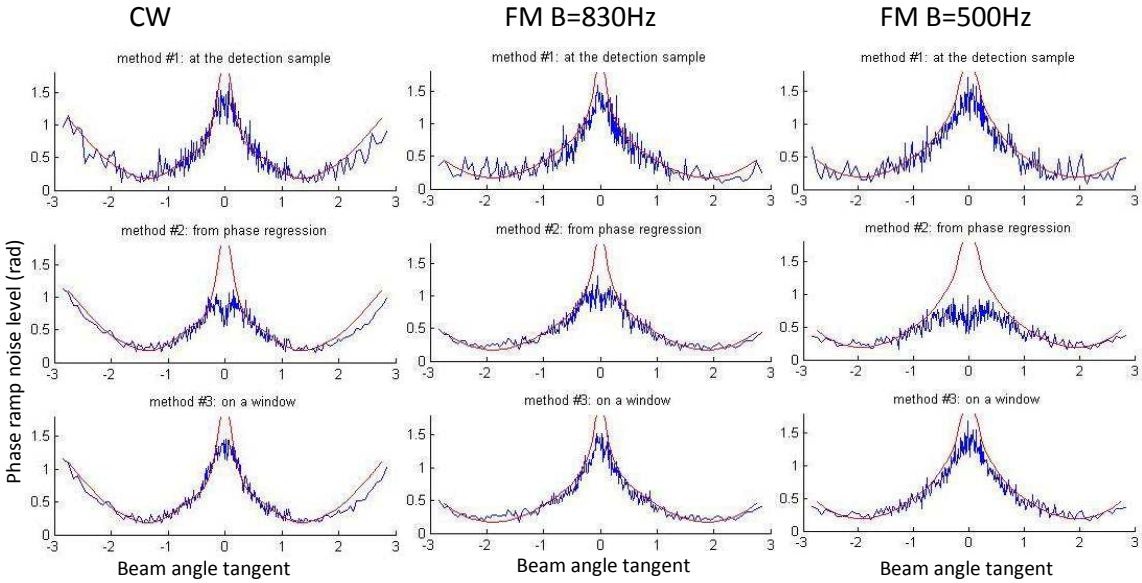

Figure 2.3.14: comparison prediction (red) and phase ramp noise level (blue) estimated on -20dB data series using estimators defined on page 86 for CW (left), FM 830 (Hz) middle), FM 500 Hz (right)

The presence of the second layer in the survey area is a disadvantage since it council the real improvement in term of coherence gain (noise reduction) obtained when reducing the sidelobes effect. However, the field data, simulation and prediction agree, confirming that the main cause of bathymetric degradation when using FM signal is the baseline decorrelation created by the presence of sidelobes in the compressed pulse.

Finally, the bathymetric measurement is not only dependent on the pulse bandwidth occupation. The pulse shape in frequency is a critical point, considering intrinsic noise (baseline decorrelation).

As a conclusion: if bathymetry using FM pulses looks noisier than when using CW this happens in domain (beam angle, range) where the main cause of interferometric noise is baseline decorrelation. Indeed, shape of FM signal envelope is quasi rectangular since the purpose is transmitting as much energy as possible thus, in order to benefit a maximum of the pulse compression (maximize signal to noise ratio regards to additive noise). However, it was not anticipated that such signals present high sidelobes after pulse compression which lengthens the observed footprint and decorrelate the interferometric signals even if the bandwidth is equivalent. The impact of sidelobes is not negligible; in some bathymetric conditions it may double or triple the observed bathymetric noise level.

2.3.6 Impact on Amplitude detection (simulation tests only)

Detection on the amplitude of the seafloor echoes is processed on vertical beams, where the phase detection is not exploitable. On vertical beams the time response is narrow and the amplitude (or intensity) detection process is the best adapted. The detection is made thanks to the calculation of the center of gravity of the signal envelope, which is more robust than estimating the maximum of the envelope. The center of gravity of the beam response envelope is assumed to give the delay associated to the seafloor point located along the beam axis direction. This is practically the case when using amplitude detection. A bias can be introduced when there is a change of reflectivity inside the beam (*i.e.* due the increase of propagation). However, this happens only when the beam angle is increased, where in practice the phase detection is preferred.

It has been shown that the longer the beam envelope, the noisier the amplitude detection. ([Lad, 2012, Lur, 2010b], see Appendix G, equation (G.3.4)). The amplitude detection is thus done iteratively to reduce the window length. A first window is defined by a threshold. A first detection is made by using the samples whose amplitude is higher the threshold (i.e higher than 610dB compared to the maximum of the beam time response). The second and third iterations reduce the window. A new window is defined centered on the previous detection and whose width is proportional to the sample spread of the previous envelope (sample standard deviation weighted by their amplitude).

The beam time response shape is not really impacted by FM signals. The first window length depends on the threshold. If the threshold is higher than the level of the compressed pulse sidelobes, the first window length is the same when using FM pulse or CW pulse. Inside steep beams, the additive noise can be assumed negligible compared to the signal. In addition, the detection window after the iterations can be assumed really short taking only samples containing useful signals. With only one of those two assumptions, it has been shown (Appendix G) that the standard deviation of the detection does not depend on noise level but only on the detection window width.

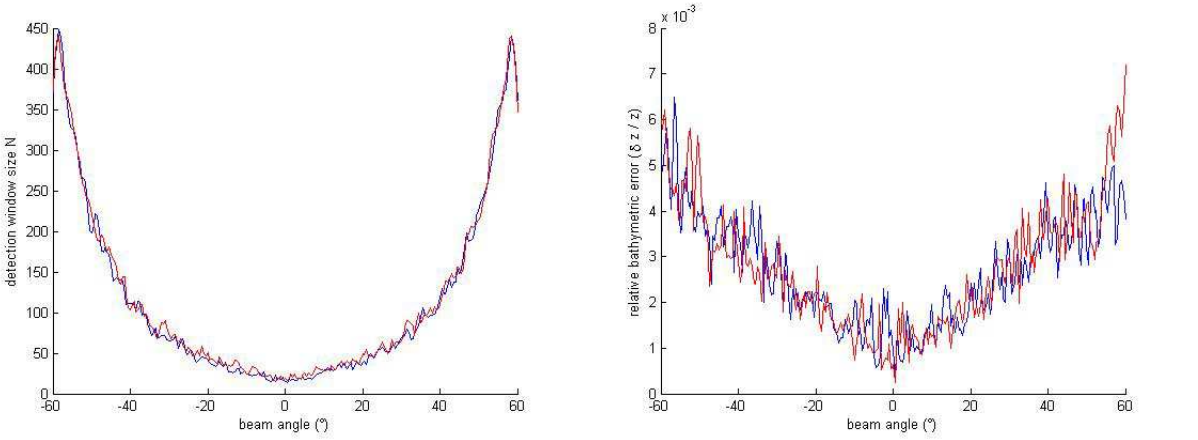

(a) Detection Window

(b) Detection results as relative bathymetric error: std(detection)/mean(detection)

Figure 2.3.15: Detection window width (left) and amplitude Detection quality (right) on 20 simulated realisations, for CW (blue), FM 830 Hz (red)

The final detection window (average on 20 realisation) is the same when using FM and CW, if the threshold (for first window detection) is chosen higher than the pulse compressed sidelobes (see Figure 2.3.15a). For a simulation (20 realisations), the relative bathymetric error when using amplitude detection is estimated thanks as the ratio of the standard deviation of the detection time and its mean value. The result as a function of beam angle is plotted in Figure 2.3.15b. As theoretically predicted, the quality is the same whatever the pulses, since the detection window is the same. The detection window is proportional to the beam envelope width which can be approximated (when the beam angle is high) by:

$$N \propto \frac{2H}{c} \frac{|\tan\theta|}{(\cos\theta)^2} \Phi f_s \propto \frac{\tan\theta}{(\cos\theta)^2} \tag{2.3.15}$$

Where $\Phi$is the beam angle aperture.

The time standard deviation of the amplitude detection (using amplitude detection) is proportional to the square root of the detection window (see Appendix G equation (G.3.5) and [Lur, 2010b, Lad, 2012]).

$$\mathrm{std}\{\hat{t}\} \propto \sqrt{N} \tag{2.3.16}$$

Thus, the relative bathymetric error follows:

$$\frac{\mathrm{std}\{\hat{t}\}}{\mathrm{mean}\{\hat{t}\}} \approx \frac{\mathrm{std}\{\hat{t}\}}{\langle \hat{t} \rangle} \propto \frac{\sqrt{\frac{2H}{c} \frac{|\tan\theta|}{(\cos\theta)^2} \Phi f_s}}{\frac{2H}{c\cos\theta}} \propto \sqrt{|\tan\theta|} \tag{2.3.17}$$

Figure 2.3.16 represents the equations (2.3.15) & (2.3.17), describing the behaviour of the detection window width and the relative bathymetric error as a function of beam angle. The comparison of Figures 2.3.15 and 2.3.16 shows the same behaviour.

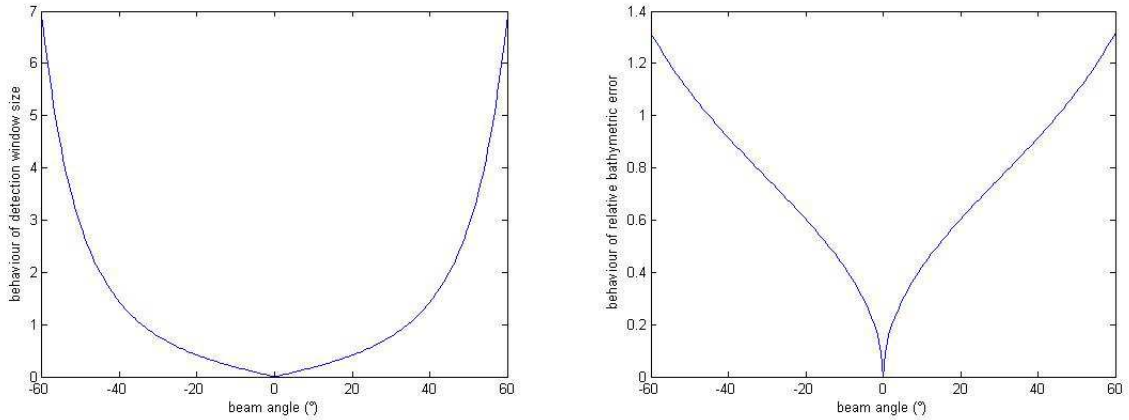

(a) Detection window size behaviour (equation (2.3.15)) (b) relative bathymetric error behaviour (equation (2.3.17))

Figure 2.3.16: Behaviour of detection window size and relative bathymetric error using amplitude detection

Finally, the bathymetric quality using amplitude detection little depends on the kind of transmitted pulses, but rather on the size of the detection window. If the sidelobes of the

pulse compression are lower than the threshold allowing to define the detection window, the bathymetry quality using FM pulses with matched filtering is the same as when using CW.

Chapter 3

Improvement proposal

The second chapter concluded that the Doppler effect to which the modulated signals respond differently (mismatch of the pulse compression) could not be the main cause of the degradation on bathymetric measurement when using modulated signal in MBES. The explanation comes from the intrinsic noise upon the phase difference measurement of the interferometric signals due to the presence of sidelobes in the FM compressed pulse. This effect of interferometric decorrelation caused the lengthening of the footprint (sidelobes) is called baseline decorrelation, and has been found being a satisfying explanation.

3.1 Discussion on the different pulse parameters

To design new signals, the different parameters, which could be played with, are :

- duration T.
- bandwidth B.

The duration T denotes the whole duration of the pulse. Of course, the envelope of the signal is important; it can change equivalent pulse duration. It also defines the amount of energy transmitted in the medium. The envelope can be changed by smoothing the envelope thanks to a tapering coefficient as defined in paragraph (2.3.1).

For FM signals, T can be theoretically increased as much as necessary since the resolution does not depend on it. However, beyond the material limitation and the statistical duration stability of the medium (which is not reached here), T is practically limited. Indeed, because of several transmitting sectors, the signal is sequentially fully-transmitted for each sector. The sounder is unable to receive when pulse transmission. If the pulse duration is long (multiplied by the number of sectors), it creates huge blind areas on water-column data. Hence, this could be reductive since nowadays more and more operators are interested in keeping the water-column data from bathymetric MBES for other applications.

The parameter B is the whole sweep bandwidth, corresponding to the whole instantaneous frequencies swept by the transmitted pulse as a function of time. The main limitation for this parameter is the bandwidth available between two sector carrier frequencies. It is remind that transmitting sectors give several advantages. They have been introduced to concentrate the transmitted pulse in more narrow beam pattern and thus increase the transmitting level. It gives also the advantage to filter frequencies for a given sector and thus reject interferences with

the other sector contributions such as the specular (strong echo from the vertical). To avoid cross-talks between the different sectors, and keep the advantages of sectors, the bandwidth is limited to a few kHz such as 2kHz for the EM 710 from Kongsberg Maritimes.

The shape of the transmitted signal in frequency domain is really important, since it defines the pulse compression. Indeed, if $w(t)$ denotes the pulse compressed signal, it can be written as:

$$w(t) = s * \overline{s(-u)} = \mathrm{FT}^{-1}\left[\mathrm{FT}(s).\mathrm{FT}(\overline{s(-u)})\right] = \mathrm{FT}^{-1}\left[S(\nu)\overline{S(\nu)}\right] = \mathrm{FT}^{-1}\left[|S(\nu)|^2\right] \quad (3.1.1)$$

The time compressed pulse is thus defined as the inverse Fourier transform of the square Fourier transform envelope of the transmitted signal. For example, a linear frequency modulation in a rectangular envelope presents a rectangular frequency-spectrum as first approximation (using stationary phase theorem Appendix A). It explains why the pulse compression shows many sidelobes (inverse Fourier transform of a rectangular function being a cardinal sine function). The smoother the frequency-domain shape, the lower the pulse-compressed sidelobes. In addition, the baseline decorrelation coherence coefficient is a particular point of the normalized cross-correlation of the square Fourier transform envelope of the signal.

From the stationary phase theorem (described in Appendix A), there is a relation linking the modulation function, time and frequency shapes of the signal.

3.2 Tapering the transmitted envelope

It has been shown in the previous chapter that pulse compressed sidelobes is the main cause of degradation when using FM signals. The aim of the whole chapter and in particular this paragraph is to propose some issues to reduce the sidelobe impact (baseline decorrelation) in order to improve the bathymetric measurement quality when using frequency modulated signal. To reduce sidelobes, the Fourier transform of the pulse compressed signal has to be smoother. The first idea is to work on the transmitted signal, by introducing a tapering on the transmitted signal.

3.2.1 Theoretical improvement on sidelobes impact

In order to reduce the sidelobes and smooth the frequency occupation of FM signals, the first idea is to smooth the transmitted envelope. The envelope shapes have been defined in the paragraph 2.3.1. The problem of tapering the envelope, while keeping the same sweep bandwidth, is the reduction in the occupied frequency bandwidth. Hence, the final compressed pulse presents a larger main lobe. The sweep bandwidth is here increased as the transmitted envelope tapering increases (Table 3.1).

tapering coefficient	10%	50%	75%	100%
sweep bandwidth	830 Hz	1120 Hz	1410 Hz	1780 Hz
colour in Figures 3.2.1,3.2.2 and3.2.3	red	magenta	black	green

Table 3.1: Chirp parameters

The equivalent bandwidth is kept as constant for all the pulses, and compressed pulses have the same main lobe. The sweep bandwidth of each FM shape has been designed in order to minimize the quadratic difference between their main lobe.

Figure 3.2.1 shows the different FM pulse transmitted envelopes (with the different tapering rates) with their pulse compressed shape. The more tapered the transmitted envelope, the lower the sidelobes of its pulse compression. In addition, Figure 3.2.1 confirms that the different FM-pulse compressions have the same main lobe.

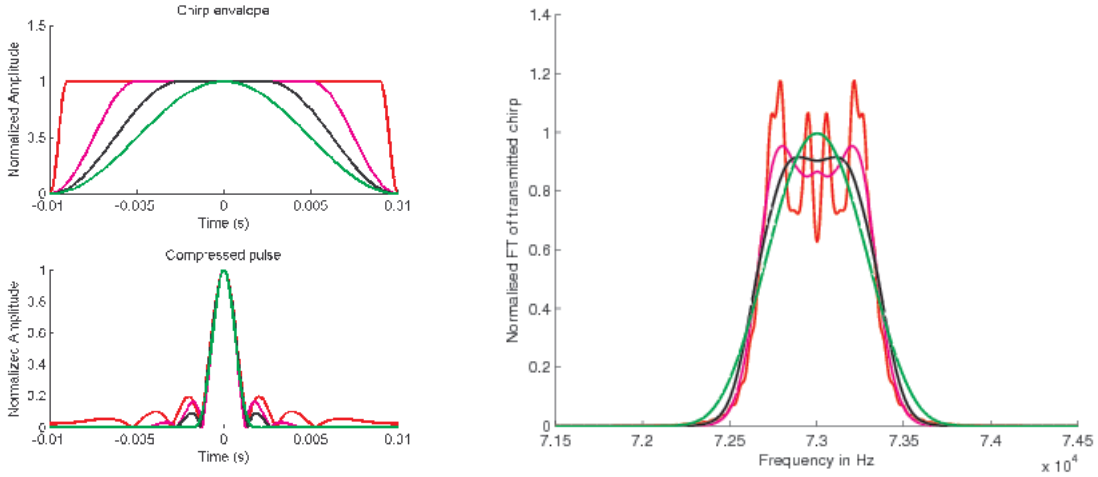

(a) temporal pulse shape

(b) frequency pulse shape (Fourier transform)

Figure 3.2.1: Different tapering rates and sidelobe level decrease(red:10%, magenta:50%, black:75%, green: 100%)

The interferometric coherence level expectation (considering only the baseline decorrelation) can once again be calculated as a particular point of the Fourier transform of the square of the pulse compressed envelope.

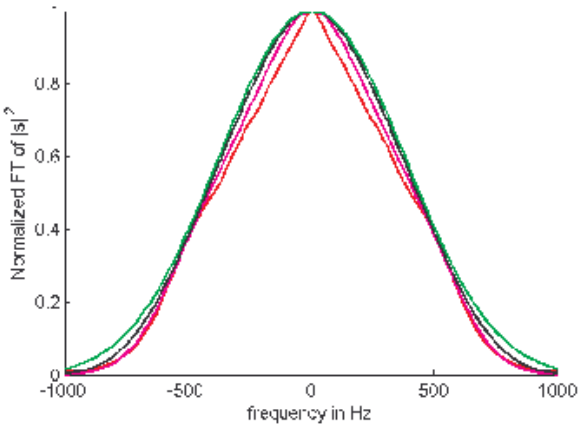

Figure 3.2.2: Fourier transform of the pulse compressed envelope square (red:10%, magenta:50%, black:75%, green: 100%)

Figure 3.2.2 shows this function (Fourier transform of the pulse compressed envelope square).

It can be noticed (Figure 3.2.2) that when tapering ratio is close to zero, the function becomes close to a triangle (cross correlation of a rectangular function), while by increasing the tapering ratio, the function is more round (cross correlation of a smoother function). The triangle is always lower (inside) the smoother function. And by increasing the tapering the function Fourier transform of the pulse compressed envelope square) becomes higher for any considered frequency. It means that the coherence level of the interferometric signal is higher (considering baseline decorrelation: intrinsic noise) whatever the interferometric configuration. It means that theoretically in area where the measurement is limited by intrinsic noise the use of tapered envelope should improve the bathymetric measurement quality (reduction of intrinsic noise).

The translation of the coherence ratio into phase ramp noise level as a function of the beam angle considering the same configuration used on the previous part.$H = 200$m, $a = 0.3$m, $f_c = 73$kHz is plotted in Figure 3.2.3. In Figure 3.2.3 only the baseline decorrelation effect is considered. The improvement in term of noise level observed on phase ramps when using tapered envelope is clearly visible.

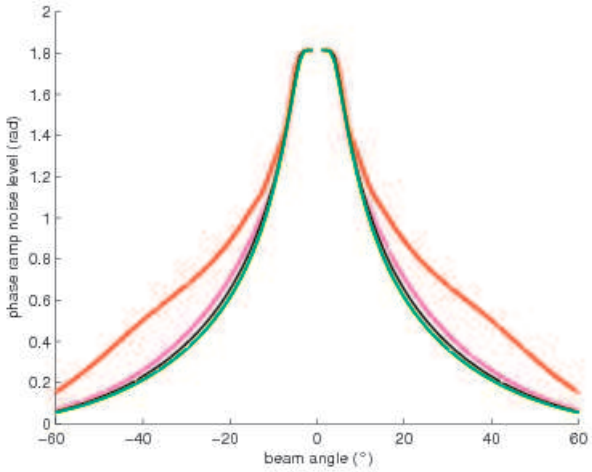

Figure 3.2.3: Prediction with different tapering rate: impact of sidelobes(red:10%, magenta:50%, black:75%, green: 100%)

3.2.2 Validation on simulations

A series of simulations has been run to ensure that the prediction and validate the assumption that tapering the chirp envelope reduces the phase noise level on the interferometric term ($\arg S_a S_b^*$). The schema of simulations is still used as defined in sections 2.2.1.3 and 2.3.4. Here, the additive noise is once again not taken into account and the measurement will be thus done by considering only the improvement on baseline decorrelation. The noise level throughout the phase ramps is estimated by the same 3 methods as defined in section 2.3.4:

1. Standard deviation at the closest sample of detection instant of the phase of $S_a S_b^*$ for the different beam angles over 20 realizations (blue line in Figure 3.2.4) ;

2. Square root of the squared error between the phase ramp and linear regression for each beam angle and realization. The results are averaged over the 20 realizations (green line in Figure 3.2.4) ;

3. Standard deviation of $S_a S_b^*$ phase for a window around the detection instant and averaging the results on this window (black line in Figure 3.2.4).

The results are plotted in Figure 3.2.4. Same as previously, the first method gives a good but noisy estimation. The second method is more robust but not compliant for low beam angles. The third estimator is a kind of a trade-off between the two first ones given less noisy estimation than the first method and reliable estimation for low beam angles.

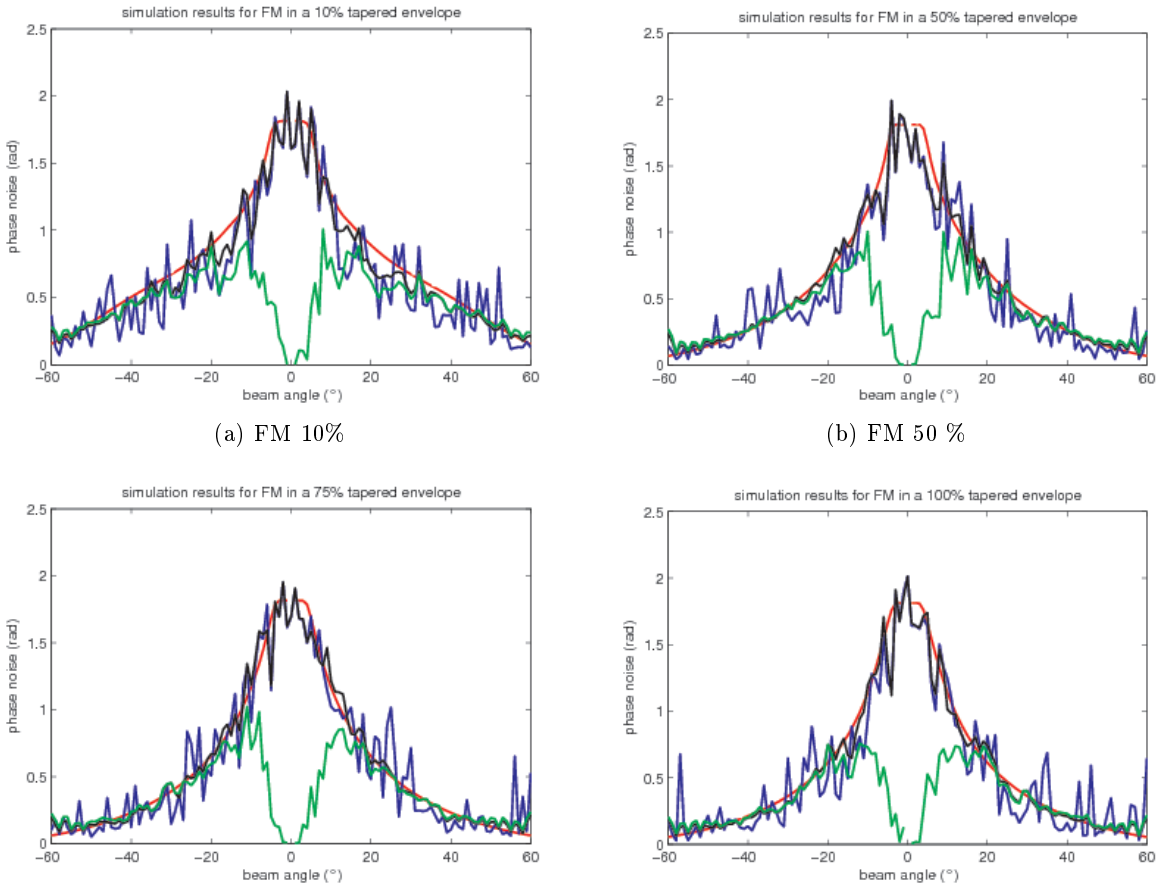

(a) FM 10%

(b) FM 50 %

(c) FM 75%

(d) FM 100 %

Figure 3.2.4: Agreement between simulations (green, blue and black as defined on the facing page) baseline decorrelation model predictions (red) for the different tapering coefficient: 10% (upper left), 50% (upper right), 75% (lower left), 100% (lower right)

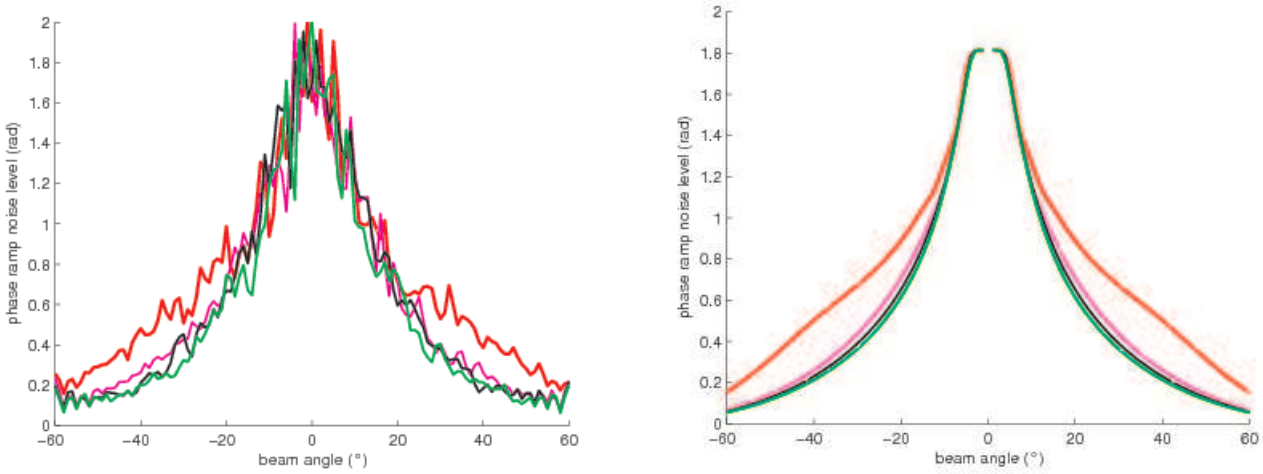

(a) Simulation phase ramp noise level estimation using estimator #3

(b) Phase ramp noise level prediction

Figure 3.2.5: noise level over phase ramp (red:10% tapering, magenta: 50%, black: 75% tapering, green: 100% tapering)

The agreement between the prediction and the simulation is evaluated thanks to the two indexes defined in the previous chapter in equations(2.3.13) and (2.3.14). The first one is the mean of the relative error between simulation (from the third estimator) and prediction. The second one is the square root of the quadratic error mean. Table (3.2) shows the agreement measurement. The relative error is lower than 5% and the quadratic error is about 0.11rad. The results measured on simulations is thus compliant to the model predictions.

tapering	10%	50%	75%	100%
Bandwidth	830Hz	1120Hz	1410 Hz	1780 Hz
index 1: g_1	4.8%	3.2%	3.9%	1.4%
index 2:g_2	0.11 rad	0.11 rad	0.09 rad	0.10 rad

Table 3.2: indexes of agreement between prediction and estimation

It means that tapering the transmitted envelope does reduce phase ramp noise level (where baseline decorrelation is main cause of degradation) for FM pulses. Finally, this technic should improve the bathymetry measurement on phase detection in some configurations (where baseline decorrelation was the limitation factor).

3.2.3 Test on survey data

3.2.3.1 Data description

Acquisitions have been made with 3 series of 7 signals : one CW signal comparable to 5 FM signals with different tapering coeficients (the latters being designed, so that their compressed main lobe is really close to the CW signal envelope), the last FM signal is the one usually used in EM710 (deep mode). This recording has been done in the same day as survey presented

in 2.3.5, in same condition and area with the same sounder (*i.e.* the *R/V Simrad echo*'s EM 710). The ship was immobile in order to ensure the seafloor statistics stability by pinging the same area. The series correspond to different maximum transmitting power levels, to seperate effect from baseline decorrelation and additive noise.

file name	signal type	duration	sweep band	tapering rate	transmitted level
F09	CW	2ms		100%	0dB
F10	FM	20ms	830Hz	10%	0dB
F11	FM	20ms	920Hz	25%	0dB
F12	FM	20ms	1120Hz	50%	0dB
F13	FM	20ms	1410Hz	75%	0dB
F14	FM	20ms	1780Hz	100%	0dB
F15	FM	20ms	500Hz	10%	0dB
F18	CW	2ms		100%	-20dB
F19	FM	20ms	830Hz	10%	-20dB
F20	FM	20ms	920Hz	25%	-20dB
F21	FM	20ms	1120Hz	50%	-20dB
F22	FM	20ms	1410Hz	75%	-20dB
F23	FM	20ms	1410Hz	75%	-20dB
F24	FM	20ms	1780Hz	100%	-20dB
F25	FM	20ms	500Hz	10%	-20dB
F20	FM	22ms	920Hz	25%	-20dB
F21	FM	27ms	1120Hz	50%	-20dB
F22	FM	35ms	1410Hz	75%	-20dB
F23	FM	50ms	1780Hz	100%	-20dB

Table 3.3: Data series description

First series is made at 0dB in order to finally reach the maximum SNR (concerning the additive noise). Second series is made with low power transmission level in order to look on the impact of the additive noise, especially the impact of the energy loss due to the envelope tapering (visible on side beams). Last series keep a low power energy transmission level but the duration of the FM transmitted pulse has been adapted to their tapering so that the contained energy is maintained for all FM tapering rates.

To make things visible, it has been chosen, among the pulses described in Table 2.13, to only plot the results of the estimations from only 3 pulses :

- CW (whose performance aims at being compared to FM pulses)
- FM 10% and B=830Hz (presenting the highest sidelobe level, thus really sensitive to baseline decorrelation)
- FM 100% and B=1780Hz (showing improvement by tapering the transmitted envelope, compressed pulse sidelobe quasi unexistant and model performance prediction, considering baseline decorrelation, reaching CW pulse)

Indeed, if on data, it is possible to observe some improvements by using FM tapered signals, the noise level on data does not fit the model prediction, especially for CW and FM100%. And

the improvement from baseline decorrelation reduction is not much visible. The explanation is the same as for the previous chapter, exposed in section 2.3.5.2. The survey has been conducted on the same area presenting a two layered seafloor structure. The analysis of the temporal response of the vertical beam for all the different pulse shapes of Table 2.13 has shown this presence of two backscattering layers on the survey area. Unfortunately the second layer contributes to make the phase ramps look noisier, by decorrelating the interferometric signals, and prevent us from correctly observing the real improvement from envelope tapering.

3.2.3.2 Noise level estimation on survey data

Figure 3.2.6 shows the results of the estimation of the noise level throughout the phase ramps using the estimator #3 defined on page 86.

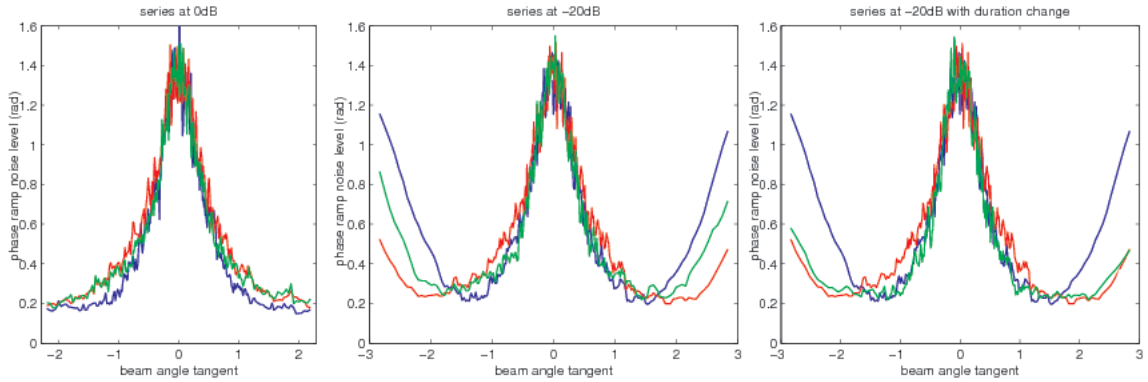

Figure 3.2.6: Phase ramp noise level estimation on survey, effect of tapering the transmitting envelope for CW (blue), FM 10% (red), FM 100% (green) with series: with high transmission level (left), with low transmission level (center) with low transmission level but with the increase of the 100% FM duration (right).

From Figure 3.2.6, even with the presence of the second layer, several interesting remarks can be made.

The first case (Figure 3.2.6 left plot) with high transmission power 0 dB is disappointing in terms of observation of the improvement on phase ramp noise by using tapered envelope. Indeed, almost no improvements are observable. The main explanation can be that when using this mode the transducer response could not have been linear. It is not impossible that the transmitted wave had suffered from a saturation cut-off in amplitude. This would have less affected the non-tapered envelope since the cut-off would not have really change its shape; whereas the tapered envelope becomes more rectangular. To support this assumption, the analysis of the vertical beam for FM 100% has shown highest sidelobes than expected before the specular response. However, in absence of more details about the exact distortion affecting the signal when transmitting at 0 dB, we will not dwell on.

The second case (3.2.6, center plot) when transmitting at -20 dB gives more interesting results. It can be noticed that for inner beams, where baseline decorrelation is the main cause of interferometric noise, the performance of the interferometric phase when tapering the FM envelope reaches the one for CW. Conversely, for outer beams, where additive noise becomes dominant compared to baseline decorrelation, since tapering the transmitted envelope has

reduced the pulse energy, 100% tapered FM gives noisier phase ramp than 10% tapered FM. Indeed, the processing gain on signal to noise for additive noise (see processing gain expression in (2.1.21)) is lower when using tapered signal.

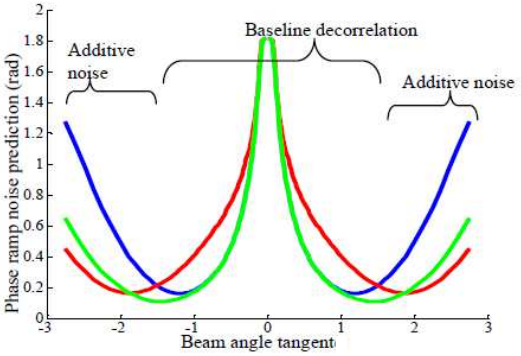

(a) Prediction

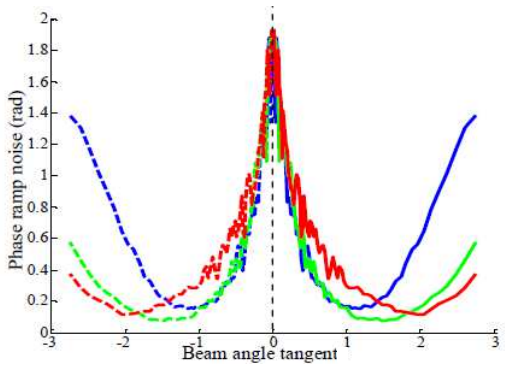

(b) Simulation

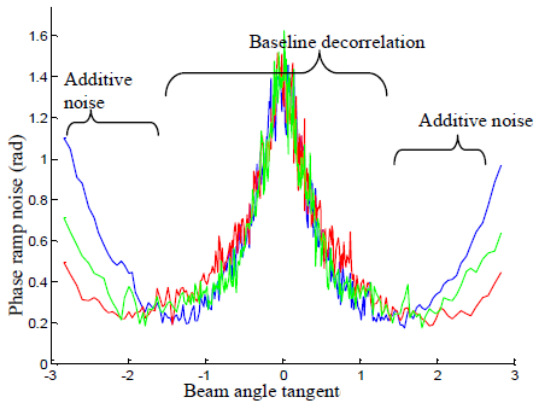

(c) Data

Figure 3.2.7: Phase ramp noise level (comparison prediction model (upper) ,simulation (middle), data (lower)) CW (blue), 10%-tapered FM (red), 100%-tapered FM (green).

A solution to keep the same transmitted energy level is to increase the pulse duration. In case of 100% tapering, the signal duration has to be changed from 20ms to 50ms to carry the same amount of energy than a 10%-tapered signal. The results (Figure 3.2.6, right plot) shows that with this consideration, in addition to the improvements due to baseline decorrelation reduction for inner beams, the phase ramps becomes as reliable as the ones 10% tapered FM for outer beams.

Thus, tapering the envelope while increasing the duration allows to gain in terms of baseline decorrelation (sidelobe reduction) without damaging as regards to additive noise. However, as said, the duration cannot be increased as much as desired, as far as applications using water-columns are concerned. In addition, the transmission duration can become also critical since it limits the ping rate (and thus survey duration or coverage density). Indeed, the systems wait for the reception of the whole echo before to ping again and in addition to propagation delay, signal duration (multiplied by the number of sectors) has to be considered.

Figure 3.2.7 shows the results of the prediction, simulation and data estimation of the second case configuration (-20dB of transmitted power maximum). In the simulation additive noise have been taken into account. The behaviour of the prediction and the simulation is the same. Central beams are more affected by baseline decorrelation so that FM10% behaves worst than the others while outer beams suffer from additive noise, that is why FM10% is the best in this case (because of better signal to noise processing gain).

Data estimations have the same behaviour as simulation estimations and model predictions, however does not fit exactly especially where baseline is the main cause of degradation.

This is caused by the two layered seafloor structure; same reason as for the previous chapter (see paragraph 2.3.5.2). The impact of the second layer on the phase ramp can be done thanks to the model developed in Appendix G.

3.2.3.3 Confrontation noise level estimated on survey data with two layers model prediction

The effect of the second layer is different considering the pulse shape. In the case of CW pulse or FM in a 100% tapered envelope, the level of coherence of the interferometric signals is better than for other FM pulses. The higher is the coherence level, the more important the loss of coherence between interferometric signals in case of two layers. Indeed the coherence loss has been shown as proportional to the initial coherence (see Appendix F). Thus CW pulse or FM in a 100% tapered envelope suffers more from the presence of the second layer than the other FM pulses.

Figure 3.2.8 shows the confrontation between the prediction taking into account the second layer and the data estimation. It can be seen that there is a slight divergence between the expectation and data. The prediction is better when introducing the impact of the second layer. However, prediction and simulation do not match exactly. This in domain where baseline decorrelation is the main cause of bathymetric degradation.

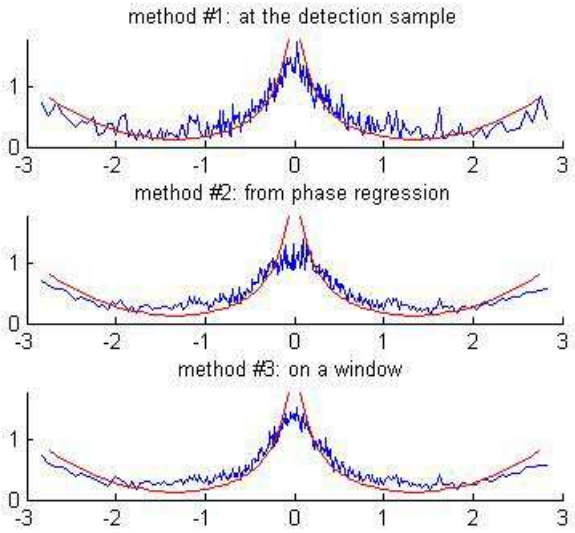

Figure 3.2.8: Confrontation prediction and data estimation (phase ramp noise level)

However the knowledge about the structure of this second layer is unknown. It is possible that if the second layer is a rough surface the backscattered signal is more powerful than modeled here. This could explain the difference between expectation from model and data results. In absence of more information on the second layer structure, it is impossible to develop more the model.

3.3 Filtering by other matched filtering

Actually, it would be interesting to keep the transmitted energy as maximum as possible. The transmitting envelope is thus preferred being rectangular. The purpose is to keep the advantage of maximizing transmitted energy in order to be the more efficient when additive noise is the limitation of the bathymetric detection, and reduce the impact of the baseline decorrelation due to the sidelobes level which is the main limitation factor. To reduce the sidelobes level, another classic method is to taper the Fourier transform of the transmitted signal by filtering [Bur, 1989, Col, 1999, Var, 2003]. There are two equivalent ways to process it. The first one is temporal by filtering with a tapered signal to process at once the pulse compression and the smoothing (this way will be preferred for the rest of the work). The second consists in applying a weighting window on frequency domain, after pulse compression. Several weighting window can be found in the literature such as Hamming, Hann, Taylor.

The problem is if this approach reduces the sidelobes, it also increases the width of the main lobe. Indeed, the resulting bandwidth is reduced by the tapered matched filtering. Thus the baseline decorrelation improvement due to the sidelobe reduction might be damaged by the main lobe width increase. The object of the paragraph is to discuss this issue.

3.3.1 Theoretical baseline improvement

Obviously, the matched filtering by a tapered unadapted filter reduces the processing gain and would be less efficient in the case of additive noise. It is the main cause of additive noise notably for the outer beams.

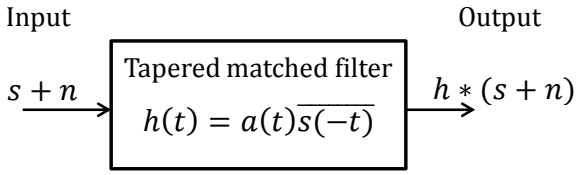

Figure 3.3.1: tapered matched-filter filtering

The pulse compression is processed by using a tapered version of the matched filter $h(t) = a(t)\overline{s(-t)}$ ($s(t)$ being the transmitted pulse). The time envelope $a(t)$ of this tapered matched filter is defined as in (2.3.1) with square cosine slopes for the tapered ends and a constant part. All this filter envelope will be characterised by their tapering ratio α (see section 2.3.1). From the stationary phase theorem, it can be seen that the Fourier transform of the filter output is approximately real and centered on the carrier, the inverse Fourier transform is thus no more modulated.

Finally, the processing gain will take the following expression. The signal to noise ratio at the input of the filtering is still the same as in the equation (2.1.19):

$$(S/N)_{in} = \frac{\max |s|^2}{N_0/T_{eq}} \tag{3.3.1}$$

The signal to noise ratio at the output of the filter is:

$$(S/N)_{out} = \frac{|\int_{-\infty}^{+\infty} s(-u)h(u)du\,|^2}{N_0 \int_{-\infty}^{+\infty} |h(u)|^2\,du} \tag{3.3.2}$$

In case of matched filter (considering that $a(t)$ is a rectangular function with the pulse duration T), the signal to noise after matched filtering is maximum and equals:

$$(S/N)_{out} = \frac{|\int_{-\infty}^{+\infty} |s(u)|^2\,du\,|^2}{N_0 \int_{-\infty}^{+\infty} |s(u)|^2\,du} = \frac{|\int_{-T/2}^{T/2} du\,|^2}{N_0 \int_{-T/2}^{T/2} du} = \frac{T}{N_0} \tag{3.3.3}$$

In case of unadapted matched filter, the signal to noise at the output of the filter is:

$$(S/N)_{out} = \frac{|\int_{-\infty}^{+\infty} a(u)du\,|^2}{N_0 \int_{-\infty}^{+\infty} |a(u)|^2\,du} = \frac{\left(\frac{1}{2}\alpha T + (1-\alpha)T\right)^2}{N_0\left(\frac{3}{8}\alpha T + (1-\alpha)T\right)} = \frac{(1-\frac{1}{2}\alpha)^2 T}{N_0(1-\frac{5}{8}\alpha)} \tag{3.3.4}$$

α being the tapering ratio as defined in (2.3.2). Finally the loss in processing gain improvement due to the unadapted filter is (in dB):

$$PG_{loss} = 10\log_{10}\left(\frac{(1-\frac{1}{2}\alpha)^2}{1-\frac{5}{8}\alpha}\right) \tag{3.3.5}$$

The theorem of the stationary phase (Appendix A) allows to give an approximation of the signal and the unadapted filter in the frequency domain.

$$\begin{cases} S(\nu) &= \mathbf{\Pi}\left(\frac{\nu-f_c}{B}\right)\sqrt{\frac{T}{B}}e^{-\pi i\frac{T}{B}(\nu-f_c)^2}e^{i\frac{\pi}{4}} \\ H(\nu) &= a\left(T\frac{\nu-f_c}{B}\right)\sqrt{\frac{T}{B}}e^{\pi i\frac{T}{B}(\nu-f_c)^2}e^{-i\frac{\pi}{4}} \end{cases} \tag{3.3.6}$$

The time pulse compression with unadapted filter is the convolution product of the signal with the unadapted filter. It is thus the inverse Fourier transform of the classical multiplication between the Fourier transform of the signal and the filter.

$$w(t) = \int_{-\infty}^{+\infty} s(t-u)h(u)du = \mathrm{FT}^{-1}[S(\nu)H(\nu)] = \mathrm{FT}^{-1}[S(\nu)H(\nu)] = \mathrm{FT}^{-1}[a(\frac{\nu-f_c}{B})\frac{T}{B}] \tag{3.3.7}$$

Since $a(t)$ is a smoother envelope, the pulse compressed signal with unadapted filter will present a smoother envelope in frequency domain. This leads to reduce the sidelobes in the temporal domain. However, the tapering of the filtering induces a reduction of the equivalent bandwidth of the compressed signal, so that the main lobe is increased by this process.

Figure 3.3.2 presents the filter output for different tapered filter. It shows the twofold effect: improvement considering the level of the sidelobes, and damage considering the increase of the main lobe width.

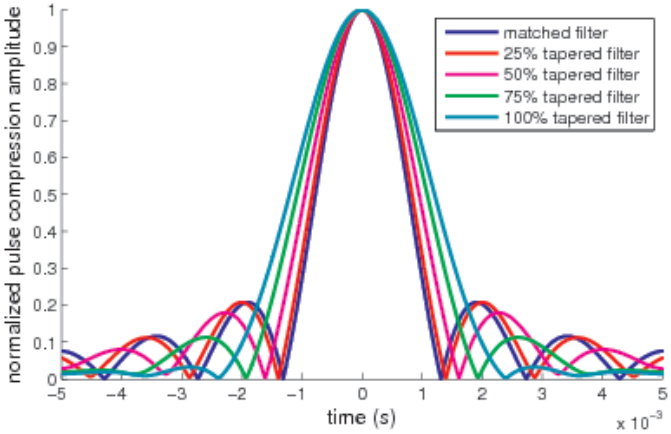

Figure 3.3.2: Filter output envelope - pulse compression using tapered matched filtering with tapering ratio 25% (red), 50% (magenta), 75% (green), 100% (light blue) compared with standard matched filter (blue)

Thus, in a way, the baseline decorrelation can be improved by the sidelobe reduction but also damaged by the main lobe width increase. Figure 3.3.3 shows the normalized Fourier transform of the compressed-signal square envelope with the different filter. Let us remind that taking this function in a particular point (which depends on the interferometer configuration)

gives the coherence coefficient of the interferometric signals S_a and S_b. The coherence level leads to the associated baseline decorrelation signal to noise ratio.

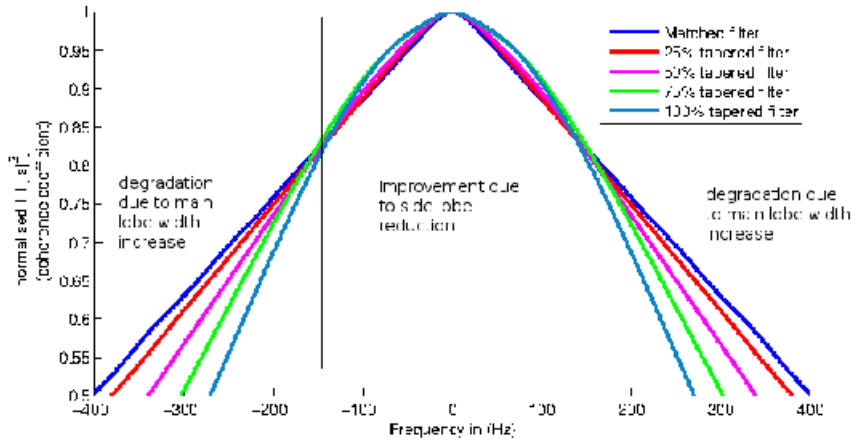

Figure 3.3.3: Normalized Fourier transform of the square pulse compressed envelope

In Figure 3.3.3, it can be seen that there are two behaviour areas. The unadapted filtering makes the signal frequency shape smoother and thus the pulse compressed sidelobes level lower. The auto correlation of the filtered signal is more curved around zero compared to the 10%-tapered FM pulse compression whose Fourier transform auto correlation looks triangular (since its FT is smoother). Let us remind that the coherence coefficient of the interferometric signals is a particular point of this auto-correlation function (see paragraph 2.3.2). Filtering reduces the sidelobes and curves the auto correlation of the filtered signal Fourier transform. It improves in this domain the coherence coefficient, when $2f_c\beta$ becomes low enough (120 Hz if considering 100% tapered filtering). However, as said, smoothing the frequency envelope also leads to an equivalent bandwidth reduction, so that the main lobe of the pulse compressed signal is increased. Because of the bandwidth reduction, the autocorrelation of the signal FT is narrower (since signal bandwidth is narrower) and the coherence ratio is lower, when $2f_c\beta$ becomes higher.

The coherence coefficient can be given as a function of beam angles, by using the relation giving $2f_c\beta = f_c \frac{1}{2} \frac{a}{H} \frac{\cos^2\theta_0}{\tan\theta_0}$ with a=33cm H=200m and f_c=73kHz. The results are plotted in Figure 3.3.4 with the different filterings (color code is the same as in Figures 3.3.3 and 3.3.2).

It means that for beams close to the vertical, the increase of the pulse-compressed main lobe width is dominant on the side lobe reduction. Conversaly, by increasing beam angles, the decrease of sidelobes (even if the main lobe width is increased) makes the footprint seen by the sounder smaller and thus baseline decorrelation lower. In this condition, by using tapered matched filtering, the bathymetry quality is improved. However, this is only valid for beams which suffer mainly from the baseline decorrelation. Indeed, above a given beam angle, outer beams are more affected by additive noise, and in this condition, tapered matched filtering damages the resulting interferometric phase (since it reduces the processing gain).

By using the link between the coherence coefficient and the predictable phase noise level from (2.1.60), a prediction in terms of phase noise level as a function of beam angle is made, and is plotted in Figure 3.3.4 .

Figure 3.3.4 presents also two behaviour domains, which correspond to the area define for the Figure 3.3.3. For the beam angles whose tangent is lower than 0.43 (beam angle=23°), the noise level on the interferometric phase difference is higher by using the tapered matched filtering. However the improvement is seen for beam angles higher than 23°, due to sidelobe reduction.

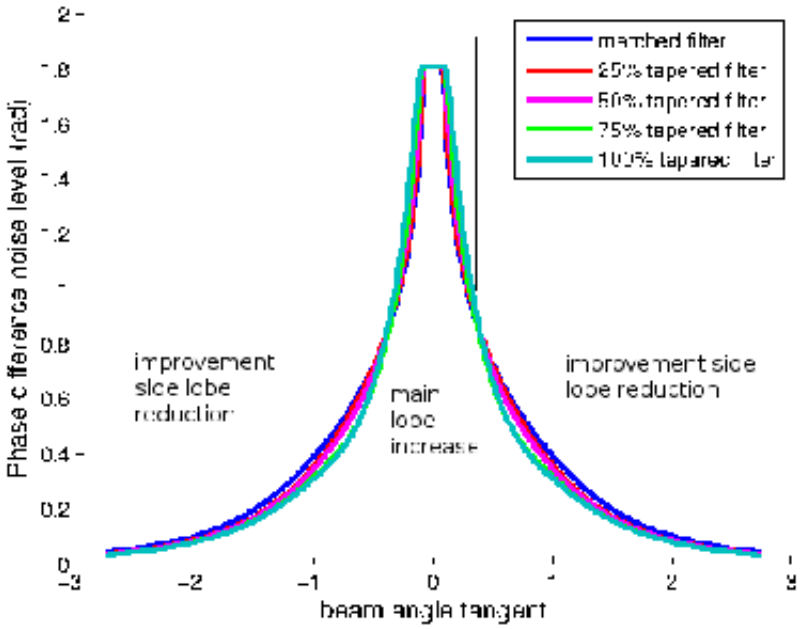

Figure 3.3.4: Noise level on the phase difference measurement

Hence, the improvement level reached by using this method (tapered matched filtering) is low since using square cosine envelope drastically reduces the equivalent bandwidth and thus significantly increases the main lobe width. In addition, when additive noise becomes the main cause of degradation, it also increases the interferometric phase difference .

3.3.2 Simulation results

It has been searched (in Appendix H) the best tapered matched filter shape following a power cosine shape. This optimal shape in frequency has been fund as a square root cosine.

$$H(\nu) = \overline{S(\nu)}\cos(\pi\frac{\nu - f_c}{B})^{1/2} \tag{3.3.8}$$

Using the stationary phase theorem (Appendix A) the temporal shape of the filter is (modulation function being $\nu = \frac{B}{T}t$):

$$h(t) = \cos(\pi\frac{t}{T})^{1/2}e^{2\pi i(f_c t - \frac{B}{2T}t^2)} \tag{3.3.9}$$

A series of simulation has been run to confirm the improvement by using the tapered matched filter allowing compressed pulse sidelobe reduction and improvement on the baseline decorrelation. The simulation scenario is still the same as in section 2.2.1.3.

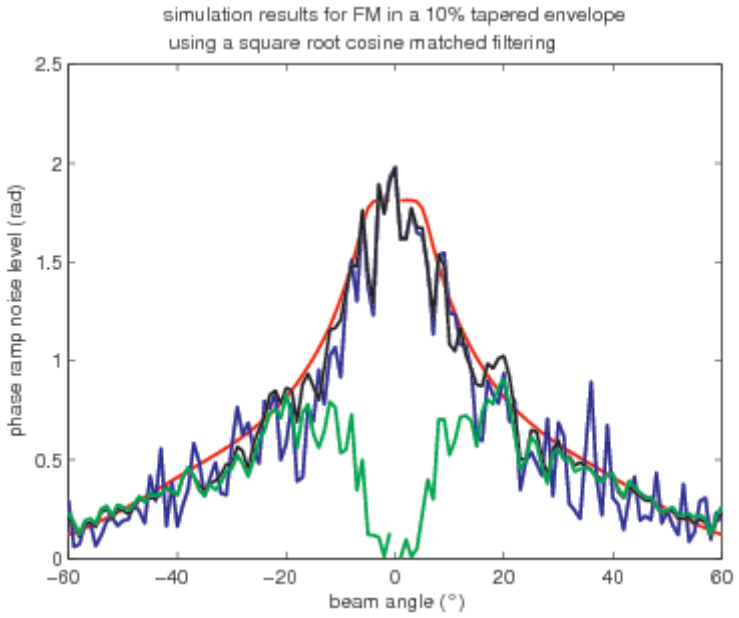

Figure 3.3.5: Phase ramp noise level estimation on simulation using a tapered matched filter (as squared root cosine). Estimations: at the detection sample (blue), with phase ramp regression (green), on a window centered on detection (black), compared with model prediction (red).

As in the two previous cases (Sections 2.3.4 and 3.2.2), the estimation of the phase ramp noise level has been done using 20 realisations using the three estimators defined on page 98 (at the detection instant in blue, from the phase ramp regression in green, on a window in black). Since only the baseline improvement was under consideration, simulations did not take into account the additive noise.

The third estimator represented in black in Figure 3.3.5 defined in section 2.3.4 on page 98 is the most robust and is compared to the prediction. The agreement between simulation results and model predictions is made using the formulas (2.3.13) and (2.3.14). Here, g_1 (defining the average of the relative error) equals 3.8% and g_2 (square root of the quadratic error mean) is equal to 0.11rad. It can be considered that the simulation results match the model predictions.

Figure 3.3.6 is another visualisation. It makes it possible to compare the phase ramp noise level (estimated on simulation by the third estimation and prediction) when using the standard and the tapered matched filtering. It allows to see the similarity between the prediction and the estimation on the simulated data, and define, for which beams (here beams higher than 20°), the second improvement proposal reduces the level of phase noise. It can be seen that the improvement is really little.

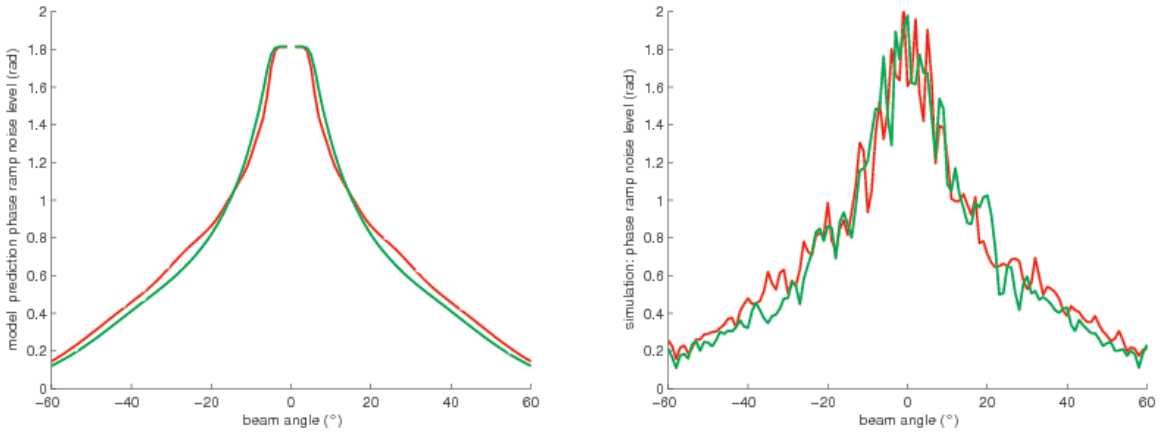

(a) Prediction

(b) Estimation on simulation (estimator 3)

Figure 3.3.6: comparison of phase ramp noise level using tapered (green) and standard (red) matched filtering as a function of beam angle from model prediction (left) and simulation (right) .

3.3.3 Results on field data

The same day as the survey data (described in section on page 85 in Table on page 101) were recorded, stave data associated to the beamformed data with the different pulse shapes were also recorded for 20 pings. These stave data have been required with the purpose: to be able to find improvements by using unadapted filtering. Indeed, as said, the change on transmitted pulse shapes reduces the transmitted energy and the idea was to be able to work only at reception to keep the maximum amount of transmitted energy.

Such stave data makes it possible to re-process the beamforming and the matched filtering. It will allows then to adapt the matched filtering as function of what kind of noise it is desired to limit. As example if the beam is in conditions where the main cause of phase ramp noise is baseline decorrelation, the matched filter will be chosen as unadapted in order to reduce sidelobes and their impact. If conversely the main noise cause comes from addtive noise, the matched filter will be the standard matched filter which maximizes the output additive signal to noise ratio.

On the stave data extracted from the file numbered 19 (see table 3.3), this corresponds to the FM 10% tapering pulse, it has been tested the filtering by the matched filter inside the squared root cosine envelope. Results in term of phase ramp noise level estimation (via the third estimator: mean of the standard deviation on a window centered on the detection, here the number of pings is 10) is plotted in Figure 3.3.7. Compared this figure with Figure 3.3.6 , results on survey data are not far from simulation data results or model predictions. The noise level is slightly higher in the re-processed data. When re-processing, some compensations (such as motion corrections) are not taken into account, and this could introduce error in ping-to-ping phase standard deviation which can explain the difference between re-processed data and simulation results and model predictions. In Figure 3.3.7, it is possible to distinguish an improvement when using the tapered matched filter (in beam angles from 20 to 60°). For beam higher than 60°, it would be certainly possible to look on the impact additive noise

considering the processing-gain loss (due to the tapered filter mismatch). However, to reduce the processing time, the received signal has been chosen to be processed on a reduced number of samples and the seafloor response for beams over 60° is missing.

Finally, the improvement by filtering with tapered matched filtering which was the objective of this part is not really visible on the field data. First of all, this improvement is theoretically really thin (Figure 3.3.6), and once again the presence of the second layer in survey area can explain why this slight improvement is vanished by its impact. The impact of the second layer is not linear and phase ramp after tapered matched filtering are more affected than the one using standard filtering. This can be enough to make this improvement as little as observed in Figure on this page.

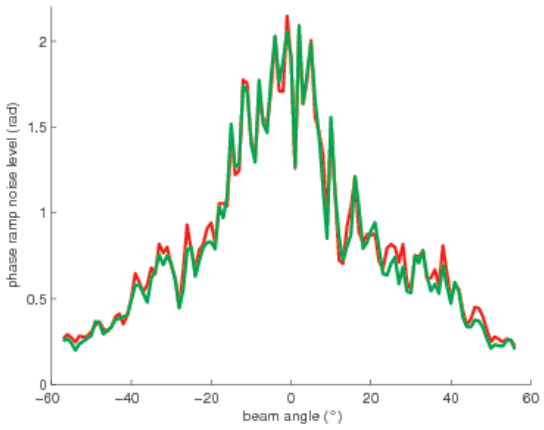

Figure 3.3.7: Phase ramp noise level estimated on reprocessed field data using standard (red) , tapered (with squared-root-cosine) (green) matched filterings

The presence of the second layer in the seafloor structure prevent us to test and clearly conclude on improvement (baseline decorrelation reduction) proposals, processing at reception.

3.4 Compromise between detect capability (limited by additive noise) and accuracy (limited by baseline decorrelation)

Tapering the transmitting signal envelope causes a loss on transmitted energy. Filtering by a unadapted matched filter is not an optimal operation. Hence, these two different approaches leads, to a decrease on the processing gain at the matched filter output. If the intrinsic noise is reduced by these methods (sidelobe reduction), the additive noise is relatively increased (because of the transmitted energy decrease). Thus in area where additive noise becomes a limitation on the bathymetric measurement the proposed techniques allowing to reduce the baseline decorrelation will be even more affected. In a certain way, it has to be defined a trade off between the capability of the detection which is limited by the additive noise and its quality limited by the intrinsic noise. The limit configuration where additive noise becomes dominant compared to baseline decorrelation (vice versa) has to be found in order to define in which conditions the unadapeted matched filter has to be used. It would also help to define

the transmitting sector where using modulated signal in tapered envelope rather than in a full envelope.

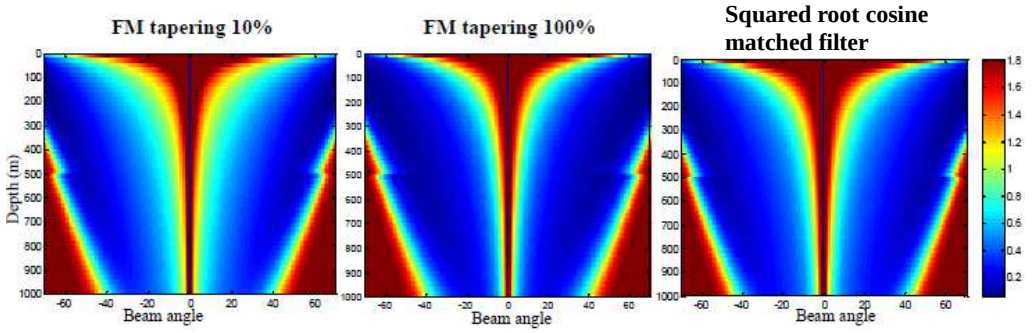

Figure 3.4.1: Phase ramp noise level as a function of depth and beam angle

Prediction of the phase ramp noise level has been done by using equation of model, using the characteristics of the EM710, as a function of depth and beam angle. Results is plotted in Figure 3.4.1. The first graph represents the 10% tapered FM pulse. The second and third graphs represent the model prediction of the phase ramp noise level by using the two proposals of improvement proposed in sections 3.2 & 3.3. The first method consists in tapering the transmitted envelope (transmission in a 100% tapered envelope). The second method consists in applying a tapered matched filter (filter in a square root cosine envelope). At 500m depth, the sounder characteristics change; transmitted power level is increased, as well as the FM pulse duration. This has been taken into account. That is why at 500m depth the phase ramps look more robust to additive noise (in outer beams). The central beams are affected by baseline decorrelation. It can be noticed that when using standard matched filtering with 10% tapered FM pulse, phase noise is higher (lighter blue color) than for the other cases. It can be noticed that the domain border in depth where additive noise seems dominant (compared to baseline) is a linear function of beam angle.

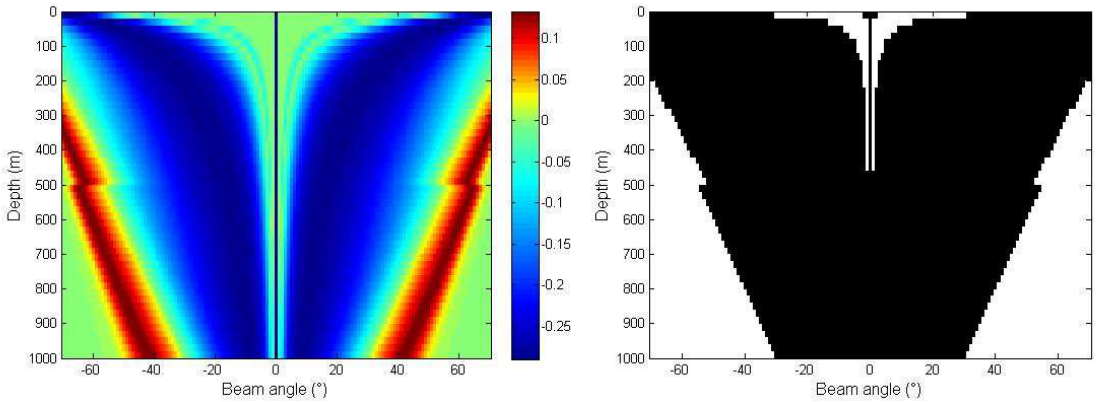

(a) Difference between 10% and 100% FM

(b) Black: Improvement domain.

Figure 3.4.2: Comparison of phase ramp noise level predictions between FM10% with FM100% with standard matched filtering as a function of depth and beam angle

Figures 3.4.3 and 3.4.2 represent the comparison between the results, and their domain of improvement by using one of the two proposed methods. The improvement brought by the first method consisting in tapering compared to the usual FM pulse (in a 10% tapered envelope) is presented in 3.4.2 . Phase ramps using this method are improved in domain configuration (in depth and angle) where baseline decorrelation was the main noise cause. This was predictable since the interferometric coherence coefficient considering only baseline decorrelation was predicted higher (whatever the interferometric configuration). However, as expected where additive noise is dominant phase ramp are strongly damages (due to the reduction of transmitted energy). The domain border (between additive noise and baseline decorrelation) in depth is a linear function of beam angle. This linear function could be numerically-estimated and makes it possible to optimise the transmitting sectors.

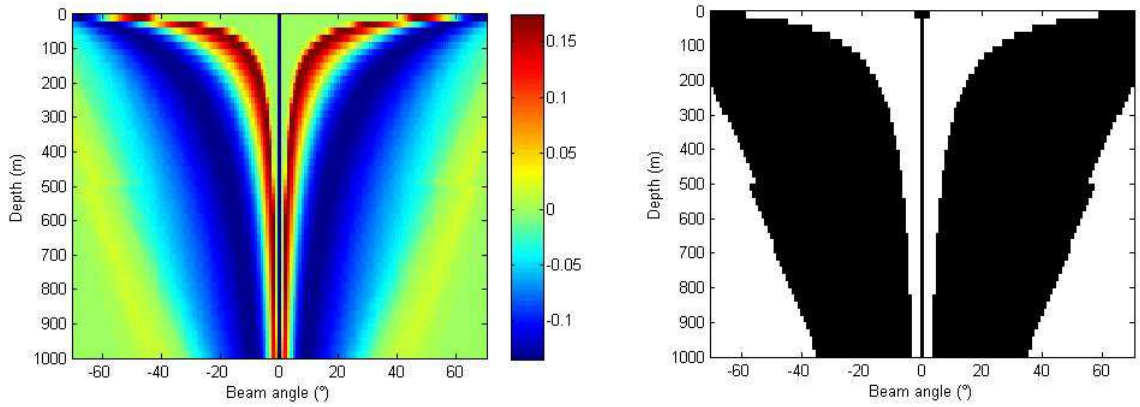

(a) Difference- standard and tapered matched filtering

(b) In black: Improvement domain

Figure 3.4.3: Comparison of the phase ramp noise level (FM10%) from model with standard matched filtering and unadapted tapered filtering (square root cosine envelope) on a 10%-tapered linear chirp as a function of depth and beam angle

The improvement by using a tapered matched filtering at reception on a rectangular transmitted pulse is presented in Figure 3.4.2. It is observed that concerning baseline decorrelation the phase ramp noise level is decreased in certain domain. Indeed, in some configurations, the decrease of pulse compression sidelobe level is enough to reduce baseline decorrelation (decrease interferometric noise). In other configurations, the increase of the pulse-compression main-lobe width prevails on side-lobe level reduction and baseline decorrelation is even worst. Comparing with the first solution, filtering with unadapted matched filter is less efficient (considering baseline decorrelation reduction). However the damage considering additive noise is lower than for the first solution. The linear border (separating additive noise and baseline decorrelation predominance domain) defines the conditions when filtering by unadapted matched filter should be preferred to standard matched filtering.

3.5 Proposal of new frequency modulation

3.5.1 Frequency modulation function maximizing transmitted energy while minimizing sidelobes

Here, the issue is to maximize the transmitted energy. Thus, the temporal transmitted pulse envelope $e(t)$ is considered as rectangular.

$$\max \int_{\mathbb{R}} e^2(t)dt \tag{3.5.1}$$

In addition, the sidelobes after pulse compression have to be minimized. The signal after pulse compression can be written as:

$$\begin{aligned} w(t) =& s(t) * s^*(-t) = \int_{\mathbb{R}} s(\tau)s^*(t-\tau)d\tau \\ =& \int_{\mathbb{R}} S(\nu)S^*(\nu)e^{2\pi jt\nu}d\nu = \int_{\mathbb{R}} |S(\nu)|^2 e^{2\pi jt\nu}d\nu \end{aligned} \tag{3.5.2}$$

$w(t)$ is the inverse Fourier transform of the square module of $S(\nu)$. In order to the compressed pulse $w(t)$ presents low sidelobes, the frequency shape $|S(\nu)|^2$ has to be really tapered.

in order to respect these two requirements,a non-linear frequency-modulation function [Col, 2002, Coo, 1993] is searched. For this purpose, some results from the stationary phase hypothesis presented in Appendix (A) will be used, notably the relation (A.2.2)

3.5.1.1 Rectangular temporal envelope and frequency-domain envelope close to cosine function

The fundamental hypothesis are the following: the temporal envelope is rectangular and frequency domain envelope takes the shape of cosines functions (which are tapered envelope shapes) :

$$\left\{ \begin{array}{rcl} a(t) & = & \Pi(\frac{t}{T}) \\ |S(\nu)|^2 & = & A_n \cos^n(\frac{\pi(\nu-f_c)}{B})\Pi(\frac{\nu-f_c}{B}) \end{array} \right. \tag{3.5.3}$$

The results obtained by using the stationary phase developments (A.2.2) are exposed below.

- **case n=1**

$$t + T/2 = A_1 \frac{B}{\pi}(\sin(\pi\frac{\nu - f_c}{B}) + 1) \tag{3.5.4}$$

In order to keep boundary conditions (which corresponds to the energy conservation of Parseval theorem) $A_1 = \frac{\pi T}{2B}$

$$t_1(\nu) = \frac{T}{2}\sin\left(\pi\frac{\nu - f_c}{B}\right) \tag{3.5.5}$$

By inversion of the previous expression, the time frequency relation is found (ν as a function of t). Reminding that the time-frequency relation is the derivative of the modulation $\omega(t)$ function, the latter can be found by integrating the previous one:

$$\begin{aligned} \omega'(t) =& \nu = f_c + \frac{B}{\pi}\arcsin(\frac{2t}{T}) \\ \Rightarrow \omega(t) =& f_c t + \frac{B}{\pi}\left(t\arcsin(\frac{2t}{T}) + \frac{T}{2}\sqrt{1-(\frac{2t}{T})^2}\right) \end{aligned} \tag{3.5.6}$$

- **case n=2**

$$t + T/2 = \frac{A_2}{2}\left(\nu - f_c + B/2 + \frac{B}{2\pi}\sin\left(2\pi\frac{\nu - f_c}{B}\right)\right) \tag{3.5.7}$$

In order to keep boundary conditions, it must be $A_2 = 2T/B$

$$t_2(\nu) = T\left(\frac{\nu - f_c}{B} + \frac{1}{2\pi}\sin(2\pi\frac{\nu - f_c}{B})\right) \tag{3.5.8}$$

Reversing the time frequency relationship is not easy in this case, but approximative polynomial relation can be done. Then, by an integration it is possible to obtain an approximative frequency modulation function $\omega(t)$ which fulfils the requirements.

3.5.1.2 Rectangular temporal envelope and Gaussian frequency envelope

As in the paragraph 3.5.1.1 the temporal envelope is chosen as rectangular. The frequency domain envelope has to approximate a Gaussian (tapered envelope shape):

$$\begin{cases} a(t) &= \Pi(\frac{t}{T}) \\ |S(\nu)|^2 &= Ae^{-\alpha(\nu-f_c)^2}\Pi(\frac{\nu-f_c}{B}) \end{cases} \tag{3.5.9}$$

By using stationary phase development (A.2.2) it leads to

$$t + \frac{T}{2} = \int_{-\frac{B}{2}+f_c}^{\nu} Ae^{-\alpha(u-f_c)^2}du \tag{3.5.10}$$

Considering that αB is high (which is actually expected since the frequency domain shape has to be a tapered function of frequency on bandwidth B. If the contrary case, the Gaussian would have been approximated to a constant function over B and Gaussian tapering would have been useless), the integral of the previous expression can be expressed thanks to the erf function (Gauss error functionerf$(x) = \frac{2}{\sqrt{\pi}}\int_0^x e^{-y^2}dy$)

$$t + \frac{T}{2} = A\int_{-\infty}^{\nu-f_c} e^{-\alpha\nu^2}d\nu = \frac{A}{2}\sqrt{\frac{\pi}{\alpha}}(\mathrm{erf}(\sqrt{\alpha}(\nu - f_c)) + 1) \tag{3.5.11}$$

In order to keep boundary condition (respect Parseval theorem):

$$T = A\sqrt{\frac{\pi}{\alpha}} \tag{3.5.12}$$

And the frequency-time relation is:

$$t = \frac{T}{2}\mathrm{erf}\left(\frac{A\sqrt{\pi}}{T}(\nu - f_c)\right) \tag{3.5.13}$$

The inversion of the time frequency relation gives the frequency ν (equal to to the derivative of the modulation function ω) as a function of the time t.

$$\nu = f_c + \frac{T}{A\sqrt{\pi}}\mathrm{erf}^{-1}(2\frac{t}{T}) \tag{3.5.14}$$

There is a polynomial development of the function erf^{-1} (inverse of the Gauss error function).

$$\nu = f_c + \frac{T}{2A}\left[2\frac{t}{T} + \frac{\pi}{12}(2\frac{t}{T})^3 + \frac{7\pi^2}{480}(2\frac{t}{T})^5 + \frac{127\pi^3}{40320}(2\frac{t}{T})^7\right] \tag{3.5.15}$$

By integration it leads to:

$$\omega(t) = f_c t + \frac{T}{2A}\left[\frac{t^2}{T} + \frac{2\pi}{3T^3}t^4 + \frac{7\pi^2}{90T^5}t^6 + \frac{127\pi^3}{2520T^7}t^8\right] \tag{3.5.16}$$

3.5.2 Non linear frequency modulation

Thanks to the previous paragraphs 3.5.1.1 and 3.5.1.2, other types of frequency modulation (non linear) has been defined allowing to taper the frequency domain signal envelope and thus to reduce the sidelobes of the pulse compression pulse shape [Col, 2002, Coo, 1993, Var, 2003, Col, 1999, Lev, 1988].

In this section, the last modulation function defined in the equation (3.5.16), paragraph 3.5.1.2, with the usual linear frequency modulation in the rectangular envelope (tapered at 10%) and the other linear frequency modulation in a 100% tapered envelope. All these modulations are designed so that their main lobe after pulse compression is the closest from one to the other.

3.5.2.1 Pulse shapes

In this paragraph, two pulse shapes are considered in the same 10% tapered envelope. The first one follows a linear frequency modulation with the sweep bandwidth B=830Hz and duration T= 40ms. The second follows the modulation defined by:

$$\omega(t) = f_c t + 0.85\frac{B}{2T}\left[\frac{t^2}{T} + \frac{2\pi}{3T^3}t^4 + \frac{7\pi^2}{90T^5}t^6 + \frac{127\pi^3}{2520T^7}t^8\right] \tag{3.5.17}$$

Figure 3.5.1 shows the time frequency relation (or criterion of the stationary phase) $\nu(t) = \omega'(t)$ for these 2 pulse shapes.

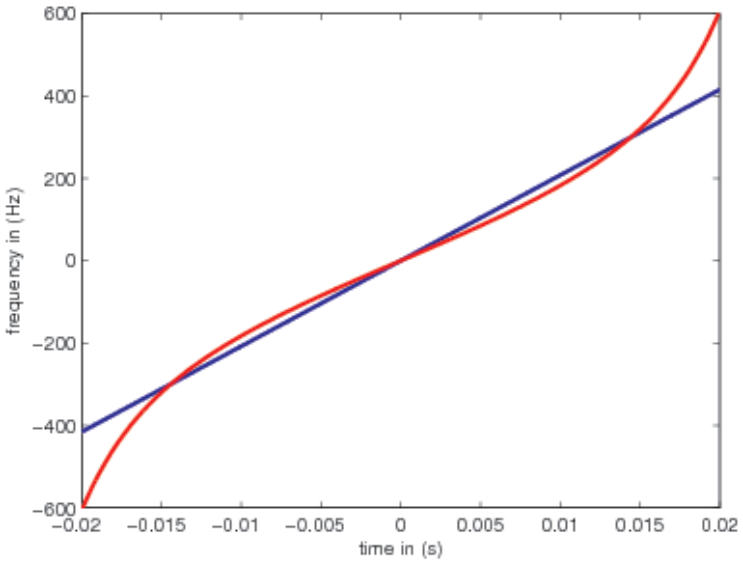

Figure 3.5.1: Time-Frequency relation (Blue: linear modulation, Red: Modulation defined by (3.5.17)).

These two pulse shapes are then compared to a chirp (linear frequency modulation) in a 100% tapered envelope with the parameters stated as T =20ms and B =1750Hz.

Figure3.5.2a shows the normalized frequency occupation of these three different pulses and their resulting compressed envelope after matched filtering.

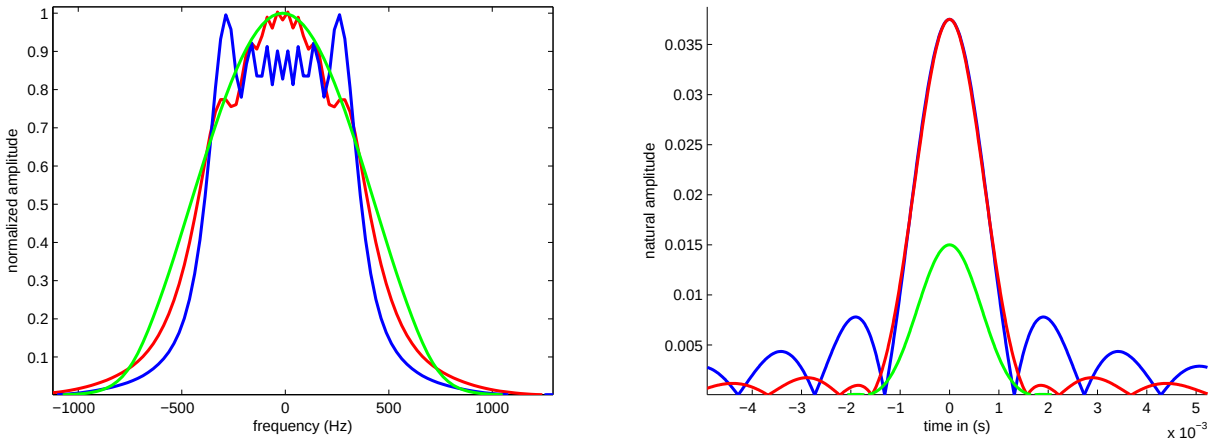

(a) Fourier transform

(b) Pulse compression envelope

Figure 3.5.2: Comparison of the three different pulses: 10% tapered linear chirp (blue), 10%-tapered chirp using modulation defined by (3.5.17) (red) , 100% tapered linear chirp (green)

The three pulses present similar bandwidth occupation. As expected, the linear modu-

lation signal with the 10% tapered envelope presents an approximately-rectangular Fourier transform, whereas the linear chirp in the 100% tapered envelope presents a really smoother Fourier transform envelope (close to a square cosine). This was predictable thanks to the stationary phase development. The pulse using the non-linear frequency modulation (polynomial close to the erf^{-1} function) presents a tapered Fourier transform envelope, which appears as trade-off between the Fourier transform shapes of the two first pulses.

From Figure 3.5.2b, it can be noticed that the main lobes of these three pulse shapes after pulse compression are really close (same effective bandwidth). The linear modulation in the 10% tapered envelope presents high sidelobes due to the quasi- rectangular aspect of its Fourier transform. The linear modulation in the 100% tapered envelope presents almost no sidelobe. However its maximum amplitude is strongly decreased (energy loss by tapering the envelope). It means that the signal to noise ratio considering additive noise will be approximately four-time lower by considering this pulse shape than when the use of signal in a 10% tapered envelope. Indeed, considering that duration and transmitted power level are the same, the transmitted energy is decreased by a factor 3/8. Here is the interest of using non-linear frequency modulation function (polynomial approximated erf^{-1}). Indeed such a modulation function allows to strongly decrease sidelobes while the transmitted energy is kept as maximum (the final SNR considering additive noise is unchanged).

3.5.2.2 Performance prediction for these pulse shapes

Let remind here that the performance level of the bathymetric measurement is directly proportional to the correlation degree of the interferometric signal S_a and S_b. This correlation coefficient is the normalized Fourier transform of the squared compressed envelope at a particular point which depends on the central frequency and the configuration parameters of the interferometer (water depth, interferometric spacing, beam angle...).

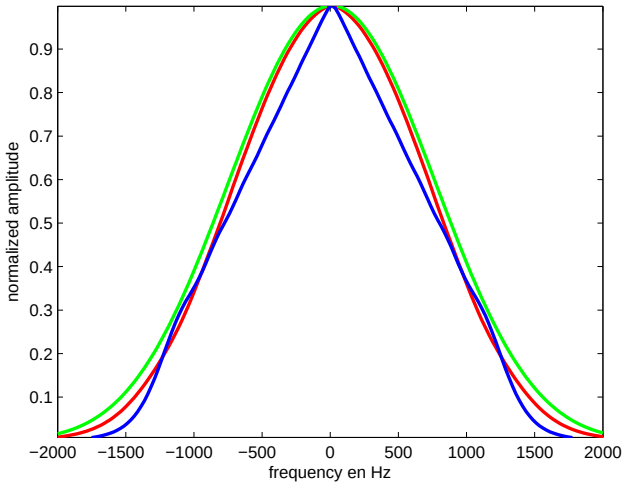

Figure 3.5.3: Normalized Fourier transform of the squared compressed envelope for the different pulses: 10% tapered linear chirp (blue), 10% tapered non-linear chirp whose modulation is defined by (3.5.17) (red), 100% tapered linear chirp (green) .

Figure 3.5.3 plots the normalized Fourier transform of the squared envelope of the three considered pulse compressed signals. The coherence coefficient using the non linear chirp gets closer to the one with the use of 100% tapered linear chirp. It is also better for a lot of interferometer configuration than the one when using the commonly-used linear chirp in the same 10%-tapered envelope.

From the coherence ratio defined as a particular point of the squared pulse-compressed envelope Fourier transform, it is possible to define the noise level over the phase difference of the interferometric signals.The interferometric configuration used for the prediction of the phase noise level is the same as all the cases defined previously: f_c =73 kHz, H =200 m, a =0.33 m. The results for the different pulses are plotted in Figure 3.5.4.

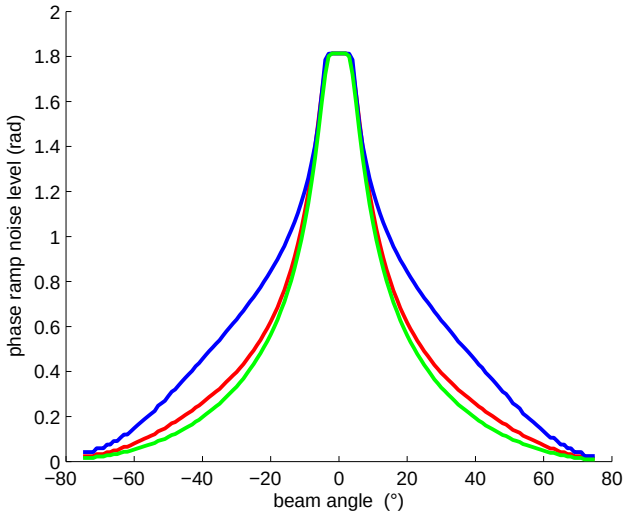

Figure 3.5.4: Phase ramp noise level prediction as function of beam angle for the different pulses: 10% tapered linear chirp (blue), 10% tapered non-linear chirp whose modulation is defined by (3.5.17) (red), 100% tapered linear chirp (green) (considering baseline decorrelation only)

Not surprisingly, the phase ramp noise level is predicted lower when using the non-linear chirp compared to linear chirp for a 10% tapered envelope, thanks to the sidelobes reduction (Figure 3.5.4) . The improvement level is really close to the improvement observed when using fully tapered transmitted pulse. In addition, considering the domain where additive noise is the main cause of bathymetry degradation, the non-linear chirps should have better performances than fully-tapered linear ones.

3.5.2.3 The Doppler effect on the non linear frequency modulation (considering baseline decorrelation)

The non-linear frequency modulation has the advantage to reduce the sidelobes level of the compressed pulse. Hence, it limits the sidelobe impact on the final bathymetric measurement (considering baseline decorrelation). However, it has the drawback to be more sensitive to the Doppler effect notably considering its performance in sidelobes reduction.

Ambiguity function In order to look at the impact of the Doppler effect, on the different pulse shape, let us use the ambiguity function defined as follows:

$$A(\tau, k) = \int_{-\infty}^{+\infty} s(\eta t) s^*(\tau - t) dt \tag{3.5.18}$$

The Doppler shift η is defined as $\eta = (1 + \frac{v_d}{c})$ where v_d is the constant radial speed.

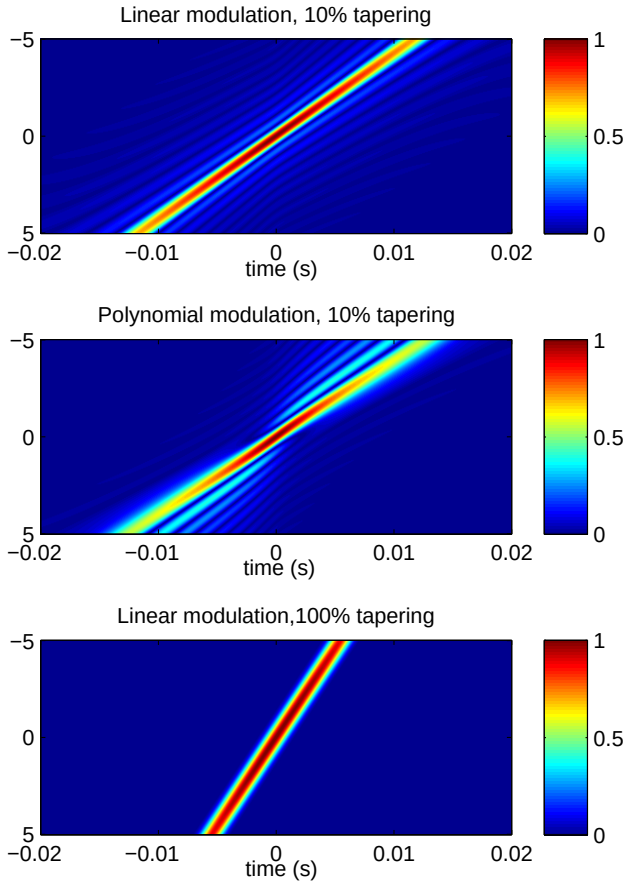

Figure 3.5.5: Ambiguity function of the three pulses: 10% tapered linear chirp (upper), 10% tapered non-linear chirp whose modulation is defined by (3.5.17) (middle), 100% tapered linear chirp (lower)

Figure 3.5.5 presents the ambiguity function of the different pulse shapes defined in the previous section :

1. linear chirp with 10% of tapering
2. linear chirp with 100% of tapering (same pulse compressed main lobe than the first chirp)

3. non-linear modulated pulse with 10% of tapering (presenting less sidelobes than the 10% tapered chirp and carrying the same amount of energy)

The results are presented as a function of τ and v_d. The ambiguity function is normalized so that it presents a maximum in (0,0) equal to 1.

It can be noticed that the maxima of the ambiguity function for eachτ follow the time-frequency relation of the modulation.

$$\delta_f = \frac{f_c}{k} - f_c = \omega'(\tau) - f_c \tag{3.5.19}$$

This relation gives the bathymetric measurement bias due to the time shift from the Doppler-shifted signal filtered by the matched filter.

As expected, the ambiguity time-frequency relation is linear when considering chirp (linear frequency modulated signal as its name indicates so).

$$\delta_f = \frac{B}{T}\tau \quad \tau = \frac{T}{B} f_c \frac{v_d}{c} \tag{3.5.20}$$

The linear modulation of the 100%-tapered pulse uses a longer sweep bandwidth. This was increased to conserve the same equivalent main lobe after pulse compression than 10%-tapered-FM pulse-compression. The time shift for this modulation is thus less important.

It can be noticed that the cross section of the ambiguity function of the polynomial modulation at $v = 0$, corresponding to no Doppler effect, effectively presents really low sidelobes. However, on the other cross sections (at $v \neq 0$) the sidelobes become very higher. In addition, the main lobe looses as much energy as the sidelobes get back.

coherence coefficient using ambiguity function Previously, considering only the intrinsic noise (baseline decorrelation), it was stated that the coherence ratio of the two interferometric signals S_a and S_b is a particular point of the normalized Fourier transform of the square of the compressed envelope. The Dopplerized compressed signals are considered as non-modulated signals. And by generalizing the previous statement, the coherence ratio is defined as a particular point of the normalized Fourier transform of the squared envelope of the matched filter output (corresponding to the different cross-sections in the v-axis of the ambiguity function). Thus, by using the ambiguity function, the coherence ratio in case of the Doppler effect defined thanks to the radial speed v (between target and transmitter and receiver), the coherence ratio is a function of v and expressed in the particular point f_p (see paragraph 2.3.3.2 and Appendix E)

$$C(f_p, v) = \frac{\int_{\infty}^{\infty} |A(\tau, 1 + \frac{v}{c})|^2 e^{-2\pi i f_p \tau} d\tau}{\int_{\infty}^{\infty} |A(\tau, 1 + \frac{v}{c})|^2 d\tau} \tag{3.5.21}$$

The representation of (3.5.21) for the three signal as a function of v and f_p is plotted in the Figure 3.5.6 .

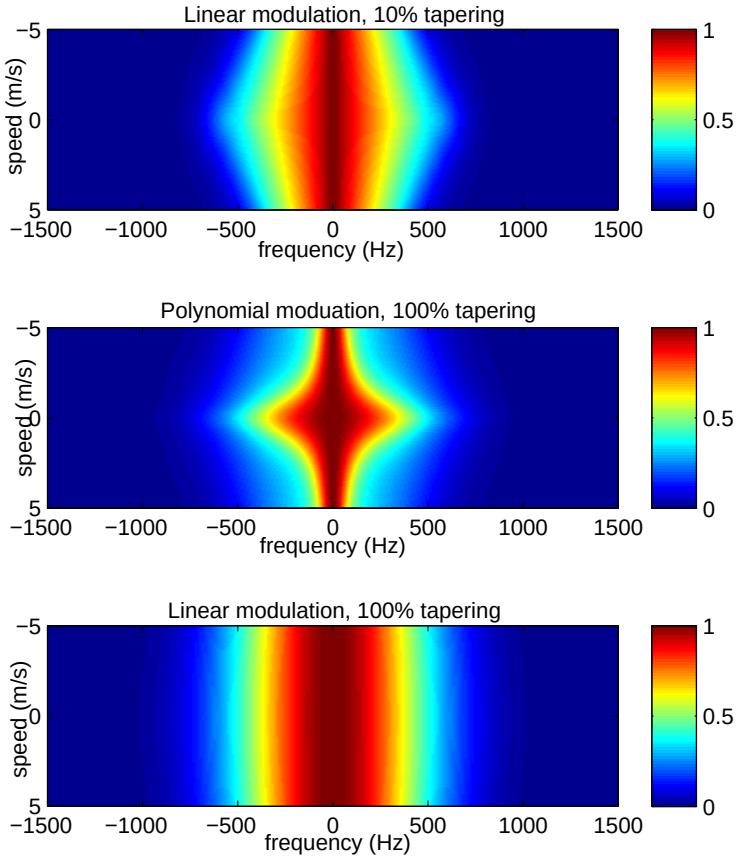

Figure 3.5.6: Coherence coefficient for the three pulse shapes: 10% tapered linear chirp (upper), 10% tapered non-linear chirp whose modulation is defined by (3.5.17) (middle), 100% tapered linear chirp (lower)

The aim is to have the coherence ratio the higher as possible since the signal to noise ratio derived from the baseline is an increasing function of the coherence ratio. From Figure 3.5.6, it can be shown that the Fourier transform of the square pulse compressed envelope is really large in the case of non linear modulation in the case of no motion $v = 0$. Indeed the pulse compression presents really low sidelobes and the behaviour of $C(f_d, 0)$ is close to the behaviour of the 100% tapered pulse compressed $C(f_d, 0)$. However, when v is not null, the pulse compression for the non linear modulation presents high sidelobes. This impacts the coherence ratio which decreases for a given f_d (vertical cross-sections of the graph). On such sections, for non linear chirp, the coherence coefficient drops when the radial speed is not null. Conversely, for linear modulation modulation, it can been seen that the coherence level of interferometric signal is not really affected (vertical cross section for a given frequency is almost a constant function). Indeed sidelobe level remains closely the same even when considering dopplerised pulse compressed shapes. This prediction comes to reinforce the conclusion made in part 2.2.2 as Doppler effect does not affect the phase ramp statistics, for

linear frequency modulated signals.

Figure 3.5.7 presents the comparison of the coherence coefficient (Fourier transform of the square pulse compressed shape) of the different considered modulated signals. Considering baseline decorrelation, the coherence ratio is always better when using tapered signal in transmission compared to 10%-tapered chirp. This is the case, when the Doppler effect. For non-linear modulation, the improvement compared to linear modulation is not robust to the Doppler effect.

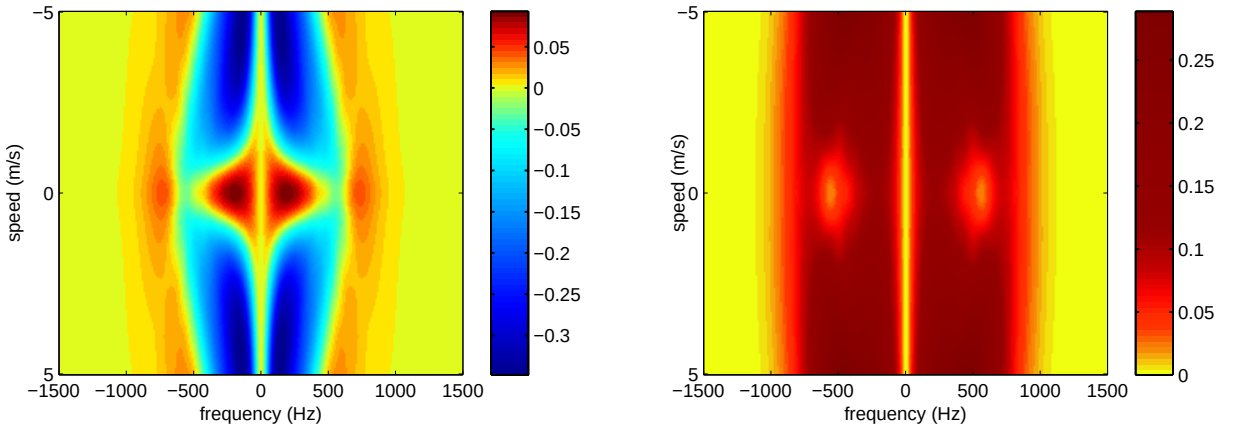

(a) non linear *vs* linear chirps in 10% tapered envelope (b) linear chirps in 100% tapered *vs* linear 10% tapered

Figure 3.5.7: comparison of coherence coefficients for the two improvement proposals: non-linear chirp (left), tapered linear chirp (right) compared to linear chirp

3.5.3 Validation on simulation

A series of simulations using the signal defined in (3.5.17) has been run with the same conditions as the previous simulations (see sections 3.2.2 and 2.3.4). 20 realisations of a random array of elementary scatterers has been generated. Received signals are processed as summation of the contribution on the motion less array. The additive noise is not taken into account. Beamforming is processed in time and the pulse compression is applied by standard matched filtering.

The noise level on the interferometric phase difference is estimated with the same three estimators (as defined on page 98):

1. Standard deviation at the detection sample (represented in blue in Figure 3.5.8)

2. Mean of estimations from phase ramp regression (equation (2.1.79)) (represented in green in Figure 3.5.8)

3. Mean of standard deviation over a window centered on the detection sample (represented in black in Figure 3.5.8)

The noise levels estimated from the simulations is compared to the model prediction (red) in Figure 3.5.8, and shows a good agreement.

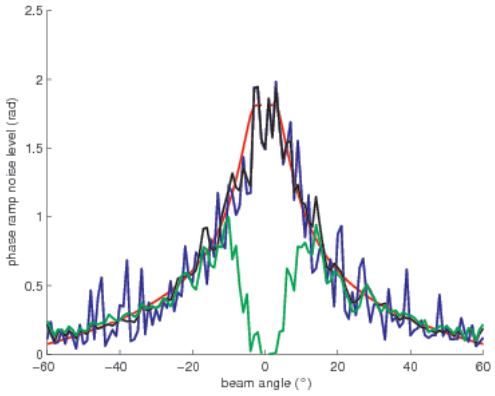

Figure 3.5.8: Phase ramp noise level on simulations (blue, green, black) and comparison with model prediction (red)

The agreement between the simulation data estimation and the model prediction is measured with g_1 and g_2, the same indices defined by (2.3.13) and (2.3.14) and used in sections 2.3.4 and 3.2.2. g_1 is the mean of the relative error between the prediction and the third estimator and is equal here to 5,7%. $g_2$is the square root of the quadratic error mean and equals 0.09 rad. Once again, the simulation results are compliant with the model predictions. Figure (3.5.9) gives another representation to compared simulation results with model prediction. It confirms that non linear frequency modulation reduces baseline decorrelation (thanks to sidelobe level reduction).

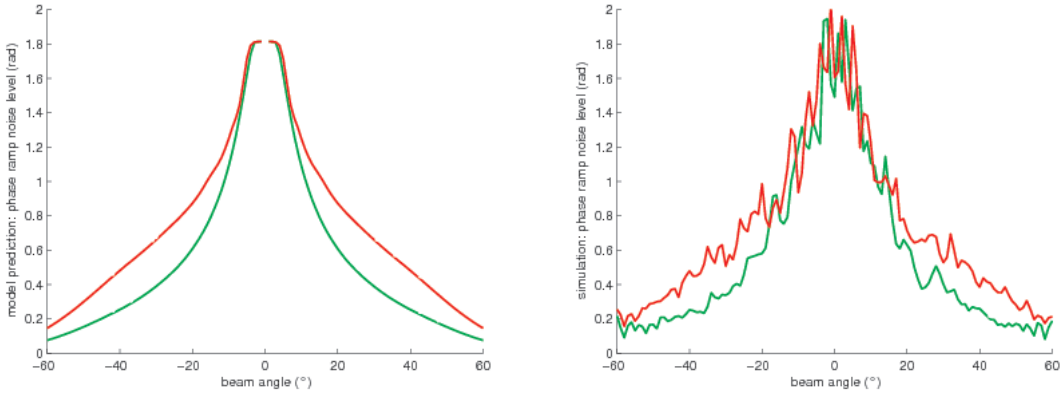

(a) Prediction (b) Simulation estimation

Figure 3.5.9: Comparison of the bathymetric performance in terms of phase ramp noise level using non linear modulation (green) *vs* linear modulation (red)

In addition, its transmitted envelope is rectangular thus the pulse can carry a maximum of energy. This kind of pulses are thus also efficient regards to additive noise.

However, as seen in paragraph 3.5.2.3, the pulse compression signal envelope is really sensitive to Doppler effect presenting high sidelobes in this case. Thus to use such pulses (non linear frequency modulated signal) the strategy of the Doppler effect compensation should

probably be changed. In this case, it would be certainly interesting to predict the Doppler effect before the matched filtering to filter with a dopplerized adapted matched filter.

3.6 Conclusion on the proposed solution of improvement

It has been shown that bathymetry using modulated signal suffers more from baseline decorrelation than CW signals. All the improvement solutions aims thus at reducing it. Three solutions has been proposed to improve bathymetric measurement.

- Transmitting in a tapered envelope (method 1);
- filtering by a tapered matched filter (method 2);
- using non linear frequency modulation (method 3);

	method 1	method 2	method 3
Baseline decorrelation reduction	***improved***	it ***depends*** (main lobe width increases as function of sidelobe level decreases)	***improved***
Additive noise reduction	***damaged*** because of transmitted energy reduction but could be ***limited*** by increasing pulse duration	could be ***optimised*** by choosing between standard and tapered matched filter	remains the ***best***
Possible need to predict Doppler effect before matched filtering	***No***	***No***	***Yes***

Table 3.4: Comparison of improvement proposal

Table 3.4 sums up the advantages and drawbacks of each improvement proposal.

The first method consisting in tapering the transmitted envelope is really efficient concerning the reduction of the pulse compression sidelobes effect. The main drawback is that by tapering the envelope, the transmitted energy is reduced. Thus, the use of this pulse (transmitted in a tapered envelope) makes the bathymetric results more sensitive to additive noise. However, the use of this kind of pulses are still better to CW-pulse one considering additive noise robustness. In addition, this can be limited by increasing the FM pulse duration. If pulse duration is not a critical parameter, the first solution is thus really convenient.

The second proposal works on filtering the reception. This is convenient when the modulated signal duration is limited. The main interest of the second solution is that conversely to

the first method the transmitted energy is maximum for a given limited pulse duration. The idea is to filter with unadapted matched filter (in a tapered envelope) in the conditions where the main bathymetric degradation cause is baseline decorrelation while keeping the standard matched filtering in the case of additive noise predominance (additive signal to noise ratio maximum for a given pulse duration). However, the main drawback of this technique is that the equivalent signal bandwidth is reduced by the tapered filter. And whereas the pulse compression sidelobe decreases, the main lobe width increases. This was not the case with the first solution since working at transmission allows to keep the pulse compressed main lobe width as constant, by increasing the transmitted sweep bandwidth while tapering the envelope. Thus the improvement observed when working at reception considering baseline decorrelation is always lower than when working at transmission.

Third method is good regarding the bathymetric-quality optimisation for additive and intrinsic noise. The transmitted envelope being rectangular the transmitted energy for a limited pulse duration is maximum relatively to it. Hence, with the matched filtering, the bathymetric quality is optimal for a given pulse duration, in the configuration where additive noise is dominant. In addition since pulse compression presents lower sidelobe, the bathymetric result is improved when baseline decorrelation was the noise main cause. And this kind of modulated signal is compliant with both additive and intrinsic noise reduction. However it advantage is lost because of its sensitiveness to Doppler effect. This raises the question about reviewing the Doppler effect compensation. However beside possible problems with platform motion, this kind of signal has not been implemented and tested yet (It may have some other problem caused by propagation distortion, backscattering) .

Conclusion

The latest generation of MBES makes use of modulated signals in order to increase the achievable swath while keeping a high resolution. Indeed modulated signals allow to increase the transmitted energy in ocean medium via pulse-duration increasing. Associated with pulse compression (matched filtering), the process is equivalent to have used more-powerful, shorter non-modulated signal. The resulting signal to noise considering the ambient noise is thus improved.

In practice, modulated signal use admittedly increases the sounder angular swath which is buried by the additive noise (in case of CW). However, bathymetric measurement quality from MBES using modulated signal (FM) (for middle swath) is observed noisier compared to the use of continuous wave (CW). It is contrary to expectation since FM signal use has precisely been introduced to improve the MBES bathymetry measurement.

This was the problematic of the PhD work: to understand why the use of FM signal causes bathymetric measurement damage and propose improvement solutions.

Concerning the different causes of bathymetric measurement damage, two possible causes were explored. The first one was the Doppler effect which was assumed to play differently on interferometric signal depending on CW or FM use. Indeed, considering Dopplerized signals, the matched filtering used to process the pulse compression in case of FM use mismatches with the received signal. A meticulous study of the Doppler effect on interferometric signal has been conducted, based on model (allowing prediction) and support by simulation, considering both CW and FM signal. If the Doppler effect is a well-known phenomenon, no study (before this PhD work) has been done to predict its effect on bathymetric signal. This study has concluded that Doppler effect also impacts CW signal causing a bias on seafloor angle localisation (unknown effect). This effect is really low and more felt on the side beams (where bathymetry measurement suffers from other degradation causes). It has thus not been considered until now. The effect on bathymetric FM signal is double; they are affected by bias in beam angle steering the same as CW, but also by a time bias introduced by the mismatched pulse compression. The latter is corrected as post processing. It has been discussed the advantages and disadvantages of such processing. However, assuming that time bias is well corrected, bathymetric FM signal is not more affected by the Doppler effect than CW. Indeed Doppler effect has been shown to not change the observed noise level. However, on simulations proposed to support the Doppler study, noise level on interferometric phase difference with FM signal appears really higher than with CW.

The second cause of degradation, which has been studied, comes from intrinsic noise causes. The only difference between FM pulse compressed signal and CW pulse is the presence of sidelobes. These side lobes bring a piece of backscattering signals which behaves as a noise on (or interferes with) the main interferometric signals (from pulse compression main lobe).

This phenomenon is baseline decorrelation. It has been shown that baseline decorrelation (from pulse-compressed sidelobe) can explain the bathymetric degradation when using FM signal, inducing the interferometric signal noise in some configuration twice higher than when using equivalent CW pulse. The baseline decorrelation study has been conducted on three supports: model, simulation and field data. If model and simulation agree, field data slightly diverges. This has been explained by the possible presence of an additional backscattering seabed layer on data area recording. However, the three approaches have concluded that the bathymetric degradation when using FM signals comes from pulse compression side lobes (via baseline decorrelation).

Improvement proposals have been done in order to reduce the impact of sidelobes (from the pulse compression) in order to improve bathymetric measurement when using modulated signal. Three different proposals have been done. The first one consists in working at the transmission with a smoother envelope. The study of such a proposal has been done based on model, simulation, field data (unfortunately once again affected by a second layer). This method allows to strongly improve the bathymetric measurement statistics in configuration where baseline was the main cause of noise. However, tapering the transmitted envelope strongly decrease the transmitted energy and in configuration where ambient noise was predominant, the tapered modulated signals are less efficient. The transmission by sectors can be used to overcome it. The second method was working at reception with not changing the transmitted pulse shape. The study of the second proposal has been done on model, simulation and field data (however this last one was not convincing probably due to the second layer presence). The main interest is to keep the maximum of transmitted energy and thus be the more efficient concerning ambient noise robustness. This solution can be also convenient because it only needs to change the processing part of the sounder. The problem with this method is by reducing the side lobe of the pulse compression the main lobe width is also increased. Thus, baseline decorrelation gains on the sidelobe level reduction but looses on mainlobe width increase. Finally the second method will always be less efficient than the first one considering baseline decorrelation reduction. However by considering that the filtering can be adapted depending to the beam, it is possible to use an optimum filtering (considering the goal: baseline or additive noise reduction) for any beam and improve bathymetric measurement for all the swath. The third method is at transmission by using non linear frequency modulation shape. The main interest of this method is to be able to keep the transmitting pulse shape, which allows to maximize the transmitted energy. The signal to noise ratio considering ambient noise is thus maintained, and this kind of pulse will give the best performance in configuration where additive noise is predominant. In addition the non linearity of the modulation allows to decrease the pulse-compression sidelobe level, which will allow to reduce baseline decorrelation as well. This kind of pulse is really promising. However, the implementation of such signal needs a change in sounder systems. And this has not been tested in real situations (only model and simulation for the PhD work). It maybe suffers, in real conditions, from other degradation causes (lost of stability in the medium, or at transducer generation). In addition, these signals would lose their interest in term of baseline reduction in presence of Doppler effect. To keep its interest, it can be imagined that the Doppler effect could be taken into account before pulse compression (creating a Dopplerized matched filtering). At this stage of the argumentation, many developments and tests remain to be done and nothing could surely be concluded concerning this last improvement proposal.

Appendix A

Stationary phase theorem

A.1 Applied to Fourier transform calculation

Let us consider the modulated signal defined as follows :

$$s(t) = a(t)e^{2\pi j\omega(t)} \tag{A.1.1}$$

where $\omega(t)$ represents the frequency modulation function. If the frequency modulation is a type of linear then $\omega(t)$ is $\omega(t) = f_c t + B/2Tt^2$. $u(t)$ is the signal envelope shape. The Fourier transform of such a signal is by definition:

$$S(\nu) = \int_{-\infty}^{+\infty} a(t)e^{-2\pi j(\nu t - \omega(t))}dt \tag{A.1.2}$$

The theory of the stationary phase [Coo, 1993, Cur, 1991] is actually an approximated the calculation of an integral which can be written as the integral defined in A.1.2.

This method of the stationary phase consists in identifying that the exponential term inside the integral is an oscillating term. When oscillation are fast the integral becomes null (since the integration duration is long). Thus the main contribution in this integral occurs when the oscillation rate is low or minimum, in other words when the derivation of the phase term becomes null.

$$-2\pi\frac{d}{dt}(\nu t - \omega(t)) = 0 \qquad \Leftrightarrow \qquad \nu = \omega'(t) \tag{A.1.3}$$

Considering that $\omega'(t) \neq cst$ (which mean that the signal is actually modulated in frequency), for each frequency ν_k of the frequency domain the criteria expressed in(A.1.3) gives the spectral contribution mainly comes from one or several given instant(s)t_k associated with ν_k by the criterion relation $\nu_k = \omega'(t_k)$). The instant(s) which mostly contribute(s) at the frequency ν_k is/are the instantst_k so that the tangent to the curve defined by the modulation function $\omega(t)$ is parallel to the straight of equation $\nu_k t$. In addition, it can be noticed that the criterion relation expressed in(A.1.3) is also named *time frequency* relation. This relation is often a bijection from the time domain t to the frequency domain ν so that for the frequency given ν_k only one instant t_k is associated. At the opposite if the time frequency relation associated with the modulation is not bijective, for the frequency ν_k, as it was said, it can be associated several $t_{k,1}, t_{k,2}...t_{k,N}$. The following calculation is made by considering that

the relation is bijective, in the other case the development is still valid by summing on the different associated $t_{k,i}$.

Considering the Fourier transform (A.1.2) for a particularν_k , only instants close to t_k (verifying the criterion (A.1.3)) can contribute (considering that by going far enough to t_k the oscillating term becomes high and its impact in the rest of the integral tends to be null).

$$S(\nu_k) = \int_{t_k-\epsilon}^{t_k+\epsilon} a(t)e^{-2\pi j(\nu_k t-\omega(t))}dt \tag{A.1.4}$$

It is possible to process to a limit development of the phase term $v_k t - \omega(t)$ nearby the instant t_k (A.1.5)

$$\nu_k t - \omega(t) = \nu_k t_k - \omega(t_k) + \underbrace{(\nu_k - \omega'(t_k))}_{=0}(t-t_k) - \frac{\omega''(t_k)}{2}(t-t_k)^2 \tag{A.1.5}$$

Considering ϵ low, the phase term could be closely-enough approximated by the three first order terms of the development. In addition, the second term of the development is null (according to the stationary phase criterion).

Let us here consider the hypothesis stating that $\omega''(t_k) \neq 0$. This hypothesis is always valid in the case of the time frequency relation is a bijection which is usually the case.

Finally the expression (A.1.5) can be simplified (by considering that the variation rate of $u(t)$ is low and this function could be approximately considered as constant equals to $u(t_k)$ on the considered interval)

$$S(\nu_k) = a(t_k)e^{-2\pi j(v_k t_k-\omega(t_k))}\int_{t_k-\epsilon}^{t_k+\epsilon} e^{2\pi j\frac{\omega''(t_k)}{2}(t-t_k)^2}dt \tag{A.1.6}$$

Considering the variable change $\sqrt{2\omega''(t_k)}(t-t_k) = y$

$$S(\nu_k) = \frac{a(t_k)}{\sqrt{2\omega''(t_k)}}e^{-2\pi j(v_k t_k-\omega(t_k))}2\int_0^{\sqrt{2\omega''(t_k)}\epsilon} e^{j\frac{\pi y^2}{2}}dt \tag{A.1.7}$$

The final integral term can be seen as the Fresnel integral if the superior born is high enough. And it thus conducts to:

$$S(\nu_k) = \frac{a(t_k)}{\sqrt{\omega''(t_k)}}e^{-2\pi j(v_k t_k-\omega(t_k))}e^{j\frac{\pi}{4}} \tag{A.1.8}$$

By generalisation on all the ν_k , and in the case of the frequency time relation ($\nu = \omega'(t)$) is forming a bijection so that to each frequency a single instant can be associated and *vice versa*, in other words, so that the inverse function is well defined and $t_\nu = [\omega']^{-1}(\nu)$, it is possible to expressed the Fourier transform of the modulated signal as follows:

$$S(\nu) = \frac{a(t_\nu)}{\sqrt{\omega''(t_\nu)}}e^{-2\pi j(vt_\nu-\omega(t_\nu))}e^{j\frac{\pi}{4}} \tag{A.1.9}$$

There is a direct relation between the spectral shape of the signal and the temporal signal envelope and the modulation function.

$$|S(\nu)|^2 = \frac{a(t_\nu)^2}{|\omega''(t_\nu)|} \tag{A.1.10}$$

This equation (A.1.10) makes it possible to get a quick approximation of the spectrum shape knowing the temporal signal characteristics: modulation type and envelope shape. But, it is also possible to define the modulation function stating the spectral and temporal envelope shapes as required criteria.

Example: Fourier transform of a linear frequency modulated signal (Chirp)

Let us take the example of a chirp (linear modulation) in a rectangular envelope to illustrate the results exposed in the previous part. Such a signal is mathematically expressed by the equation system (A.1.11)

$$\begin{cases} a(t) &= \Pi(\frac{t}{T}) \\ \omega(t) &= f_c t + \frac{B}{2T}t^2 \end{cases} \tag{A.1.11}$$

where$\Pi(t)$ denotes the rectangular function which equals 1 on the interval $[-\frac{1}{2} : \frac{1}{2}]$ and 0 otherwise. By using the stationary phase criterion defined in (A.1.3) in this case it becomes $\nu = \omega'(t) = f_c + \frac{B}{T}t$. (time frequency relation is linear). The reverse of this relation gives $t_\nu = T/B(\nu - f_c)$. Finally, using the results on (A.1.10) from the associated development of the stationary phase method.

$$|S(\nu)| = \Pi(\frac{\nu - f_c}{B})\sqrt{\frac{T}{B}} \tag{A.1.12}$$

The equation found in (A.1.12) is the expected approximation. Indeed, the Fourier transform of a chirp is commonly approximated by a rectangular function with bandwidth equal to B (if the product B.T is high).

A.2 Applied to define frequency modulation function

Indeed, since $\omega''(t) = \frac{d\nu}{dt}$, the substitution in (A.1.10)leads to a differential equation linking the spectral and temporal shapes.

$$|S(\nu)|^2 d\nu = a(t)^2 dt \tag{A.2.1}$$

And the link between ν and t (time frequency relation of a modulated signal) can be found out by solving the integral equation(A.2.2)

$$\int_{-\infty}^{\nu} |S(f)|^2 df = \int_{-\infty}^{t} u(\tau)^2 d\tau \tag{A.2.2}$$

Thanks to the relation (A.2.2) by stating the spectral and temporal envelope shapes as required criteria, it is possible to define the modulation function $\omega(t)$ allowing to approach these criteria. Indeed, solving (A.2.2) gives the relation ν as a function of t (as a bijective form of the time frequency relation) and by integrating the results given that $\nu(t) = \omega'(t)$ an associated modulation function $\omega(t)$ is found.

Appendix B

Interferometric phase difference statistics calculation

Consider that the interferometric signals S_a and S_b are random variables modelled as Gaussian-distributed. This hypothesis could be justified by the backscattering formation of the received signal. Indeed by considering that the number of scatterers is statistically high in a resolution cell, the central limit theorem confirms this Gaussian statistic model [Hel, 2003, Hel,1998, Che, 2004]. n addition the additive noise is considered as Gaussian as well. And thus, the summation of the contribution of the backscatterers (which constituted a Gaussian variable thanks to the central limit theorem) plus a Gaussian additive noise, has a random Gaussian behaviour which is modelled by:

$$\begin{cases} S_a & = x_a + iy_a = r_a e^{i\varphi_a} \\ S_b & = x_b + iy_b = r_b e^{i\varphi_b} \end{cases} \tag{B.0.1}$$

Where x_i and y_i are zeros mean Gaussian variables and thus r_i presents a Rayleigh distribution with parameter σ^2 (equal for the two sensors since the two signals statistics have same amplitude) and φ_i is uniformly distributed between $-\pi$ and π. It is reminded that we search the statistic (density, mean, standard deviation) of the random variable $\Delta\phi$ defined as $\Delta\phi = \arg(S_a S_b^*) = \varphi_a - \varphi_b$. Its probability density repartition is calculated from the probability density of the interferometric signals S_a and S_b [Puj, 2007].

B.1 Probability density

The vector $S = [S_a\ S_b]$has the following probability density (2-component complex Gaussian density):

$$f(S) = \frac{1}{\pi^2 |K|} \exp\left(-SK^{-1}S^*\right) \tag{B.1.1}$$

Where K is the covariance matrix of the random vector S and$|.|$denotes the determinant, the star operator $*$ is the conjugate transpose operator. The real and imaginary parts of an interferometric signal ($x_i$and y_i) are uncorrelated. Then the expected value $\langle . \rangle$ and variance of the interferometric signal are:

$$\begin{cases} \langle S_a \rangle = \langle S_b \rangle = 0 \\ \langle S_a S_a^* \rangle = \langle S_b S_b^* \rangle = \sigma^2 \end{cases} \tag{B.1.2}$$

Let us introduce the correlation coefficient η which will help to simplify the covariance matrix writing (K).

$$\eta = \frac{\langle S_a S_b^* \rangle}{\sqrt{\langle S_a S_b^* \rangle \langle S_b S_b^* \rangle}} = \mu e^{i\psi} \tag{B.1.3}$$

In equation (B.1.3), the coherence coefficient μ as it has previously been defined in (2.1.44), is used.

Thanks to the correlation coefficient the covariance matrix can be written as:

$$K = \langle SS^* \rangle = \begin{bmatrix} \langle S_a S_a^* \rangle & \langle S_a S_b^* \rangle \\ \langle S_b S_a^* \rangle & \langle S_b S_b^* \rangle \end{bmatrix} = \sigma^2 \begin{bmatrix} 1 & \eta \\ \eta^* & 1 \end{bmatrix} \tag{B.1.4}$$

Its inverse is:

$$K^{-1} = \frac{1}{\sigma^2(1-\mu^2)} \begin{bmatrix} 1 & -\eta \\ -\eta^* & 1 \end{bmatrix} \tag{B.1.5}$$

Thus by replacing in(B.1.1) the density function of S is:

$$f(S_a, S_b) = \frac{1}{\pi^2 \sigma^4 (1-\mu^2)} \exp\left(-\frac{1}{\sigma^2(1-\mu^2)} (S_a S_a^* + S_b S_b^* - 2\mathcal{R}\{\eta^* S_a S_b^*\} \right) \tag{B.1.6}$$

Where $\mathcal{R}$ is the real part.

By expressing the vector S in rotational coordinates as in (B.0.1) (as a function of $r_a, r_b, \varphi_a$and φ_b) (Transformation Jacobian determinant being $r_a r_b$) it leads to:

$$f(r_a, r_b, \varphi_a, \varphi_b) = \frac{r_a r_b}{\pi^2 \sigma^4 (1-\mu^2)} \exp\left(-\frac{1}{\sigma^2(1-\mu^2)} \left(r_a^2 + r_b^2 - 2 r_a r_b \mu \cos(\varphi_a - \varphi_b - \psi) \right) \right) \tag{B.1.7}$$

Here let us introduce another transformation :

$$\begin{aligned} [0+\infty[\times]-\infty+\infty[&\to [0+\infty[\times[0+\infty[\\ \begin{pmatrix} z \\ v \end{pmatrix} &\to \begin{pmatrix} r_a \\ r_b \end{pmatrix} = \begin{pmatrix} \frac{1}{\sqrt{2}} \sqrt{\sigma^2(1-\mu^2)} z^{1/2} \exp\frac{v}{2} \\ \frac{1}{\sqrt{2}} \sqrt{\sigma^2(1-\mu^2)} z^{1/2} \exp\frac{v}{2} \end{pmatrix} \end{aligned} \tag{B.1.8}$$

whose Jacobian is $\sigma^2(1-\mu^2)/4$

$$f(z, v, \varphi_a, \varphi_b) = \frac{z}{2\pi^2} \frac{(1-\mu^2)}{4} \exp\left(-\frac{1}{2} \left(z \exp(v) + z \exp(-v) - 2z\mu \cos(\varphi_a - \varphi_b - \psi) \right) \right) \tag{B.1.9}$$

by integrating on v and z on their respective domain the joint probability density ofφ_a and$\varphi_b$is found as:

$$\begin{aligned} f(\varphi_a,\varphi_b) &= \frac{(1-\mu^2)}{8\pi^2}\int_0^{+\infty} z\exp(zY)\overbrace{\int_{-\infty}^{+\infty}\exp-(z\cosh(v))\,dv}^{\text{twice the second kind modified Bessel function}}\,dz \\ &= \frac{(1-\mu^2)}{4\pi^2}\int_0^{+\infty} z\exp(zY)\,K_0(z)dz \\ &= \frac{(1-\mu^2)}{4\pi^2}\left[\frac{1}{1-Y^2}+\frac{Y}{(1-Y^2)^{3/2}}\left(\frac{\pi}{2}+\text{asin}Y\right)\right] \end{aligned} \tag{B.1.10}$$

Where

$$Y = \mu\cos(\varphi_a-\varphi_b-\psi) = \mu\cos(\Delta\phi-\psi) \tag{B.1.11}$$

Finally, the probability density of the phase difference between S_a and $S_b$is

$$\begin{aligned} f(\Delta\phi) &= \int_0^{2\pi} f(\Delta\phi,\varphi)d\varphi \\ &= \frac{(1-\mu^2)}{2\pi}\left[\frac{1}{1-Y^2}+\frac{Y}{(1-Y^2)^{3/2}}\left(\frac{\pi}{2}+\text{asin}Y\right)\right] \end{aligned} \tag{B.1.12}$$

It can be noticed from this expression than when the coherence μ between the two interferometric signals drops to 0, the density repartition of the phase difference between these two signals tends to an uniform function on the interval -π toπ. This seems evident if the two signals S_a and S_b do not have any coherent part, that the phase difference between can take any value between -π and π with equi-chance. If the coherence reaches one the repartition function looks like to a Dirac function in ψ.

By considering that ψ is null, the probability density depends only on the coherence coefficient μ. The lower the coherence ratio μ, the more spread the probability density (until reach the equi-probable repartition when $\mu = 0$). The variance (noise level on the phase difference estimator) is thus a decreasing function of the coherence ratio.

B.2 Phase difference Expected value

By definition the expected value of$\langle\Delta\phi\rangle$is:

$$\langle\Delta\phi\rangle = \int_{-\pi}^{\pi}\Delta\phi\, f(\Delta\phi)\, d\Delta\phi \tag{B.2.1}$$

Following [Tou, 1995] let us introduce the function $F(\Delta\phi)$ as:

$$\begin{aligned} F(\Delta\phi) &= \Delta\phi - \frac{1}{2}(\pi\frac{\partial}{\partial\Delta\phi}\text{asin}(\mu\cos\Delta\phi) + \frac{\partial}{\partial\Delta\phi}\left[\text{asin}(\mu\cos\Delta\phi)\right]^2 \\ &= \Delta\phi + \frac{\mu\sin\Delta\phi}{\sqrt{1-(\mu\cos\Delta\phi)^2}}\left[\frac{\pi}{2}+\text{asin}\left(\mu\cos\Delta\phi\right)\right] \end{aligned} \tag{B.2.2}$$

It can be shown that the derivative of this function F is close to the probability density of $\Delta\phi$ ($f(\Delta\phi)$)

$$\frac{1}{2\pi}\frac{\partial F(\Delta\phi)}{\partial\Delta\phi} = f(\Delta\phi+\psi) \tag{B.2.3}$$

Proof. with $Y_2 = \mu\cos(\Delta\phi)$:

$$\begin{aligned}
\frac{\partial F(\Delta\phi)}{\partial\Delta\phi} &= 1 + \frac{Y_2\sqrt{1-Y_2^2} - \frac{Y_2(\mu\sin\Delta\phi)^2}{\sqrt{1-Y_2^2}}}{1-Y^2}\left[\frac{\pi}{2} + \operatorname{asin}\left(\mu\cos\Delta\phi\right)\right] - \frac{(\mu\sin\Delta\phi)^2}{1-(\mu\cos\Delta\phi)^2} \\
&= 1 + \frac{Y_2\left(1-Y_2^2\right) - Y_2\left(\mu\sin\Delta\phi\right)^2}{\left(1-Y_2^2\right)^{3/2}}\left[\frac{\pi}{2} + \operatorname{asin}Y_2\right] - \frac{(\mu\sin\Delta\phi)^2}{1-Y_2^2} \\
&= \frac{1-(\mu\cos\Delta\phi)^2-(\mu\sin\Delta\phi)^2}{1-Y_2^2} + \frac{Y_2\left(1-Y_2^2\right) - Y_2\left(\mu\sin\Delta\phi\right)^2}{\left(1-Y_2^2\right)^{3/2}}\left[\frac{\pi}{2} + \operatorname{asin}Y_2\right] \\
&= \left(1-\mu^2\right)\left[\frac{1}{1-Y_2^2} + \frac{Y_2}{\left(1-Y_2^2\right)^{3/2}}\left[\frac{\pi}{2} + \operatorname{asin}Y_2\right]\right] = 2\pi f(\Delta\phi+\psi)
\end{aligned} \tag{B.2.4}$$

□

Then by firstly a variable change and secondly a parts integration, the expected value of $\Delta\phi$is :

$$\begin{aligned}
\langle\Delta\phi\rangle &= \int_{-\pi-\psi}^{\pi-\psi}(\Delta\phi+\psi)\, f(\Delta\phi+\psi)\, d\Delta\phi \\
&= \psi + \frac{1}{2\pi}\int_{-\pi-\psi}^{\pi-\psi}\Delta\phi\,\frac{\partial F(\Delta\phi)}{\partial\Delta\phi}\, d\Delta\phi \\
&= \psi + \frac{1}{2\pi}\left[\Delta\phi F(\Delta\phi)\right]_{-\pi-\psi}^{\pi-\psi} - \int_{-\pi-\psi}^{\pi-\psi}F(\Delta\phi)\, d\Delta\phi
\end{aligned} \tag{B.2.5}$$

By definition the expected value of$\langle\Delta\phi\rangle$is:

$$\langle\Delta\phi\rangle = \int_{-\pi}^{\pi}\Delta\phi\, f(\Delta\phi)\, d\Delta\phi \tag{B.2.6}$$

Then by firstly a variable change and secondly a parts integration, the expected value of $\Delta\phi$File

$$\begin{aligned}
\langle\Delta\phi\rangle &= \int_{-\pi-\psi}^{\pi-\psi}(\Delta\phi+\psi)\, f(\Delta\phi+\psi)\, d\Delta\phi \\
&= \psi + \frac{1}{2\pi}\int_{-\pi-\psi}^{\pi-\psi}\Delta\phi\,\frac{\partial F(\Delta\phi)}{\partial\Delta\phi}\, d\Delta\phi \\
&= \psi + \frac{1}{2\pi}\left(\left[\Delta\phi F(\Delta\phi)\right]_{-\pi-\psi}^{\pi-\psi} - \int_{-\pi-\psi}^{\pi-\psi}F(\Delta\phi)\, d\Delta\phi\right)
\end{aligned} \tag{B.2.7}$$

F is the function defined in(B.2.2) and thus the first term of the above equation (B.2.7) is

$$\begin{aligned}
\left[\Delta\phi F(\Delta\phi)\right]_{-\pi-\psi}^{\pi-\psi} &= (\pi-\psi)\,F(\pi-\psi) + (\pi+\psi)\,F(-\pi-\psi) \\
&= (\pi-\psi)\left(\pi-\psi+\frac{\mu\sin\psi}{\sqrt{1-(\mu\cos\psi)^2}}\left[\frac{\pi}{2}-\operatorname{asin}(\mu\cos\psi)\right]\right) \\
&+ (\pi+\psi)\left(-\pi-\psi+\frac{\mu\sin\psi}{\sqrt{1-(\mu\cos\psi)^2}}\left[\frac{\pi}{2}-\operatorname{asin}(\mu\cos\psi)\right]\right) \\
&= 2\pi\frac{\mu\sin\psi}{\sqrt{1-(\mu\cos\psi)^2}}\left[\frac{\pi}{2}-\operatorname{asin}(\mu\cos\psi)\right]-4\pi\psi
\end{aligned} \tag{B.2.8}$$

The second part of the equation (B.2.7) is:

$$\begin{aligned}
\int_{-\pi-\psi}^{\pi-\psi} F(\Delta\phi)\,d\Delta\phi &= \int_{-\pi-\psi}^{\pi-\psi}\Delta\phi - \frac{\pi}{2}\frac{\partial}{\partial\Delta\phi}\operatorname{asin}(\mu\cos\Delta\phi)\,d\Delta\phi \\
&\qquad + \frac{1}{2}\frac{\partial}{\partial\Delta\phi}\left[\operatorname{asin}(\mu\cos\Delta\phi)\right]^2 d\Delta\phi \\
&= \frac{1}{2}\left[\Delta\phi^2\right]_{-\pi-\psi}^{\pi-\psi} - \frac{\pi}{2}\left[\operatorname{asin}(\mu\cos\Delta\phi)\right]_{-\pi-\psi}^{\pi-\psi} \\
&\qquad + \frac{1}{2}\left[\operatorname{asin}(\mu\cos\Delta\phi)^2\right]_{-\pi-\psi}^{\pi-\psi} \\
&= -2\pi\psi
\end{aligned} \tag{B.2.9}$$

Finally, the expected value of the phase of $S_a S_b^*$ is:

$$\begin{aligned}
\langle\Delta\phi\rangle &= \psi + \frac{1}{2\pi}\left(\left[\Delta\phi F(\Delta\phi)\right]_{-\pi-\psi}^{\pi-\psi} - \int_{-\pi-\psi}^{\pi-\psi} F(\Delta\phi)\,d\Delta\phi\right) \\
&= \psi + \frac{\mu\sin\psi}{\sqrt{1-(\mu\cos\psi)^2}}\left[\frac{\pi}{2}-\operatorname{asin}(\mu\cos\psi)\right] - 2\psi + \psi \\
&= \frac{\mu\sin\psi}{\sqrt{1-(\mu\cos\psi)^2}}\left[\frac{\pi}{2}-\operatorname{asin}(\mu\cos\psi)\right] \\
&= \frac{\mu\sin\psi}{\sqrt{1-(\mu\cos\psi)^2}}\left[\operatorname{acos}(\mu\cos\psi)\right]
\end{aligned} \tag{B.2.10}$$

As expected when the coherence between the two interferometric signals drops to 0, the mean value of the phase difference tends to 0 whatever the value ofψ. This is predictable since in this case, it tends to be the expected value of a uniform random variable whose value is between $-\pi$and π . If the coherence value tends to 1, the expected value of the phase difference tends to ψ and the estimator is unbiased. Here it is found back that if ψ equals zeros (case at the theoretical detection instant) the expected value is null and the estimator is unbiased.

If ψ is not null and the coherence level of interferometric signal is low, the estimator of ψ given by the phase difference of the interferometric signals is bias. (i.e $\langle \arg S_a S_b^* \rangle \neq \arg \langle S_a S_b^* \rangle$) This can be explained by the fact that the expected value operator $\langle . \rangle$ processed before the operator $\arg\{.\}$ operates as a smooting operation. If the operator $\arg\{.\}$ is process before when the coherence level of interferometric signal is low, the phase of $S_a S_b^*$is really noisy and have a non null probability to jump over π or below $-\pi$. If in addition ψ is not null for example positive, the phase has more chances to jump over π. Since the operator $\arg\{.\}$ is defined modulo 2π the observed phase is pulled down. And thus its expected value of the estimator is biased.

B.3 Phase difference Variance

By definition the variance is expressed as:

$$\operatorname{var}\{\Delta\phi\} = \left\langle \Delta\phi^2 \right\rangle - \langle \Delta\phi \rangle^2 \tag{B.3.1}$$

The second term has been calculated in the previous part, the first term can be calculated using similar development.

$$\begin{aligned}
\left\langle \Delta\phi^2 \right\rangle &\triangleq \int_{-\pi}^{\pi} \Delta\phi^2 \, f(\Delta\phi) \, d\Delta\phi \\
&= \int_{-\pi-\psi}^{\pi-\psi} (\Delta\phi + \psi)^2 \, f(\Delta\phi + \psi) \, d\Delta\phi \\
&= \psi^2 + \frac{\psi}{\pi} \int_{-\pi-\psi}^{\pi-\psi} \Delta\phi \, \frac{\partial F(\Delta\phi)}{\partial \Delta\phi} \, d\Delta\phi + \frac{1}{2\pi} \int_{-\pi-\psi}^{\pi-\psi} \Delta\phi^2 \, \frac{\partial F(\Delta\phi)}{\partial \Delta\phi} \, d\Delta\phi \\
&= \psi^2 + 2\psi \left(\langle \Delta\phi \rangle - \psi \right) + \frac{1}{2\pi} \int_{-\pi-\psi}^{\pi-\psi} \Delta\phi^2 \, \frac{\partial F(\Delta\phi)}{\partial \Delta\phi} \, d\Delta\phi
\end{aligned} \tag{B.3.2}$$

The second term has been calculated in the previous part, the first term can be calculated using similar development.

The last term of this equation is calculated by part:

$$\int_{-\pi-\psi}^{\pi-\psi} \Delta\phi^2 \, \frac{\partial F(\Delta\phi)}{\partial \Delta\phi} \, d\Delta\phi = \left[\Delta\phi^2 F(\Delta\phi) \right]_{-\pi-\psi}^{\pi-\psi} - 2 \int_{-\pi-\psi}^{\pi-\psi} \Delta\phi \, F(\Delta\phi) \, d\Delta\phi \tag{B.3.3}$$

where the first term is:

$$\begin{aligned}\left[\Delta\phi^2 F(\Delta\phi)\right]_{-\pi-\psi}^{\pi-\psi} &= (\pi-\psi)^2 F(\pi-\psi) - (\pi+\psi)^2 F(-\pi-\psi) \\ &= (\pi-\psi)^2 \left(\pi-\psi+\frac{\mu\sin\psi}{\sqrt{1-(\mu\cos\psi)^2}}\left[\frac{\pi}{2}-\operatorname{asin}(\mu\cos\psi)\right]\right) \\ &- (\pi+\psi)^2 \left(-\pi-\psi+\frac{\mu\sin\psi}{\sqrt{1-(\mu\cos\psi)^2}}\left[\frac{\pi}{2}-\operatorname{asin}(\mu\cos\psi)\right]\right) \\ &= -4\pi\psi\frac{\mu\sin\psi}{\sqrt{1-(\mu\cos\psi)^2}}\left[\frac{\pi}{2}-\operatorname{asin}(\mu\cos\psi)\right]+2\pi^3-6\pi\psi^2\end{aligned} \tag{B.3.4}$$

and the second term:

$$\begin{aligned}\int_{-\pi-\psi}^{\pi-\psi}\Delta\phi F(\Delta\phi)\,d\Delta\phi = \int_{-\pi-\psi}^{\pi-\psi}&\Delta\phi^2-\frac{\pi}{2}\Delta\phi\frac{\partial}{\partial\Delta\phi}\operatorname{asin}(\mu\cos\Delta\phi) \\ &-\frac{1}{2}\Delta\phi\frac{\partial}{\partial\Delta\phi}\operatorname{asin}(\mu\cos\Delta\phi)^2 d\Delta\phi\end{aligned} \tag{B.3.5}$$

The three term of this equation equal:
First one:

$$\int_{-\pi-\psi}^{\pi-\psi}\Delta\phi^2 d\Delta\phi = 2\frac{\pi^3}{3}+2\psi^2\pi \tag{B.3.6}$$

Second one:

$$\begin{aligned}\int_{-\pi-\psi}^{\pi-\psi}\Delta\phi\frac{\partial}{\partial\Delta\phi}\operatorname{asin}(\mu\cos\Delta\phi)d\Delta\phi &= \left[\Delta\phi\operatorname{asin}(\mu\cos\Delta\phi)\right]_{-\pi-\psi}^{\pi-\psi} \\ &- \int_{-\pi-\psi}^{\pi-\psi}\operatorname{asin}(\mu\cos\Delta\phi)d\Delta\phi \\ &= -2\pi\operatorname{asin}(\mu\cos\psi)+12\psi^2\end{aligned} \tag{B.3.7}$$

Third one:

$$\begin{aligned}\int_{-\pi-\psi}^{\pi-\psi}\Delta\phi\frac{\partial}{\partial\Delta\phi}\operatorname{asin}(\mu\cos\Delta\phi)^2 d\Delta\phi &= \left[\Delta\phi\operatorname{asin}(\mu\cos\Delta\phi)^2\right]_{-\pi-\psi}^{\pi-\psi} \\ &- \int_{-\pi-\psi}^{\pi-\psi}\operatorname{asin}(\mu\cos\Delta\phi)^2 d\Delta\phi \\ &= 2\pi\left[\operatorname{asin}(\mu\cos\psi)\right]^2-\pi\sum_{i=1}^{+\infty}\frac{\mu^{2i}}{i^2}\end{aligned} \tag{B.3.8}$$

By summing the three terms

$$\int_{-\pi-\psi}^{\pi-\psi} \Delta\phi F(\Delta\phi)\, d\Delta\phi = 2\frac{\pi^3}{3} - 4\psi^2\pi + \pi^2 \text{asin}(\mu\cos\psi) - \pi\left[\text{asin}(\mu\cos\psi)\right]^2 + \frac{\pi}{2}\sum_{i=1}^{+\infty}\frac{\mu^{2i}}{i^2} \tag{B.3.9}$$

The equation (B.3.3) can be simplified to :

$$\frac{1}{2\pi}\int_{-\pi-\psi}^{\pi-\psi} \Delta\phi^2 \frac{\partial F(\Delta\phi)}{\partial\Delta\phi} d\Delta\phi = -2\psi\frac{\mu\sin\psi}{\sqrt{1-(\mu\cos\psi)^2}}\left[\frac{\pi}{2} - \text{asin}\left(\mu\cos\psi\right)\right] + \frac{\pi^2}{3} + \psi^2 - \pi\text{asin}(\mu\cos\psi) + \text{asin}(\mu\cos\psi) - \frac{1}{2}\sum_{i=1}^{+\infty}\frac{\mu^{2i}}{i^2} \tag{B.3.10}$$

Finally the expected value $\left\langle \Delta\phi^2 \right\rangle$ is

$$\begin{aligned}\left\langle \Delta\phi^2 \right\rangle &= \psi^2 + 2\psi\left(\langle\Delta\phi\rangle - \psi\right) + \frac{1}{2\pi}\int_{-\pi-\psi}^{\pi-\psi} \Delta\phi^2 \frac{\partial F(\Delta\phi)}{\partial\Delta\phi}\, d\Delta\phi \\ &= \frac{\pi^2}{3} - \pi\text{asin}(\mu\cos\psi) + \text{asin}(\mu\cos\psi) - \frac{1}{2}\sum_{i=1}^{+\infty}\frac{\mu^{2i}}{i^2}\end{aligned} \tag{B.3.11}$$

And the variance of the interferometric phase difference is:

$$\begin{aligned}\text{var}\left\{\Delta\phi\right\} &= \left\langle \Delta\phi^2 \right\rangle - \langle\Delta\phi\rangle^2 \\ &= \frac{\pi^2}{3} - \pi\text{asin}(\mu\cos\psi) + \text{asin}(\mu\cos\psi) - \frac{1}{2}\sum_{i=1}^{+\infty}\frac{\mu^{2i}}{i^2} \\ &- \frac{\mu^2\sin^2\psi}{1-(\mu\cos\psi)^2}\left[\frac{\pi^2}{4} - \pi\text{asin}\left(\mu\cos\psi\right) + \left[\text{asin}\left(\mu\cos\psi\right)\right]^2\right] \\ &= \frac{1-\mu^2}{1-(\mu\cos\psi)^2}\left[\frac{\pi^2}{4} - \pi\text{asin}\left(\mu\cos\psi\right) + \left[\text{asin}\left(\mu\cos\psi\right)\right]^2\right] + \frac{\pi^2}{3} - \frac{\pi^2}{4} - \frac{1}{2}\sum_{i=1}^{+\infty}\frac{\mu^{2i}}{i^2} \\ &= \frac{1-\mu^2}{1-(\mu\cos\psi)^2}\left[\frac{\pi^2}{4} - \pi\text{asin}\left(\mu\cos\psi\right) + \left[\text{asin}\left(\mu\cos\psi\right)\right]^2\right] + \frac{\pi^2}{12} - \frac{1}{2}\sum_{i=1}^{+\infty}\frac{\mu^{2i}}{i^2} \\ &= \frac{1-\mu^2}{1-(\mu\cos\psi)^2}\left[\frac{\pi^2}{4} - \pi\text{asin}\left(\mu\cos\psi\right) + \left[\text{asin}\left(\mu\cos\psi\right)\right]^2\right] + \frac{1}{2}\sum_{i=1}^{+\infty}\frac{1-\mu^{2i}}{i^2}\end{aligned} \tag{B.3.12}$$

then the variance is [Puj, 2007, Sin, 2002, Oli, 1996]:

$$\text{var}\left\{\Delta\phi\right\} = \frac{1-\mu^2}{1-(\mu\cos\psi)^2}\left(\frac{\pi^2}{4} - \pi\text{asin}\left(\mu\cos\psi\right) + \left[\text{asin}\left(\mu\cos\psi\right)\right]^2\right) + \frac{1}{2}\sum_{i=1}^{\infty}\frac{1-\mu^{2i}}{i^2} \tag{B.3.13}$$

The variance is maximal when the coherence is null and equals $\pi^2/3$ (uniformly distributed random variable between $-\pi$ and π) and minimum equaling 0 when interferometric signals are fully coherent $\mu = 1$. the variance of the phase difference $\Delta\phi$ is a decreasing function of the coherence level of the interferometric signals

Appendix C

Phase ramp Linear regression

Let us consider a noisy linear function. whose noise expected value is null and variance is σ. The mathematical expression of this function is as follows:

$$\Delta\phi(t) = \alpha t + \beta + n(t) \tag{C.0.1}$$

The linear regression consists in estimating $\alpha$and β by minimizing the quadratic error between the regression and the real phase ramp so that:

$$[\widehat{a}, \widehat{b}] = \min_{a,b} \sum_{i=1}^{N} e_i^2 = \min_{a,b} \sum_{i=1}^{N} \left(\Delta\phi(t_i) - at_i - b\right)^2 \tag{C.0.2}$$

Here the linear regression is made on N samples.
Finally the estimator takes the values:

$$\begin{cases} \widehat{a} & = \frac{\sum_{i=1}^{N}(\Delta\phi(t_i)-\tilde{\Delta\phi})(t_i-\widetilde{t})}{\sum_{i=1}^{N}(t_i-\widetilde{t})^2} = \alpha + \frac{\sum_{i=1}^{N}(n_i-\tilde{n})(t_i-\widetilde{t})}{\sum_{i=1}^{N}(t_i-\widetilde{t})^2} \\ \widehat{b} & = \tilde{\Delta\phi} - \widehat{a}\widetilde{t} = \beta + (\alpha - \widehat{a})\widetilde{t} + \widetilde{n} \end{cases} \tag{C.0.3}$$

Where $\tilde{\Delta\phi}$and $\widetilde{t}$are respectively the mean on the detection windows of the phase difference value and the time. $\tilde{\Delta\phi} = \frac{1}{N}\sum_{i=1}^{N}\Delta\phi(t_i)$ and $\tilde{t} = \frac{1}{N}\sum_{i=1}^{N} t_i$. From Gauss-Markov theorem, the estimators $\widehat{a}$and $\widehat{b}$ is the best linear unbiased estimators of α andβ. Indeed the expected value of this estimators are:

$$\begin{cases} \langle\widehat{a}\rangle & = \alpha + \frac{\sum_{i=1}^{N}\langle(n_i-\tilde{n})\rangle(t_i-\widetilde{t})}{\sum_{i=1}^{N}(t_i-\widetilde{t})^2} = \alpha \\ \left\langle\widehat{b}\right\rangle & = \beta + \langle(a-\widehat{a})\rangle\,\widetilde{t} + \langle\widetilde{n}\rangle = \beta \end{cases} \tag{C.0.4}$$

Their variances are:

$$\begin{cases} \left\langle(\widehat{a}-\alpha)^2\right\rangle & = \frac{\sum_{i=1}^{N}\sum_{j=1}^{N}\langle(n_i-\tilde{n})(n_j-\tilde{n})\rangle(t_i-\widetilde{t})(t_j-\widetilde{t})}{\left[\sum_{i=1}^{N}(t_i-\widetilde{t})^2\right]^2} = \frac{\sigma^2\sum_{i=1}^{N}(t_i-\widetilde{t})^2 - \frac{\sigma^2}{N}\left[\sum_{i=1}^{N}(t_i-\widetilde{t})\right]^2}{\left[\sum_{i=1}^{N}(t_i-\widetilde{t})^2\right]^2} \\ & = \frac{\sigma^2}{\sum_{i=1}^{N}(t_i-\widetilde{t})^2} \\ \left\langle\left(\widehat{b}-\beta\right)^2\right\rangle & = \left\langle(\alpha-\widehat{a})^2\right\rangle\widetilde{t}^2 + \left\langle\widetilde{n}^2\right\rangle + 2\left\langle(\alpha-\widehat{a})\widetilde{n}\right\rangle\widetilde{t} = \frac{\sigma^2\widetilde{t}^2}{\sum_{i=1}^{N}(t_i-\widetilde{t})^2} + \frac{\sigma^2}{N} \end{cases} \tag{C.0.5}$$

Indeed$\langle(\alpha-\widehat{a})\widetilde{n}\rangle = -\frac{\sum_{i=1}^{N}\left(\langle n_i\tilde{n}\rangle-\langle\tilde{n}^2\rangle\right)\left(t_i-\widetilde{t}\right)}{\sum_{i=1}^{N}(t_i-\widetilde{t})^2} = 0$

The estimated phase ramp $\widehat{\Delta\phi}(t) = \widehat{a}t + \widehat{b}$ is an unbiased estimation of the phase ramp. Indeed its expected value equals the expected phase ramp $\left\langle\widehat{\Delta\phi}(t)\right\rangle = \langle\widehat{a}\rangle\, t + \left\langle\widehat{b}\right\rangle = \alpha t + \beta$.

The variance of the phase ramp estimator $\widehat{\Delta\phi}(t)$ is:

$$\begin{aligned}
\left\langle\left(\widehat{\Delta\phi}(t) - \left\langle\widehat{\Delta\phi}(t)\right\rangle\right)^2\right\rangle &= \left\langle\left((\widehat{a}-\alpha)\,t + \widehat{b} - \beta\right)^2\right\rangle = \left\langle(\widehat{a}-\alpha)^2\right\rangle t^2 + \left\langle\left(\widehat{b}-\beta\right)^2\right\rangle + 2t\left\langle(\widehat{a}-\alpha)\left(\widehat{b}-\beta\right)\right\rangle \\
&= \left\langle(\widehat{a}-\alpha)^2\right\rangle t^2 + \left\langle\left(\widehat{b}-\beta\right)^2\right\rangle + 2t\left[-\left\langle(\widehat{a}-\alpha)^2\right\rangle\widetilde{t} + \langle(\alpha-\widehat{a})\widetilde{n}\rangle\right] \\
&= \frac{\sigma^2}{\sum_{i=1}^{N}(t_i-\widetilde{t})^2}t^2 + \frac{\sigma^2\widetilde{t}^2}{\sum_{i=1}^{N}(t_i-\widetilde{t})^2} + \frac{\sigma^2}{N} - 2t\,\tilde{t}\frac{\sigma^2}{\sum_{i=1}^{N}(t_i-\widetilde{t})^2} \\
&= \sigma^2\left[\frac{(t-\tilde{t})^2}{\sum_{i=1}^{N}(t_i-\widetilde{t})^2}t^2 + \frac{1}{N}\right]
\end{aligned} \tag{C.0.6}$$

The variance of the phase estimation is minimum at the center of the regression window. That is why it is important to center the detection window on the expected detection instant. So that the phase ramp estimation has the less variability at this instant. The projection of the phase ramp variability on the time axis gives the variability of the time detection.

Finally the variance of the time detection is:

$$\left\langle(\widehat{\tau}-\tau)^2\right\rangle = \frac{\left\langle\left(\widehat{\Delta\phi}(\tau) - \left\langle\widehat{\Delta\phi}(\tau)\right\rangle\right)^2\right\rangle}{\alpha^2} \geq \frac{\sigma^2}{\alpha^2 N} \tag{C.0.7}$$

If the detection windows is centered in the expected value of the time detection the standard deviation of the time detection estimator is (same as in [Lur, 2010b]):

$$\mathrm{std}\left\{\widehat{\tau}\right\} = \frac{\mathrm{std}\left\{\Delta\phi\right\}}{\alpha\sqrt{N}} \tag{C.0.8}$$

An unbiased estimator of the noise level over the phase ramp is given by:

$$\widehat{\sigma}^2 = \frac{1}{N-2}\sum_{i=1}^{N} e_i^2 = \frac{1}{N-2}\sum_{i=1}^{N}\left(\Delta\phi(t_i) - \widehat{a}t_i - \widehat{b}\right)^2 \tag{C.0.9}$$

Indeed

$$\begin{aligned}
\left\langle \sum_{i=1}^{N} \left(\Delta\phi(t_i) - \widehat{a}t_i - \widehat{b} \right)^2 \right\rangle &= \sum_{i=1}^{N} \left\langle \left((\alpha - \widehat{a})\, t_i - \left(\beta - \widehat{b} \right) + n_i \right)^2 \right\rangle \\
&= \sum_{i=1}^{N} \left[\left\langle (\alpha - \widehat{a})^2 \right\rangle t_i^2 + \left\langle \left(\beta - \widehat{b} \right)^2 \right\rangle + \langle n_i^2 \rangle \right. \\
&\qquad \left. + 2 \left\langle (\alpha - \widehat{a}) \left(\beta - \widehat{b} \right) \right\rangle t_i + 2 \langle (\alpha - \widehat{a})\, n_i \rangle\, t_i + 2 \left\langle n_i \left(\beta - \widehat{b} \right) \right\rangle \right] \\
&= \sum_{i=1}^{N} \left[\frac{\sigma^2}{\sum_{i=1}^{N} (t_i - \widetilde{t})^2} t_i^2 + \frac{\sigma^2}{\sum_{i=1}^{N} (t_i - \widetilde{t})^2} \widetilde{t}^2 + \frac{\sigma^2}{N} + \sigma^2 \right. \\
&\qquad \left. - 2 \frac{\sigma^2}{\sum_{i=1}^{N} (t_i - \widetilde{t})^2} \widetilde{t} t_i - 2 \frac{\sigma^2}{\sum_{i=1}^{N} (t_i - \widetilde{t})^2} (t_i - \widetilde{t})^2 - 2 \frac{\sigma^2}{N} \right] \\
&= \sigma^2 \left[\frac{\sum_{i=1}^{N} (t_i - \widetilde{t})^2}{\sum_{i=1}^{N} (t_i - \widetilde{t})^2} + N - 2 \frac{\sum_{i=1}^{N} (t_i - \widetilde{t})^2}{\sum_{i=1}^{N} (t_i - \widetilde{t})^2} - 1 \right] = (N-2)\, \sigma^2
\end{aligned} \tag{C.0.10}$$

Appendix D

Matched Filter Calculation

The aim of this part is to calculate the pulse compression signal when considering Linear frequency modulated signal (Chirp) whose temporal expression is defined as:

$$s(t) = e^{2\pi i(f_c t + \frac{B}{2T}t^2)} \qquad \text{for} - T/2 \leq t \leq T/2, \text{ otherwise=0} \tag{D.0.1}$$

Here the chirp is considered in a rectangular envelope whose duration is T
The result after matched filtering in case of no Doppler effect is:

$$w(t) = \int_{-\infty}^{+\infty} s(u)\overline{s(u-t)}du \tag{D.0.2}$$

The result after matched filtering in case of Doppler effect is:

$$w(t) = \int_{-\infty}^{+\infty} s(ku)\overline{s(u-t)}du \tag{D.0.3}$$

D.1 Matched filter calculation without Doppler

To perform the calculation, we here separate different cases depending on the value of t : since the domains (for which the functions inside the integral are not null) are centered respectably on 0 and t and with the duration T . The calculation [Hei, 2004] is developed below.

If $-T/2 < T/2 + t < T/2$, in other words $-T < t < 0$ then the pulse compression result is:

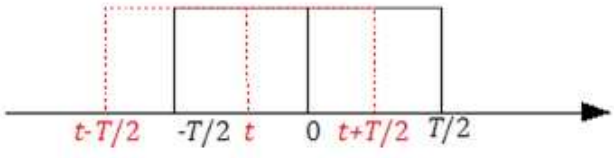

$$w(t) = \int_{-T/2}^{T/2+t} s(u)\overline{s(u-t)}du \tag{D.1.1}$$

The development leads to:

$$
\begin{aligned}
w(t) &= \int_{-T/2}^{T/2+t} e^{2\pi i\left(f_c u+\frac{B}{2T}u^2\right)} e^{-2\pi i\left(f_c(u-t)+\frac{B}{2T}(u-t)^2\right)} du \\
&= e^{2\pi i\left(f_c t-\frac{B}{2T}t^2\right)} \int_{-T/2}^{T/2+t} e^{2\pi i\left(\frac{B}{2T}2ut\right)} du \\
&= e^{2\pi i\left(f_c t-\frac{B}{2T}t^2\right)} \frac{\left[e^{2\pi i\frac{B}{2T}2t(T/2+t)} - e^{-2\pi i\frac{B}{2T}2t(T/2)}\right]}{2\pi\frac{B}{T}t} \\
&= e^{2\pi i f_c t} \frac{\left[e^{2\pi i\frac{B}{2T}t(T+t)} - e^{-2\pi i\frac{B}{2T}t(T+t)}\right]}{2\pi\frac{B}{T}t} \\
&= e^{2\pi i f_c t}(t+T)\mathrm{sinc}\left(2\pi\frac{B}{2T}t(T+t)\right)
\end{aligned}
\tag{D.1.2}
$$

Second case, if $-T/2 < t-T/2 < T/2$, in other words $0 < t < T$ then the pulse compression result is:

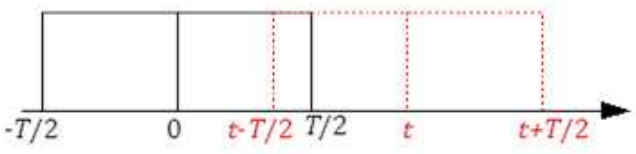

$$
w(t) = \int_{t-T/2}^{T/2} s(u)\overline{s(u-t)}du \tag{D.1.3}
$$

The development leads to:

$$
\begin{aligned}
w(t) &= \int_{t-T/2}^{T/2} e^{2\pi i\left(f_c u+\frac{B}{2T}u^2\right)} e^{-2\pi i\left(f_c(u-t)+\frac{B}{2T}(u-t)^2\right)} du \\
&= e^{2\pi i\left(f_c t-\frac{B}{2T}t^2\right)} \int_{t-T/2}^{T/2} e^{2\pi i\left(\frac{B}{2T}2ut\right)} du \\
&= e^{2\pi i\left(f_c t-\frac{B}{2T}t^2\right)} \frac{\left[e^{2\pi i\frac{B}{2T}2t(T/2)} - e^{-2\pi i\frac{B}{2T}2t(T/2-t)}\right]}{2\pi\frac{B}{T}t} \\
&= e^{2\pi i f_c t} \frac{\left[e^{2\pi i\frac{B}{2T}t(T-t)} - e^{-2\pi i\frac{B}{2T}t(T-t)}\right]}{2\pi\frac{B}{T}t} \\
&= e^{2\pi i f_c t}(T-t)\mathrm{sinc}\left(2\pi\frac{B}{2T}t(T-t)\right)
\end{aligned}
\tag{D.1.4}
$$

Finally, considering (D.1.2) and(D.1.4) it leads that the results of the pulse compression is:

$$
w(t) = e^{2\pi i f_c t} T\mathbf{\Lambda}(\frac{t}{T})\mathrm{sinc}\left(2\pi\frac{B}{2}t\Lambda(\frac{t}{T})\right) \tag{D.1.5}
$$

where $\mathbf{\Lambda}(t)$ denotes the triangle function whose maximum value is 1 at 0 and values are null if $t \leq -1$ or$t \geq 1$

D.2 Matched filter calculation with Doppler

This part aim to have a approximated expression of the matched filter in case of Doppler effect $w(t) = \int_{-\infty}^{+\infty} s(\eta u)\overline{s(u-t)}du$. From this calculation,and with simple variable changes it will makes it possible to get the expression of the received signal at the sources A and B of the interferometer.

$$\begin{aligned} w(t) &= \int_{-\infty}^{+\infty} s(\eta u)\overline{s(u-t)}du \\ &= \int_{-\infty}^{+\infty} e^{2\pi i\left(f_c\eta u+\frac{B}{2T}\eta^2u^2\right)}e^{-2\pi i\left(f_c(u-t)+\frac{B}{2T}(u-t)^2\right)}1_T(u-t)1_T(ku)du \end{aligned} \tag{D.2.1}$$

The expression after of matched filtering becomes:

$$\begin{aligned} w(t) &= \int_{-\infty}^{+\infty} e^{2\pi i\left(f_c(1+\alpha)u+\frac{B}{2T}(1+\alpha)^2u^2\right)}e^{-2\pi i\left(f_c(u-t)+\frac{B}{2T}(u-t)^2\right)}1_T(u-t)1_T(ku)du \\ &= e^{2\pi i\left(f_ct-\frac{B}{2T}t^2\right)}\int_{-\infty}^{+\infty} e^{2\pi i\left(f_c\alpha u+\frac{B}{2T}2ut\right)}e^{2\pi i\left(\frac{B}{2T}(2\alpha+\alpha^2)u^2\right)}1_T(u-t)1_T(ku)du \end{aligned} \tag{D.2.2}$$

By neglecting the term $e^{2\pi i\left(\frac{B}{2T}(2\alpha+\alpha^2)u^2\right)}$. This approximation is possible by considering that $f_c \gg B$ and $BT(\eta-1) \ll 1$. Actually neglecting this term comes down to consider that the Doppler effect is shifting the chirp only on its central frequency (the band remains equal to B instead to be affected and becomes ηB) and on its duration which become T/η. Similarly, we separate the case in function of the value of t since the functions inside the integral have their domains centered on 0 and t with the durations T/η and T.

If $-T/2/\eta < T/2 + t < T/2/\eta$, in other words $-T + \alpha T/2 < t < -\alpha T/2$ then the pulse compression result is:

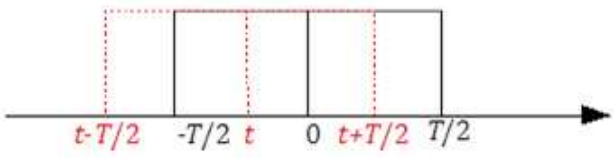

$$\begin{aligned} w(t) &= e^{2\pi i\left(f_ct-\frac{B}{2T}t^2\right)}\int_{-\frac{T}{2}(1-\alpha)}^{T/2+t} e^{2\pi i\left(f_c\alpha+\frac{B}{T}t\right)u}du \\ &= e^{2\pi i\left(f_ct-\frac{B}{2T}t^2\right)}\frac{e^{2\pi i\left(f_c\alpha+\frac{B}{T}t\right)\left(\frac{T}{2}+t\right)}-e^{-2\pi i\left(f_c\alpha+\frac{B}{T}t\right)\frac{T}{2}(1-\alpha)}}{2\pi i\left(f_c\alpha+\frac{B}{T}t\right)} \\ &= e^{2\pi i\left(f_ct-\frac{B}{2T}t^2\right)}e^{2\pi i\frac{1}{2}\left(f_c\alpha+\frac{B}{T}t\right)(t-\alpha T/2)}\frac{\sin\left[\pi\left(f_c\alpha+\frac{B}{T}t\right)(T+t-\alpha T/2)\right]}{\pi\left(f_c\alpha+\frac{B}{T}t\right)} \\ &= e^{2\pi if_c(1+\frac{\alpha}{2})t}e^{-2\pi i\frac{\alpha}{4}Bt}\frac{\sin\left[\pi\left(f_c\alpha+\frac{B}{T}t\right)(T+t)-\alpha Bt/4\right]}{\pi\left(f_c\alpha+\frac{B}{T}t\right)} \\ &\approx e^{2\pi if_c(1+\frac{\alpha}{2})t}(T+t)\mathrm{sinc}\left[\pi\left(f_c\alpha+\frac{B}{T}t\right)(T+t)\right] \end{aligned} \tag{D.2.3}$$

The maximum in amplitude is reached for $\left(f_c\alpha + \frac{B}{T}t\right) = 0$ we find back the expression of the time shift $\delta t = -\alpha f_c T/B = -\frac{v_e+v_r}{c} f_c T/B$ and the loss of energy $m = 1 - \alpha f_c/B$.

If $-T/2/k < t - T/2 < T/2/k$, in other words $\alpha T/2 < t < T - \alpha T/2$ then the pulse compression result is:

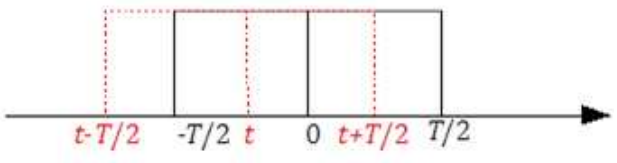

$$
\begin{aligned}
w(t) &= e^{2\pi i\left(f_c t - \frac{B}{2T}t^2\right)} \int_{t-T/2}^{\frac{T}{2}(1-\alpha)} e^{2\pi i\left(f_c\alpha + \frac{B}{T}t\right)u} du \\
&= e^{2\pi i\left(f_c t - \frac{B}{2T}t^2\right)} \frac{e^{2\pi i\left(f_c\alpha + \frac{B}{T}t\right)\frac{T}{2}(1-\alpha)} - e^{2\pi i\left(f_c\alpha + \frac{B}{T}t\right)(t-T/2)}}{2\pi i\left(f_c\alpha + \frac{B}{T}t\right)} \\
&= e^{2\pi i\left(f_c t - \frac{B}{2T}t^2\right)} e^{2\pi i\frac{1}{2}\left(f_c\alpha + \frac{B}{T}t\right)(t-\alpha T/2)} \frac{\sin\left[\pi\left(f_c\alpha + \frac{B}{T}t\right)(T - t - \alpha T/2)\right]}{\pi\left(f_c\alpha + \frac{B}{T}t\right)} \\
&= e^{2\pi i f_c(1+\frac{\alpha}{2})t} e^{-2\pi i\frac{\alpha}{4}Bt} \frac{\sin\left[\pi\left(f_c\alpha + \frac{B}{T}t\right)(T-t) - \alpha Bt/4\right]}{\pi\left(f_c\alpha + \frac{B}{T}t\right)} \\
&\approx e^{2\pi i f_c(1+\frac{\alpha}{2})t}(T-t)\mathrm{sinc}\left[\pi\left(f_c\alpha + \frac{B}{T}t\right)(T-t)\right]
\end{aligned}
\tag{D.2.4}
$$

At the first estimation we can say that the result of the matched filter is:

$$
w(t) == \int_{-\infty}^{+\infty} s(ku)\overline{s(u-t)}du \approx e^{2\pi i f_c(1+\frac{\alpha}{2})t} T\mathbf{\Lambda}(\frac{t}{T})\mathrm{sinc}\left[\pi\left(f_c\alpha + \frac{B}{T}t\right)T\mathbf{\Lambda}(\frac{t}{T})\right] \tag{D.2.5}
$$

As we said previously from this formula it is possible to find back the time shift and the loss of energy expression we had pointed out during the training period. Indeed the maximum of the signal envelop is reached when $\left(f_c\alpha + \frac{B}{T}t\right) = 0$ conducting to the expression of the time shift $\delta t = -\alpha f_c T/B = -\frac{v_e+v_r}{c} f_c T/B$ and the loss of energy $m = 1 - \alpha f_c/B$.

Appendix E

Coherence coefficient calculation in the case of Doppler

In the case of Doppler effect, the received signals S_a and S_b are expressed as the summation of scatterers contribution on the instantaneous responding footprint. Let us assume that the Doppler shift is the same for all this scatterers. It means that the projection of radial speed are the same on all the angular direction defined by the scatterers. This is a good approximation if the angular aperture of the instantaneous footprint is narrow compared to the angular position of the footprint center. And the S_a and S_b are :

$$\begin{aligned} S_a &= \int_{\Delta_x} a_x s\left(\frac{k_r}{k_e}(t-\tau_x) - \frac{a}{2c}\frac{1}{k_e}\sin\theta_x\right) dx \\ S_b &= \int_{\Delta_x} a_x s\left(\frac{k_r}{k_e}(t-\tau_x) + \frac{a}{2c}\frac{1}{k_e}\sin\theta_x\right) dx \end{aligned} \tag{E.0.1}$$

Let us estimate the coherence ration in the case of Dopplerized CW signals :

$$\mu = \frac{\left|\langle S_a \overline{S_b}\rangle\right|}{\sqrt{\langle S_a \overline{S_a}\rangle \langle S_b \overline{S_b}\rangle}} \tag{E.0.2}$$

The received signal are time shifted to process the time beamforming and the expected value of the interferometric term is:

$$\langle S_a \overline{S_b}\rangle = \langle a^2\rangle \int_{\Delta_x} s\left(\frac{k_r}{k_e}(t-\tau_x) - \frac{a}{2c}\frac{1}{k_e}(\sin\theta_x - k_r\sin\theta)\right) \overline{s\left(\frac{k_r}{k_e}(t-\tau_x) - \frac{a}{2c}\frac{1}{k_e}(\sin\theta_x - k_r\sin\theta)\right)} dx \tag{E.0.3}$$

The same linearisation as in paragraph 2.1.3 is made:

$$\begin{cases} \tau_x = \tau_0 + \dfrac{2}{c}\sin\theta_0(x-x_0) = \tau_0 + T\dfrac{k_r}{k_e}\dfrac{x-x_0}{\Delta x} \\ \sin\theta_x = \sin\theta_0 + \dfrac{x-x_0}{H}\cos^3\theta_0 \end{cases} \tag{E.0.4}$$

By taking $t = \tau_0$ (which is equivalent to study the coherence level of interferometric signals at the detection instant), in addition by considering that$(\sin\theta_0 - k_r\sin\theta) = 0$ (which

correspond to the detection on the beam axis (but with the steering error due to steering angle bias caused by the Doppler effect) :

$$\begin{aligned}\left\langle S_a\overline{S_b}\right\rangle &= \left\langle a^2\right\rangle \int s\left(T\frac{(x-x_0)}{\Delta x}\frac{k_r}{k_e}(1-\beta\frac{1}{k_r})\right)\overline{s\left(T\frac{(x-x_0)}{\Delta x}\frac{k_r}{k_e}\left(1+\beta\frac{1}{k_r}\right)\right)}dx \\ &= \left\langle a^2\right\rangle \frac{\Delta_x}{T}\frac{k_e}{k_r}\int s\left(\left(1-\beta\frac{1}{k_r}\right)t\right)\overline{s\left(\left(1+\beta\frac{1}{k_r}\right)t\right)}dt\end{aligned} \tag{E.0.5}$$

Futhermore the calculation of$\left\langle S_a\overline{S_a}\right\rangle$and $\left\langle S_b\overline{S_b}\right\rangle$gives:

$$\begin{aligned}\left\langle S_a\overline{S_a}\right\rangle &= \left\langle a^2\right\rangle \int s\left(T\frac{(x-x_0)}{\Delta x}\frac{k_r}{k_e}(1-\beta\frac{1}{k_r})\right)\overline{s\left(T\frac{(x-x_0)}{\Delta x}\frac{k_r}{k_e}\left(1-\beta\frac{1}{k_r}\right)\right)}dx \\ &= \left\langle a^2\right\rangle \frac{\Delta_x}{T}\frac{k_e}{k_r}\left(1-\beta\frac{1}{k_r}\right)\int |s|^2\,dt\end{aligned} \tag{E.0.6}$$

And:

$$\left\langle S_b\overline{S_b}\right\rangle = \left\langle a^2\right\rangle \frac{\Delta_x}{T}\frac{k_e}{k_r}\left(1+\beta\frac{1}{k_r}\right)\int |s|^2\,dt \tag{E.0.7}$$

Thus

$$\sqrt{\left\langle S_a\overline{S_a}\right\rangle\left\langle S_b\overline{S_b}\right\rangle} \approx \left\langle a^2\right\rangle \frac{\Delta_x}{T}\frac{k_e}{k_r}\int |s|^2\,dt \tag{E.0.8}$$

And finally the coherenec ratio can be expressed as:

$$\mu = \frac{\int s\left(\left(1-\beta\frac{1}{k_r}\right)t\right)\overline{s\left(\left(1+\beta\frac{1}{k_r}\right)t\right)}dt}{\int |s|^2\,dt} \tag{E.0.9}$$

Where the factor β is still the same as defiened in 2.1.31.

In the case of a CW signal (or pulse compressed signal $s(t) = |s|e^{2\pi i f_c t}$), the ambiguity function can be simplified (time delay being still null). Indeed, the distortion of the whole envelope can be neglected since $\beta \ll 1$. Finally, the dilation or the compression of the signal is approximated by a frequency shift (common radar-community approximation).

$$\mu = \frac{\int |s|^2 e^{-2\pi i f_c(2\frac{\beta}{k_r}t)}dt}{\int |s|^2 dt} = \frac{\mathrm{FT}[|s|^2](2f_c\beta/k_r)}{\mathrm{FT}[|s|^2](0)} = \frac{\mathrm{FT}[|s|^2](f_c\frac{1}{2}\frac{a}{H}\frac{\cos^2\theta_0}{\tan\theta_0}(1+\frac{v_r}{c}))}{\mathrm{FT}[|s|^2](0)} \tag{E.0.10}$$

In the case of FM signals, the interferometric signal are:

$$\begin{cases} w_a(t) \approx \int_x a_x e^{2\pi i f_c(1+\frac{\alpha}{2})\left(t-\tau_x-\frac{a}{2c}\left(\frac{1}{k_r}\sin\theta_x-\sin\theta\right)\right)}\left|A(t-\tau_x,\frac{k_r}{k_e})\right|dx \\ w_b(t) \approx \int_x a_x e^{2\pi i f_c(1+\frac{\alpha}{2})\left(t-\tau_x+\frac{a}{2c}\left(\frac{1}{k_r}\sin\theta_x-\sin\theta\right)\right)}\left|A(t-\tau_x,\frac{k_r}{k_e})\right|dx \end{cases} \tag{E.0.11}$$

The calculation is made by following alays the same process. Hence, Firstly, the linearisation is applied. Let $t = \tau_0$ (which is equivalent to study the coherence level of interferometric signals at the detection instant), and $(\sin\theta_0 - k_r \sin\theta) = 0$ (which correspond to the detection on the beam axis (but with the steering error due to steering angle bias caused by the Doppler effect) . Secondly, with the variable change $t = \frac{T}{\Delta_x}(1 + \alpha/2)(x - x_0)$, the expected value of the interferometric term is:

$$\left\langle S_a \overline{S_b} \right\rangle = \left\langle a^2 \right\rangle \frac{\Delta_x}{T} \frac{1}{(1 + \frac{\alpha}{2})} \int e^{-2\pi i f_c (2\frac{\beta}{k_r} t)} \left| A(t, \frac{k_r}{k_e}) \right|^2 dt \tag{E.0.12}$$

The coherence coefficient can be considered as:

$$\begin{aligned} \mu(\eta) &= \frac{\int e^{-2\pi i f_c (2\frac{\beta}{k_r} t)} |A(t,\eta)|^2 \, dt}{\int |A(t,\eta)|^2 \, dt} = \frac{\mathrm{FT}[|A(t,\eta)|^2](2 f_c \beta / k_r)}{\mathrm{FT}[|\,|A(t,\eta)|^2](0)} \\ &= \frac{\mathrm{FT}[|\,|A(t,\eta)|^2](f_c \frac{1}{2} \frac{a}{H} \frac{\cos^2\theta_0}{\tan\theta_0}(1 + \frac{v_r}{c}))}{\mathrm{FT}[|A(t,\eta)|^2](0)} \\ &\approx \frac{\mathrm{FT}[|\,|A(t,\eta)|^2](f_c \frac{1}{2} \frac{a}{H} \frac{\cos^2\theta_0}{\tan\theta_0})}{\mathrm{FT}[|A(t,\eta)|^2](0)} \end{aligned} \tag{E.0.13}$$

Appendix F

Coherence coefficient calculation with seabed penetration

Here, it is considered that a part of the signal penetrates inside the seafloor. So, the backscatterers are not only spread on the sea bottom line across-track sounding but also along the depth axis.

F.1 Continuous layer

As previously, infinitesimal backscatterers situated in x and h are considered to send back a delayed signal copy (delayed by $\tau_{x,h}$) of the received signal weighted by a random coefficient $a_{x,h}$. The resulting signal is the double summation in x-axis and h-axis of the backscatterer contributions.

$$\begin{aligned} S_a &= \int_0^{h_m} \int_{-\infty}^{+\infty} a_{x,h} s\left(t - \tau_{x,h} - \frac{a}{2c}\left(\sin\theta_{x,h} - \sin\theta\right)\right) dx dh \\ S_b &= \int_0^{h_m} \int_{-\infty}^{+\infty} a_{x,h} s\left(t - \tau_{x,h} + \frac{a}{2c}\left(\sin\theta_{x,h} - \sin\theta\right)\right) dx dh \end{aligned} \tag{F.1.1}$$

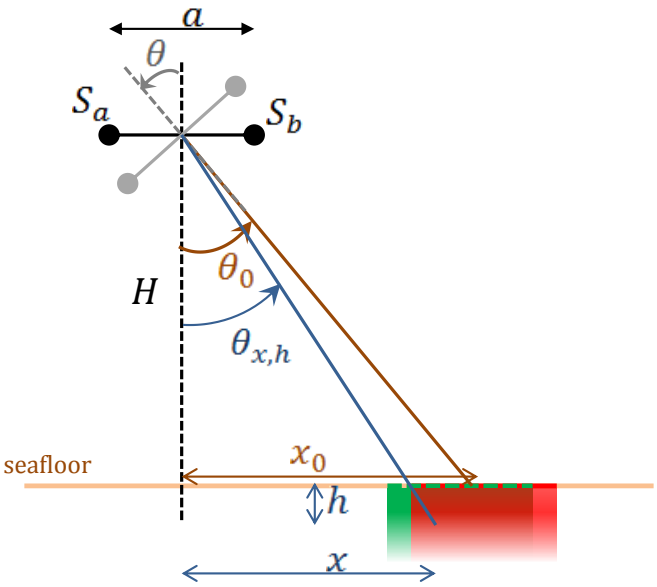

Figure F.1.1: Receiving configuration with seabed penetration

The cross expected value $\langle S_a \overline{S_b} \rangle$is:

$$\begin{aligned}\langle S_a \overline{S_b} \rangle &= \iiiint \langle a_{x,h} a_{x',h'} \rangle \, s\left(t - \tau_{x,h} - \frac{a}{2c}\left(\sin\theta_{x,h} - \sin\theta\right)\right) \\ &\qquad \overline{s\left(t - \tau_{x',h'} + \frac{a}{2c}\left(\sin\theta_{x',h'} - \sin\theta\right)\right)} dx dx' dh dh' \\ &= \int \langle a_h^2 \rangle \int s\left(t - \tau_{x,h} - \frac{a}{2c}\left(\sin\theta_{x,h} - \sin\theta\right)\right) \overline{s\left(t - \tau_x + \frac{a}{2c}\left(\sin\theta_{x,h} - \sin\theta\right)\right)} dx dh\end{aligned} \tag{F.1.2}$$

Each backscattering random coefficients are commonly assumed to be statistically independent from one another. Thus $\langle a_{xh} a_{x'h'} \rangle$ is null if x is different from x' or h different from h'. The backscattering power $\langle a_{x,h} a_{x,h} \rangle$ can be a function of h. Let us consider that the point contributions at a given instant can be gathered to form a footprint centered in the direction θ_0. The propagation delay associated with the footprint center (situated along direction θ_0) is τ_0. Considering that the footprint dimension is relatively small compared to the depth H and lateral distance x, simplification using first-order Taylor series can be done. Here in first approximation, the velocity is the same in the seabed medium than in the water medium, assuming no refraction at the interface.

$$\begin{cases} \tau_{x,h} = \tau_0 + \dfrac{2}{c}\left[\sin\theta_0 (x - x_0) + \cos\theta_0 h\right] + o(x - x_0) + o\left(h\right) \\ \qquad\quad = \tau_0 + T\dfrac{x - x_0}{\Delta x} + \dfrac{2}{c}\cos\theta_0 h + o(x - x_0) + o\left(h\right) \\ \sin\theta_{x,h} = \sin\theta_0 + \dfrac{x - x_0}{H}\cos^3\theta_0 - \dfrac{h}{H}\cos^2\theta_0 \sin\theta_0 + o(x - x_0) + o\left(h\right) \end{cases} \tag{F.1.3}$$

By taking $t = \tau_0$ and $\theta_0 = \theta$ which corresponds to study the coherence level of the

interferometric signals at the theoretical detection sample and in the beam direction, the coherence ratio becomes:

$$\left\langle S_a\overline{S_b}\right\rangle = \int \left\langle a_h^2\right\rangle \int s\left((1-\beta)\,t - \left(\frac{2}{c}\cos\theta + \frac{a}{2cH}\cos^2\theta\sin\theta\right)h\right) \overline{s\left((1+\beta)\,t - \left(\frac{2}{c}\cos\theta - \frac{a}{2cH}\cos^2\theta\sin\theta\right)h\right)}dtdh \tag{F.1.4}$$

Where the factor β is still (see (2.1.31)) defined as:

$$\beta = \frac{a}{2cT}\frac{\Delta x}{H}\cos^3\theta = \frac{1}{4}\frac{a}{H}\frac{\cos^2\theta}{\tan\theta} \tag{F.1.5}$$

Here lets assumed that the transmitted signal can be written as $s(t) = |s|e^{2\pi i f_c t}$and $\left\langle S_a\overline{S_b}\right\rangle$ can be thus approximated (assuming that the delay and distortion do not affect much the signal envelope) and thanks to Fubbini integral separability.

$$\left\langle S_a\overline{S_b}\right\rangle = \int_0^{h_m} \left\langle a_h^2\right\rangle e^{2\pi i f_c \frac{a}{cH}h\cos^2\theta\sin\theta}dh \int |s|^2 e^{-2\pi i f_c(2\beta t)}dt \tag{F.1.6}$$

By a similar development it can be shown that:

$$\left\langle S_a\overline{S_a}\right\rangle = \left\langle S_b\overline{S_b}\right\rangle = \int_0^{h_m} \left\langle a_h^2\right\rangle dh \int |s|^2 dt \tag{F.1.7}$$

Finally the coherence coefficient writes as the ratio:

$$\begin{aligned}\mu &= \frac{\left|\left\langle S_a\overline{S_b}\right\rangle\right|}{\sqrt{\left\langle S_a\overline{S_a}\right\rangle\left\langle S_b\overline{S_b}\right\rangle}} = \frac{\left|\int_0^{h_m}\left\langle a_h^2\right\rangle e^{2\pi i f_c\frac{a}{cH}h\cos^2\theta\sin\theta}dh.\int|s|^2e^{-2\pi i f_c(2\beta t)}dt\right|}{\int\left\langle a_h^2\right\rangle dh.\int|s|^2dt} \\ &= \underbrace{\left|\frac{\int_0^{h_m}\left\langle a_h^2\right\rangle e^{2\pi i f_c\frac{a}{cH}h\cos^2\theta\sin\theta}dh}{\int\left\langle a_h^2\right\rangle dh}\right|}_{\text{degradation factor } p}.\mu_0\end{aligned} \tag{F.1.8}$$

The coherence coefficient, when considering penetration is the product of the interface coherence coefficient by a degradation factor caused by penetration.

Considering that $\left\langle a_h^2\right\rangle$is constant, independent on h:

$$p = \mathrm{sinc}(\pi f_c\frac{a}{c}\frac{h_m}{H}\cos^2\theta\sin\theta) \simeq 1 - \frac{1}{3}\left(\pi f_c\frac{a}{c}\frac{h_m}{H}\cos^2\theta\sin\theta\right)^2 \tag{F.1.9}$$

Assuming that $\left\langle a_h^2\right\rangle$is an exponential decreasing function of h , $\left\langle a_h^2\right\rangle = e^{-\alpha h}$

$$\begin{aligned}p &= \left|\frac{1}{1-2\pi i f_c\frac{a}{cH\alpha}\cos^2\theta\sin\theta}\right| = \frac{1}{\sqrt{1+\left(2\pi f_c\frac{a}{cH\alpha}\cos^2\theta\sin\theta\right)^2}} \\ &\simeq 1 - \frac{1}{2}\left(2\pi f_c\frac{a}{cH\alpha}\cos^2\theta\sin\theta\right)^2\end{aligned} \tag{F.1.10}$$

It can be noticed that if the penetration is low (magnitude of a few cm) compared to depth (which is about hundreds meters) the coherence loss p is really close to 1 and the seabed penetration does not really influence the coherence thus the noise level on phase ramp, and at last the bathymetric measurement. This is due to the fact that even if the signal penetrates the seabed the responding backscatterers at a given time are locally gathered inside the beam direction. Penetration comes to impact the noise level when the ratio between the penetration depth and the seafloor surface depth is about 10^{-2}.

F.2 Two separated layers

In this part the seafloor is considered as being constituted of two layers. The model is based on two lines of backscatterers. The upper interface is at the depth H while the lower is at $H + h$. The interferometric signals are the sum of their contributions. Let us considered that the two layers are independent. In addition the second one has an attenuation coefficient compared to the first one calledα.

$$\begin{aligned} S_a &= S_{a,1} + \alpha S_{a,2} \\ S_b &= S_{b,1} + \alpha S_{b,2} \end{aligned} \tag{F.2.1}$$

To simplify the attenuation of the second layer compared to the first one is considered as the same for the two interferometric signals.

The expected values of$S_a S_b^*$, $S_a S_a^*$ and $S_b S_b^*$are:

$$\begin{cases} \langle S_a S_b^* \rangle = \left\langle S_{a,1} S_{b,1}^* \right\rangle + \alpha^2 \left\langle S_{a,2} S_{b,2}^* \right\rangle \\ \langle S_a S_a^* \rangle = \left\langle S_{a,1} S_{a,1}^* \right\rangle + \alpha^2 \left\langle S_{a,2} S_{a,2}^* \right\rangle \\ \langle S_b S_b^* \rangle = \left\langle S_{b,1} S_{b,1}^* \right\rangle + \alpha^2 \left\langle S_{b,2} S_{b,2}^* \right\rangle \end{cases} \tag{F.2.2}$$

The coherence ratio is thus:

$$\mu = \left| \frac{\langle S_a S_b^* \rangle}{\sqrt{\langle S_a S_a^* \rangle \langle S_b S_b^* \rangle}} \right| = \left| \frac{\left\langle S_{a,1} S_{b,1}^* \right\rangle + \alpha^2 \left\langle S_{a,2} S_{b,2}^* \right\rangle}{\sqrt{\left(\left\langle S_{a,1} S_{a,1}^* \right\rangle + \alpha^2 \left\langle S_{a,2} S_{a,2}^* \right\rangle \right) \left(\left\langle S_{b,1} S_{b,1}^* \right\rangle + \alpha^2 \left\langle S_{b,2} S_{b,2}^* \right\rangle \right)}} \right| \tag{F.2.3}$$

At first approximation we can consider that $\left\langle S_{a,1} S_{a,1}^* \right\rangle = \left\langle S_{a,2} S_{a,2}^* \right\rangle = \left\langle S_{b,1} S_{b,1}^* \right\rangle = \left\langle S_{b,2} S_{b,2}^* \right\rangle$. It means that considering a given layer, the contributing energy received by sensors A and B is the same. In addition excepting the attenuation the two layer backscattered the same amount of energy.

Under this approximation, the coherence ratio becomes the modulus of weighted mean of each layer correlation ratio η_i(η_i as defined in 2.1.53).

$$\mu = \left| \frac{\eta_1 + \alpha^2 \eta_2}{1 + \alpha^2} \right| \quad \text{with} \quad \eta_i \frac{\left\langle S_{a,i} S_{b,i}^* \right\rangle}{\sqrt{\left\langle S_{a,i} S_{a,i}^* \right\rangle \left\langle S_{b,i} S_{b,i}^* \right\rangle}} \tag{F.2.4}$$

Let us derive the two layer-correlation ratios η_i. The started point is to evaluate the received signals by A and B.

$$\begin{aligned} S_{a,i} &= \int a_{x,i} s\left(t - \tau_{x,i} - \frac{a}{2c}\left(\sin\theta_{x,i} - \sin\theta\right)\right) dx \\ S_{b,i} &= \int a_{x,i} s\left(t - \tau_{x,i} + \frac{a}{2c}\left(\sin\theta_{x,i} - \sin\theta\right)\right) dx \end{aligned} \tag{F.2.5}$$

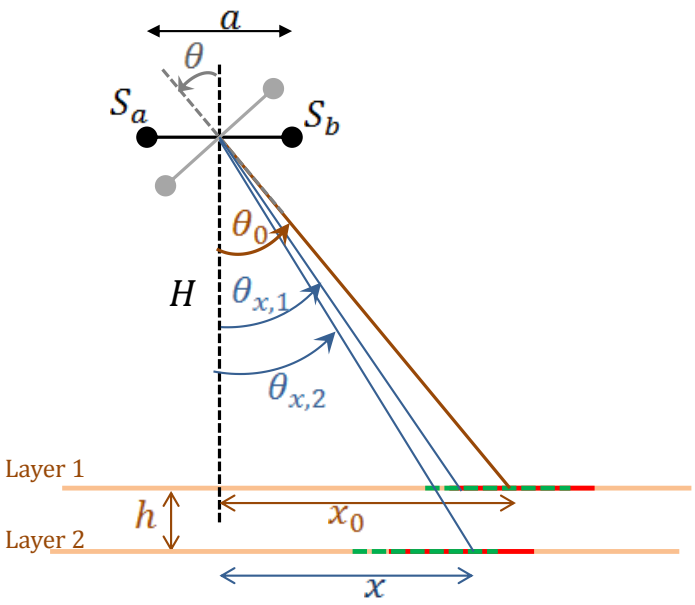

Figure F.2.1: Receiving configuration with two layers

Considering that the random backscattering coefficients are statistically independent from one to the other ($\langle a_{x,i} a_{x',i'}\rangle = \langle a_{x,i}\rangle \langle a_{x',i'}\rangle = 0$ if $i \neq i'$ or $x \neq x'$else $\left\langle a_{x,i}^2 \right\rangle = \langle a^2 \rangle$) , the hypothesis of independence between the two layer signals is found back.

$$\begin{aligned} \langle S_{a,i} S_{b,i}^* \rangle &= \langle a^2 \rangle \int s\left(t - \tau_{x,i} - \frac{a}{2c}\left(\sin\theta_{x,i} - \sin\theta\right)\right) \bar{s}\left(t - \tau_{x,i} + \frac{a}{2c}\left(\sin\theta_{x,i} - \sin\theta\right)\right) dx \\ \langle S_{a,i} S_{a,i}^* \rangle &= \langle a^2 \rangle \int s\left(t - \tau_{x,i} - \frac{a}{2c}\left(\sin\theta_{x,i} - \sin\theta\right)\right) \bar{s}\left(t - \tau_{x,i} - \frac{a}{2c}\left(\sin\theta_{x,i} - \sin\theta\right)\right) dx \\ \langle S_{b,i} S_{b,i}^* \rangle &= \langle a^2 \rangle \int s\left(t - \tau_{x,i} + \frac{a}{2c}\left(\sin\theta_{x,i} - \sin\theta\right)\right) \bar{s}\left(t - \tau_{x,i} + \frac{a}{2c}\left(\sin\theta_{x,i} - \sin\theta\right)\right) dx \end{aligned} \tag{F.2.6}$$

The linearisation of $\tau_{x,i}$ and $\sin\theta_{x,i}$ around τ_0 and $\sin\theta$ where θ is the beam angle and τ is associated with the delay corresponding to the two-way propagation from the array to the seafloor surface point at the direction θ.

$$\begin{cases} \tau_{x,1} = \tau_0 + \dfrac{2}{c}\sin\theta(x - x_0) \\ \tau_{x,2} = \tau_0 + \dfrac{2}{c}\left((x - x_0)\sin\theta + h\cos\theta\right) \\ \sin\theta_{x,1} = \sin\theta + \dfrac{x - x_0}{H}\cos^3\theta \\ \sin\theta_{x,2} = \sin\theta + \dfrac{x - x_0}{H}\cos^3\theta - \dfrac{h}{H}\cos^2\theta\sin\theta \end{cases} \tag{F.2.7}$$

And the different expected values are evaluated at the theoretical instant of detection $t = \tau_0$

- **Layer 1**

$$\left.\begin{aligned} \left\langle S_{a,1}S_{b,1}^*\right\rangle &= \left\langle a^2\right\rangle \int \overline{s\left((x - x_0)\left(\frac{2}{c}\sin\theta + \frac{1}{2c}\frac{a}{H}\cos^3\theta\right)\right)} s\left((x - x_0)\left(\frac{2}{c}\sin\theta - \frac{1}{2c}\frac{a}{H}\cos^3\theta\right)\right) dx \\ &= \left\langle a^2\right\rangle \frac{c}{2\sin\theta}\int \overline{s\left(t\left(1+\beta\right)\right)} s\left(t\left(1-\beta\right)\right) dt \end{aligned}\right\} \text{V.C} \tag{F.2.8}$$

Similarly it is shown that

$$\begin{aligned} \left\langle S_{a,1}S_{a,1}^*\right\rangle &= \left\langle a^2\right\rangle \frac{c}{2\sin\theta(1+\beta)}\int \bar{s}\left(t\right) s\left(t\right) dt \\ \left\langle S_{b,1}S_{b,1}^*\right\rangle &= \left\langle a^2\right\rangle \frac{c}{2\sin\theta(1-\beta)}\int \bar{s}(t) s\left(t\right) dt \end{aligned} \tag{F.2.9}$$

No surprisingly, because it is the same expression that if the seafloor is constituted by only one layer, we find that:

$$\eta_1 = \frac{\int \bar{s}\left(t\left(1+\beta\right)\right) s\left(t\left(1-\beta\right)\right) dt}{\int \overline{s\left(t\right)} s\left(t\right) dt} \tag{F.2.10}$$

- **Layer 2**

By the same development using the variable change since that the signal can be written as $s(t - \delta t) = e^{-2i\pi f_c \delta t} s(t)$.

$$\begin{aligned} \left\langle S_{a,2}S_{b,2}^*\right\rangle = \left\langle a^2\right\rangle \int \bar{s}\left((x - x_0)\left(\frac{2}{c}\sin\theta + \frac{1}{2c}\frac{a}{H}\cos^3\theta\right) + \frac{2}{c}h\cos\theta + \frac{a}{2c}\frac{h}{H}\cos^2\theta\sin\theta\right) \\ s\left((x - x_0)\left(\frac{2}{c}\sin\theta - \frac{1}{2c}\frac{a}{H}\cos^3\theta\right) + \frac{2}{c}h\cos\theta - \frac{a}{2c}\frac{h}{H}\cos^2\theta\sin\theta\right) dx \\ = \left\langle a^2\right\rangle \frac{c}{2\sin\theta} e^{-2i\pi\frac{f_c}{c}a\frac{h}{H}\cos^2\theta\sin\theta}\int \bar{s}\left(t\left(1+\beta\right)\right) s\left(t\left(1-\beta\right)\right) dt \end{aligned} \tag{F.2.11}$$

Similarly it is shown that

$$\begin{aligned} \left\langle S_{a,2}S_{a,2}^*\right\rangle &= \left\langle a^2\right\rangle \frac{c}{2\sin\theta(1+\beta)}\int \bar{s}(t) s\left(t\right) dt \\ \left\langle S_{b,2}S_{b,2}^*\right\rangle &= \left\langle a^2\right\rangle \frac{c}{2\sin\theta(1-\beta)}\int \bar{s}(t) s\left(t\right) dt \end{aligned} \tag{F.2.12}$$

Finally the correlation coefficient for layer 2 is:

$$\eta_2 = e^{-2i\pi\frac{f_c}{c}\frac{h}{H}\cos^2\theta\sin\theta}\frac{\int \bar{s}\left(t\left(1+\beta\right)\right)s\left(t\left(1-\beta\right)\right)dt}{\int \overline{s\left(t\right)}s\left(t\right)dt} = e^{-2i\pi\frac{f_c}{c}\frac{h}{H}a\cos^2\theta\sin\theta}\eta_1 \tag{F.2.13}$$

Finally the whole coherence ratio becomes:

$$\mu = \left|\frac{\eta_1 + \alpha^2 e^{-2i\pi\frac{f_c}{c}a\frac{h}{H}\cos^2\theta\sin\theta}\eta_1}{1+\alpha^2}\right| = \left|\frac{1+\alpha^2 e^{-2i\pi\frac{f_c}{c}a\frac{h}{H}\cos^2\theta\sin\theta}}{1+\alpha^2}\right|\mu_1 \tag{F.2.14}$$

The coherence ratio is degraded by the second layers as a multiplicative term which only depends from the geometrical configuration of the interferometer and layers localisation. In addition, α can depend on the beam angle as the propagation path inside the upper layer is angle dependent (being longer as beam angle function). The penetration distance can be approximated to:

$$d = \frac{2h}{\cos\theta} \tag{F.2.15}$$

and thus :

$$\alpha = \alpha - 2h(1-\frac{1}{\cos\theta})\varrho \tag{F.2.16}$$

Where α is expressed in dB and the parameter ϱ (in dB/m) represents the linear absorption introduced by the propagation inside the first layer medium.

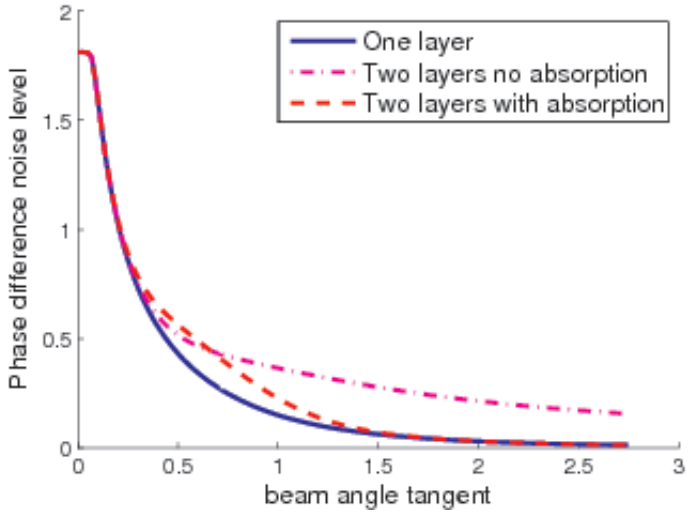

Figure F.2.2: Influence of two layers on phase difference noise level

Figure (F.2.2) presents the impact of the presence of two layers separated by 3 m the upper one being 200m-deep. Blue line present the level of noise in case of CW signal in a square cosine envelope whose duration is 3ms, when considering only the upper layer contribution (as baseline decorrelation). The magenta presents the results by considering the impact

of the second layer. The second layer presents an attenuation constant equal to α^2=1/8 (non dependent of the beam angle, it means that the absorption by the first layer is not considered). At the vertical the signals from the two layer are timely separated. When the two backscattering signals merge, the backscattered signal from the second layer becomes like a noise on the interferometric phase from the first layer signals. In red, it has been introduced the impact of the attenuation from the propagation in the first layer (as $\alpha^2 = \frac{1}{2}10^{-2h(1-\frac{1}{\cos\theta})\varrho/10}$ whereϱ = 5dB/m). By increasing the beam angle the propagation path in the layer 1 is increased and the impact of the second layer is attenuated.

Appendix G

Final bathymetric noise using Amplitude detection

In case of amplitude detection, the detected time is given by the barycenter of the beamformed signal amplitude, and by definition [Lad, 2012]:

$$\hat{t} = \frac{\sum_{i=-N/2}^{N/2} t_i a(t_i)}{\sum_{i=-N/2}^{N/2} a(t_i)} \tag{G.0.1}$$

Where $a(t_i)$ denotes the sampled received signal amplitude of a beam for the whole receiving array. $N+1$ is the number of samples used on the detection window and the window is centered. The amplitude $a(t_i)$is a random variable. The common hypothesis is that the envelope of the temporal signal for a given beam is constitutes by a determinist shape which is the projection of the beam on the seafloor multiplied by an intrinsic noise (baseline decorrelation) plus an additive noise.

$$a(t_i) = A(t_i)X(t_i) + B(t_i) \tag{G.0.2}$$

$A(t_i)$ is the multiplicative noise following as a Rayleigh law; $B(t_i)$ is the additive noise. The multiplicative noise is justified since the received signal at a given instant is the summation of several micro-reflector (from micro relief) present in the cell resolution (scatterer model). By the central limit theorem the received signal tends to be Gaussian.

$$S(t) = x(t) + jy(t) = A(t)e^{j\phi(t)} \tag{G.0.3}$$

Where $x(t)$ $y(t)$ Gaussian variables inducing that A follows Rayleigh distribution and ϕ is uniformly distributed. Here the same hypothesis is used for the received signal by the whole array than for the sub arrays (see paragraph 2.1.5.1). In addition the received signal is modulated by the projection of the beam on the seafloor $X(t)$.

And considering only the multiplicative noise:

$$a(t) = |S(t)| = A(t)X(t) \tag{G.0.4}$$

The multiplicative and the additive noise are independent. It seems to be correct hypothesis since physically they do not come from the same phenomenon (multiplicative from

the backscattering formation and additive from ambient noise)). The beam temporal signal envelope is the independent summation of both contribution as expressed in G.0.2.

G.1 Modeling

The shape of the beam $X(t)$ can be approximated as square envelope of length N_X+1 (using modeling from [Lad, 2012, Ewa, 2011]). $N+1$ is the number of sample used for the detection window.

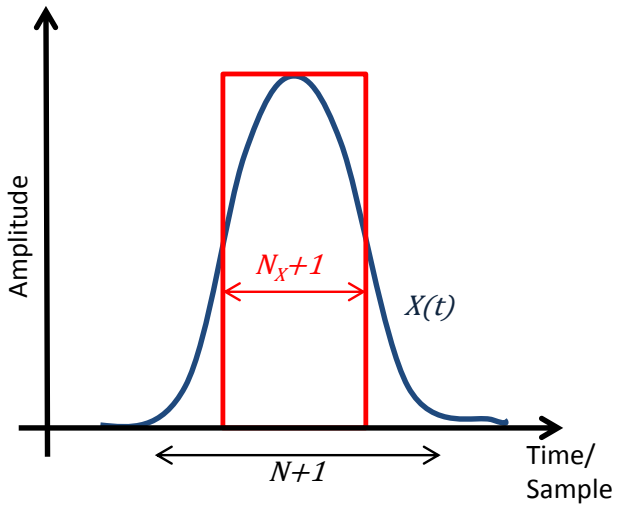

Figure G.1.1: Beam shape approximation

The useful signal is present on the samples from $-N_x/2$ and $N_x/2$ where $X(t)$ is approximated to 1. The received signal in this domain is thus the square envelope affected by the multiplicative noise. Outside this domain the signal is only composed by the additive noise (no signal envelope contribution $X(t)$ thus no multiplicative noise). If N_X higher than the chosen N let N_X equals N.

The signal in useful envelope is the summation of two Gaussian complex variable thus is a complex Gaussian variable whose amplitude thus follows a Rayleigh law. By combination of the two complex Gaussian variable, it is found that the random variable $|a(t_i)|$ has a Rayleigh distribution whose mean m verifies the equation $m^2 = |X|^2 m_A^2 + m_B^2$ and variance $\sigma^2 = |X|^2 \sigma_A^2 + \sigma_B^2$ in the useful envelope (for sample from $-N_X/2$ to $N_X/2$) and $m = m_b$and $\sigma = \sigma_B$ for the other samples.

G.2 Expected value of the detection estimator

The estimator is not linear. However at first approximation the denominator can be replace by its expected value $\sum_{i=-N/2}^{N/2} \langle |a(t_i)| \rangle = m(N_X+1) + m_B(N-N_x)$.

$$\left\langle \hat{t} \right\rangle \approx \frac{\sum_{i=-N/2}^{N/2} t_i \left\langle |a(t_i)| \right\rangle}{\sum_{i=-N/2}^{N/2} \left\langle |a(t_i)| \right\rangle} = \frac{m \sum_{i=-N_x/2}^{N_x/2} t_i + m_B \left(\sum_{i=-N/2}^{-N_X/2} t_i + \sum_{i=N_x/2}^{N/2} t_i \right)}{m(N_X+1) + m_B(N-N_X)} \tag{G.2.1}$$

The sample time are $t_i = t_0 + iT/N$. By considering that the beam shape is square:

$$\left\langle \hat{t} \right\rangle \approx t_0 \tag{G.2.2}$$

The estimator expected value gives the barycenter of the no-noisy beam envelope. It can be noticed in (G.2.1) the importance to have the whole window centered on the detection time (barycenter of the expected useful signal envelope. Indeed the additive noise which is present whatever the place of the useful signal and this can bias the time detection. However the presence of additive noise can often be neglected since on the vertical beam the backscattered signal is powerful enough. Without considering additive noise, the detected instant expected value is unbiased and equal the barycenter of the expected beam envelope on the detection window.

G.3 Variance of the detection estimator

Here the objective is to estimate the variance of the time detection using the amplitude envelope of the beam. Let us considered the estimation minus its expected value.

$$\hat{t} - \left\langle \hat{t} \right\rangle = \frac{\sum_{i=-N/2}^{N/2} t_i a(t_i)}{\sum_{i=-N/2}^{N/2} a(t_i)} - t_0 = \frac{\sum_{i=-N/2}^{N/2} (t_i - t_0)\, a(t_i)}{\sum_{i=-N/2}^{N/2} a(t_i)} = \frac{\sum_{i=-N/2}^{N/2} (t_i - t_0) \left(a(t_i) - \langle a(t_i) \rangle \right)}{\sum_{i=-N/2}^{N/2} a(t_i)} \tag{G.3.1}$$

The variance of the estimator is the expected value of the previous equation, giving:

$$\begin{aligned} \operatorname{var}\left\{\hat{t}\right\} &\approx \frac{\sum_{i=-N/2}^{N/2} (t_i - t_0)^2 \operatorname{var}\left\{a(t_i)\right\}}{\left[\sum_{i=0}^{N} \langle a(t_i) \rangle\right]^2} \\ &\approx \frac{\sum_{i=-N_X/2}^{N_X/2} (t_i - t_0)^2 |X|^2 \sigma_A^2 + \sum_{i=-N/2}^{N/2} (t_i - t_0)^2 \sigma_B^2}{\left[m(N_X+1) + m_B(N-N_X)\right]^2} \end{aligned} \tag{G.3.2}$$

Let us considered that $\sum_{i=-N/2}^{N/2} (t_i - t_0)^2 = \frac{T^2}{N^2} 2 \sum_{i=0}^{N/2} i^2 = \frac{T^2}{N} \frac{1}{12} (N+2)(N+1) = f_s^2 \frac{1}{12} N(N+2)(N+1)$. The variance of the detection time is:

$$\begin{aligned} \operatorname{var}\left\{\hat{t}\right\} &\approx \frac{f_s^2}{12} \frac{N_X(N_X+2)(N_X+1)\,|X|^2 \sigma_A^2 + N(N+2)(N+1)\sigma_B^2}{\left[\sqrt{|X|^2 m_A^2 + m_B^2}(N_X+1) + m_B(N-N_x)\right]^2} \\ &= \frac{f_s^2}{12} \frac{N_X(N_X+2)(N_X+1)(\sigma^2 - \sigma_B^2) + N(N+2)(N+1)\sigma_B^2}{\left[m(N_X+1) + m_B(N-N_X)\right]^2} \end{aligned} \tag{G.3.3}$$

It can be shown that this function is an increasing function of multiplicative noise level (σ_A) and the additive noise level(σ_B). By supposing that the additive noise is neglecting on

the detection window (m_B and $\sigma_B = 0$), we found back the expression from [Lad, 2012] (with $T_{eff} = N_X.f_s$)

$$\text{var}\left\{\hat{t}\right\} \approx \frac{T_{eff}^2}{12}\frac{\sigma_A^2}{m_A^2}\frac{(N_X+2)}{N_X(N_X+1)} = \frac{T_{eff}^2}{12}(\frac{4}{\pi}-1)\frac{(N_X+2)}{N_X(N_X+1)} \tag{G.3.4}$$

By considering that on the whole detection window samples the useful signal is present, the expression can be simplified into:

$$\text{var}\left\{\hat{t}\right\} \approx \frac{f_s^2}{12}\frac{N(N+2)}{(N+1)}\frac{|X|^2\sigma_A^2+\sigma_B^2}{\left[|X|^2 m_A^2+m_B^2\right]} = \frac{f_s^2}{12}\frac{N(N+2)}{(N+1)}(\frac{4}{\pi}-1) \tag{G.3.5}$$

It can be seen that if the additive noise is negligible, which is the case at the vertical beam (strong backscattering echo specular) the detection time standard is not depending on the level of multiplicative noise on the beam envelope (G.3.4). The standard deviation is linked to the number of samples in the detection window and the shape of the beam.

Appendix H

Optimisation tapering shape or filtering shape

The aim of this chapter is to find the best shape to filter the signal in order to reduce baseline decorrelation. Filtered by a tapered matched filtering remains to tapered the frequency domain wave form allowing to reduce sidelobe. The idea is actually to find the frequency domain shape with a cosine form allowing to maximize the normalized cross correlation of this shape around zero. Indeed the coherence coefficient of the interferometric signal is given by a cross correlation of frequency-domain shape of the filtered transmitted pulse.

Let us consider, the initial pulse is a linear frequency modulated signal in a quasi rectangular transmitted temporal envelope $s(t)$. Its frequency domain envelope $S(\nu)$ can thus be approximated by a rectangular function. The matched filter ($h(t)$ or $H(\nu)$) allows to remove the modulation. And after filtering, the frequency domain function ($S(\nu).H(\nu)$) is real centered on the carrier frequency. The filter is supposed adapted to the transmitted pulse allowing to annul the imaginary part of the transmitted pulse Fourier transform (thus $H(\nu) = a(\nu)S^*(\nu)$). The shape of the filter $a(\nu)$ is assumed to follow the shape of a cosine function:

$$a(\nu) = \begin{cases} \cos^{\alpha}\left(\pi \frac{\nu}{B}\right) & \text{if } -\frac{B}{2} < \nu < \frac{B}{2} \\ 0 & \text{otherwise} \end{cases} \tag{H.0.1}$$

where α takes its values from 0 to $+\infty$. α equalling 0 correspond to the rectangular envelope.

Here we aim to improve the coherence ration considering baseline decorralation, expressed as a particular point of the normalized Fourier transform of the square of the filtered-pulse envelope:

$$\mu = \frac{\mathrm{FT}[|s_h|^2](f_a)}{\mathrm{FT}[|s_h|^2](0)} = \frac{\int S_h(\nu) S_h(\nu - f_a) d\nu}{\int S_h(\nu)^2 d\nu} \approx \frac{\int a(\nu) a(\nu - f_a) d\nu}{\int a(\nu)^2 d\nu} \tag{H.0.2}$$

Where $f_a = f_c \frac{1}{2} \frac{a}{H} \frac{\cos^2 \theta_0}{\tan \theta_0}$ as shown in (2.1.36). $a(\nu)$ is a continuous derivative function thus if f_a is low (which is the case since we search to limit baseline decorrelation for medium and wide swath thus when f_a relatively low), the developpement using Taylors series is possible:

$$\mu \approx 1 + \sum_{i=1}^{\infty} \frac{\{f_a\}^i}{i!} \frac{\int a(\nu) a^{(i)}(\nu) d\nu}{\int a(\nu)^2 d\nu} \tag{H.0.3}$$

Every odd derivates of $a(\nu)$ gives the integrale $\int a(\nu)a^{(i)}(\nu)d\nu$equal to 0.
The even derivate of the function $a(\nu)$ are polynomial expression of cosine:

$$a^{(2i)}(\nu) = \sum_{n=0}^{i} b_{i,n} \sin(\frac{\pi\nu}{B})^{2n} \cos(\frac{\pi\nu}{B})^{\alpha-2n} \tag{H.0.4}$$

thus:

$$\int a(\nu)a^{(2i)}(\nu)d\nu = \sum_{n=0}^{i} b_{i,n} \int \sin(\frac{\pi\nu}{B})^{2n} \cos(\frac{\pi\nu}{B})^{2\alpha-2n} d\nu \tag{H.0.5}$$

The integration by part gives:

$$\begin{aligned} \int a(\nu)a^{(2i)}(\nu)d\nu =& \sum_{n=0}^{i} b_{i,n} \left[-\frac{B}{\pi(2\alpha-2n+1)} \sin(\frac{\pi\nu}{B})^{2n-1} \cos(\frac{\pi\nu}{B})^{2\alpha-2n+1} \right] \\ &+ \frac{1}{(2\alpha-2n+1)} \int \sin(\frac{\pi\nu}{B})^{2n-2} \cos(\frac{\pi\nu}{B})^{2\alpha-2n+2} d\nu \\ =& \sum_{n=0}^{i} b_{i,n} \left[-\frac{2B}{\pi(2\alpha-2n+1)} (\frac{\pi\,|f_a|}{2B})^{2\alpha-2n+1} \right] \\ &+ \frac{1}{(2\alpha-2n+1)} \int \sin(\frac{\pi\nu}{B})^{2n-2} \cos(\frac{\pi\nu}{B})^{2\alpha-2n+2} d\nu \end{aligned} \tag{H.0.6}$$

If $\alpha > 1/2$ and f_a is low, all the$\{f_a\}^{2i} \int a(\nu)a^{(2i)}(\nu)d\nu = o(f_a^2)$ for i>1.
And for f_a low the coherence coefficient can be approximated by;

$$\mu \approx 1 + \frac{\{f_a\}^2}{2} \frac{\int a(\nu) a^{(2)}(\nu) d\nu}{\int a(\nu)^2 d\nu} \tag{H.0.7}$$

Using the expression of the second derivative of $a(\nu)$:

$$a^{(2)}(\nu) = \left(\frac{\pi}{B}\right)^2 \alpha(\alpha-1) \sin(\frac{\pi\nu}{B})^2 \cos(\frac{\pi\nu}{B})^{\alpha-2} - \left(\frac{\pi}{B}\right)^2 \alpha \cos(\frac{\pi\nu}{B})^{\alpha} \tag{H.0.8}$$

And the realation obtained by integration by part:

$$\int \sin(\frac{\pi\nu}{B})^2 \cos(\frac{\pi\nu}{B})^{2\alpha-2} d\nu = o(f_a) + \frac{1}{2\alpha-1} \int \cos(\frac{\pi\nu}{B})^{2\alpha} d\nu \tag{H.0.9}$$

The integrative part of in the expression of the coherence level is:

$$\int a(\nu)a^{(2)}(\nu)d\nu = \left(\frac{\pi}{B}\right)^2 \left[\frac{\alpha(\alpha-1)}{2\alpha-1} - \alpha \right] \int \cos(\frac{\pi\nu}{B})^{2\alpha} d\nu \tag{H.0.10}$$

The term μ (coherence level) given at first approximation by if α is between $1/2$ and $+\infty$:

$$\mu \approx 1 + \frac{1}{2}\left(\frac{\pi}{B} f_a\right)^2 \left[\frac{\alpha(\alpha-1)}{2\alpha-1} - \alpha\right] = 1 + \frac{1}{2}\left(\frac{\pi}{B} f_a\right)^2 g(\alpha) \tag{H.0.11}$$

Let us find the maximum of $g(\alpha)$:

$$g'(\alpha) = -\frac{2\alpha^2(\alpha-1)}{(2\alpha-1)^2} \tag{H.0.12}$$

The maximum happens when $\alpha = 1$.

When the parameter α is higer than $1/2$ for f_a low the coherence level can be approximated by the second order polynom (H.0.11). It can be noticed that the function $g(\alpha)$ is a negative fonction (which is logical since the coherence coefficient has to be lower than 1). In this condition, the optimal degree is 1 for the filter shape.

If α lower than $1/2$ the behaviour of the coherence ratio change with introducing power of f_a lower than 2. If $\alpha = 0$ the coherence ratio is a triangle function of f_a. By changing α from $1/2$ to 0 the polynomial shape is not anymore a second order of f_a, but a shape introducing degree of $|f_a|$ between 1 and 2. Actually the dominant power of the coherence ratio as a function of f_a is in this case $1 + 2\alpha$. With α going from from $1/2$ to 0 the coherence goes from a second order polynome shape towards the triangular shape (triangle being inside rhe polynome shape for low f_a). Thus for f_a low the better power α between 0 and $1/2$ is $1/2$.

The numerical approach shows that between $1/2$ and 1, $1/2$ is better, since it keep arround 0 a behaviour around 0 of a second order polynome whil when f_a increases it takes the characteristic of the triangle function.

Annexe I

Résumé en Français : Impact des signaux modulés sur la précision de mesures bathymétriques issues de sondeurs multifaisceaux

Cette partie d'une dizaine de pages a pour but de résumer succinctement en français l'ensemble de ce manuscrit de thèse conformément aux accords de dérogation conclus avec l'école doctorale Matisse.

Buts et problématiques de cette thèse

La nouvelle génération de sondeurs multifaisceaux utilise des signaux modulés combinés avec un filtrage adapté, ce qui permet d'atteindre des portées plus importantes (grâce a l'amélioration du rapport signal sur bruit) tout en gardant une bonne résolution (compression d'impulsion). Cependant, il a été observé qu'en pratique ces sondeurs utilisant la modulation de fréquence (FM) n'atteignent pas les niveaux de performance attendus. L'objectif de la thèse consiste à comprendre pourquoi les signaux FM utilisés en bathymétrie sont plus dégradés que les signaux à bande-étroite (CW) afin d'ensuite proposer des solutions. Une première hypothèse sur la cause de cette dégradation est l'impact de l'effet Doppler. En effet, les antennes fixées sous la coque du bateau sont soumises aux mouvements du bateau, ce qui induit un effet Doppler sur le signal reçu qui n'est alors plus « adapté » au filtre adapté. Le travail de thèse s'attache donc à modéliser et interpréter l'impact du Doppler sur les signaux FM en comparaison avec les signaux CW. D'autre part, il se concentre également sur la recherche d'autres causes des pertes de qualité liées à l'utilisation de signaux FM. Finalement, nous proposerons des solutions d'amélioration soit par post-traitement, soit en utilisant des signaux modulés mieux adaptés.

Le manuscrit est donc divisé en trois grandes parties. La première est un état de l'art permettant au lecteur de se familiariser avec les bases du travail de thèse telles que les principes de fonctionnement des systèmes multifaisceaux et le traitement du signal associé : mesure bathymétrique, compression d'impulsion, modulation, etc. La seconde partie rentre dans le vif du sujet et présente l'analyse des causes de dégradations observées lors de l'utilisation de

signaux modulés. La troisième donne des pistes d'amélioration réalisables qui ont été testées en simulation et sur le terrain.

I.1 Partie 1 : État de l'art

Les différentes notions exposées dans cette partie ont pour but d'éclairer le lecteur en présentant les notions clés afin de mieux appréhender la problématique du travail de thèse : comprendre pourquoi les signaux modulés ne permettent pas d'atteindre les améliorations de qualité de mesure attendues ; trouver différentes causes et proposer des solutions d'amélioration. Nous expliquerons succinctement les principes de fonctionnement des sondeurs multifaiseaux bathymétriques et l'intérêt d'utiliser les signaux modulés (compression d'impulsion)

I.1.1 Principe de fonctionnement du sondeur multifaisceaux bathymétrique

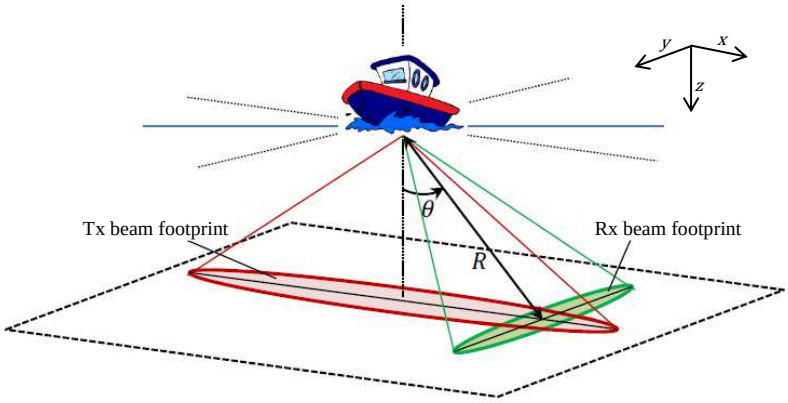

FIGURE I.1.1 – Principe du sondeur multifaisceaux

Le système sondeur multifaisceaux est fixé sur une plateforme en surface. Il est divisé en une partie émission et une partie réception. Le faisceau d'émission de l'antenne d'émission est très étroit selon la direction y (longitudinale au porteur) et très étroit selon x (direction transversale). La partie réception est constituée d'un éventail de faisceaux chacun déterminé par l'angle θ présentant un diagramme inverse à l'émission (étroit selon x, large selon y). Le signal reçu est le signal rétro-diffusé par la section du fond marin par l'intersection des deux diagrammes.

La bathymétrie consiste à estimer le couple θ et R. A chaque impulsion émise, une ligne de points sonde (selon x) est donc décrite. La direction y est décrite au fur et à mesure des impulsions lors de l'avancée du porteur. L'angle θ est supposé connu par la formation de voies ou faisceaux. En effet, pour former l'ensemble des faisceaux de réception, l'antenne de réception est dépointée en introduisant le retard associé au dépointage d'angle θ. La formation de voie est dite « en phase » lorsque le retard de dépointage est introduit grâce à la multiplication par le terme de phase associé. La formation de voie est « temporelle » lorsque l'on retient l'échantillon temporel le plus proche du retard à appliquer auquel on ajoute le terme de phase résiduel. L'estimation du paramètre R est faite grâce à l'estimation du retard associé à la propagation.

Il y a deux manières d'estimer ce retard :

- Pour les faisceaux proches de la verticale, la détection se fait à partir de l'enveloppe temporelle du signal reçu à l'aide du barycentre.
- Pour les faisceaux extérieurs, la détection est faite par interférométrie.

Dans ce dernier cas, l'antenne de réception est divisée en deux sous antennes (la distance séparant les deux centres des sous antennes par rapport à la longueur totale de l'antenne définit la baseline). La différence de phase des deux signaux issues de ces sous antennes est mesurée (pour chacun des faisceaux). Sur les parties cohérentes des signaux interférométriques, elle forme des rampes de phase en fonction du temps. L'estimation du retard se fait par détection du passage à zéro de ces rampes de phase.

I.1.2 Filtrage adapté et compression d'impulsion

L'utilisation de signaux modulés en fréquence (FM) permet d'accroitre l'énergie émise dans le milieu (via la durée d'émission) et ainsi gagner en rapport signal à bruit en réception par rapport au bruit ambiant, tout en gardant une bonne résolution. En effet la modulation permet de dissocier la durée de l'impulsion et son occupation spectrale. La résolution est liée à la durée de l'impulsion. Grâce à la compression d'impulsion, en appliquant le filtrage adapté (filtrage par le conjugué de l'inverse temporel du signal), l'impulsion est équivalente à un signal plus court et plus puissant.

I.1.3 Observation de la dégradation sur données réelles

La dégradation de la qualité de mesures bathymétriques a été observée sur les données issues de plusieurs systèmes. Ici, nous ne présenterons qu'une série de données issues du EM710 du R/V Falkor (avec le consentement de J. Beaudoin, UNH).

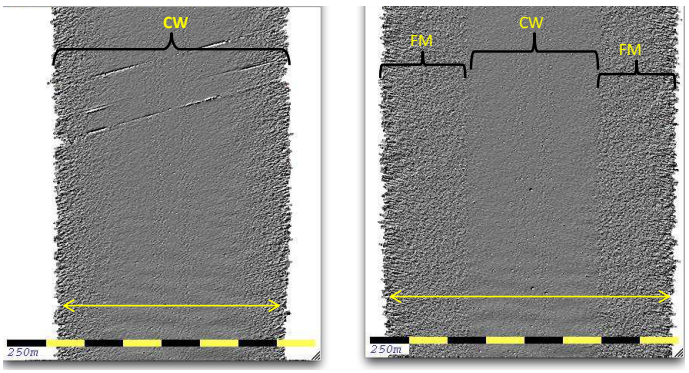

FIGURE I.1.2 – Mesures bathymétriques EM710

La partie de droite de la figure I.1.2 présente la mesure bathymétrique lors de l'utilisation de signaux non modulés (CW), celle de gauche présente le résultat de mesure lorsque le mode modulé (FM) a été activé sur les secteurs extérieurs. La portée du système a été améliorée puisque cette action a permis d'accroitre la fauché. Cependant, la mesure bathymétrique est plus bruitée pour les faisceaux utilisant des signaux modulés.

I.2 Partie 2 : Études des causes de dégradation

I.2.1 L'effet Doppler

I.2.1.1 Modélisation

L'antenne fixée sur le porteur est soumise au mouvement du porteur (roulis, tangage, lacet, pilonnement etc..). Le signal reçu est donc influencé par l'effet Doppler et n'est donc plus adapté par rapport au filtrage adapté (la compression d'impulsion ne se produit pas correctement). La question ici est : l'effet Doppler influence-t-il plus la mesure issue lors de l'utilisation des signaux modulés plutôt que les signaux non modulés ? Une étude méthodique de l'effet Doppler sur la mesure bathymétrique par interférence (détection sur la rampe de phase) dont les résultats ont été confirmés sur donnée simulée, a été menée. Les sous antennes de réception sont modélisées par deux récepteurs ponctuels et on s'intéresse à la contribution d'un réflecteur situé à la direction γ. Cette modélisation a montré que l'effet Doppler affectait le signal reçu de deux manières créant une erreur sur l'estimation de la fréquence mais aussi de la différence de marche. Dans le cas ou la formation de voies est formée en temps, seulement l'erreur de différence de marche va affecter la mesure bathymétrique. Cela résulte en une erreur sur l'estimation de l'angle de pointage de voie qui se trouve biaisé ceci de la même manière lors de l'utilisation de la FM ou du CW.

	Formation de voies en "phase"	Formation de voies "temporelle"
CW	$-\frac{v_e}{c}\tan\theta$	$\frac{v_r}{c}\tan\theta$
FM	$\frac{v_r - v_e}{2c}\tan\theta$	$\frac{v_r}{c}\tan\theta$

TABLE I.1 – erreur d'estimation de l'angle de pointage

Le tableau I.1 récapitule les erreurs d'estimation de l'angle de pointage (valable pour les signaux FM et CW), où θ est l'angle de pointage théorique. Cette erreur dans l'estimation de l'angle de pointage entraine une erreur sur l'instant de détection.

De plus si on utilise la FM, un biais sur l'instant de détection est introduit parce que le signal reçu n'est plus adapté au filtrage adapté (ce qui crée un décalage temporel du lobe principal de l'enveloppe du signal compressé) Cependant ce biais est déjà pris en compte par les sonars bathymétriques multifaisceaux et est corrigé. Dans ces conditions, l'effet Doppler n'affecte pas plus les mesures bathymétriques issues à partir des signaux FM que celles issues du CW.

I.2.1.2 Simulation

Les résultats du modèle sont confrontés à une série de simulations permettant leur validation.

Chaque observation est simulée dans le plan vertical-transversal. Le fond marin est constitué par une ligne de micro réflecteurs (en moyenne une dizaine de micros réflecteurs contribue pour un instant donné). A chaque instant, la distance micro réflecteurs et éléments de l'antenne (constituée de 128 éléments) de réception est calculée. Cette distance est variable, ce

qui introduit l'effet Doppler. Les mouvements pris en compte peuvent être paramétriques (sinusoïdal, paramètre amplitude A et période T) ou issus d'un fichier d'enregistrement d'une centrale d'attitude. A chaque instant, la contribution des micro réflecteurs est calculée. La formation de voies est faite "en temps". Pour l'interférométrie, la "baseline" choisie est de 1/3. Ici, on présente les résultats (tableau I.2) pour un mouvement paramétrique vertical sur la voie à 40° pour deux signaux équivalents : un signal non modulé (CW) de 2ms et un signal modulé en fréquence (FM) d'une durée 20ms et avec une bande de 500Hz.

	Sans mouvement	A=1m,T=10s	A=5m,T=10s	A=10m,T=10s
Simulation				
Bruit sur rampe de phase CW	0,138 rad	0,143 rad	0,146 rad	0,299 rad
Bruit sur rampe de phase FM	0,452 rad	0,392 rad	0,245 rad	0,551 rad
Erreur instant de detection CW	0 s	4,0 10^{-4} s	2,0 10^{-3} s	3,9 10^{-3} s
Erreur instant de detection FM	0 s	-3,0 10^{-4} s	-2,7 10^{-3} s	-5,4 10^{-3} s
Prédiction				
Erreur instant de detection CW	0 s	3,9 10^{-4}s	2,0 10^{-3} s	3,9 10^{-3} s
Erreur instant de detection FM	0 s	-5,4 10^{-4} s	-2,7 10^{-3} s	-5,4 10^{-3} s

TABLE I.2 – Erreur sur l'instant de detection et niveau de bruit sur rampe de phase, cas n°1: sans Doppler (référence) cas n°2, 3 et 4: mouvement vertical sinusoidal d' amplitude A= 1, 5, 10 m

Les résultats des simulations concordent avec les prédictions du modèle théorique. L'effet Doppler introduit un biais de mesure dans le cas des signaux FM et CW. Le biais introduit par la compression d'impulsion (non adapté) est corrigé après détection en utilisant les données de vitesse de la centrale d'attitude. Il reste donc le biais dû à l'erreur de pointage. Cette erreur était inconnue précédemment probablement noyée dans d'autres causes de dégradation (erreur importante pour des angles de voie importants). De ce point de vue, les signaux FM ou CW ne sont pas influencés différemment. La statistique des rampes de phase lors de l'utilisation des signaux FM est bien plus bruitée que celle provenant des signaux CW (les résultats des simulations tableau I.2) et ceci également sans effet Doppler. Une autre question s'est posée : la statistique des rampes de phase (donc la statistique sur instant de détection ou niveau de bruit) est-elle plus impactée par l'effet Doppler dans le cas des signaux FM que pour les signaux CW ? Une série de simulations a démontré que l'impact de l'effet Doppler sur la statistique des rampes de phase est négligeable par rapport aux différences observées entre les deux types de signaux.

I.2.1.3 Conclusion

L'effet Doppler ne permet pas d'expliquer la perte de performance. Après correction du biais dû à la compression d'impulsion, la détection n'est pas plus impacté lors de l'utilisation de signaux FM que CW. La perte en amplitude causée par le filtrage adapté appliqué sur un signal ayant subi l'effet Doppler ne réduit pas de façon significative le rapport signal sur bruit. Qui plus est, nous avons montré que l'effet Doppler n'influençait pas sur la statistique de la détection (les statistiques des rampes de phase restent inchangées). Cependant, il a bien été noté que les rampes de phase sont plus bruitées lors de l'utilisation de signaux FM.

I.2.2 Recherche d'autres causes de dégradation : impact des lobes secondaires

Finalement, notre étude a démontré que l'effet Doppler n'était pas une cause suffisante d'explication des dégradations observées sur la qualité des mesures bathymétriques lorsque l'on utilise la FM.

Les résultats des simulations pour confirmer les impacts théoriques de l'effet Doppler ont montré que le bruit de phase du signal interférométrique était plus important sur les signaux FM après compression d'impulsion que sur les signaux CW, ceci même dans le cas d'immobilité des antennes de réception et d'émission. Ce bruit est intrinsèque à la mesures puisque cette observation à été faite sur des signaux simulés sans bruit additif.

Ici nous listons l'ensemble des causes possibles de bruit impactant sur la qualité des rampes de phase :

- Bruit ambiant ou bruit additif (qui n'est certainement pas prépondérant pour les données FM puisque le rapport signal à bruit est amélioré d'un facteur $B.T$ de ce point de vue)
- Multi-trajet (non pris en compte/ puisqu'il s'agit de sondeurs moyen-grand fond)
- Décorrélation spatiale ou glissement d'empreinte (qui consiste à dire que les deux sous antenne ne voit pas tout à fait la même empreinte (mais chacun une empreinte légèrement décalée) ce phénomène est négligeable pour les sondeurs multifaisceaux puisque la mesure bathymétrique est faite dans l'axe de la voie.
- Décorrélation angulaire ou *baseline decorrelation* (certainement le phénomène prépondérant lors de l'utilisation des signaux FM)

La décorrélation angulaire est souvent décrite en considérant que l'empreinte de fond marin contribuant à un instant donné comme une source propre de diffusion. Les centres de phase des 2 sous-antennes sont perçus du point de vue de cette empreinte selon des directions angulaires différentes. La durée d'impulsion du signal FM-compressé apparait plus longue que CW du à la présence de lobes secondaires temporels, donc l'empreinte sur le fond à un instant donné est plus large en considérant ce signal équivalent FM (signal compressé) qu'en CW. Plus l'empreinte est étendue, plus le diagramme de rayonnement de l'empreinte est fluctuant. Le résultat est une perte de cohérence des deux signaux reçus par les sous-antennes.

Une analyse théorique a été réalisée permettant de prédire le niveau de bruit sur la différence de phase interférométrique (rampes de phase) en fonction de la configuration de l'interféromètre (profondeur de l'eau H, l'angle du faisceau θ_0, de la distance entre les deux sous

antennes a...) et la forme des impulsions s (dans le cas de la FM, il s'agit de la forme du signal compressé).

La cohérence des signaux interférométriques considérant la décorrélation angulaire (bruit intrinsèque au signal utilisé) est donné par (I.2.1), ou TF est la transformée de fourrier.

$$\mu = \frac{\left|\left\langle S_a \overline{S_b} \right\rangle\right|}{\sqrt{\left\langle S_a \overline{S_a} \right\rangle \left\langle S_b \overline{S_b} \right\rangle}} = \frac{\mathrm{TF}[|s|^2](f_c \frac{1}{2} \frac{a}{H} \frac{\cos^2 \theta_0}{\tan \theta_0})}{\mathrm{TF}[|s|^2](0)} \tag{I.2.1}$$

Ce coefficient peut être transformé en rapport signal à bruit intrinsèque :

$$d_{in} = \frac{\mu}{1-\mu} \tag{I.2.2}$$

Le rapport signal à bruit incluant bruit intrinsèque et bruit additif est donné par l'équation (I.2.3), le rapport signal à bruit venant du bruit additif étant prédit à partir de l'équation sonar.

$$\frac{1}{d_{tot}} = \frac{1}{d_{in}} + \frac{1}{d_{add}} + \frac{1}{d_{in} d_{add}} \tag{I.2.3}$$

L'impact sur la statistique de la rampe (écart type) de phase est donné par :

$$\sigma(\Delta\phi) = \frac{2}{\sqrt{\frac{12}{\pi^2} + d}\left(1 - 0.05 \frac{d}{d+1} \ln d\right)} \tag{I.2.4}$$

I.2.2.1 Impact théorique des lobes secondaires

Ici on considèrera deux signaux comparables :

- CW 3 ms dans une enveloppe en cosinus carré (signal non modulé utilisé par l'EM710).
- FM 20 ms, bande 830Hz. Ce signal compressé présente un lobe principal très proche du signal précédent, la différence entre ce signal compressé et le signal CW précédent est la présence des lobes temporels secondaires.

La figure (I.2.1) présente le résultat en terme de prédiction par rapport au bruit intrinsèque. La première sous figure présente le niveau de cohérence des signaux interférométriques, rappelons que celui ci est donné par la transformée de Fourrier normalisée du carrée de l'enveloppe du signal en un point particulier dépendant des paramètres géométriques. Le niveau de cohérence est plus faible quelque soit la configuration interférométrique lors de l'utilisation de signaux FM. Les lobes secondaires temporels du signal compressé entraine une décorrélation des signaux. Le niveau de bruit des rampe de phase (donc de l'instant de détection) est donc plus important (deuxième sous figure). La configuration choisie ici est $H = 200$m, $a = 0.33$m, $f_c = 73000$Hz.

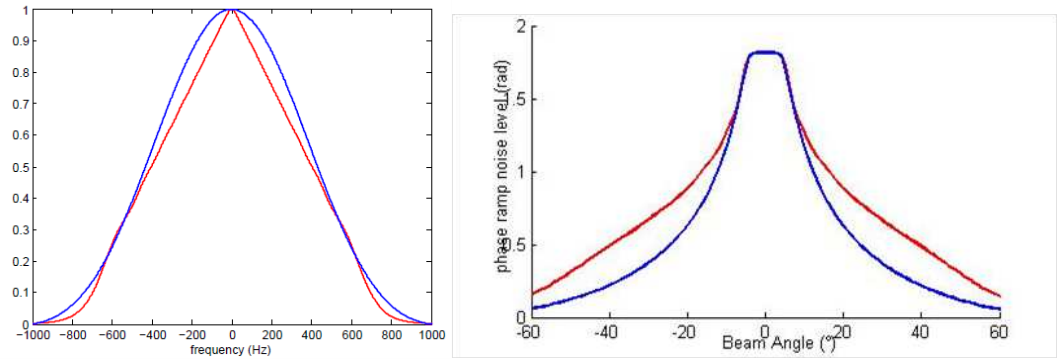

(a) niveau de cohérence des signaux interférométriques

(b) prédiction niveau de bruit sur rampes de phase en fonction de l'angle de voie

FIGURE I.2.1 – Prédiction du niveau de cohérence des signaux interférométriques et de bruit sur rampes de phase, rouge: signal FM, bleu: signal CW

I.2.2.2 Simulations

La prédiction est comparée à une série de simulations prenant en compte l'antenne complète de réception pour validation. Ici, on compare (fig I.2.2) les deux signaux précédents (rouge et bleu) avec un troisième signal (vert) : FM 20 ms, bande 500Hz, signal habituellement utilisé par l'EM710. La statistique (ou niveau de bruit) des rampes de phase est estimée sur une fenêtre autour de l'instant théorique de détection sur 20 réalisations.

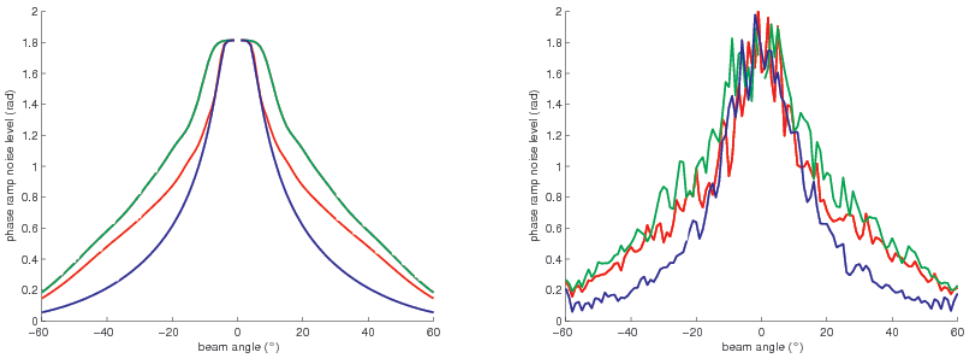

(a) prédiction du modèle théorique

(b) simulation

FIGURE I.2.2 – Comparaison estimation du bruit sur rampe de phase avec prédiction du modèle théorique CW (bleu), FM 500 Hz (vert), FM 830 Hz (rouge)

I.2.2.3 Données réelles

Une série de données réelles a été enregistrée en juin 2012 par Kongsberg Maritime à l'aide de l'EM710 du M/K Simrad-Echo. Le fond marin est plat situé à 200m de profondeur. Le système explore une très petite zone pour préserver la statistique de l'observation.

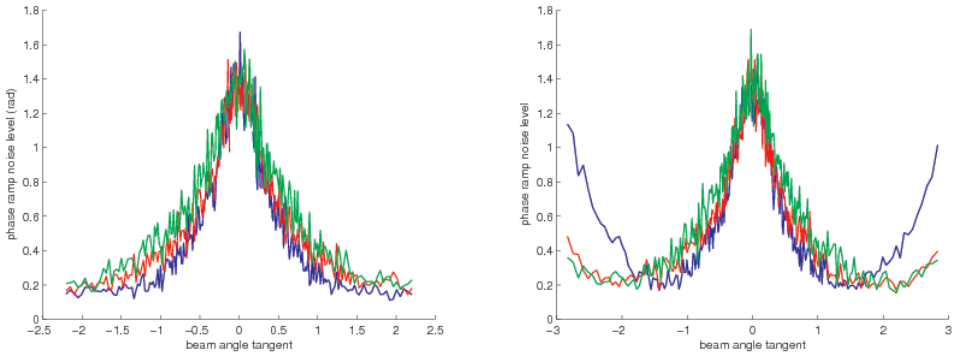

(a) série de données à 0dB (b) série de données à -20dB

FIGURE I.2.3 – Niveau de bruit sur rampes de phase en fonction de la tangente de l'angle de voie (proportionel à la distance), CW (bleu); FM 830 Hz (rouge); FM 500 Hz (vert).

Les conditions interférométriques sont les mêmes que pour les simulations et prédictions du modèle. Chacun des trois signaux précédents a été utilisé pour deux série de mesures (données après formation de voies et données capteurs disponibles) ; la première utilisant le niveau maximal d'émission (0dB) ; la seconde avec un niveau d'émission beaucoup moins important -20dB du niveau maximal (fig I.2.3). Dans la première série de mesure à 0 dB, les signaux sont très peu impactés par le bruit ambiant ; le bruit présent sur les rampes de phase vient principalement du bruit intrinsèque. Dans la seconde série de mesures, le bruit ambiant impacte les sondes principalement pour les angles de voies importants ; la compression d'impulsion donne de l'avantage aux signaux FM.

I.3 Partie 3 : Proposition d'amélioration

I.3.1 Apodisation de l'enveloppe du signal émis

Il est possible d'améliorer la qualité bathymétrie, en réduisant les niveaux des lobes secondaires après compression d'impulsion. Le lissage de l'enveloppe du signal FM émis permet de réduire ces lobes secondaires après compression d'impulsion.

Cette amélioration sur la mesure bathymétrique a été confirmée par des simulations et testée *in situ* (se reporter au manuscrit principal).

Cette méthode améliore la mesure bathymétrique lorsque le bruit intrinsèque est la principale cause de bruit. Cependant dans le cas ou la cause de bruit principale est le bruit ambiant, on perd un certaine avantage de la compression d'impulsion. En effet, l'apodisation de l'enveloppe du signal réduit l'énergie du signal transmis donc le rapport signal à bruit (du point de vue du bruit additif). Cette faiblesse peut être compensée en ré-augmentant la durée du signal. Cependant la durée du signal ne peut être indéfiniment allongée (matériel, exploration colonne d'eau). Une nouvelle piste est donc de garder le maximum d'énergie transmis en gardant une enveloppe carrée est de travailler en réception par filtrage.

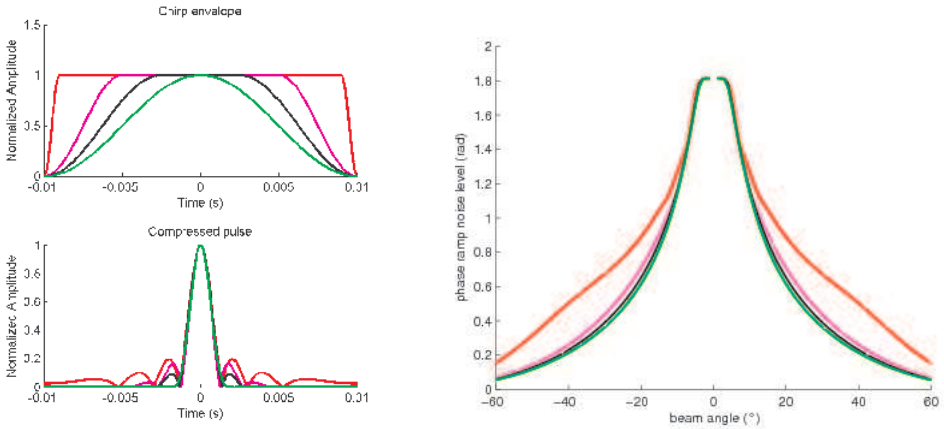

(a) Forme temporelle des impulsion (avant et après compression d'impulsion)

(b) Prediction: niveau de bruit sur rampes de phase

Figure I.3.1: Prédiction du niveau de bruit sur rampes de phase dépendant de la forme des impulsions. réduction des lobes secondaires en utilisant des envelopes apodisés (rouge:10%, magenta:50%, noir:75%, vert: 100%)

I.3.2 Filtrage par un filtre adapté apodisé

Une autre piste pour réduire les lobes secondaires de la compression d'impulsion consiste à utiliser un filtrage adapté dans une fenêtre de pondération (apodisation). Cependant, cette méthode réduit la bande du signal. Le lobe principal du signal compressé se trouve alors élargi. Les avantages de cette méthode dépendent donc de la configuration. La réduction de la bande (et donc élargissement du lobe principal du signal compressé) était compensé dans le cas précédent car travaillant en émission la bande balayé avait été élargi afin de préservé la bande équivalente du signal. Cette méthode est donc moins intéressante considérant la réduction du bruit intrinsèque que la précédente. Cependant elle permet de mieux conserver l'intérêt de la compression d'impulsion, puisqu'il est possible de choisir le type de filtrage : filtrage adapté classique ou apodisé suivant si le bruit intrinsèque ou bruit additif est prédominant.

Cette méthode à été testée en simulation et sur les données réelles à partir des signaux capteurs (de l'antenne) qui ont été traités (se reporter au manuscrit principal).

I.3.3 Utilisation de modulation de fréquence non linéaire

Afin de conserver une enveloppe d'émission rectangulaire (maximum d'énergie émise) et réduire les lobes secondaires de la compression d'impulsion, il est possible de changer la forme de modulation de fréquence. Une forme non linéaire de modulation (fig I.3.2) permet de changer la forme de l'occupation spectrale du signal. La compression d'impulsion présente des lobes secondaire d'amplitude plus faible (fig I.3.3).

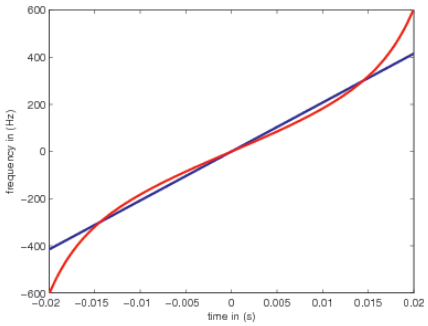

Figure I.3.2: relation temps-fréquence de la modulation (Bleu: modulation linéaire de fréquence, Rouge: Modulation non linéaire de fréquence)

Le niveau de bruit sur rampes de phase (considérant le bruit intrinsèque seul) est donc prédit moins important. De plus comme l'enveloppe est rectangulaire le lobe principal conserve le maximum d'énergie (contrairement à la méthode qui consiste à pondérer l'enveloppe du chirp), donc on garde l'intérêt complet de compression d'impulsion vis à vis au bruit ambiant.

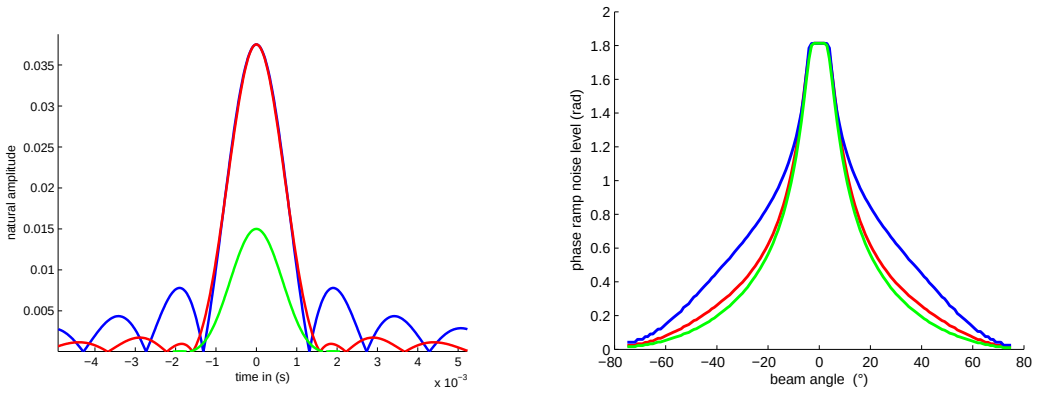

(a) Compression d'impulsion

(b) Prédiction bruit rampe de phase en fonction de l'angle de voie

FIGURE I.3.3 – Compression d'impulsion et prédiction bruit sur rampe de phase: Chirp linéaire dans enveloppe rectangulaire (bleu), Chirp non-linear dans enveloppe rectangulaire (rouge), Chirp linéaire dans envelopppe en cos2 (vert) (considérant bruit intrinsèque)

Néanmoins cette méthode présente une faiblesse en cas d'effet Doppler : la diminution des lobes secondaires de la compression d'impulsion n'est effective que lorsque le signal est bien adapté au filtrage adapté. Il faudrait donc envisager de prédire l'effet Doppler avant filtrage adapté afin de procéder à la compression d'impulsion à l'aide d'un filtre adapté 'dopplerisé'.

Conclusion

La nouvelle génération de sondeurs multifaisceaux utilise des signaux modulé en fréquence afin d'atteindre des porté plus importante tout en gardant une bonne résolution. Il est ainsi

possible d'émettre plus d'énergie en augmentant la durée d'émission. Grâce à la compression d'impulsion, le procédé est équivalent à émettre une impulsion plus puissante d'une durée plus courte.

En pratique, la portée des système a bien été accru, cependant la mesure issue de ces système apparait plus bruité. Cette observation apparait contradictoire puisque la compression d'impulsion permet théoriquement d'augmenter le rapport signal à bruit.

Deux causes de dégradation possible ont été étudiées ici. La première piste était l'effet Doppler. En effet la compression d'impulsion ne s'effectuant pas correctement en cas d'effet Doppler. Les signaux FM pourraient être plus impactés que les signaux classique lors des mouvement des antennes d'émission et réception soumis au roulis, tangage, pilonnement etc. L'étude a conclu que l'effet Doppler entrainait des biais de mesures. Un premier biais présent dans le cas de signaux FM et CW est créé par un dépointage de la voie dû à l' effet Doppler. Le second présent dans les cas de signaux FM uniquement est dû à la compression d'impulsion. Considérant que ce biais est corrigé après traitement à partir des données de vitesse enregistrées par la centrale d'attitude, l'effet Doppler n'impacte pas plus les signaux FM que CW.

La deuxième piste d'étude est centrée sur la recherche de cause de bruit intrinsèque. Il a été montré que la contribution des lobes secondaires de la compression d'impulsion entraine une décorrélation des signaux interférométriques, bruitant les rampes de phase, ce qui impacte la statistique de la détection.

Il a donc été exploré trois pistes d'amélioration permettant de réduire les lobes secondaires. Une méthode classique pour réduire les lobes secondaire consiste à pondérer l'enveloppe du signal. La première proposition est d'appliquer cette méthode en émission. La bande équivalente du signal est préservée de tel sorte que les lobes secondaires sont diminués sans élargir le lobe principal. Cette apodisation a été testé en simulation et in situ. Elle permet de réduire le bruit intrinsèque au signal, cependant en utilisant une enveloppe d'émission pondérée on réduit l'énergie de l'impulsion. La compression d'impulsion (utile vis à vis du bruit ambiant) n'est donc pas utilisée de manière optimale. Pour pallier ce problème dépendant du niveau de gain souhaité pour la compression d'impulsion, on peut augmenter la durée de l'impulsion. La seconde proposition est de garder l'émission dans une enveloppe rectangulaire et de travailler en réception en utilisant le filtrage adapté dans une fenêtre pondérée. Elle a été également testée en simulation et in situ. Cette méthode permet d'adapter le filtrage en fonction du type de bruit prépondérant. Cependant elle est moins efficace que la première car si le niveau des lobes secondaires est abaissé, le lobe principal est élargi ce qui crée un décorrélation additionnelle des signaux interférométriques selon certaines configurations. Afin de garder une compression d'impulsion optimale tout en réduisant les lobes secondaires, on propose comme troisième méthode d'utiliser d'autres formes de modulation de fréquence. Cette méthode semble prometteuse (testée en simulation) car elle présente dans tous les cas de figure des mesures théoriquement moins bruitées (gain en compression d'impulsion, gain vis à vis des lobes secondaires atténués). Cependant, elle n'a pas été testée in situ (nécessitant une adaptation mineure du système d'émission). D'autre part, elle nécessite certainement d'adapter le traitement en réception (en prenant en compte l'effet Doppler pour le filtrage adapté).

Bibliography

[Ain, 2010] M.A. Ainslie, *Principles of sonar performance modeling*, Springer, 2010

[Bea, 2012] J. Beaudoin, X. Lurton X. & J.M. Augustin, *R/V Falkor Multibeam Echosounder System Review*, UNH-Ifremer joint technical report, 2012.

[Bea, 2013] J. Beaudoin, P. Johnson and F. Flinders *R/V Falkor Multibeam Echosounder System Review*. UNH-CCOM/JHC Technical Report 13-001, 77 pp, March. 21, 2013.

[Bir, 2005] J.S. Bird, G.K. Mullins, "Analysis of swath bathymetry sonar accuracy", *IEEE Journal of Oceanic engineering* vol 30, n°2, p 372-390, 2005.

[Bou, 1992] M. Bouvet, *Traitement des signaux pour les systèmes sonar*, Masson, 1992

[Bur, 1989] W.S. Burdic, *Underwater Acoustic System Analysis*, Prentice Hall, 1984

[Cer, 2012] P. Cervenka, "Baseline Decorrelation in Acoustic Tools for Surveying the Seafloor", 11th *European Conference on Underwater Acoustics (ECUA)*, 2nd - 6th July 2012, Edinburgh, UK. *Proceeding in POMA 17, 070073*, 2013

[Che, 2004] G. L. Chenadec, *Analyse de descripteurs énergétiques et statistiques de signaux sonar pour la caractérisation des fonds marins*, PhD thesis, University of Maine, 2004.

[Col, 2002] J. M. Colin, *Le radar: Théore et Pratique* , Ellipse, 2002

[Col, 1999] T. Collins and P. Atkins, "Non linear frequency modulation chirp for active sonar", *IEE Proc.-Radar: Sonar Navig.*, Vol. 146, No. 6, December 1999

[Coo, 1993] C.E. Cook and M. Bernfeld, *Radar signals An Introduction to Theory and Application*, Artech House, 1993

[Cos, 1984] J.P. Costas, "A study of a Class of Detection Waveforms Having Nearly Ideal Range-Doppler Ambiguity Properties", *Proc. of the IEEE*, Vol. 72, n°8, pp. 996-1009, 1984.

[Cur, 1991] J.C. Curlander, *Synthetic Aperture Radar - Systems & Signal Processing*, Wiley, 1991

[DeM, 1988] C. De Moustier, "State of the art in swath bathymetry survey systems", *International Hydrographic Review*, Vol. 64, pp. 25-54, 1988

[Ewa, 2011] A. Ewart, *Improving Quality of Multibeam Data from Amplitude Detection*, University College London, MSc Project report, 2011.

[Fra, 1982a] R.E Francois, G.R. Garrison, "Sound absorbtion based on ocean measurements, Part I: Pure water and magnesium sulffate contributions". *Journal of the Acoustical Society of America*, Vol. 72, pp 896-907, 1982.

[Fra, 1982b] R.E Francois, G.R. Garrison, "Sound absorbtion based on ocean measurements, Part II: Boric acid contribution and equation for total absorption". *Journal of the Acoustical Society of America*, Vol 72, pp 1879-1890, 1982.

[Gat, 1994] F. Gatelli, A. Monti Guarnieri, F. Parizzi, P. Pasquali, C. Prati, F. Rocca, "The wavenumber shift in SAR interferometry", *IEEE Trans. Geoscience Remote Sensing*, vol 32, n°4, p 855-865, 1994.

[Har, 1995] R. Hare, A. Godin, L. Mayer. *Accuracy Estimation of Canadian Swath (Multibeam) and Sweep (Multitransducer) Sounding Systems.* Canadian Hydrographic Service Internal Report, 1995.

[Hei, 2004] A. Hein, *Processing of SAR Data: Fundamentals, Signal Processing, Interferometry*, Springer, 2004.

[Hel, 2003] L. Hellequin, J.-M. Boucher et X. Lurton, "Processing of high-frequency multibeam echo sounder data for seafloor characterization", *IEEE Journal of Oceanic Engineering*, vol. 28, no. 1, p. 78–89, 2003.

[Hel,1998] L. Hellequin, *Analyse statistique et spectrale des signaux de sondeurs multifaisceaux EM950. Application à l'identification des fonds sous-marins*, PhD Thesis, Université de Rennes 1, 1998.

[Hug, 2010] John Hughes-Clarke, *Multibeam course,* 2012

[Jam, 2008] M. Jamil, H. J. Zepernick and M.I. Pettersson, "Performance Assesment of Polyphase pulse compression codes", *ISSSTA 2008, IEEE 10th International Symposium on*, 2008

[Jin, 1996] G.Jin, D.Tang, "Uncertainties of Differential phase Estimation Associated with Interferometric Sonar", *IEEE Journal of Oceanic engineering*, vol 21, no 1, January 1996

[Kon, EM122] Kongsberg, *short specification EM122*, March 2009

[Kon, EM302] Kongsberg, *short specification EM302*, Sept 2009

[Kon, EM710] Kongsberg, *short specification EM710*, Sept 2009

[Lad, 2012] Y. Ladroit, *Amélioration des méthodes de détection et de qualication des sondes pour les sondeurs multifaisceaux bathymétriques*, PhD Thesis, Université Rennes 1,2012

[LeC, 1989] F. Le Chevalier, *Principe de Traitement des Signaux Radar et Sonar*, Masson, 1989

[Lev, 1988] N. Levanon, *Radar principles*, Wiley, 1988

[Lur, 1998] X. Lurton, *Acoustique sous-marine Présentation et application*, Ifremer 1998

[Lur, 2001] X. Lurton, "Précision de mesure des sonars bathymétriques en function du rapport signal sur bruit", *Traitement du signal* ,vol 18, no.3, pp 179-194, 2001

[Lur, 2010a] X. Lurton, *An Introduction to Underwater Acoustics, Principles and Application*, Second edition, Springer, 2010

[Lur, 2010b] X. Lurton and J.M. Augustin, "A Measurement Quality Factor for Swath Bathymetry Sounders", *IEEE Journal of Oceanic Engineering*, Vol. 35, n° 4, October 2010

[Mil, 1990] J. Millet and G. Jourdain, "Signaux à fort pouvoir de résolution temps fréquence: Comparaison entre signaux de Costas et les signaux à modulation binaire de phase BPSK", *Traitement du signal*, Vol 7, n°1, 1990

[Mit, 1985] R.L. Mitchel, *Radar Signal simulation*, Mark Ressources, 1985

[Oli, 1996] C. Oliver, S. Quegan, *Understanding Synthetic Aperture Radar Image*s, Artech House, 1996

[Puj, 2007] G. LLort Pujol, *Amélioration de la résolution spatiale des sondeurs multifaisceaux*, PhD Thesis, université Rennes 1, 2007

[Ric, 2005] M.A Richards, *Fundamentals of Radar Signal Processing*, McGraw-Hill Companies, 2005

[Ron, 1999] A. Rønhovde et L. Yang, "High-resolution beamforming for multibeam echo sounders using raw em3000 data", *OCEANS Poc.*, 1999.

[Sin, 2002] Ch. Sintes, *Déconvolution Bathymétrique d'images Sonar Lateral par des Méthodes Interférométriques et de Traitement de l'Image*, PhD Thesis, 2002

[Sin, 2010] Ch. Sintes, G. LLort Pujol and D. Gueriot, "Coherent Probabilistic Error Model for Interferometric Sidescan Sonars", *IEEE Journal of Oceanic engineering*, vol. 35, no. 2, pp. 412-435, 2010

[Sin, 2012] Ch. Sintes, G. LLort Pujol "Empirical Interferometric Phase Variance Formulas for Bathymetric Applications", *IEEE Trans. Geoscience and Remote Sensing,* Vol. 50, n°6, pp 2079 - 2097, 2012

[Tou, 1995] R. Tough, D. Blacknell and S. Quegan, "A statistical description of polarimetric and interferometric synthetic aperture radar data", *Proc. Royal Society*, vol. 449, pp. 567-589, 1995

[Uri, 1983] Urick, *Principles of Underwater Sound*, New York, MacGraw Hill 1983

[Var, 2003] L.R. Varsney and D. Thomas, sidelobe reduction for Matched filter range processing, *IEEE Radar conference*, 2003

[Vin, 2010] P. Vincent, Ch. Sintes, X. Lurton, R. Garello, "Influence of the Doppler Effect on Multibeam Echo Sounder Bathymetry", *OCOSS Proc.* (Brest, France), June 2010.

[Vin, 2011a] P. Vincent, Ch. Sintes, F. Maussang, X. Lurton, R. Garello, "Doppler Effect on Bathymetry using Frequency Modulated Multibeam Echo Sounders", *OCEANS Proc.* (Santander, Spain), June 2011.

[Vin, 2011b] P.Vincent, F. Maussang, X. Lurton, Ch. Sintes, R. Garello, "Effet Doppler : Impact sur la mesure bathymétrique issue des sondeurs multifaisceaux", *GRETSI Proc.* (Bordeaux, France), Septembre 2011

[Vin, 2012a] P. Vincent, F. Maussang, X. Lurton, Ch. Sintes, R. Garello, "Impact of FM Pulse Compression Sidelobes on Multibeam Bathymetry Measurements", *ECUA Proc.* (Edinburg, UK) , July 2012

[Vin, 2012b] P. Vincent, F. Maussang, X. Lurton, Ch. Sintes, R. Garello, "Bathymetry Degradation Causes for Frequency Modulated Multibeam Echo Sounders", *OCEANS Proc.* (Hampton Roads, USA), October 2012

[Yan, 2007] J. Yang, T.K Sarkar, "A New Doppler-Tolerant Polyphase Pulse Compression Codes based on hyperbolic fraquency modulation", IEEE Radar Conference, (Syrakus), April 2007

[Yuf, 2011] G. Yufit, E. Maillard, "The influence of ship motion on bathymetric sonar performance in FM mode of operation", *OCEANS Proc.* (Kona, USA), September 2011.

[You, 1804] T. Young, "The Bakerian Lecture: Experiments and Calculations Relative to Physical Optics", *Philosophical Transactions of the Royal Society of London*, Vol 94, pp. 1-16, 1804.

[Zeb, 1992] H.A. Zebker, J. Villasenor, "Decorrelation in interferometric radar echoes", *IEEE Trans. Geosci. Remote Sens.* Vol 30, n°5, pp 950-959, 1992.